

**CELLULAR MECHANISMS OF ECOLOGICAL INTERACTIONS
AMONG MARINE PHYTOPLANKTON**

A Dissertation
Presented to
The Academic Faculty

by

Emily R. Brown

In Partial Fulfillment
of the Requirements for the Degree
Doctor of Philosophy in the
School of Biological Sciences

Georgia Institute of Technology
August 2021

COPYRIGHT © 2021 BY EMILY R. BROWN

**CELLULAR MECHANISMS OF ECOLOGICAL INTERACTIONS
AMONG MARINE PHYTOPLANKTON**

Approved by:

Dr. Julia Kubanek, Advisor
School of Biological Sciences
School of Chemistry and Biochemistry
Georgia Institute of Technology

Dr. Pamela Peralta-Yahya
School of Chemistry and Biochemistry
School of Chemical and Biomolecular
Engineering
Georgia Institute of Technology

Dr. Mark E. Hay
School of Biological Sciences
Georgia Institute of Technology

Dr. Vinayak Agarwal
School of Chemistry and Biochemistry
School of Biological Sciences
Georgia Institute of Technology

Dr. Joseph P. Montoya
School of Biological Sciences
Georgia Institute of Technology

Date Approved: July 23, 2021

To my husband and parents.

ACKNOWLEDGEMENTS

The journey to this thesis was much longer than the six years I have spent at Georgia Tech. Therefore, I would like to start by thanking some of my early teachers and mentors. First, I would like to thank my 10th grade honors English teacher, Mr. Ed Kramer, who assigned our class a research project where we were asked to explore our greatest curiosities and deepest concerns about the world around us. This project is what piqued my interest in harmful algal blooms so I am forever indebted to Mr. Kramer for helping me discover this area of study for which I have become so passionate. My gratitude to Dr. Christopher Reddy at Woods Hole Oceanographic Institute who allowed me to shadow in his lab for two weeks as a naïve high school senior and provided me guidance in how to begin my path toward a PhD in marine biology. Finally, I must thank Dr. Jeffrey Wright, Dr. Carmelo Tomas, and Dr. Wendy Strangman who mentored me as an undergraduate at UNCW and encouraged me to stay the course toward pursuing a PhD even in the face of rejection.

While at Georgia Tech, I have struggled and grown as both as an individual and a scientist. My growth was made possible by the support of many individuals. I first and foremost would like to thank my advisor Dr. Julia Kubanek for her mentorship and support. She has been instrumental in my development as a scientist through our insightful scientific discussions, her constructive critiques, and her drive and support in helping me achieve my goals. I am also indebted to my thesis committee: Dr. Mark Hay, Dr. Pamela Peralta-Yahya, Dr. Joe Montoya, and Dr. Vinny Agarwal, who have provided me with resources and feedback which have improved my research. I would also like to thank Dr. Emily

Weigel for giving me a chance to grow my teaching chops and providing support and encouragement during the latter part of my graduate career.

I must also acknowledge my many lab mates and friends that I have made over my six years who have helped me in countless ways. In particular I would like to thank Dr. Nicole Johnston who was my scientific “other half” during some of the more difficult segments of my graduate career. She engaged with me in critical conversations regarding my research, and science in general, and as a friend she buoyed me when I was struggling. I would also like to thank all the Kubanek lab members, both past and present, including: Dr. Sam Mascuch, Dr. Nazia Mojib, Dr. Serge Lavoie, Dr. Remy Poulin, Dr. Anne Marie Sweeney-Jones, Bhuwan Chhetri, Marisa Cepeda, Nolan Barrett, and Gabi Chebli for their insight, support, and spirit lifting conversations which have carried me through my research. I am also grateful for the friendship, support, and assistance of post docs and fellow graduate students from our “neighboring” labs including Dr. Andrew Burns, Dr. Hem Thapa, Dr. Jinu Mathew Valayil, Dr. Deanna Beatty, Maddie Willert, Alex Draper, Cara Lin, Ipsita Mohanty, Stephanie Bilodeau, Sarah Roney, and Noam Altman-Kurosaki.

Finally, I would like to thank my family and many friends outside of Georgia Tech who encouraged and supported me through this endeavor. A special shout-out to Megan Wolff and Rochelle Dumm who were both shoulders to cry on when I needed relief and made sure I came up to breathe, workout, eat, and enjoy life. Also, my parents deserve an extra special thank you for their love, support, and encouragement as I pursued my dream to study marine science and earn a PhD. Last but definitely not least, I want to thank my husband David for his patience, love, support, and general awesomeness throughout my graduate school career.

TABLE OF CONTENTS

ACKNOWLEDGEMENTS	iv
LIST OF TABLES	ix
LIST OF FIGURES	xi
LIST OF SYMBOLS AND ABBREVIATIONS	xviii
SUMMARY	xix
CHAPTER 1. Introduction: Chemical ecology of marine plankton	1
1.1 Abstract	1
1.2 Introduction	1
1.3 Intraspecific Signaling	3
1.3.1 Reproductive signaling	3
1.3.2 Quorum sensing	7
1.3.3 Other intraspecific signaling	12
1.4 Facilitation and mutualism	13
1.5 Host-parasite interactions	20
1.6 Allelopathy	27
1.7 Predator-prey interactions	34
1.7.1 Chemical defenses	34
1.7.2 Prey capture and predator avoidance	49
1.8 Community and ecosystem effects	58
1.8.1 Community and ecosystem effects	58
1.8.2 Bacterial dynamics	63
1.8.3 Effects of global change	67
1.9 Conclusions	69
CHAPTER 2. Harmful alga trades off growth and toxicity in response to cues from dead phytoplankton	71
2.1 Abstract	71
2.2 Introduction	72
2.3 Materials and methods	75
2.3.1 Phytoplankton cultivation	75
2.3.2 Experimental design	76
2.3.3 Intracellular toxin analysis	81
2.3.4 Extracellular toxin analysis	82
2.3.5 Statistical analysis	83
2.4 Results	84
2.5 Discussion	93
CHAPTER 3. Predator Cues Target Signaling Pathways in Toxic Algal Metabolome	99

3.1	Abstract	99
3.2	Introduction	100
3.3	Methods	102
3.3.1	Phytoplankton culturing	102
3.3.2	Metabolomics experimental design and execution	102
3.3.3	Metabolite analysis and annotation	103
3.3.4	Signaling pathway inhibition experiments and cell membrane permeability assay	104
3.4	Results	105
3.4.1	Copepodamides trigger subtle but measurable changes in the metabolome of <i>Alexandrium minutum</i>	105
3.4.2	Jasmonic acid biosynthesis and signaling are involved in toxin production initiated by copepodamides	109
3.4.3	Copepodamides appear not to behave as GPCR agonists and do not disrupt cell membranes in <i>Alexandrium minutum</i>	112
3.5	Discussion	115
CHAPTER 4. Differentiating toxic and nontoxic congeneric harmful algae using the non-polar metabolome		122
4.1	Abstract	122
4.2	Introduction	123
4.3	Materials and methods	127
4.3.1	Phytoplankton culturing	127
4.3.2	Experimental design	127
4.3.3	Harvesting and extraction	130
4.3.4	Toxin analysis	131
4.3.5	NMR sample preparation and spectral data acquisition	132
4.3.6	NMR spectral processing and analysis	133
4.3.7	UPLC/MS sample preparation and data acquisition	134
4.3.8	UPLC/MS data processing and analysis	136
4.3.9	Metabolite annotation	136
4.4	Results	138
4.4.1	The non-polar metabolomes of <i>Alexandrium</i> spp. vary considerably between closely related toxic and non-toxic species	138
4.4.2	Only a small portion of the non-polar metabolome of <i>Alexandrium</i> spp. is likely associated with toxicity	142
4.5	Discussion	144
CHAPTER 5. Conclusions and future directions		150
APPENDIX A. Supplementary Figures for Chapter 2		156
APPENDIX B. Supplementary Materials for Chapter 3		157
B.1	Methods	157
B.1.1	Copepodamide extraction and isolation	157
B.1.2	Harvesting and extraction of <i>Alexandrium minutum</i> for metabolomics experiment	158

B.1.3	Metabolomic sample preparation and spectral data acquisition	161
B.1.4	Data processing and analysis	166
B.1.5	Metabolite annotation	168
B.1.6	Signaling pathway inhibition experiments	169
B.1.7	Cell membrane permeability assay	176
B.2	Results: Supplementary figures and tables	177
APPENDIX C. Supplementary Figure and Tables for Chapter 4		183
REFERENCES		187

LIST OF TABLES

Table 2.1	Comparison of the cell size, biomass, and concentration of lysed phytoplankton added to <i>Alexandrium minutum</i> replicates for Experiments 1.	76
Table 2.2	Distribution of treatments of chemical cues from dead phytoplankton and replicates across batches (Experiment 1).	78
Table 2.3	Measured nutrient concentrations used to calculate concentrations of ammonia and nitrate used for dilute media control in Experiment 2.	81
Table 4.1	Lipid classes identified by MS-based models with significantly different concentrations in toxic <i>Alexandrium catenella</i> or <i>Alexandrium pacificum</i> compared to non-toxic <i>A. tamarense</i> . The number of compounds in each class and the average fold-change is included for each class. Average fold-change is the mean change in concentration for each lipid in <i>A. catenella</i> relative to <i>A. tamarense</i> (Experiment 1) and in <i>A. pacificum</i> relative to <i>A. tamarense</i> (Experiment 2).	142
Table 4.2	Candidate metabolites tentatively identified that were in significantly different concentrations in both toxic <i>Alexandrium catenella</i> and <i>Alexandrium pacificum</i> compared to non-toxic <i>A. tamarense</i> . The change in concentration is the compound's concentration in <i>A. catenella</i> relative to <i>A. tamarense</i> (Experiment 1) and its concentration in <i>A. pacificum</i> relative to <i>A. tamarense</i> (Experiment 2). P values were calculated using an unpaired t-test. Lipid classifications: phosphatidylcholines (PCs), phosphatidylinositols (PIs), and triacylglycerols (TGs).	144
Table B1	Identification of metabolites whose concentrations differed in <i>Alexandrium minutum</i> based upon exposure to copepodamides, based on UPLC/-MS data. The retention time (in minutes), <i>m/z</i> , detected ion, molecular formula, and mass error (ppm) are provided for each tentatively identified metabolite. Additionally, the fold-change based on <i>A. minutum</i> exposed to copepodamides relative to <i>A. minutum</i> exposed to a solvent control is provided where possible. Confidence levels were assigned based on available spectral details. Confidence level 1: exact match both in fragmentation and retention time to an authentic standard; 2: observed MS/MS data and shifts in the ¹ H NMR loadings plots and raw spectra were consistent with predicted spectra from databases; 3: observed MS/MS data were consistent with predicted spectra from databases; 4: relatively high FISH coverage calculated by Compound Discoverer and retention	178

time relative to other metabolites matches the literature; 5: close match mass match and retention time relative to other metabolites matches the literature.

- Table C1 Putatively identification of metabolites whose concentrations are significantly different in *Alexandrium catenella* compared to *Alexandrium tamarense* based on UPLC/MS data from experiment 1. The m/z , detected ion, molecular formula, and mass error (mDa), and lipid class are provided for each tentatively identified metabolite which differs significantly in concentration between *A. catenella* and *A. tamarense* from Experiment 1 but do not differ significantly between *A. tamarense* from Experiment 1 and 2. Additionally, the p -value and fold-change based on *A. catenella* relative to *A. tamarense* is provided. Confidence levels were assigned based on available spectral details. Confidence level 1: exact match both in fragmentation and retention time to a purchased standard; 2: observed MS/MS data consistent with predicted spectrum from databases and exact mass match in LOBSTAHS or LIPDMAPS to corresponding lipid class; 3: exact mass match in LOBSTAHS or LIPDMAPS to corresponding lipid class or partial match of MS/MS data to databases. 184
- Table C2 Putatively identification of metabolites whose concentrations different significantly in *Alexandrium pacificum* compared to *Alexandrium tamarense* based on UPLC/MS data from experiment 2. The m/z , detected ion, molecular formula, and mass error (mDa), and lipid class are provided for each tentatively identified metabolite which differs significantly in concentration between *A. pacificum* and *A. tamarense* from Experiment 2 but do not differ significantly between *A. tamarense* from Experiment 1 and 2. Additionally, the p -value and fold-change based on *A. pacificum* relative to *A. tamarense* is provided. Confidence levels were assigned based on available spectral details. Confidence level 1: exact match both in fragmentation and retention time to a purchased standard; 2: observed MS/MS data consistent with predicted spectrum from databases and exact mass match in LOBSTAHS or LIPDMAPS to corresponding lipid class; 3: exact mass match in LOBSTAHS or LIPDMAPS to corresponding lipid class or partial match of MS/MS data to databases. 186

LIST OF FIGURES

Figure 1.1	A class of compounds exuded by copepods: Copepodamides A-H (1-8).	4
Figure 1.2	Bacterial auto-inducers: <i>N</i> -(3-oxo-hexanoyl)-L-homoserine lactone (9), <i>N</i> -octanoyl-L-homoserine lactone (10), <i>N</i> -butanoyl-L-homoserine lactones (11), <i>N</i> -hexanoyl-L-homoserine lactones (12), <i>N</i> -decanoyl-L-homoserine lactones (13), <i>N</i> -dodecanoyl-L-homoserine lactones (14), and <i>N</i> -tetradecanoyl-L-homoserine lactone (15).	9
Figure 1.3	Quorum sensing molecules <i>N</i> -(3-hydroxyhexanoyl)-L-homoserine lactone (16) and <i>N</i> -(3-oxo-decanoyl)-L-homoserine lactone (17) involved in antiphage defense in <i>Vibrio anguillarum</i> .	12
Figure 1.4	Intraspecific signaling molecule indole-3-acetic acid (18) produced by <i>Emiliana huxleyi</i> .	13
Figure 1.5	Molecules potentially involved in cross-talk between phytoplankton and bacteria: L-tryptophan (19), dimethylsulfoniopropionate (DMSP) (20), and 2,3-dihydroxypropane-1-sulfonate (DHPS) (21).	15
Figure 1.6	Paralytic shellfish toxins (PSTs): saxitoxin (22), neosaxitoxin (23), gonyautoxins (GTX) -1 (24), -2 (25), -3 (26), -4 (27), -5 (28), <i>N</i> -sulfocarbamoyl saxitoxin C1 (29), and <i>N</i> -sulfocarbamoyl saxitoxin C2 (30), produced by the dinoflagellate <i>Alexandrium fundyense</i> .	21
Figure 1.7	Metabolites involved in bacterial-algal interactions. Phenylacetic acid (31) and trophodithietic acid (32) are molecules produced by <i>Phaeobacter inhibens</i> which promote algal growth and have antipathogenic properties. <i>p</i> -Coumaric acid (33) and <i>N</i> -(3-hydroxydecanoyl)-L-homoserine lactone (36) promote production of algicidal roseobacticides A (34) and B (35) in <i>P. inhibens</i> .	25
Figure 1.8	Molecules from algicidal bacteria studies. β -cyclodextrin (37) is a homoserine lactone quorum sensing inhibitor. <i>N</i> -(3-oxo-octanoyl)-L-homoserine lactone (38) is an autoinducer produced by the algicidal bacterium <i>Ponticoccus</i> sp. Prolyl-methionine (39) and hypoxanthine (40) are potential algicides produced by <i>Bacillus</i> sp. against <i>Phaeocystis globosa</i> .	27

Figure 1.9	Molecules proposed to possess allelopathic properties: the monohydroxy fatty acid 15(S)-hydroxyeicosa-5Z,8Z,11Z,13E,17Z-pentaenoic acid (15(S)-HEPE) (41) and the peptide TYR-PRO-PHE-PRO-GLY-NH ₂ (42) produced by the diatom <i>Skeletonema costatum</i> and the raphidophyte <i>Heterosigma akashiwo</i> , respectively.	29
Figure 1.10	Chemical structure of the algal toxins yessotoxin (43) and domoic acid (44) produced by the dinoflagellate <i>Protoceratium reticulatum</i> and some diatoms from the genus <i>Pseudo-nitzschia</i> , respectively. Sterol sulfates, β -sitosterol sulfate (45), dihydrobrassicasterol sulfate (46), and cholesterol sulfate (47) which have self-inhibitory activity in the diatom <i>Skeletonema marinoi</i> .	33
Figure 1.11	Chemical structures of the toxins karlotoxins 1 (48), 2 (49), 8 (50), and 9 (51) and karmitoxin (52) produced by dinoflagellate of the genus <i>Karlodinium</i> .	36
Figure 1.12	Chemical structures of algal toxins: prymnesin-B1 (53) and -2 (54), produced by the haptophyte <i>Prymnesium parvum</i> , and azaspiracids (AZA) -1 (55), -36 (56), and -37 (57), produced by the dinoflagellate <i>Azadinium poporum</i> . Chemical structure of the diatom oxylipin 2E-decenal.	38
Figure 1.13	Algal toxin goniiodomin A (59) produced by the dinoflagellate <i>Alexandrium pseudogonyaulax</i> .	48
Figure 1.14	Chemical structure of 4-methyl-5-thiazoleethanol (60), a metabolite produced by both <i>Oxyrrhis marina</i> and <i>Emiliana huxleyi</i> .	58
Figure 1.15	Polyunsaturated aldehydes produced by diatoms: (2E,4E)-2,4-octadienal (61), (2E,4E)-2,4-heptadienal (62), and (2E,4E)-2,4-decadienal (63).	59
Figure 1.16	Brevetoxins (PbTx) -2 (64), -3 (65), -6 (66), and -9 (67) produced by the dinoflagellate <i>Karenia brevis</i> .	61
Figure 1.17	Bacterial quorum sensing molecules <i>N</i> -(3-oxo-tetradecanoyl)-L-homoserine lactone (69) and <i>N</i> -(3-hydroxybutanoyl)-L-homoserine lactone (71). Chemical structures of the autoinducer precursor 2-heptyl-4-quinolone (68), produced by <i>Pseudoalteromonas piscicida</i> , and propionate (70), a precursor of DMSP (20).	64
Figure 1.18	Polycyclic hydrocarbons, naphthalene (72) and phenanthrene (73), which are degraded by microbial communities associated with the diatom <i>Skeletonema costatum</i> .	67

- Figure 2.1 Effects of chemical cues from dead phytoplankton (as an indication of predation risk) on (a) cellular toxin concentration of GTX 1-4 and (b) percent growth of *Alexandrium minutum* (Experiment 1). Data were analyzed using a random intercept model whereby the dark bars represent the line of best fit and the symbols show the contribution of each batch to the mean. The lower case letters show statistical differences between treatments via Tukey tests ($p \leq 0.05$). 86
- Figure 2.2 Effects of chemical cues from dead phytoplankton (as an indication of predation risk) on bulk (molar) toxin concentration of GTX 1-4 of *Alexandrium minutum* (Experiment 1). Data were analyzed using a random intercept model whereby the dark bars represent the line of best fit and the symbols show the contribution of each batch to the mean. The lower case letters show statistical differences between treatments via Tukey post-hoc test ($p \leq 0.05$). 88
- Figure 2.3 Effects of phylogenetic relatedness on (a) cellular toxin production of GTX 1-4 and (b) growth of *Alexandrium minutum* relative to controls in response to chemical cues from dead phytoplankton, as an indication of predation risk (Experiment 1). Data from exposure to chemical cues from *A. minutum*, *A. tamarense*, and *A. pacificum* are nested under “congeneric” and *P. lima*, *P. micans*, and *C. monotis* are nested under “distantly related”. Data are shown as mean \pm standard deviation and were analyzed using a nested ANOVA. Lower case letters show statistical differences between treatments ($p \leq 0.05$). 89
- Figure 2.4 Effects of historical, geographic co-occurrence on (a) cellular toxin production of GTX 1-4 and (b) growth of *Alexandrium minutum* relative to controls, in response to chemical cues from dead phytoplankton, as an indication of predation risk (Experiment 1). Data from exposure to chemical cues from *A. minutum* and *A. tamarense* are nested under “co-occurring” and *A. pacificum* is under “non-co-occurring”. Data are shown as mean \pm standard deviation and were analyzed using a nested ANOVA. Lower case letters show statistical differences between treatments ($p \leq 0.05$). 90
- Figure 2.5 Effects of nutrients and chemical cues from dead *Alexandrium pacificum* (as an indication of predation risk) on (a) cellular toxin concentration of GTX 1-4 and (b) growth of *Alexandrium minutum* (Experiment 2). *A. minutum* was exposed to *A. pacificum* lysate at a 1:3 and 2.6:3 ratio of *A. pacificum* lysate biomass to *A. minutum* biomass, equivalent to 0.38:3 and 1:3 ratio of *A. pacificum* lysate to *A. minutum* by cell number. Additionally, either full strength K media (“media control”) or K media diluted to reflect the nitrate and ammonia concentration present in the 2.6:3 ratio of *A. pacificum* lysate biomass to *A. minutum* biomass (“dilute media control”) were 92

added to *A. minutum* as controls. Data are shown as mean \pm standard deviation and were analyzed using a Welch's ANOVA. Lower case letters show statistical differences between treatments via Games-Howell post-hoc test ($p \leq 0.05$).

- Figure 3.1 Exposure to copepodamides induced toxicity and reduced growth in *Alexandrium minutum*. Bars represent the mean \pm standard deviation of (a) cellular toxin concentration of gonyautoxins 1-4 and (b) percent growth of *A. minutum* when exposed to a solvent control (No copepodamides) or 1 nM copepodamides (Copepodamides). Data were analyzed using an unpaired Welch's t-test for the toxin analysis and an unpaired t-test for the growth analysis. Asterisks indicate level of statistical significance; **** $p < 0.001$. 106
- Figure 3.2 PCA models of UPLC/MS data revealed that both polar and non-polar metabolites moderately distinguished metabolomes of *Alexandrium minutum* based on copepodamide exposure. Orange squares represent metabolomes of *A. minutum* exposed to copepodamides and green circles represent metabolomes of *A. minutum* not exposed to copepodamides (controls). PCA scores plots from UPLC/MS analysis using positive (a and b) and negative (c and d) mode MS for both polar (a and c) and non-polar (b and d) metabolites. 107
- Figure 3.3 Jasmonic acid biosynthesis and signaling are involved in toxin production in *Alexandrium minutum* induced by copepodamide exposure. Bars represent the mean \pm standard deviation of cellular toxin concentration of gonyautoxins 1-4 in *A. minutum* in response to inhibition of (a) serine/threonine phosphatases by cantharidin and (b) jasmonic acid signaling by neomycin when exposed to a solvent control (No copepodamides, green) or 1 nM copepodamides (Copepodamides, orange). Data were analyzed using two-way ANOVAs with a Tukey HSD post hoc tests for multiple comparisons. Asterisks indicate the level of statistical significance; **** $p < 0.001$, *** $p < 0.001$, ns = not significantly different. 111
- Figure 3.4 Copepodamides appear not to be agonists of GPCRs nor do they disrupt cell membranes in *Alexandrium minutum*. (a) Points represent the mean \pm standard percent growth of *A. minutum* in response to inhibition of GPCRs by SCH-202676 at varying doses when exposed to a solvent control (No copepodamides, green circles) or 1 nM copepodamides (Copepodamides, orange squares). The data were analyzed using a sigmoidal fitted non-linear regression, excluding the highest dose. (b) Bars represent the mean \pm standard deviation percent *A. minutum* cells alive with permeable cell membranes when exposed to a solvent control (No copepodamides) or 1 nM copepodamides (Copepodamides). Data were analyzed 114

using an unpaired t-test. Asterisks indicate the level of statistical significance; **** $p < 0.001$.

- Figure 3.5 Cellular pathways and metabolites impacted in *Alexandrium minutum* by copepodamide exposure based on data from MS and NMR metabolomics, pathway inhibition experiments, and toxin analysis. Metabolites, enzymes, and pathways upregulated in response to copepodamides are indicated in blue. Red designates pathway and metabolites downregulated in response to copepodamides. Grey indicates equivocal regulation in response to copepodamides. 116
- Figure 4.1 The non-polar metabolomes of toxic *Alexandrium* species, *A. catenella* and *A. pacificum*, differ considerably from non-toxic *A. tamarense* based on PCA models from UPLC/MS data. Yellow diamonds represent metabolomes of *A. catenella*, orange squares represent metabolomes of *A. pacificum*, and green circles represent metabolomes of *A. tamarense*. Scores plots from PCA models based on UPLC/MS analysis of Experiment 1 (A and B) and 2 (C and D) metabolites using both positive (A and C, “MS+”) and negative mode (B and D, “MS-”). Lipid classes identified by MS-based models with significantly different concentrations in toxic *Alexandrium catenella* or *Alexandrium pacificum* compared to non-toxic *A. tamarense*. The number of compounds in each class and the average fold-change is included for each class. Average fold-change is the mean change in concentration for each lipid in *A. catenella* relative to *A. tamarense* (Experiment 1) and in *A. pacificum* relative to *A. tamarense* (Experiment 2). 140
- Figure 4.2 oPLS-DA models of NMR spectral data revealed that non-polar metabolomes of toxic *Alexandrium* (*A. catenella* and *A. pacificum*) species differ from non-toxic *A. tamarense*. Yellow diamonds represent metabolomes of *A. catenella*, orange squares represent metabolomes of *A. pacificum*, and green circles represent metabolomes of *A. tamarense*. oPLS-DA models based on ¹H NMR spectral analysis of Experiment 1 (A and B) and 2 (C and D) with scores plots (A and C) and their corresponding loadings plots on the first latent variable (B and D). Positive loading values signify metabolites in greater concentration in *A. catenella* (B) and *A. pacificum* (D) than *A. tamarense*, whereas negative loads show metabolites enhanced in *A. tamarense*. 141

- Figure A1 Relationship between cellular toxicity and growth in *Alexandrium minutum* in response to chemical cues from dead phytoplankton (Experiment 1). Data were analyzed by linear regression analysis using the mean growth and toxicity for the media control and each dead phytoplankton treatment. 156
- Figure B1 oPLS-DA models of NMR data revealed that both polar and non-polar metabolomes of *Alexandrium minutum* change in response to copepodamide exposure. Orange squares represent metabolomes of *A. minutum* exposed to copepodamides and green circles represent metabolomes of *A. minutum* not exposed to copepodamides (controls). oPLS-DA scores plots from ¹H NMR analysis (*a* and *c*) and their corresponding loadings plots on the first latent variable (*b* and *d*) for both polar (*a* and *b*) and non-polar (*c* and *d*) metabolomes, which are composed of 1,176 and 1,305 features, respectively. 177
- Figure B2 Inhibition of jasmonic acid biosynthesis reduced growth and exposure to copepodamides had variable impacts on growth in *Alexandrium minutum*. Bars represent the mean \pm standard deviation of percent growth of *A. minutum* in response to inhibition of (*a*) serine/threonine phosphatases by cantharidin and (*b*) jasmonic acid signaling by neomycin when exposed to a solvent control (No copepodamides, green) or 1 nM copepodamides (Copepodamides, orange). Data were analyzed using two-way ANOVAs with a Tukey HSD post hoc tests for multiple comparisons. Asterisks indicate the level of statistical significance; **** $p < 0.001$, *** $p < 0.001$. 180
- Figure B3 Inhibition of GPCRs did not block induction of toxin production or cause reduction in growth in *Alexandrium minutum*. Bars represent the mean \pm standard deviation of (*a*) cellular toxin concentration of gonyautoxins 1-4 and (*b*) percent growth of *A. minutum* in response to inhibition of GPCRs by SCH-202676 when exposed to a solvent control (No copepodamides, green) or 1 nM copepodamides (Copepodamides, orange). Data were analyzed using two-way ANOVAs with a Tukey HSD post hoc tests for multiple comparisons. Asterisks indicate the level of statistical significance; **** $p < 0.001$, *** $p < 0.001$, ** $p < 0.01$. 181
- Figure B4 Exposure to copepodamides when GPCRs were inhibited caused a reduction in growth in *Alexandrium minutum*. Points represent the mean \pm standard percent growth of *A. minutum* in response to inhibition of GPCRs by SCH-202676 at varying doses when exposed to a solvent control (No copepodamides, green) or 1 nM copepodamides (Copepodamides, orange). The uninhibited solvent controls were assigned a dose of 0.001 μ M for the purposes of log- 182

transformation. The data were analyzed using a non-linear regression, excluding the highest dose. Asterisks indicate the level of statistical significance; *** $p < 0.001$.

Figure C1 Representative ^1H NMR spectra from NMR metabolomics experiments 1-2. A single representative ^1H NMR spectrum of the non-polar metabolome from each *Alexandrium* species: *A. catenella* (yellow) and *A. tamarense* (light green) (Experiment 1) and *A. catenella* (yellow) and *A. tamarense* (dark green) (Experiment 2) from (A) 3.5-5.6 ppm and (B) 5.7-8.7 ppm. 183

LIST OF SYMBOLS AND ABBREVIATIONS

ppt	parts per thousand
nM	nanomolar (nanomoles per liter)
μ M	micromolar (micromoles per liter)
fmol	femtomole
μ m	micrometer
μ mol m ⁻² s ⁻¹	micromoles per meter square per second
pgC cell ⁻¹	picograms of carbon per cell
sp.	species
spp.	several species
GPCR	G protein-coupled receptors
GTX	gonyautoxin
PST	paralytic shellfish toxins
¹ H	proton
NMR	nuclear magnetic resonance
MS	mass spectrometry
UPLC	ultrahigh performance liquid chromatography
LC/MS	liquid chromatography-mass spectrometry
MS/MS	tandem mass spectrometry
dd-MS ²	tandem mass spectrometry collected in a data-dependent manner
HCD	higher-energy collisional dissociation
PCA	principal component analysis
oPLS-DA	orthogonal partial least squares discriminant analysis

SUMMARY

Understanding predator-prey interactions is a fundamental part of the study of ecology. In order to survive, prey are advantaged by recognizing predators and assessing predation risk, and predators must successfully select and capture prey. As many planktonic organisms lack advanced eyes or ears these interactions are predominately chemically mediated (Chapter 1). To date, our knowledge of the chemical cues and cellular mechanisms underpinning interactions between zooplankton and phytoplankton is still underdeveloped. The current body of work seeks to expand this discipline by investigating chemical mechanisms involved in predator-prey interactions using species from the chemically defended phytoplankton genus *Alexandrium* and cues from one type of predatory zooplankton, copepods.

Many potential prey judge the likelihood that predators are nearby based on cues from injured or dead competitors (i.e., other prey). For some organisms that respond to dead competitor cues, injury of a closely related competitor is perceived as a reliable indicator of high predation risk. However, in other cases organisms respond more strongly to cues from injured co-occurring competitors, which may be more distantly related, as they might indicate that hungry predators are nearby. There has been relatively little study of this form of predation risk assessment in single-celled organisms, particularly chemically defended phytoplankton. Several species of marine phytoplankton belonging to the genus *Alexandrium* produce toxins which appear to function as chemical defenses against copepod grazing. In fact, *Alexandrium minutum* increases production of toxins in response to compounds exuded by copepods (i.e., predator cues). However, whether

A. minutum uses other cues, such as damaged phytoplankton, to assess predation risk is unknown. Therefore, to explore the role of dead phytoplankton cues in chemical defense plasticity, we exposed *A. minutum* to chemical cues from six different lysed phytoplankton species (Chapter 2). Chemical cues from dead conspecifics and congeners drastically suppressed *A. minutum* toxicity and modestly enhanced growth regardless of whether they co-occur geographically. In contrast, exposure to cues from distantly related, but historically co-occurring phytoplankton species induced toxin production and decreased growth in *A. minutum* by roughly the same magnitude. This study revealed that *A. minutum* perceives cues from dead competitors and that phylogenetic relatedness of the competitor is important in determining the defense response. Ultimately, the degree of relatedness matters in how *A. minutum* trades-off utilization of resources, such as nutrients from cell lysates, for either growth or chemical defense. Furthermore, it implies that phytoplankton may respond to similar types of cues as multicellular organisms but that their response may be more strongly governed by the trade-off between nutrient acquisition and reduced predation risk.

To better understand the chemosensory mechanisms of predator-prey interactions in phytoplankton, we investigated how *A. minutum* perceives copepodamides, a suite of copepod metabolites known to induce resistance against predators in diverse phytoplankton taxa, and the metabolic pathways involved in initiating *A. minutum*'s chemical defense (Chapter 3). In *A. minutum*, recognition of copepodamides caused subtle, targeted changes in the metabolome including dysregulation of valine biosynthesis and enhancement of butanoate metabolism and arginine biosynthesis, as determined by ¹H nuclear magnetic resonance (NMR) and mass spectrometry (MS) based metabolomics. Additionally,

inhibition experiments led to the discovery that copepodamides trigger signal transduction via disruption of serine/threonine phosphatases, which leads to increased jasmonic acid biosynthesis and signaling, and ultimately results in amplified toxin biosynthesis in *A. minutum*. While we did not decipher the exact mechanism by which *A. minutum* recognizes copepodamides we found that they might interact, in a manner that is still ambiguous, with GPCRs and G protein signaling. This study was an important step in enhancing our knowledge of the chemosensory ecology of phytoplankton.

In addition to understanding how phytoplankton recognize and respond to predators, it is also valuable to understand how predators, such as copepods, select prey. Some copepods seem capable of distinguishing live toxic and non-toxic cells, discriminating against more toxic individual prey, even though these toxins are produced and stored within phytoplankton cells and only leak into the water column upon cell death. We proposed that copepods may detect chemical cues on phytoplankton cell surfaces that are associated with toxicity rather than sensing the intracellular toxins. Using MS and NMR-based metabolomics, we discovered that the non-polar metabolomes of two toxic species (*Alexandrium catenella* and *Alexandrium pacificum*) vary considerably from their non-toxic congener *Alexandrium tamarense* even though all three are very closely related. Metabolites belonging to seven different lipid classes (free fatty acids, mono-, di-, and triacylglycerols, sphingolipids, glycerophospholipids, and sterols) were implicated in distinguishing the non-polar metabolomes of the *Alexandrium* species based on toxicity. We determined that the phosphatidylcholines and sterol classes are most likely to function as toxin-related cues for copepods based on enhanced concentrations of these lipids in both toxic species. Ultimately, we partially identified three metabolites which exhibited the

greatest enrichment in both toxic species relative to the non-toxic *A. tamarense* and which may serve as targets in future experiments aimed at fully deciphering the chemoreception mechanism copepods use to perceive *Alexandrium* toxicity.

Overall, my dissertation research provides insight into mechanisms behind ecological interactions involving marine phytoplankton including assessment of predation risk, physiological mechanisms behind predator cue recognition and response, and cellular traits that may enable predators to distinguish toxic and non-toxic cells, leading to increased fitness for chemically defended prey. This thesis further demonstrates the complexity of planktonic interactions at both organismal and molecular levels.

CHAPTER 1. INTRODUCTION: CHEMICAL ECOLOGY OF MARINE PLANKTON

This section is adapted from Brown, E.R., Cepeda, M.R., Mascuch, S.J., Poulson-Ellestad, K.L., Kubanek, J., 2019. Chemical ecology of the marine plankton. *Natural Product Reports* **36**(8): 1093-1116; <https://doi.org/10.1039/C8NP00085A> with permission from the Royal Society of Chemistry.

1.1 Abstract

This review focuses on recent studies on the chemical ecology of planktonic marine ecosystems, with the objective of presenting a comprehensive overview of new findings in the field in the time period covered. In order to highlight the role of chemically mediated interactions in the marine plankton this review has been organized by ecological concepts starting with intraspecific communication, followed by interspecific interactions (including facilitation and mutualism, host-parasite, allelopathy, and predator-prey), and finally the effects of plankton secondary metabolites on community and ecosystem-wide interactions.

1.2 Introduction

In the previous three years, research in planktonic marine chemical ecology has focused especially on quorum sensing and how it impacts algal-bacterial interactions as well as chemical defense in predator-prey interactions. This review summarizes the new studies in the whole field of chemical ecology of the marine plankton from January 2015 through December 2017. Previous reviews in this series summarized the advances in the

field between 2006 and 2008 (Poulson et al. 2009), January 2009 to September 2010 (Sieg et al. 2011), October 2010 to December 2012 (Roy et al. 2013), and January 2013 to December 2014 (Schwartz et al. 2016).

Several recent reviews centered on quorum sensing in algal associated bacteria and intraspecific communication among microalgae (Rolland et al. 2016, Zhou et al. 2016, Venuleo et al. 2017). Zhou and colleagues published a comprehensive review of quorum sensing in marine bacteria with a particular focus on how quorum sensing impacts symbiotic interactions between bacteria and algae (2016). They explored how quorum sensing is involved in modulating behaviors in bacteria that are mutualistic as well as antagonistic to the rest of the microbial community and their algal host. Additionally, they investigated co-evolution between bacteria and algae and the potential role of quorum sensing-induced behaviors to help predict and control harmful algal blooms (Zhou et al. 2016). Rolland and colleagues focused exclusively on how quorum sensing and quorum quenching (disruption of quorum sensing) are involved in bacterial dynamics in the phycosphere, defined as the microenvironment immediately surrounding phytoplankton cells, dominated by algal exudates (2016). These authors reviewed the types of molecules involved and the ecological role of quorum sensing and quenching among bacteria that live in the phycosphere, commenting on how quorum sensing and quenching are likely important in regulating the relationship between bacteria and algal hosts (Rolland et al. 2016). In another review, Venuleo and colleagues surveyed how, like bacteria, microalgae extensively participate in intraspecific communication (2017). They explored what constitutes “intraspecific” in these highly variable organisms that can reproduce either sexually and asexually, and the evolution of intraspecific

communication. Additionally, they reviewed what is known about the ecological roles of intraspecific communication in many microalgal species.

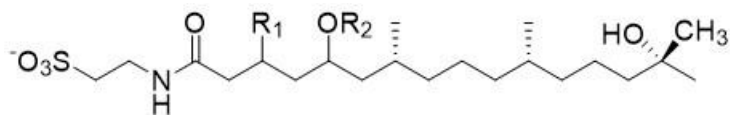
Other reviews examined the ecology and chemical diversity of harmful algal blooms (Gleason et al. 2015, Rasmussen et al. 2016a). Gleason and colleagues discussed interactions between fungi of the phylum Chytridiomycota, or chytrids, and toxic phytoplankton (2015). Additionally, they commented on the paucity of studies regarding the effects of parasitism on toxin production in these phytoplankton (Gleason et al. 2015). Rasmussen and colleagues highlighted the chemical diversity of toxins produced by phytoplankton, particularly dinoflagellates, by reviewing 59 algal toxins (2016a). They organized their review by structural class and discussed the algae responsible for toxin production and the mode of action of the toxins, when known (Rasmussen et al. 2016a). These authors concluded their review with the current state of knowledge for several species of algae previously implicated in large-scale fish kills (Rasmussen et al. 2016a).

1.3 Intraspecific Signaling

1.3.1 Reproductive signaling

The existence and involvement of pheromones in copepod reproduction has been established through behavioral assays, but the nature and identities of these cues have remained elusive (Heuschele and Selander 2014). Mathematical modeling of copepod mating behavior predicts that males, which correct their courses with high fidelity after initially tracing a female track in the wrong direction, may establish the directionality of a female pheromone trail through detection of a multicomponent signal (Hinow et al. 2017). In a scenario in which a signal comprised of two components, each differing in its

environmental persistence, was compared to a single component signal, a hypothetical male able to sense a ratio between two signal components was more likely to successfully reorient toward the female than a male only able to sense gradients in the absolute concentration of a single chemical (Hinow et al. 2017). It is possible that the more persistent signal may serve as a “track” while the less persistent signal specifies direction (which way is upstream). It will be necessary to determine whether the findings, in light of assumptions based on a laminar flow environment, are relevant to the natural environment in which female pheromones may take the form of ‘clouds’ rather than delineated trails (Seuront and Stanley 2014). Further examination of the sensory capabilities of male copepods may also provide context to the findings.



Copepodamides

A (1) R₁= -CH₃ R₂= Docosahexaenoyl

B (2) R₁= -CH₃ R₂= Eicosapentaenoyl

C (3) R₁= -CH₃ R₂= Stearidonoyl

D (4) R₁= =CH₂ R₂= Docosahexaenoyl

E (5) R₁= =CH₂ R₂= Eicosapentaenoyl

F (6) R₁= =CH₂ R₂= Stearidonoyl

G (7) R₁= -CH₃ R₂=H

H (8) R₁= =CH₂ R₂=H

Figure 1.1. A class of compounds exuded by copepods: Copepodamides A-H (1-8).

Attempts to structurally describe exuded metabolites and pheromones from copepods have been reported for *Temora longicornis* and *Oithona davisae* (Heuschele et

al. 2016, Selander et al. 2016). Comparisons of male and female exudates were facilitated by continually recirculating live copepod-containing water through extraction media to adsorb diffusible cues (Heuschele et al. 2016, Selander et al. 2016). Untargeted metabolomics analyses of *T. longicornis* extracts revealed sex-specific differences in exudate composition and component abundance, and provided proof-of-principle that copepod-specific metabolites, such as copepodamide G (**7**) (which is one of eight compounds that make up a class of copepod-specific compounds), may be captured and measured with this technique (Selander et al. 2016). Female *T. longicornis* extracts did not retain the ability of unextracted water exudates to elicit mate-seeking swimming behavior in males, confounding pheromone identification (Selander et al. 2016). Similarly, analyses of exuded metabolites from *O. davisae* revealed sex-specific differences, but those extracts, too, did not recapitulate the ability of unmanipulated water exudates to induce mate-seeking swimming behavior in males (Heuschele et al. 2016). The methods used in these studies have the tantalizing potential to expand the understanding of copepod diffusible chemistry and chemical signaling and its influence on plankton ecology, but are hindered by the apparent lability of many copepod pheromones.

In the rotifer *Brachionus manjavacas*, analysis of excreted proteins has yielded new information about the identity of the quorum sensing pheromone ‘misis-inducing protein’, responsible for inducing a shift from asexual to sexual reproduction (misis) in this microscopic animal (Snell 2017). Two excreted proteins of molecular weights 39 and 45 kDa made up the majority of a mixture which induced misis; however, the most promising candidate for the misis-inducing protein was a 22 kDa protein which, when

precipitated out of solution, significantly reduced mixis in female progeny. Initial protein sequencing efforts indicated that the precipitated protein was similar to five known proteins (Snell 2017). Additional experiments are needed to determine whether the 22 kDa protein is sufficient for mixis induction and whether other proteins are involved.

Rather than attempt to isolate chemical signals, Basu and colleagues instead characterized transcriptional changes that occur when the diatom *Pseudo-nitzschia multistriata* is exposed to unmanipulated, reproductive chemical cues produced in an experimental setting (2017). The *P. multistriata* life cycle is divided into two phases: vegetative reproduction in which cells divide and become progressively smaller due to the restriction imposed by their rigid silica thecae, and sexual reproduction which occurs when a minimum size threshold is reached (D'Alelio et al. 2009). In the sexual reproduction phase, chemical signals trigger cells of opposite mating types to generate genetically diverse zygotes from which cells of maximal size are ultimately formed (Scalco et al. 2014). The authors found that different *P. multistriata* mating types maintained in contact-free co-culture responded to chemical cues by altering their growth (possibly as a means of synchronization) and initiating transcriptional changes which indicated cells were likely preparing for meiosis and integrating environmental sensing and cell signaling (Basu et al. 2017). Differences were observed in the numbers, identities, and magnitudes of regulated genes in each mating type, a possible indication that each produces a different pheromone signal. The work is an elegant approach to investigating the downstream effects of waterborne cues that avoids laborious pheromone isolation and possible complications should the signal be multicomponent, present in a specific ratio, or modified in some way following production. Manipulation

of the pathways identified in the study followed by phenotypic evaluation may further clarify the mechanism of pheromone reception by and action on *P. multistriata*.

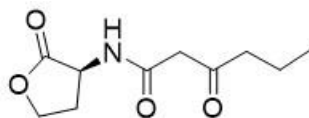
1.3.2 *Quorum sensing*

In addition to intraspecific signaling as it relates to reproduction, new insights have been gained into the cooperative interaction of quorum sensing, its distribution in phytoplankton, new quorum sensing-regulated activities, and implications for phytoplankton ecology.

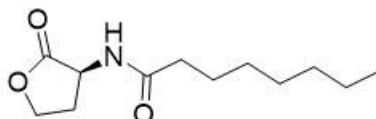
While a subset of marine organisms have been shown to produce self-signaling autoinducer molecules or have been inferred to produce these molecules based on sequence information (e.g., bacteria, rotifers), little was known about the distribution of quorum sensing pathways in the oceans. Classically, bacterial quorum sensing was not thought to play a prominent role in the ocean because the density of bacteria in seawater is usually below the quorum sensing threshold. However, quorum sensing may become relevant in situations where bacteria aggregate on particles or are present during high-density phytoplankton blooms. Examination by Doberva and colleagues of publicly available metagenomic sequence information from the Global Ocean Sampling (GOS) database for the incidence of autoinducer (AI) synthases revealed previously unknown AI sequences (2015). This indicates that quorum sensing is diverse and widespread in the marine environment, often involving uncultivated bacteria (Doberva et al. 2015). Phylogenetic differences in the distributions of LuxI (AI-1), HdtS (AI-1), LuxS (AI-2), and AinS (AI-1) AI synthases were observed, but evolutionary conclusions are difficult to draw since pathways are known to be transferred horizontally (Doberva et al. 2015).

Because pathway identification was limited to matches from pre-constructed databases, it is likely that quorum sensing diversity and distribution were underestimated and richer than results reflect.

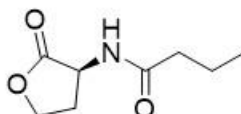
While the work discussed above did not investigate expression of quorum sensing pathways in free-living versus particle-associated bacteria, a separate study of bacterial communication on marine snow directly revealed known autoinducers *N*-(3-oxo-hexanoyl)-L-homoserine lactone (**9**) and *N*-octanoyl-L-homoserine lactone (**10**), indicating that bacterial concentrations on particles can indeed be high enough to facilitate quorum sensing (Jatt et al. 2015). Of the cultured marine snow isolates, 10 of 53 produced acyl homoserine lactones. The gram-negative alphaproteobacterium *Paracoccus carotinifaciens* produced **9**, the first report of this molecule for this species (Jatt et al. 2015). The gammaproteobacterium *Pantoea ananatis* was found to produce the L-homoserine lactones *N*-butanoyl (**11**), *N*-hexanoyl (**12**), *N*-decanoyl (**13**), *N*-dodecanoyl (**14**), and *N*-tetradecanoyl-L-homoserine lactone (**15**). Additionally, *P. ananatis* produced five extracellular hydrolytic enzymes, including alkaline phosphatase which was inhibited by the addition of a quorum sensing inhibitor (Jatt et al. 2015). While the relative importance of alkaline phosphatase to particle remineralization remains to be seen, the findings provide initial support for the idea that quorum sensing is an important contributor to biogeochemical cycling dynamics and supply of organic matter to other residents of the plankton.



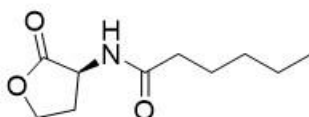
N-(3-oxo-hexanoyl)-L-homoserine lactone (9)



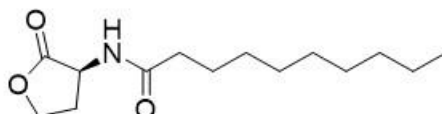
N-octanoyl-L-homoserine lactone (10)



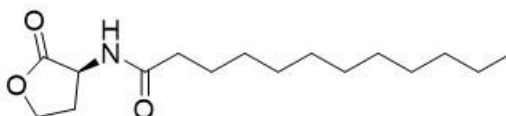
N-butanoyl-L-homoserine lactones (11)



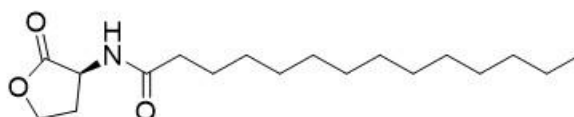
N-hexanoyl-L-homoserine lactones (12)



N-decanoyl-L-homoserine lactones (13)



N-dodecanoyl-L-homoserine lactones (14)



N-tetradecanoyl-L-homoserine lactone (15)

Figure 1.2 Bacterial auto-inducers: *N*-(3-oxo-hexanoyl)-L-homoserine lactone (9), *N*-octanoyl-L-homoserine lactone (10), *N*-butanoyl-L-homoserine lactones (11), *N*-hexanoyl-L-homoserine lactones (12), *N*-decanoyl-L-homoserine lactones (13), *N*-dodecanoyl-L-homoserine lactones (14), and *N*-tetradecanoyl-L-homoserine lactone (15).

New observations of quorum sensing involvement in organismal defense have also been reported. The pathogenic bacterium *Vibrio cholerae* living in biofilms established on chitinous substrates experienced reduced predation by the flagellate *Rhynchomonas nasuta* than did *V. cholerae* biofilms established on abiotic or non-chitinous substrates (Sun et al. 2015). The biofilms formed on chitin exuded ammonium, a toxic byproduct of chitin metabolism, which conferred protection from predation (Sun et al. 2015). A quorum sensing mutant with reduced deterrence to *R. nasuta* was found to be impaired in *N*-acetylglucosamine catabolism, chemotaxis, and chitin-regulated pilus synthesis, but interestingly was not impaired in its ability to form a biofilm (Sun et al. 2015). Biofilm formation on zooplankton by *V. cholerae* is an important protective mechanism that contributes both to its environmental persistence and periodic outbreaks. Metabolism of chitin appears to augment the protective capacity of *V. cholerae* biofilms through the production of antiprotozoal ammonium, a phenomenon the authors refer to as “metabolite-based grazing resistance” and which they propose may be a common defense property of biofilm (Sun et al. 2015). Effects of ammonium on potential hosts were not explored.

In addition to quorum sensing-regulated grazing defense in *V. cholerae*, a recent report details the quorum sensing-dependent mechanism by which another pathogenic marine *Vibrio*, *V. anguillarum*, defends against viral infection (Tan et al. 2015b). Bacterial mutation of membrane-based phage receptors to prevent viral entry into the cell is a common antiviral defense mechanism recognized as an important driver of bacterial evolution. However, mutation of receptors or transporters important for satisfying the cell’s metabolic demands could bring fitness costs (Tan et al. 2015b). Non-mutational

means of antiphage defense that circumvent or mitigate this liability include aggregate formation, exopolysaccharide production and temporary downregulation of phage receptors (Høyland-Kroghsbo et al. 2013, Tan et al. 2014, Tan et al. 2015a). *V. anguillarum*, which produces the quorum sensing molecules *N*-(3-hydroxyhexanoyl)-L-homoserine lactone (**16**) and *N*-(3-oxo-decanoyl)-L-homoserine lactone (**17**) and **12** at high densities, protected itself against KVP40 phage infection by alternately forming aggregates and producing exopolysaccharide at low cell densities, as well as temporarily downregulating the phage receptor universal outer membrane protein K at high cell densities (Tan et al. 2015b). This strategy may allow the bacterium to dynamically respond to differences in phage pressure while minimizing fitness costs (assuming that the magnitude of phage threat correlates with host bacterial density). A quorum sensing mutant locked into a low density phenotype expressed high levels of phage receptor and remained vulnerable to phage infection regardless of culture density (Tan et al. 2015b). These findings suggest that in certain instances in which phage therapy is being considered, it may be beneficial to combine it with methods to inhibit quorum sensing. This may constrain bacteria to a phenotype that is vulnerable to viral attack and therefore increase the effectiveness of phage therapy.

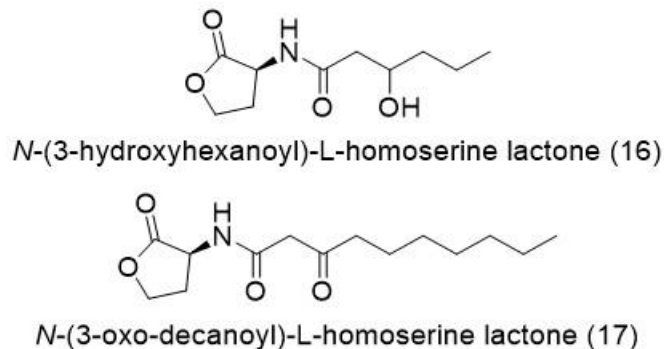


Figure 1.3 Quorum sensing molecules *N*-(3-hydroxyhexanoyl)-L-homoserine lactone (16) and *N*-(3-oxo-decanoyl)-L-homoserine lactone (17) involved in antiphage defense in *Vibrio anguillarum*.

Because quorum sensing has consequences on marine communities and ecosystems, additional studies on this topic are presented in the bacterial dynamics subsection of the community and ecosystem effects section.

1.3.3 Other intraspecific signaling

Indole-3-acetic acid (18) is a well-known auxin, or plant hormone, that influences plant growth and differentiation and is now appreciated to be important in intraspecific signaling between cell types of the coccolithophore *Emiliana huxleyi* (Labeeuw et al. 2016). Coccolith-bearing *E. huxleyi* produce indole-3-acetic acid. This metabolite is then sensed by non-coccolith-bearing, bald cells which respond by undergoing a physiological shift that is characterized by increased quantum yield (an indicator of photosystem II health), a decrease in growth and chlorophyll fluorescence, and an increase in cell size and membrane permeability (Labeeuw et al. 2016). This work is the first to report auxin production by a bacteria-free haptophyte, an observation of note as auxin production by algae has been a controversial topic with some attributing the presence of these molecules

to production by associated bacteria. Detection in *E. huxleyi* of homologs of tryptophan-dependent indole-3-acetic acid genes from the mustard plant *Arabidopsis thaliana* supported the conclusion that the coccolithophore biosynthesizes the metabolite (Labeeuw et al. 2016). The significance of the observed signaling coordination between coccolith-bearing and bald *E. huxleyi* cell types is not clear. Labeeuw and colleagues note that while the two cell types co-occur in blooms, generally coccolith-bearing cells are present at higher densities during a bloom while bald cells increase in number towards the end of a bloom (2016). Further investigation is necessary to establish the benefit of signaling coordination for *E. huxleyi* and its implications for phytoplankton bloom dynamics and biogeochemical cycling.

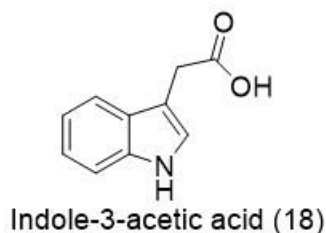


Figure 1.4 Intraspecific signaling molecule indole-3-acetic acid (18) produced by *Emiliana huxleyi*.

1.4 Facilitation and mutualism

Several recent studies have focused on chemical cross-talk between species. These interactions include both facilitative and perhaps mutualistic interactions; however true mutualisms between planktonic organisms have rarely been unequivocally demonstrated. Most studies reviewed here focused on the influence of bacteria on the growth or physiology of eukaryotic phytoplankton. Only two studies unambiguously

identified the presence of signaling molecules, while several studies infer the presence of a signaling molecule. For the purposes of this review, only papers that demonstrated signaling or cuing functions of nutritional molecules (e.g., amino acids, vitamins) are considered. Thus, studies that established growth effects due to the exchange of dissolved organic nutrients (including vitamins) among organisms are not reviewed here.

Two recent studies have demonstrated a new ecological role for algal-derived tryptophan (**19**) as a biosynthetic substrate that can be used by bacteria to produce the plant hormone indole-3-acetic acid (**18**), which in turn acts as a growth promoter of eukaryotic phytoplankton (Amin et al. 2015, Segev et al. 2016). In these cases, specific plankton-bacterial relationships were described (Amin et al. 2015, Segev et al. 2016). For instance, Amin and colleagues showed that **18** produced by the Roseobacter *Sulfitobacter* sp. stimulated the growth of some strains of the diatom *Pseudonitzschia multiseriis* (2015). When *Sulfitobacter* sp. grew alone, or with *P. multiseriis*, **18** was detected at micromolar concentration ranges demonstrating that bacteria produce and release **18** into the environment. These authors confirmed the ecological relevance of their laboratory findings by demonstrating that **18** was present in field samples at similar concentrations and using metatranscripts for *Sulfitobacter* sp. to identify active **18** biosynthesis pathways in these samples (Amin et al. 2015). The authors suggested that *P. multiseriis* provides necessary organic carbon to promote bacterial growth as bacterial numbers increased when grown with the *P. multiseriis* strain whose growth had been enhanced, while the diatom preferentially utilizes ammonium derived from bacterial metabolism (Amin et al. 2015). Additionally, transcriptomic data indicated that *P. multiseriis* increased the production of **19** when grown with *Sulfitobacter* sp. Coupling the above

data with the observations that extracellular **19** concentrations significantly decreased in the presence of the bacterium suggests that bacteria rapidly take up diatom-produced **19** (Amin et al. 2015). The authors speculated that diatom-derived tryptophan served as the biosynthetic precursor for bacterially produced **18**, potentially through several **18** pathways including indole 3-acetonitrile, indole 3-acetamide, and tryptamine pathways, although no isotope tracer studies were confirmed to test this hypothesis (Amin et al. 2015).

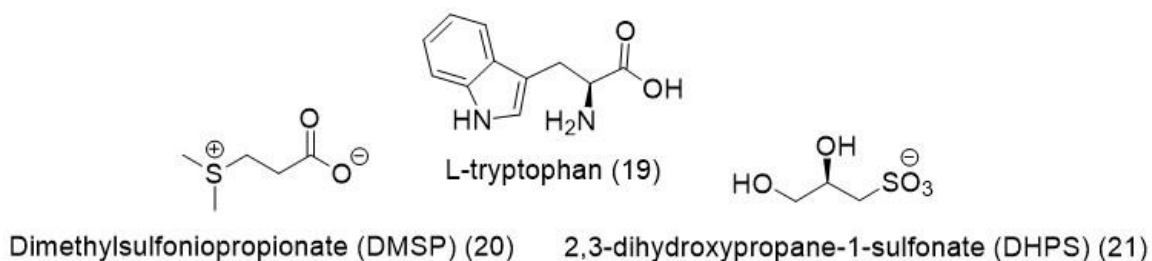


Figure 1.5 Molecules potentially involved in cross-talk between phytoplankton and bacteria: L-tryptophan (19), dimethylsulfoniopropionate (DMSP) (20), and 2,3-dihydroxypropane-1-sulfonate (DHPS) (21).

The coccolithophorid *Emiliana huxleyi* releases **19** that is used by the alphaproteobacterium *Phaeobacter inhibens* to produce **18**, which in turn stimulates the growth of *E. huxleyi* (Segev et al. 2016). *P. inhibens* only grew effectively when with *E. huxleyi*, which provided several nutrients, dimethylsulfoniopropionate (DMSP) (**20**), and fixed carbon, that supported bacterial growth (Segev et al. 2016). The authors speculated that free-living *P. inhibens* may also use dissolved **20** as a cue to locate *E. huxleyi* cells (Segev et al. 2016). *E. huxleyi* grew more rapidly in the presence of the bacterium and additions of **18** to bacteria-free *E. huxleyi* increased its maximum cell density (Segev et

al. 2016). When *P. inhibens* was fed isotopically labeled **19**, fully labeled **18** was produced, confirming that **19** is used by *P. inhibens* to make **18** and *E. huxleyi* was shown to produce extracellular **19**. Therefore, this work demonstrates that “crosstalk” between these organisms is possible within the phycosphere (Segev et al. 2016). Similar to the results of the study by Amin and colleagues (2015), **18** was undetectable in coccolithophore-bacterium co-cultures, indicating a rapid turnover of this molecule among organisms (Segev et al. 2016). Considering the taxonomic diversity of the organisms used, these studies provide evidence for the potential of widespread, chemically mediated facultative relationships among eukaryotic phytoplankton and bacterial counterparts (Amin et al. 2015, Segev et al. 2016).

Other studies have demonstrated the potential for chemical signaling or cuing among eukaryotic phytoplankton and bacteria (Durham et al. 2015, Durham et al. 2017, Landa et al. 2017). Authors of these studies inferred chemical cross-talk between organisms by tracking an organism’s transcriptomic or metabolomic changes in response to the presence of another species. Durham and colleagues investigated the relationship between the Roseobacter *Rugeria pomeroyi* and the diatom *Thalassiosira pseudonana* (2015). Because bacterial transcriptomes showed increased expression of 2,3-dihydroxypropane-1-sulfonate (**21**) transporters and catabolism genes when in the presence of the diatom, the authors suggested the bacterium provided vitamin B12 to the diatom, and in return the diatom provided **21** to the bacterium. In addition, sulfur metabolism genes of *T. pseudonana* were down-regulated when exposed to the bacterium (Durham et al. 2015). While this may signal a tight relationship between *R. pomeroyi* and *T. pseudonana*, the authors state that there is little evidence that the relationship is

mediated by non-nutritional molecules, since production of **21** by diatoms did not appear to be stimulated by the bacterium (Durham et al. 2015). However, the presence of signaling molecules was not explicitly tested in this study. A more recent study used mutant *R. pomeroyi* to test the role of **21** as a bacterial growth substrate (Landa et al. 2017). Bacteria incapable of expressing key **21** transporters were unable to grow when provided with **21** as sole carbon source, and limited growth was observed when this bacterium was grown with *T. pseudonana* (Landa et al. 2017). These results support the hypotheses that *T. pseudonana*-produced **21** serves as a carbon source, not as a signaling molecule, for *R. pomeroyi*.

Yet, *T. pseudonana* appears to be capable of recognizing *R. pomeroyi* (Durham et al. 2017). In the presence of *R. pomeroyi*, *T. pseudonana* regulated expression of genes related to cell signaling and recognition functions, including pathways similar to bacterial recognition pathways found in plants (Durham et al. 2017). The authors proposed that these signaling and secondary messenger genes indicate active recognition of the bacterium by the diatom (Durham et al. 2017). Presumably, this recognition occurs via dissolved organic compounds, since few *R. pomeroyi* cells were attached to *T. pseudonana* cells and *R. pomeroyi* had upregulated genes for protein excretion/organic molecule excretion (Durham et al. 2017). Which signal(s) *T. pseudonana* responds to is as of yet unknown. Future work in this study system to characterize the dissolved organic compounds of the culture medium, as well as more classical conditioned media-based experiments will help to confirm the presence of chemical signaling used by *T. pseudonana* to detect bacteria.

EroS was recently identified as an enzyme exuded by the marine gammaproteobacterium *Vibrio fischeri* which stimulates sexual reproduction and a newly described swarming behavior in the choanoflagellate *Salpingoeca rosetta* (Woznica et al. 2017). The amino acid sequence of EroS contains a glycosaminoglycan lysase domain, revealing that it acts specifically on chondroitin (a specific glycosaminoglycan). Amino acid substitutions at the catalytic site eliminated the ability of EroS to elicit swarming and mating behaviors in *S. rosetta*, indicating that enzymatic activity of EroS is critical in its function to stimulate mating/swarming (Woznica et al. 2017). This study demonstrated several previously underappreciated aspects of *S. rosetta* biology: the presence of sulfated glycosaminoglycans in *S. rosetta* membranes, aggregation behavior to increase the rate of sexual reproduction, and the ability of bacteria to influence behaviors and reproduction in *S. rosetta* (Woznica et al. 2017). Aggregating makes evolutionary sense in the pelagic environment, since cells are likely to be greatly dispersed and finding mates should be challenging. The authors suggest that the ability of *S. rosetta* to respond to the presence of certain bacteria may signify appropriate environments for successful sexual production (Woznica et al. 2017).

A few recent studies investigated the impacts of eukaryotic phytoplankton on bacterial metabolism or physiology (Wang et al. 2015, Landa et al. 2017). The alphaproteobacterium *Dinoroseobacter shibae* was found to influence the growth of the dinoflagellate *Prorocentrum minimum*, by shifting from a mutualist, which increases growth, to a pathogen, which promotes rapid decline, during different growth phases of *P. minimum* (Wang et al. 2015). Transcriptomics revealed quorum sensing, *CtrA* phosphorelay, and flagella biosynthesis genes were consistently and significantly

upregulated after this switch from mutualism to pathogenicity (Wang et al. 2015). Various knockout mutants were more inhibitory towards *P. minimum* than wild type bacteria, indicating that these genes modulate the deleterious effects of *D. shibae* on the dinoflagellate. However, two mutants, both lacking a plasmid encoding for type IV secretion systems, had no effect on the growth of *P. minimum*, demonstrating that *D. shibae* contains several genes for pathogenicity (Wang et al. 2015). To date, no work has yet been done in this study to isolate or investigate any chemical signals that may turn on the expression of pathogenic genes in *D. shibae*.

The dinoflagellate *Alexandrium tamarense* influences the metabolism of *R. pomeryoi* by causing the bacterium to increase expression of quorum sensing genes (Landa et al. 2017). This appears to be a species-specific effect, as the presence of the diatom *T. pseudonana* did not cause differential expression of these quorum sensing genes (Landa et al. 2017). *R. pomeryoi* also enhanced expression of genes involved in degradation of **20** in the presence of *A. tamarense* (Landa et al. 2017). Landa and colleagues speculated that the presence of **20** (likely produced by *A. tamarense* in the presence of *R. pomeryoi*) served not only as a carbon and sulfur source for the bacterium, but also as a signal to alter *R. pomeryoi* metabolism. In support of this hypothesis *R. pomeryoi* enhanced expression of quorum sensing genes, phosphorelay and flagellum assembly genes as well as gene transfer agent cassette when grown with *A. tamarense* (Landa et al. 2017).

Proteomics revealed that compounds exuded by the diatom *Thalassiosira weissflogii* cause changes in the metabolism of the gammaproteobacterium *Marinobacter adhaerens* (Stahl and Ullrich 2016). Ten bacterial proteins involved in nitrogen

metabolism and amino acid transport were differentially expressed in *M. adhaerens* in response to *T. weissflogii*, even though the bacterium was physically separated from the diatom (Stahl and Ullrich 2016). This led Stahl and colleagues to conclude that the presence of *T. weissflogii* provides a different nutritional environment for *M. adhaerens*, which is then reflected in the changes in the proteome to accommodate amino acid released by the diatom (2016). The authors did not discuss the potential for cues or signals released by either the bacteria or the diatoms to cause changes in metabolism unrelated to nutrition; however, they noted the insensitivity of their methodological approach indicating that other signaling possibilities cannot be excluded (Stahl and Ullrich 2016).

These studies, as well as the large body of work showing that dissolved vitamins are readily exchanged among members of plankton (as reviewed by Sañudo-Wilhelmy et al. (2014)) showcase the myriad enigmatic exchanges of metabolites among planktonic organisms. The identification of such metabolites, whether they are nutritional or for signaling, is challenging due to the rapid turnover of such compounds within the phycosphere, which results in low standing stock concentrations. This type of cross-talk, as evidenced by the large taxonomic and ecological variation in organisms described above, is likely common throughout the pelagic and remains an underexplored area of research. Future studies to assess whether these species-specific relationships constitute true mutualisms are also needed.

1.5 Host-parasite interactions

Waterborne cues emitted by predators induce defenses in some marine prey (Hay 2009, Scherer and Smee 2016). A pair of recent studies suggest that phytoplankton might

respond to chemical cues from parasites in an analogous way, reducing their risk of infection (Lu et al. 2016, Lee and Park 2017). Lu and colleagues reported that the dinoflagellate *Alexandrium fundyense* detects waterborne cues from the parasitic dinoflagellate *Amoebophrya* sp. resulting in differential gene regulation (2016). When infected by *Amoebophrya* sp. or exposed to its exuded metabolites, *A. fundyense* was found to upregulate its genes associated with energy production, signal transduction, stress, and (putatively) defense. However, there were still distinct differences in gene regulation between the two types of parasite exposure indicating that the molecular mechanisms responsible for detecting and responding to parasitic threat, as well as changes in energy usage and signaling, differ in each case. Production of paralytic shellfish toxins (PSTs) (e.g. **22-30**) by *A. fundyense* was not significantly altered by the presence of the parasite or its diffusible metabolites (Lu et al. 2016). Overall, this study suggests that recognition of *Amoebophrya* sp. waterborne cues alone might ‘prime’ a protective, defensive response in the host before encounter.

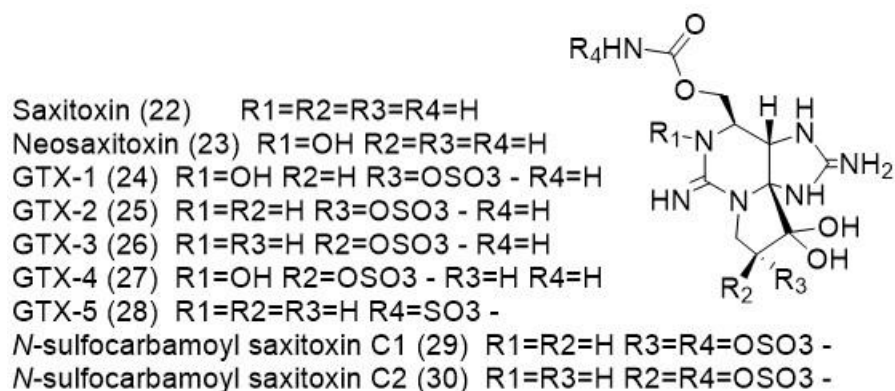


Figure 1.6 Paralytic shellfish toxins (PSTs): saxitoxin (22), neosaxitoxin (23), gonyautoxins (GTX) -1 (24), -2 (25), -3 (26), -4 (27), -5 (28), *N*-sulfocarbamoyl saxitoxin C1 (29), and *N*-sulfocarbamoyl saxitoxin C2 (30), produced by the dinoflagellate *Alexandrium fundyense*.

Another dinoflagellate, *Fragilidium duplocampanaeforme*, did not sense the waterborne cues of its parasite; only the physical presence of live zoospores of the parasitic dinoflagellate *Parvilucifera infectans*, and not dead zoospores or zoospore exuded compounds, triggered cells to form temporary, ecdysal cysts (Lee and Park 2017). These results contrast with those previously reported for *Alexandrium ostenfeldii* which was observed to form ecdysal cysts in response to waterborne cues from *P. infectans* (Toth et al. 2004). More data are needed to understand whether ecdysal cyst formation in diverse dinoflagellates in response to waterborne cues is a common phenomenon affecting plankton community composition and dynamics.

In addition to host sensation of parasites, the reverse case, parasite reception of host exuded metabolites, also occurs. Chytrid zoospores distinguish metabolic nuances in host exudates and increase chemotactic behavior toward attractive diatom hosts (Scholz et al. 2017). Abiotic factors influenced host attractiveness; extracts from light-stressed diatoms elicited the greatest chemotactic response from zoospores. Scholz and colleagues also attempted to identify differences in broad metabolite classes between species of diatoms within the same genus that differed in their susceptibility to parasite infection (Scholz et al. 2017). Differences were noted, but due to the experimental setup it was not possible to determine whether the compounds originated from the diatoms or the parasites, nor to draw conclusions about the chemical characteristics of parasite-resistant diatoms (Scholz et al. 2017). However, both exuded compounds and internal compounds from parasite-resistant diatoms increased protection against parasite infection, hinting at the production of unidentified protective chemical compound(s) by parasite-resistant diatoms.

Once inside its host a parasite may manipulate the host to its own advantage. A recent study by van Tol and colleagues investigated interactions between the flavobacterium *Croceibacter atlanticus* and diatoms (van Tol et al. 2016). The bacterium is a member of the microbial consortium which attaches to diatom surfaces (van Tol et al. 2016). Once attached, *C. atlanticus* inhibited the growth of about half of the tested diatoms (van Tol et al. 2016). Interestingly, the resistant diatoms each still possessed their natural microbial consortia hinting that their microbiome may counteract the negative influence of *C. atlanticus* (van Tol et al. 2016). When the model diatom *Thalassiosira pseudonana* was infected with *C. atlanticus* it stopped dividing, grew larger, became polyploid, and increased its plasmid number and chlorophyll a abundance (van Tol et al. 2016). The authors hypothesized that these outcomes benefit the parasitic bacterium by creating a more colonizable surface area and greater excretion of metabolites that aid in growth. The compounds exuded by *C. atlanticus* when grown alone caused no deleterious effects to *T. pseudonana* indicating that either the inhibitor compounds are not constitutively released or that the interaction is not chemically mediated (van Tol et al. 2016). However, no further steps were taken to identify any induced compound(s) that might be responsible for the growth inhibition of *T. pseudonana* caused by *C. atlanticus*.

Not all cases of host-parasite interaction are antagonistic at all life stages. The marine Roseobacter *Phaeobacter inhibens* associates with the coccolithophore *Emiliana huxleyi* in a mutualist-to-parasite switch model (Wang et al. 2016a), similar to its interaction with the dinoflagellate *Prorocentrum minimum* (Wang et al. 2015). While acting as mutualists, other *Phaeobacter* spp. have been found to co-opt DMSP (20) from

E. huxleyi to produce phenylacetic acid (**31**), a growth promoter in some algae, and tropodithietic acid (**32**), an antibiotic that protects microalgae from marine pathogens (González et al. 1999, Thiel et al. 2010, D'Alvise et al. 2012). During senescence, the alga produces *p*-coumaric acid (**33**) which triggers *Phaeobacter* spp. to produce algicidal roseobactin (**34** and **35**), in a switch to parasitism (Seyedsayamdost et al. 2011). A recent effort by Wang and colleagues to uncover the roseobactin biosynthetic gene cluster in *P. inhibens* determined that genes required for biosynthesis of **32** were also required for roseobactin biosynthesis and that genes from three different loci are needed for roseobactin production (2016a). They also discovered that *P. inhibens* requires two signals, **33** and the QS molecule *N*-(3-hydroxydecanoyl)-L-homoserine lactone (**36**) to switch to parasitism and initiate roseobactin production. Additionally, the authors uncovered a new biosynthetic mechanism for thiol insertion in the biosynthesis of roseobactin (Wang et al. 2016a). The necessity for the dual presence of **33** and **36** for roseobactin biosynthesis may point to tight regulation of the switch from mutualism to parasitism. For the most part, by utilizing the same biosynthetic enzymes to produce **32**, **34** and **35**, a rapid switch from mutualism to parasitism can be accomplished.

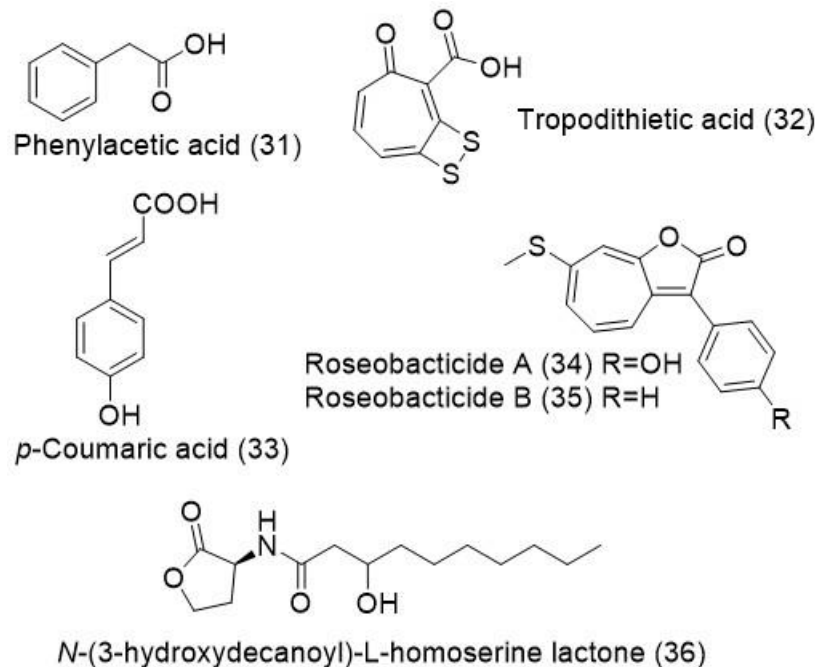


Figure 1.7 Metabolites involved in bacterial-algal interactions. Phenylacetic acid (31) and trophodithietic acid (32) are molecules produced by *Phaeobacter inhibens* which promote algal growth and have antipathogenic properties. p-Coumaric acid (33) and N-(3-hydroxydecanoyl)-L-homoserine lactone (36) promote production of algicidal roseobacticides A (34) and B (35) in *P. inhibens*.

Recently, the algicidal effects of some marine bacteria have been studied in an attempt to better understand algal-bacterial interactions (Yang et al. 2015, Chi et al. 2017). Many bacteria that are algicidal only appear to be so when at high concentrations (Imai et al. 1992, 1993, Roth et al. 2007, Li et al. 2014). Therefore, a recent study by Chi and colleagues was founded on the hypothesis that bacterial quorum sensing is important in controlling algal blooms and more specifically, involved in controlling production of algicidal compounds (2017). The algicidal bacterium *Ponticoccus* sp., isolated from *P. donghaiense*, killed cultures of *P. donghaiense*, *A. tamarensis*, and the prymnesiophyte *Phaeocystis globosa* when they were in exponential growth phase. When treated with β -

cyclodextrin (**37**), a known binder of acyl homoserine lactones, *Ponticoccus* sp. became less algicidal, suggesting that quorum sensing might be at least partially involved in its algicidal activity (Chi et al. 2017). The homoserine lactones, *N*-(3-oxo-octanoyl)-L-homoserine lactone (**38**) and *N*-(3-oxo-decanoyl)-L-homoserine lactone (**17**), as well as, the autoinducer synthases (*zlaI* and *zlbI*) and luxR transcriptional regulator genes (*zlaR* and *zlbR*) for were identified as being involved in quorum sensing in *Ponticoccus* sp (Chi et al. 2017). However, the algicidal compounds were never identified. Another study characterized prolylmethionine (**39**) and hypoxanthine (**40**) as involved in the algicidal activity of a *Bacillus* sp. against *P. globosa*, the alga from which it was isolated (Yang et al. 2015). However, *P. globosa* only experiences growth inhibition when exposed to **39** and **40** at well above ecologically relevant concentrations (Yang et al. 2015).

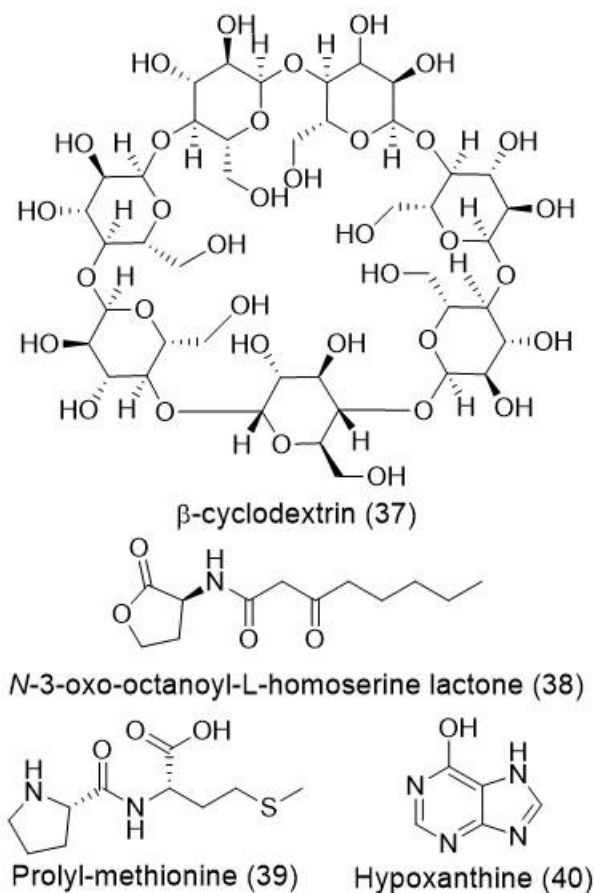


Figure 1.8 Molecules from algicidal bacteria studies. β -cyclodextrin (37) is a homoserine lactone quorum sensing inhibitor. *N*-(3-oxo-octanoyl)-L-homoserine lactone (38) is an autoinducer produced by the algicidal bacterium *Ponticoccus* sp. Prolyl-methionine (39) and hypoxanthine (40) are potential algicides produced by *Bacillus* sp. against *Phaeocystis globosa*.

1.6 Allelopathy

Understanding interactions among phytoplankton species is important in order to predict bloom dynamics. For example, not all phytoplankton species that share a fundamental ecological niche co-occur in the field, and for the ones that do, we do not know all the factors that allow for coexistence. In 2009 the rhabdophyte *Chattonella marina* var. *marina* and the dinoflagellate *Gymnodinium catenatum* co-bloomed in Bahía

de La Paz, Gulf of California, but *C. marina* consistently occurred at double or greater concentration relative to *G. catenatum* (López-Cortés et al. 2011). Therefore, a study was undertaken by Fernández-Herrera and colleagues to gain insight into how *C. marina* outcompeted *G. catenatum* during the bloom (2016). *C. marina* was found to cause loss of flagella, nuclear swelling, and cyst formation in *G. catenatum*. Compounds exuded by *C. marina* appeared to account for approximately 50% of the outcome on *G. catenatum* (Fernández-Herrera et al. 2016). Additionally, some *G. catenatum* cells lysed after contact with *C. marina* cells. Overall, the study showed that *C. marina* has deleterious effects on *G. catenatum* physiology and growth, but the exuded compounds responsible for the allelopathic portion of these effects were not identified (Fernández-Herrera et al. 2016).

Both the dinoflagellate *Alexandrium minutum* and the diatom *Skeletonema costatum* grow off the coast of China, but only *S. costatum* is known to form blooms there (Wang et al. 2017a). Wang and colleagues found that compounds exuded by *S. costatum* inhibited the growth of *A. minutum*. Yet when *A. minutum* was exposed to 15(S)-hydroxyeicosa-5Z,8Z,11Z,13E,17Z-pentaenoic acid (15(S)-HEPE) (**41**), a known auto-inhibitor of *S. costatum*, it acted as a stimulant at low concentrations and an inhibitor at unnaturally high concentrations (Wang et al. 2017a). Therefore, **41** was not the allelochemical exuded by *S. costatum* responsible for the observed growth inhibition of *A. minutum* despite being produced. The allelopathy of *S. costatum* against *A. minutum* may explain why only low concentrations of *A. minutum* are reported in the East China Sea. However, the authors of the study warned that this favoring of diatoms could change

if coastal pollution continues because eutrophication promotes dominance of dinoflagellates over diatoms in the East China Sea (Wang et al. 2017a).

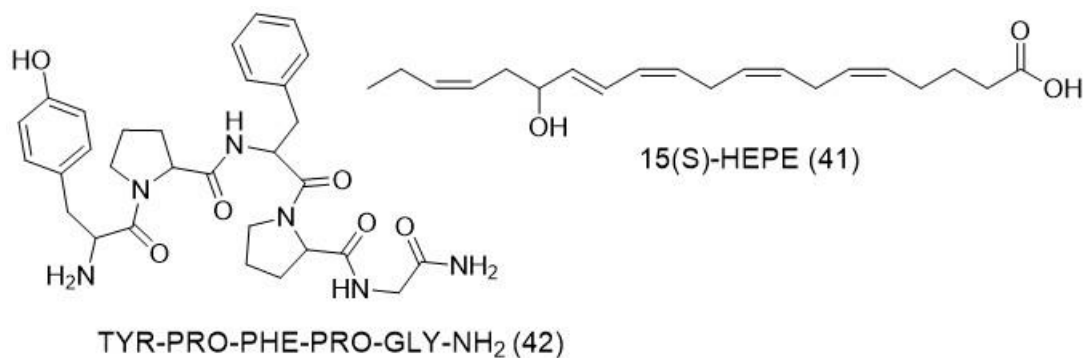


Figure 1.9 Molecules proposed to possess allelopathic properties: the monohydroxy fatty acid 15(S)-hydroxyeicosa-5Z,8Z,11Z,13E,17Z-pentaenoic acid (15(S)-HEPE) (41) and the peptide TYR-PRO-PHE-PRO-GLY-NH₂ (42) produced by the diatom *Skeletonema costatum* and the raphidophyte *Heterosigma akashiwo*, respectively.

In a pair of studies by Wang and colleagues the diatom *Phaeodactylum tricornutum* was found to be allelopathic against the raphidophyte *Heterosigma akashiwo* (2016b, 2017b). Additionally, using mass spectrometry, an allelopathic peptide with putative primary sequence TYR-PRO-PHE-PRO-GLY-NH₂ (42) was identified, although the authors cautioned that further investigation is needed to verify its three dimensional structure (Wang et al. 2016b). At ecologically relevant concentrations 42 caused increased activity of esterases, cell membrane disruption, and disturbance of cell membrane potential in *H. akashiwo* (Wang et al. 2017b). None of the deleterious effects lasted the full length of the experiment suggesting that either *H. akashiwo* acclimated to

the allelochemical, the *H. akashiwo* cells that survived gave rise to a population that was more resistant to the allelochemical, or that **42** degraded over time (Wang et al. 2017b).

Allelopathic interactions are not limited to larger phytoplankton. In a recent series of studies Śliwińska-Wilczewska and colleagues explored the effects of the picocyanobacterium *Synechococcus* sp. on the phytoplankton community in the Baltic Sea (2016, 2017a, 2017b). Compounds exuded by *Synechococcus* sp. inhibited the growth of all the phytoplankton in a natural community, except the cyanobacteria *Nodularia spumigena* and *Gloeocapsa* sp. (Śliwińska-Wilczewska et al. 2017b). This caused a shift in the phytoplankton community whereby *Synechococcus* sp. became even more dominant and green algal species decreased in relative abundance.

Allelopathic effects of the same *Synechococcus* sp. were also measured against the filamentous cyanobacteria *Aphanizomenon flos-aquae*, *Nostoc* sp., *Phormidium* sp., and *Rivularia* sp. (Śliwińska-Wilczewska et al. 2017a). Compounds exuded from *Synechococcus* sp. inhibited the growth of *Nostoc* sp. and *Phormidium* sp., but enhanced the growth of *A. flos-aquae*. The decrease in growth of *Phormidium* sp. was accompanied by a decrease in chlorophyll a abundance and fluorescence suggesting that its photosynthesis efficiency was reduced by *Synechococcus* sp. exudates. In contrast, in *Nostoc* sp. carotenoids, a class of accessory photosynthetic pigments, increased in the presence of *Synechococcus* sp. exudates despite overall growth inhibition (Śliwińska-Wilczewska et al. 2017a). Therefore, further studies should investigate the mechanism by which *Synechococcus* sp. inhibits the growth of *Nostoc* sp. In an additional study, Śliwińska-Wilczewska and colleagues found that *Synechococcus* sp. was most allelopathic towards the diatom *Navicula perminuta*, as measured by the rate and

efficiency of photosynthesis, at optimal growing conditions for *Synechococcus* sp. (Śliwińska-Wilczewska et al. 2016). Unfortunately, the allelochemicals produced by *Synechococcus* sp. were not identified in any of the aforementioned studies.

Allelopathic potency often varies within species (Chen et al. 2015, Xu et al. 2015, Sala-Pérez et al. 2016). Fifteen strains of *Alexandrium tamarense* caused different levels of growth inhibition in *C. marina*, with weakly inhibitory strains themselves strongly suppressed by *C. marina*.(Chen et al. 2015). The inhibitory effect caused by each *A. tamarense* strain correlated with the lytic activity of exuded compounds greater than 1 kDa. However, lytic activity of exudates were tested using rabbit blood cells and not *C. marina* (Chen et al. 2015). Therefore, further studies are needed to explore to what extent exploitation competition, in addition to allelopathy, might be responsible for the decreased growth of *C. marina* when co-cultured with *A. tamarense*.

The lytic effects of six arctic strains of the dinoflagellate *Protoceratium reticulatum* against the cryptomonad *Rhodomonas salina* were tested by Sala-Pérez and colleagues (2016). Lytic activity was found to be strain- and growth phase-dependent, but independent of temperature. Exudates alone from *P. reticulatum* caused lysis in *R. salina* but did not recapitulate the levels of lysis caused by co-culture, suggesting that the compounds responsible for causing the lysis might be unstable. Additionally, lysis of *R. salina* did not appear to be associated with yessotoxin (**43**) (Sala-Pérez et al. 2016).

A study by Xu and colleagues found that the growth of the dinoflagellate *Akashiwo sanguinea* was inhibited by one of two strains of the diatom *Pseudo-nitzschia multiseriis* (2015). Compounds exuded in stationary phase by *P. multiseriis* strain

CLNN16, but not strain CLNN21, inhibited growth in *A. sanguinea*, thereby suggesting that only CLNN16 is allelopathic against *A. sanguinea*. However, no allelochemicals were identified (Xu et al. 2015). In another part of this study these authors tested the effects of a strain of *Pseudo-nitzschia pungens* from the South China Sea against *A. sanguinea* and four other co-occurring phytoplankton species (*Prorocentrum minimum*, *Phaeocystis globosa*, *C. marina*, and *R. salina*) (Xu et al. 2015). *P. pungens* inhibited growth of *A. sanguinea*, and to a lesser extent *C. marina* and *R. salina*, in a density-independent manner. Additionally, compounds exuded by lysed cells of both *P. pungens* and *P. multiseriata* strain CLNN16 inhibited the growth of *A. sanguinea* and *R. salina* (Xu et al. 2015). The authors of the study suggest that both *Pseudo-nitzschia* spp. are allelopathic but that domoic acid (**44**) is not the allelochemical, since the tested strain of *P. pungens* was allelopathic despite not being a known producer of **44** (Xu et al. 2015). However, concentrations of **44** were not measured in this study and compounds released only by cell lysis are likely not effective at mediating competition.

Some phytoplankton appear to inhibit their own growth (Zhang et al. 2015b, Gallo et al. 2017). In a follow-up to their 2013 study (Wang et al.), Zhang and colleagues tested the effect of compounds exuded by declining phase *S. costatum* on the interactions between *S. costatum* and the dinoflagellate *Prorocentrum donghaiense* using more field-relevant nutrient concentrations and bacteria free culture conditions (Zhang et al. 2015b). Once again they found that self-inhibition by *S. costatum* is likely what drives the successional bloom of *P. donghaiense* after *S. costatum* in the East China Sea (Wang et al. 2013, Zhang et al. 2015b). Despite continued study of this system, additional

experiments are still warranted because the self-inhibitory compound(s) produced by *S. costatum* have yet to be identified.

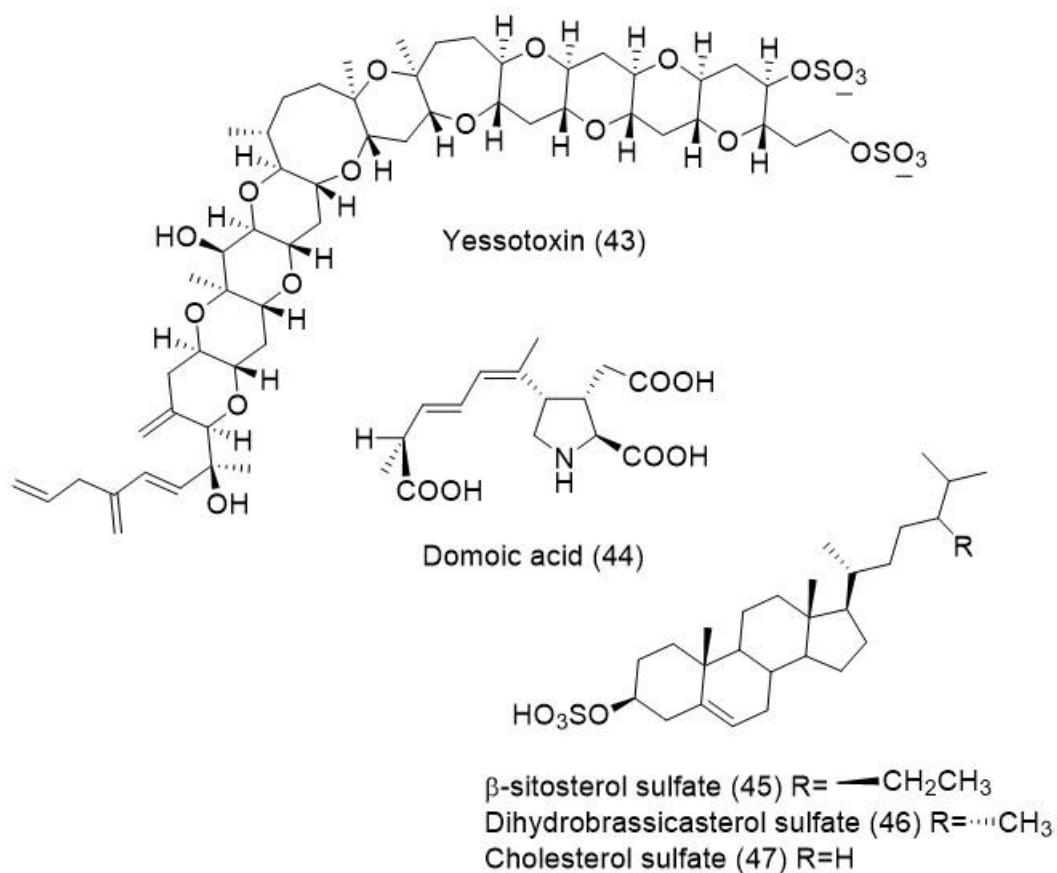


Figure 1.10 Chemical structure of the algal toxins yessotoxin (43) and domoic acid (44) produced by the dinoflagellate *Protoceratium reticulatum* and some diatoms from the genus *Pseudo-nitzschia*, respectively. Sterol sulfates, β -sitosterol sulfate (45), dihydrobrassicasterol sulfate (46), and cholesterol sulfate (47) which have self-inhibitory activity in the diatom *Skeletonema marinoi*.

The sterol sulfates, β -sitosterol sulfate (45), dihydrobrassicasterol sulfate (46), and cholesterol sulfate (47), have been found to regulate cell death programming in the diatom *Skeletonema marinoi* (Gallo et al. 2017). Early exponential phase cultures of *S.*

marinoi declined immediately when exposed to their own stationary phase filtrates or the individual compounds **45**, **46**, and **47**. Exposure to **47** alone induced processes associated with cell stress and apoptosis in *S. marinoi*. The role of these compounds in the self-inhibition was further confirmed when interruption of the biosynthesis of **45**, **46**, and **47** resulted in an extended stationary phase and an increase in final cell density of *S. marinoi* (Gallo et al. 2017).

1.7 Predator-prey interactions

1.7.1 Chemical defenses

Marine plankton are well-known producers of secondary metabolites hypothesized to act as defenses against predators. Over the past decade, several species of dinoflagellates of the genus *Karlodinium* which produce karlotoxin 1, 2, 8, and 9 (**48-51**) (Waters et al. 2015), have been implicated in fish kills. These molecules act by binding to cholesterol and disrupting cell membranes (Deeds et al. 2015, Rasmussen et al. 2016a). Recently, a novel karlotoxin-like molecule was identified by Rasmussen and colleagues from the newly identified ichthyotoxic dinoflagellate species *Karlodinium armiger* (2017). Karmitoxin (**52**) differs from the previously described **48-51** in that it possesses a primary amine at one end. In a rainbow trout gill cell toxicity assay, **52** lysed cells with an LC₅₀ value of 125 nM (Rasmussen et al. 2017). Additionally, **52** exhibited an LC₅₀ of 400 nM for adult female *Acartia tonsa* copepods (Rasmussen et al. 2017). The concentrations used to establish LC₅₀ values were in the measured range for extracellular **52** from *K. armiger* (Rasmussen et al. 2017). However, an ecological assay for planktonic organisms would typically involve exposing copepods to toxins within food particles, not

dissolved in seawater. Therefore, it is unclear whether **52** would actually play an important role as a chemical defense against copepods or as an ichthyotoxin in natural populations.

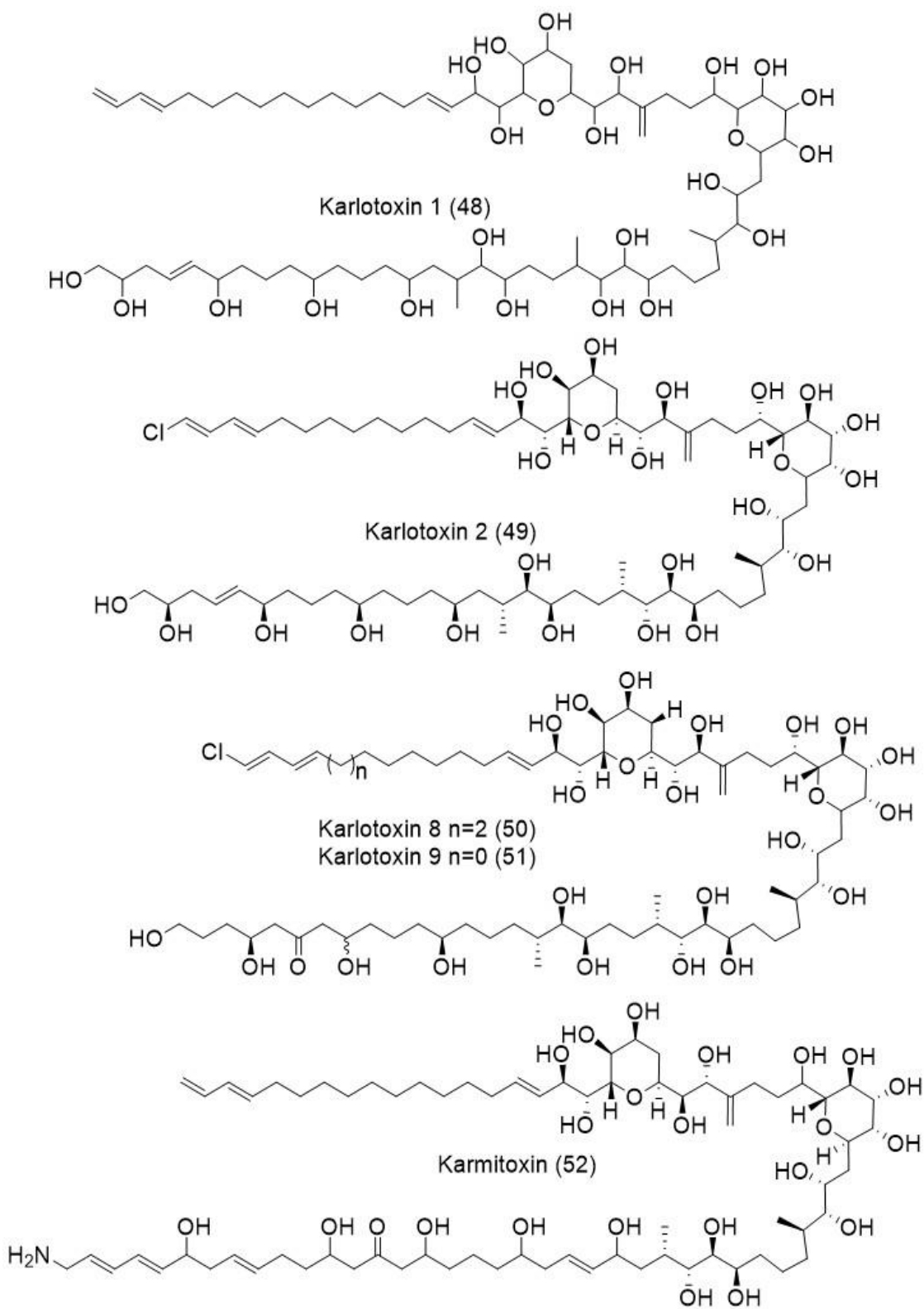


Figure 1.11 Chemical structures of the toxins karlotoxins 1 (48), 2 (49), 8 (50), and 9 (51) and karmitoxin (52) produced by dinoflagellate of the genus *Karlodinium*.

The haptophyte *Prymnesium parvum* has also been implicated in massive fish kills (Roelke et al. 2016). Recently, Rasmussen and colleagues characterized a new prymnesin that contains a novel ladder-frame polyether backbone (2016b). Prymnesin-B1 (**53**) differs from the previously described prymnesin-2 (**54**) in the elimination of rings H and I from the polyether ladder-frame resulting in six fewer carbon atoms in the polyketide backbone, substitution of the α -L-xylofuranose moiety for α -D-galactopyranose, and loss of a chlorine before the terminal alkynyl groups. Additionally, by screening 10 strains of *P. parvum* from all around the world they putatively identified 13 new prymnesins by liquid chromatography high-resolution mass spectrometry, eight of which appear to possess a novel, more heavily chlorinated backbone (Rasmussen et al. 2016b). By a rainbow trout gill cell assay **53** was found to have an EC₅₀ value of 5.98 nM, which makes **53** much less toxic than **54**; therefore, the authors speculated that all prymnesins are ichthyotoxic to varying degrees (Rasmussen et al. 2016b). Nevertheless, they failed to determine whether the potencies of toxins fall within the expected natural concentrations for prymnesins during a *P. parvum* bloom.

Recently two new toxic azaspiracids (**55** and **56**) were isolated from the dinoflagellate *Azadinium poporum* (Krock et al. 2015). These new analogues differ from the previously described **57** by minor alterations to methylation, hydroxylation, and unsaturation patterns. In a cytotoxicity assay with lymphocytes **55** and **56** were much less toxic than **57** (Krock et al. 2015). Although the azaspiracids have previously been proposed to function as chemical defenses (Jaufrais et al. 2012), this study did not address an ecological function for the novel natural products; further studies should be performed to identify the ecological roles, if any, of azaspiracids in *Azadinium* sp.

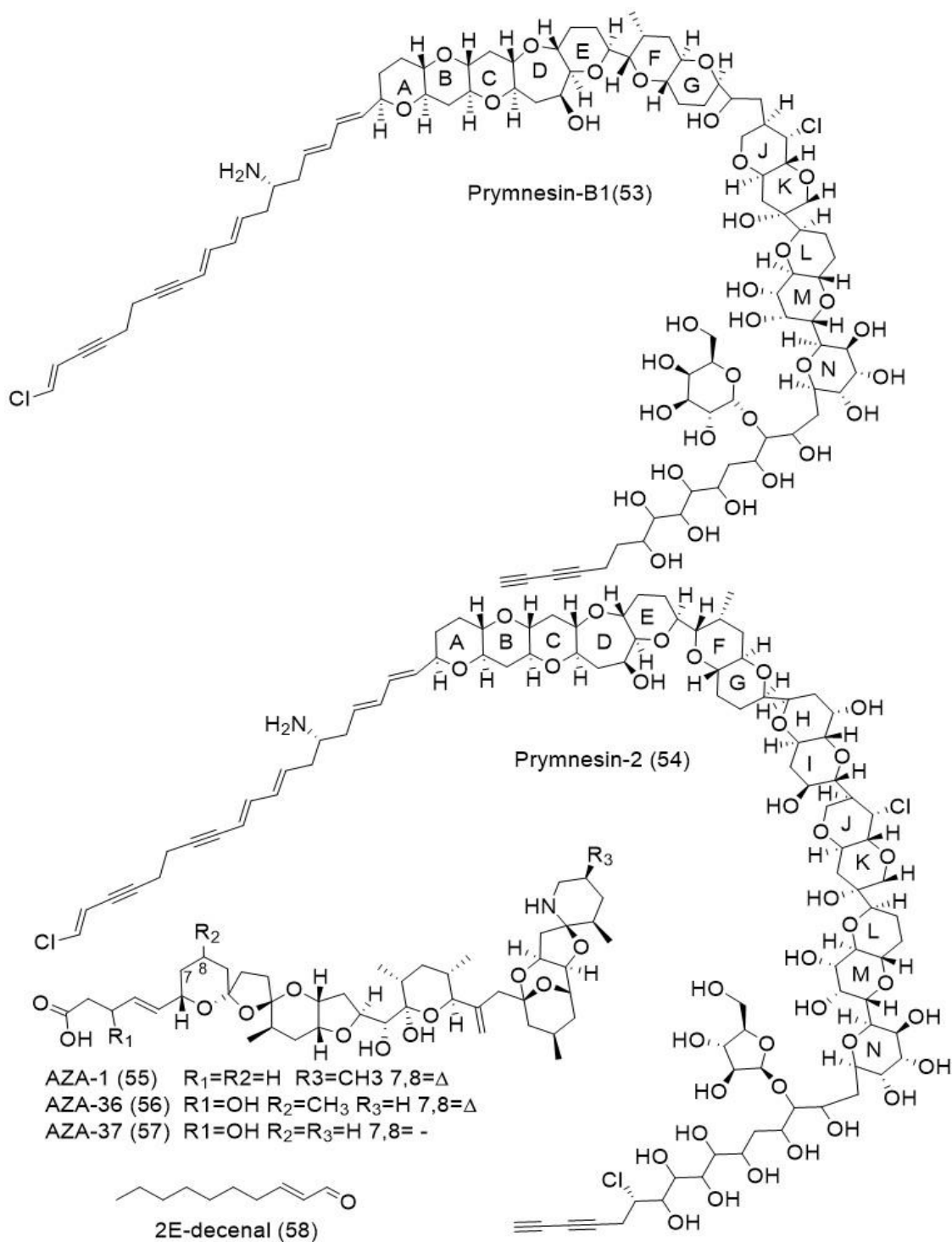


Figure 1.12 Chemical structures of algal toxins: prymnesin-B1 (53) and -2 (54), produced by the haptophyte *Prymnesium parvum*, and azaspiracids (AZA) -1 (55), -36 (56), and -37 (57), produced by the dinoflagellate *Azadinium poporum*. Chemical structure of the diatom oxylipin 2E-decenal.

A 2015 study on winter phytoplankton blooms in 2004 and 2005 in the northern Adriatic Sea attempted to link diatoms and non-volatile oxylipins, such as 15(S)-HEPE (41) and 2E-decenal (58), to reduced reproductive success in copepods (Ianora et al. 2015). The study found that mean phytoplankton density during winter blooms increased between 2004 and 2005 driven largely by diatoms, which increased in abundance from 10.3% to 50.1% of the phytoplankton composition. Among the diatoms, *Skeletonema marinoi* was the most dominant species in 2005; whereas in 2004, *Pseudo-nitzschia galaxiae*, *S. marinoi*, and *Chaetoceros* spp. were all close to equally dominant among diatom species (Ianora et al. 2015). The higher diatom abundance in 2005 was mirrored by higher egg production in copepods *Acartia tonsa* and *Calanus helgolandicus*; yet, hatching success was significantly lower in 2005 than in 2004. Ianora and colleagues suggested that hatching success was compromised because of higher concentrations of oxylipins, particularly non-volatile oxylipins, recorded in 2005, which might have been the result of diatom population booms (2015). A study in 2012 had shown a pattern of downregulation in aldehyde detoxification and apoptosis regulator genes in *C. helgolandicus* in response to a diet of *S. marinoi*, the predominant diatom in the 2005 winter Adriatic Sea blooms, providing further support for the hypothesis that the increase in *S. marinoi* and oxylipins in 2005 was responsible for deleterious effects on copepods (Lauritano et al.). In 2015, a similar study to the 2012 one was completed exploring the effects of a diet of *S. marinoi* on gene expression in the copepod *Calanus sinicus* (Lauritano et al.). While after the first two days aldehyde detoxification genes, a heat shock protein, and an antioxidant enzyme gene were downregulated in *C. sinicus* fed *S. marinoi* similar to the response in *C. helgolandicus*, by the fifth day these genes had

switched to being upregulated (Lauritano et al. 2015). This suggests that, unlike *C. helgolandicus* (Lauritano et al. 2012), *C. sinicus* is capable of restoring initially damaged proteins and activating an antioxidant response (Lauritano et al. 2015). The results of these studies support the generalized hypothesis that oxylipins contribute to the poor food value of diatoms for copepods.

The dinoflagellates *Akashiwo sanguinea* and *Alexandrium catenella* and the raphidophyte *Chattonella marina* negatively impact the growth of the predatory dinoflagellate *Noctiluca scintillans* despite the ability of *N. scintillans* to feed and grow on several other chemically defended dinoflagellates and raphidophytes (Stauffer et al. 2017). When provided with a mixed assemblage diet of *A. catenella*, a producer of PSTs (e.g. **22-30**), and a non-toxic strain of the raphidophyte *Heterosigma akashiwo*, the growth rate of *N. scintillans* increased with increasing proportion of *H. akashiwo* at a rate greater than expected if toxicity of *A. catenella* was undermining its value as a food (Jonasdottir et al. 1998, Stauffer et al. 2017). Therefore, it is unlikely that toxicity is responsible for the negative growth rate of *N. scintillans* when feeding on *A. catenella*. In further support of this hypothesis, *H. akashiwo* cultures spiked with compounds exuded by *A. catenella*, and not ones spiked with saxitoxin (**22**), significantly decreased the growth rate of *N. scintillans* (Stauffer et al. 2017). Therefore, there may be unidentified compounds produced, and possibly exuded, by *A. catenella* that either detract from its nutritional value or deter feeding by *N. scintillans* without imposing direct toxicity.

The newly described *Alexandrium pohangense* uses its chemical defense to kill potential protist predators before they even begin grazing (Kim et al. 2016). *A.*

pohangense forms blooms off the coast of Pohang, South Korea despite having an extremely slow growth rate when growing autotrophically (Lim et al. 2015). Consequently, one hypothesis is that *A. pohangense* blooms less by growing and more by avoiding predation, relative to its competitors (Kim et al. 2016). In a recent study, pre-bloom concentrations of *A. pohangense* immobilized and then lysed nine different heterotrophic protist predators known to prey upon other chemically defended phytoplankton (Kim et al. 2016). Compounds exuded by *A. pohangense* alone killed the majority of protists in a natural assemblage and were nearly as potent at killing the predators as live *A. pohangense*. In conclusion, *A. pohangense* likely forms blooms, at least in part, by killing many would-be protists predators; however, rates of predation on other competitors in a natural assemblage still needs to be measured for comparison and the post-ingestion effects of *A. pohangense* on metazoan predators has yet to be studied (Kim et al. 2016). Without these additional studies there is no way of knowing if *A. pohangense* experiences lower predation rates than its competitors. Additionally, future studies should identify the compound(s) responsible for the lytic effects recorded in this study.

Bivalve mollusks are commonly negatively impacted by the chemical composition of phytoplankton. A recent study by Tran and colleagues found that the toxic dinoflagellate *Alexandrium minutum* impacts the daily rhythms of the oyster, *Crassostrea gigas* (2015). Bloom concentrations of *A. minutum* caused loss of the cyclic pattern of expression of *Cgcry*, a circadian rhythm-controlling gene, in *C. gigas* (Tran et al. 2015). Similarly, digestive processes and gene expression of genes involved in oxidative stress defense, immunity, and respiration were no longer cyclically regulated when oysters ate

A. minutum (Tran et al. 2015). Moreover, the study found oysters that had accumulated *A. minutum* toxins in their digestive glands remained open throughout the 24 hours, regardless of cycling of the tides or *Cgcry* gene expression, revealing another mechanism by which such compounds can affect grazers (Tran et al. 2015). The full consequences of the loss of biological daily rhythms on the long term fitness of oysters have yet to be studied and the authors suggest that the loss of rhythm, and subsequent changes in digestion pattern, may actually protect the oysters from more serious adverse effects when they experience ephemeral blooms of *A. minutum* (Tran et al. 2015).

Toxic phytoplankton may also indirectly harm bivalve mollusks by making bivalve mollusks more vulnerable to infection. Several recent studies have suggested that exposure to blooms of toxic *Alexandrium* spp. makes shellfish prone to parasitism (Lassudrie et al. 2015) and infection (Abi-Khalil et al. 2016). A study by Abi-Khalil and colleagues showed that exposure to toxic *A. catenella* increased the susceptibility of adult *C. gigas* to mortality from infection by the pathogen *Vibrio tasmaniensis* (2016). Additionally, the authors found an association between *V. tasmaniensis* infection, mortality, and toxin (i.e., GTX-2 (25) and GTX-C2 (30)) accumulation in adult oysters (Abi-Khalil et al. 2016). In contrast, *C. gigas* larvae did not experience increased susceptibility of infection by *Vibrio* sp when to fed *A. catenella* (Lassudrie et al. 2016). However, larvae did experience an increased immune response, but this was unrelated to accumulation of PSTs (e.g. 22-30) (Lassudrie et al. 2016). On the other hand, other recent studies have shown that 22 induces apoptosis of immune cells in *C. gigas* (Abi-Khalil et al. 2017) and decreases phagocytosis, increases reactive oxygen species production (Astuya et al. 2015), and causes an upregulation of immune pattern recognition receptor

genes and their signaling pathways in the Chilean mussel, *Mytilus chilensis* (Detree et al. 2016). Unfortunately, these three studies (Astuya et al. 2015, Detree et al. 2016, Abi-Khalil et al. 2017) involved either bathing the immune cells in dissolved **22** (or other related toxins (**23-30**)) or directly injecting **22** into mussel muscle, which is not how mussels would be exposed in under natural conditions.

Shellfish larvae may be especially vulnerable to phytoplankton compounds. Sperm and oocytes exposed to the dinoflagellate *Karenia brevis* just prior to fertilization experienced decreased fertilization success and increased mortality (Rolton et al. 2015). Additionally, long term exposure to live *K. brevis* or its exuded compounds caused increased mortality in all larvae, whether they were initially exposed pre- or post-fertilization (Rolton et al. 2015). Even after the removal of *K. brevis*, larvae exposed to high concentrations of *K. brevis* cells continued to experience higher rates of mortality and lower growth rates indicating *K. brevis* can have deleterious effects on oyster larvae long after it is gone (Rolton et al. 2015). Because these effects were also experienced by larvae which were only exposed to exuded compounds, the source of the deleterious effects is likely chemical in nature; but, the compound(s) responsible were not investigated in this study (Rolton et al. 2015) and therefore are a source of future studies.

Some algae modulate their own toxin production in response to chemical cues from predators. In a study by Tammilehto and colleagues, the diatom *Pseudo-nitzschia seriata* increased its production of domoic acid (**44**) when in the presence of two different species of copepods, *Calanus hyperboreus* and *C. finmarchicus* that were feeding on other *P. seriata* cells, separated by a permeable membrane (2015). Unlike toxin production, chain length in *P. seriata* was only affected when in direct contact with

grazers, in which case *P. seriata* maintained a small proportion of large (four cell) chains whereas without the grazer *P. seriata* increased the proportion of large chains over time (Tammilehto et al. 2015). Lysed conspecific cells caused no changes in *P. seriata*, thereby indicating that the copepods and not the dead conspecifics were responsible for the chemical cue that resulted in the more defensive behaviors (Tammilehto et al. 2015). In a follow-up study by Harðardóttir and colleagues copepodites (sexually immature copepods) induced toxin production in *P. seriata* and the previously assumed non-toxic *Pseudo-nitzschia obtusa* (2015). Despite *P. seriata* having overall higher toxin production than its congener, both *Pseudo-nitzschia* spp. were eaten in equal proportion by the copepodites, which were found to bioaccumulate **44** (Harðardóttir et al. 2015). This suggests that copepodites are as resistant to **44** as their adult counterparts and brings into question if **44** is a chemical defense against *Calanus* copepods at all. On one hand, *Pseudo-nitzschia* spp. increased production of **44** in response to the copepods; however, it does not appear to be toxic to various life stages of *C. finmarchicus* (Harðardóttir et al. 2015, Tammilehto et al.). One hypothesis is that **44** was once an effective deterrent against grazing by *Calanus* copepods but the copepods have evolved resistance to the toxin. Alternatively, the nutritional benefits of *Pseudo-nitzschia* spp. may outweigh the deleterious effects of **44**.

The toxic dinoflagellate *Alexandrium fundyense* increased its production of PSTs (**22-30**) when exposed to copepods with which it has historically co-occurred; whereas with other copepods it requires a feeding cue before toxin induction (Senft-Batoh et al. 2015a, Senft-Batoh et al. 2015b). The greatest increase in toxin production in *A. fundyense*, in most cases, was when it was exposed to a predator that was feeding or had

recently eaten *A. fundyense* (Senft-Batoh et al. 2015a, Senft-Batoh et al. 2015b). As part of the study, the authors attempted to decouple the response to a predator from the response to an injured conspecifics by measuring toxin induction in *A. fundyense* in the presence of lysed conspecifics and congeners in the absence of predators (Senft-Batoh et al. 2015b). While not as dramatic as the response to the feeding predator cues, there was an increase in toxin production in response to lysed algal cells alone indicating the *A. fundyense* was likely responding to some sort of cue from the damaged conspecifics in addition to the predator cues (Senft-Batoh et al. 2015b).

Phytoplankton also modulate toxin production based on the type of predators. Senft-Batoh and colleagues hypothesized that, because PSTs (*e.g.* 22-30) act by blocking voltage-gated sodium channels, if *A. fundyense* produces PSTs as an inducible chemical defense they will only increase production of PSTs in the presence of metazoan grazers, which have at least perfunctory nervous systems, but not in the presence of protist grazers (2015a). In support of their hypothesis, *A. fundyense* increased its toxin production in response to seven different metazoan predators from across three phyla, but not in response to either of two protist predators, each from a different phylum (Senft-Batoh et al. 2015a). Additionally, the magnitude of toxin induction showed a positive asymptotic relationship with the total number of algal cells ingested by predators (Senft-Batoh et al. 2015a). Overall, the study suggests that grazer-induced production of PSTs in *A. fundyense* is phylum- and species-specific and that the induction becomes greater when the proximity of the grazer and the likelihood of being eaten increases. As an opportunity for future investigation, we don't yet know the identity of the chemical cues from ciliate

predators which elicit induction of toxin production in *A. fundyense* (Senft-Batoh et al. 2015a).

In 2015, a study identified copepodamides (**1-8**) as predatory cues produced by copepods which induce toxin production in *Alexandrium minutum* (Selander et al.). Copepodamides are polar lipids whose backbone is likely biosynthesized by attachment of taurine via an amide bond to a hydroxylated phytanic acid analog, to which is appended an unsaturated fatty acid moiety. The copepodamides induced up to a 20-fold increase in toxin production at pico- to nanomolar concentrations (Selander et al. 2015). Additionally, the study showed copepodamides to be active at ecologically relevant concentrations by measuring the exudation rate of copepodamides from field-collected copepods and by measuring copepodamide concentrations in field samples (Selander et al. 2015).

Chemical defenses utilized by phytoplankton are typically not effective against all potential predators. Often there are predators sensitive to a chemical defense which experience deleterious effects, whereas others are partially or wholly resistant. The copepod *C. finmarchicus* is sensitive to *A. fundyense* toxicity, producing fewer eggs when fed a diet including *A. fundyense* (Roncalli et al. 2016b). However, reduced egg production may be due to nutritional inadequacy of *A. fundyense* rather than toxicity. Other copepods such as *Acartia hudsonica* appear to have evolved partial resistance to *Alexandrium* spp. toxicity (Chen 2010). The initial hypothesis was that *A. hudsonica* mitigated *Alexandrium fundyense* toxicity via a mutant sodium channel; however, the mutant isoform was found to be just as sensitive as the wild-type (Chen 2010). Therefore, later studies suggested that it is the ratio of the isoforms that is important for mitigating

toxicity (Finiguerra 2013). In contrast, more recent studies have found that there is no difference in the ratio of wild-type to mutant isoforms in populations more frequently exposed to *Alexandrium* blooms (Finiguerra et al. 2014, Roncalli et al. 2017). Consequently, a recent study by Finiguerra and colleagues found that, even when fed a sole diet of *Alexandrium fundyense*, the mutant isoform conferred no advantage (2015). Additionally, expression of the mutant isoform appeared to be disadvantageous for *Acartia hudsonica*, causing decreased growth in individuals who predominantly express it when eating a diet without *A. fundyense* (Finiguerra et al. 2015). Therefore, the mechanism of resistance of *Acartia hudsonica* to the toxicity of *A. fundyense* still requires further investigation. Roncalli and colleagues found that adult *Calanus finmarchicus* copepods upregulated genes involved in digestive processes when eating a diet enriched in *A. fundyense*, possibly in an attempt to limit toxin absorption (2017). Nonetheless, in this study toxin accumulation or biotransformation in the copepods was not measured so this hypothesis cannot yet be verified.

In order to avoid the deleterious effects of consuming chemically defended *Alexandrium* spp., the copepod *Temora longicornis* changed its feeding behavior in a species- and strain-specific way (Xu et al. 2017). The copepods exhibited normal feeding behavior in response to the nontoxic dinoflagellate *Protoceratium reticulatum* and a strain of *Alexandrium tamarense* which displays lytic activity and produces large quantities of PSTs (e.g. **22-30**). The copepods also consumed prey at a normal rate in response to *Alexandrium pseudogonyaulax* which produces goniodomin A (**59**) and to a strain of *A. tamarense* that is lytic and produces only low quantities of PSTs (Xu et al. 2017). However, copepods subsequently rejected most cells after an hour of exposure to

A. pseudogonyaula and regurgitated most of the *A. tamarensis* cells. In contrast to all the other *Alexandrium* spp. treatments, the copepods reduced their rate of feeding in response to a non-lytic strain of *A. tamarensis* that produces moderate concentrations of PSTs (Xu et al. 2017). Since the least favored prey was neither the most toxic nor lytic, the copepods are likely using another cue to assess food quality (Xu et al. 2017). These different feeding behaviors affect predator-prey dynamics and may also have drastic impacts on apparent competition dynamics among the phytoplankton. Prey that are captured and rejected may experience an advantage over competitors whereas prey that cause a decrease in copepod feeding behavior provide equal predation relief to their competitors and therefore lose their competitive advantage (Xu et al. 2017).

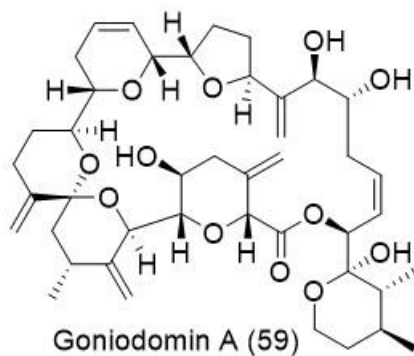


Figure 1.13 Algal toxin goniiodomin A (59) produced by the dinoflagellate *Alexandrium pseudogonyaulax*.

The copepod *Acartia tonsa* avoids thin layers of *K. brevis* exudates in order to avoid negative effects of consuming or exposure to *K. brevis* (True et al. 2017). In a recent study by True and colleagues *A. tonsa* swimming behaviors were quantified after

exposure to a distinct layer of cell-free exudates from various concentrations of *K. brevis*. As concentration of *K. brevis* cells used to make the exudates increased, *A. tonsa* increasingly avoided the exudate layer (True et al. 2017). This avoidance response (True et al. 2017) is starkly different from an attraction response in *A. tonsa* which was observed previously as a result of contact with a layer of exudates from the more palatable green alga *Tetraselmis* sp. (Woodson et al. 2007). This suggests that exudates alone are enough for *A. tonsa* to distinguish preferable and non-preferable prey sources and cause them to change their swimming and foraging behavior. Avoidance of *K. brevis* exudates allows *A. tonsa* to minimize time wasted potentially capturing less favorable prey (True et al. 2017). For *K. brevis* this avoidance could cause a positive feed-back loop as higher concentrations of exuded compounds trigger stronger avoidance which reduces grazing on the dinoflagellate, allowing the bloom to grow. The authors of the study warned that *A. tonsa* individuals in this particular study were from Georgia, not the Florida gulf coast where *K. brevis* predominantly blooms, and therefore represent naïve predators which may be more sensitive to the deleterious effects of *K. brevis* (True et al. 2017). In spite of this, they postulated that the interaction is still relevant when considering the expansion of bloom-forming species distributions due to climate change (True et al. 2017).

1.7.2 *Prey capture and predator avoidance*

The detection of suitable food is imperative for the survival of predators. For nearly 40 years scientists have assumed that current-feeding copepods detect non-motile prey using long-range chemoreception. However, in a recent study Gonçalves and Kiørboe challenged this view and suggested instead that the copepods use near-field

chemoreception (2015). Through critical analysis of foundational studies and with the addition of their own data they showed that prey need to be within a few prey lengths of the setae of a copepod in order to elicit a capture response. At these distances diffusion through the thick boundary layer encompassing the setae would take longer than most reported beat cycles for current-feeding copepods (Gonçalves and Kiørboe 2015). Furthermore, using models Gonçalves and Kiørboe showed that previously reported distances for prey detection falls within the limits of fluid mechanical signal and detection for the copepods. Finally, they argued that the rate of leakage from an individual phytoplankton cell is not high enough to result in a detectable concentration of solutes outside the chemical boundary layer of the cell (Gonçalves and Kiørboe 2015). In 2016 Paffenhöfer and Jiang responded to the study and suggested that Gonçalves and Kiørboe (2015) used too low of a leakage rate in their calculations. Moreover, they argued that phytoplankton cells might go through short bursts of intense leakages that result in concentrations of solutes inside their boundary layer building up high enough for copepod detection (Paffenhöfer and Jiang 2016). Paffenhöfer and Jiang therefore concluded that it is in fact possible for copepods to use long-range chemoreception and disputed that without long-range chemoreception it would be very difficult for copepods which use feeding-currents to survive in environments with lots of particulates and low food concentrations (2016). In a rebuttal Kiørboe and colleagues used new reasoning and evidence to demonstrate that mechanoreception is sufficient for copepods to detect adequate amounts of food to survive even in environments with low concentrations of food (2016). In part Kiørboe and colleagues (Kiørboe et al. 2016) argued that Paffenhöfer and Jiang (2016) incorrectly assumed that the forces of the feeding current perfectly

balance gravity so that the copepods hover as they feed; however, a previous study showed that feeding currents are often so strong that copepods are driven through the water (Kiørboe et al. 2010). Additionally, Kiørboe and colleagues reported observations that even at realistically low phytoplankton concentrations copepods detect prey at distances consistent with mechanoreception (2016). Finally, they argued that intense bursts of leakage by phytoplankton should be rare and therefore only a few phytoplankton cells at any given time would be detectable to copepods if the burst are necessary for the use of chemoreception for prey detection (Kiørboe et al. 2016). This represents a partial paradigm shift in our understanding of how current-feeding copepods interact with their phytoplankton prey, whereby the copepods may first sense potential prey using mechanoreception of hydrodynamic cues, followed by assessment of palatability via contact chemoreception. Overall, this novel perspective necessitates re-evaluation of conclusions from former studies.

Volatile organic compounds released by wounded phytoplankton may act as chemical cues which zooplankton, such as copepods, can use to easily find prey. In a well-controlled and innovative study, Maibam and colleagues assessed the effects of volatile organic compounds from three diatoms (*Pseudonitzschia delicatissima*, *Chaetoceros affinis*, and *Skeletonema marinoi*), and a dinoflagellate (*Prorocentrum minutum*) on the behavior of the copepod *Centropages typicus* both at current and future ocean pH conditions (2015). The copepods clearly recognized the volatile organic compounds; however, for three of four species tested the response of the copepods to the volatile organic compounds was inconsistent with what would be expected if they were used as prey cues (Maibam et al. 2015). Additionally, the behavior by copepods in

response to volatile organic compounds from dinoflagellates suggests that pH may affect either the chemical structure of some volatile organic compounds or chemoreception of these molecules by *C. typicus* (Maibam et al. 2015).

In some cases their surface chemistry may help prey avoid being captured by predators. Pelagic bacterial community composition changes after being filtered by either benthic and pelagic tunicates (Dadon-Pilosof et al. 2017). A study by Dadon-Pilosof and colleagues revealed that retention of bacteria by tunicates may be less size- and shape-dependent and more surface chemistry-dependent than previously thought (2017). The tunicates had some of the a lowest retention efficiencies for the SAR11 clade of Alphaproteobacteria despite them being similar in size to other bacteria and beads (Dadon-Pilosof et al. 2017). Therefore, the authors of the study proposed that the “stickiness” of the bacteria, or their ability to adhere to the hydrophobic mucous net of the tunicates, explains the retention efficiency of different groups of bacteria. In support of this hypothesis, bacteria in the SAR11 clade that possessed more hydrophilic cell surfaces experienced low retention efficiency by the tunicates; however, this was not the case for all the bacteria tested, as Flavobacteriaceae NS5 and SAR116 bacteria both had highly hydrophobic cell surfaces and experienced low retention efficiency by the tunicates (Dadon-Pilosof et al. 2017). Therefore, the hydrophobicity of the surface of bacteria could play a role in how some, but not all, bacteria, like the SAR11 clade, escape predation by filter feeders.

While surface chemistry might reduce predation for some organisms, certain proteins on the surface of cyanobacterium *Synechococcus* sp. increase its susceptibility of predation (Strom et al. 2017). The glycoprotein SwmA as well as the large surface

protein SwmB are required for motility in this strain (McCarren et al. 2005, McCarren and Brahamsha 2007, Strom et al. 2017). Additionally, SwmA has previously been implicated in the formation of the S layer around the cell which protects and stabilizes the cell (Brahamsha 1996). Therefore, SwmA and SwmB were hypothesized to protect *Synechococcus* sp. against ciliate and nanoflagellate predators (Strom et al. 2017). Nonetheless, when Strom and colleagues tested this hypothesis they found that there was a lower predation rate on mutants lacking SwmA mutant than either the wild-type or mutants lacking SwmB (2017). This study indicates that SwmA and the presence of the S layer actually increased predation rate, contrary to the original hypothesis.

Just as predators use chemical cues to find their prey, some prey use chemical cues from predators to avoid predation. However, little is known about how organisms integrate visual and chemical cues to avoid predation. Crab larvae are a particularly good model organism to study the integration of visual and chemical cues because they tend to live at the edge of their photo detection capabilities and one species, *Rhithropanopeus harrisi*, has previously been shown to increase the frequency of swimming descents in the presence of fish kairomones (Cohen and Forward Jr 2003). In a study by Charpentier and Cohen, the effect of fish exudates on crab visual acuity was compared between larvae of *R. harrisi*, an exclusively estuarine crab (Cronin 1982) which likely experiences higher predation pressure (Christy 2011), and larvae of *Hemigrapsus sanguineus*, an intertidal crab that spends a portion of its larval phase in the pelagic zone to escape predation (2015, Cohen et al. 2015). In response to fish mucus, *R. harrisi* larvae showed a less dramatic increase in defensive behavior and immediate physiological response but showed long-term phenotypic plasticity in the form of changes in eye structure; whereas,

H. sanguineus larvae experienced more drastic increases in defensive behavior and retinal response, which would greater assist it in avoiding visual predators only in the short-term (Charpentier and Cohen 2015). This study was successful in uncovering how crab larvae integrate both chemical and visual cues when assessing predation pressure; nevertheless, future studies should ensure that both sets of cues, particularly the chemical cues, are provided to the study organisms at realistic concentrations. In another study Charpentier and colleagues showed that, a more advanced larval stage, called zoea, of these same crab species experienced increased spine length in response to fish mucus (2017). The estuarine dwelling *R. harrisii* zoea is shorter in body length but has longer spines than the transitory *H. sanguineus* zoea. During the study, *R. harrisii* zoea exposed to fish mucus for their entire development were consumed less by the fish *Fundulus heteroclitus* and their mean spine length was longer than zoea exposed to fish mucus for only a couple hours (Charpentier et al. 2017). This indicates that longer spines in *R. harrisii* zoea reduces predation by gape-limited predators. Overall, these two studies demonstrate that crab zoea use multiple forms of inducible defenses (behavioral, physiological, and morphological) to avoid predation (Charpentier and Cohen 2015, Charpentier et al. 2017).

Like zooplankton, phytoplankton use chemical cues of predators to induce defenses and avoid predation. In a study by Lindström and colleagues, the dinoflagellates *Lingulodinium polyedra* and *Alexandrium tamarense* increased the intensity of their bioluminescence in response to copepodamides (**1-8**), the previously described compounds exuded by predatory copepods (2017). The greatest increase in light intensity in both species was in response to copepodamides combined with mechanostimulation,

which mimics how algae might experience attack by copepods (Lindström et al. 2017). In contrast to previous studies with live copepods (Selander et al. 2011, Selander et al. 2012), copepodamides did not induce changes in cell size or swimming behavior in either dinoflagellate (Lindström et al. 2017). While the study demonstrates that bioluminescence intensity is induced by predator chemical cues further work is needed to show that the increased bioluminescence results in lower grazing rates on *L. polyedra* and *A. tamarensis* due to release from predation mediated by a tritrophic interaction.

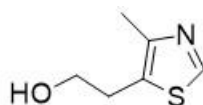
In a pair of studies Wohlrab and colleagues analyzed how gene expression (2016) and phenotype (2017) varied between two strains of *A. fundyense* with respect to predator response. One strain formed larger chains, produced less PSTs (**22-27**), and was lytic against the cryptomonad *Rhodomonas* sp. (hereby called the lytic strain) and the other strain formed some small chains, produced high levels of PSTs, but was non-lytic (hereby called the non-lytic strain) (Wohlrab et al. 2016, Wohlrab et al. 2017). Many genes which were more highly expressed in the lytic strain belonged to proteins known to be involved in secondary metabolism; yet these genes were not differentially expressed in either strain in response to chemical cues from a caged grazing predator (Wohlrab et al. 2016). Exposure of the lytic strain of *A. fundyense* to a caged dinoflagellate predator, *Polykrikos kofoidii*, grazing on the non-lytic conspecific strain did not result in upregulation of secondary metabolism genes that were differentially expressed between the two strains (Wohlrab et al. 2016). Therefore, the authors suggest that secondary metabolism genes that were more highly expressed in the lytic strain in the absence of the predator are either not involved in the production of the lytic compound(s) or production of the lytic compounds is not an inducible anti-predatory trait (Wohlrab et al. 2016). However,

assays have not yet been carried out to directly assess if lytic capability changes in this environment. Additionally, it would be valuable to test whether induction of the lytic compound(s) is strain-specific. Furthermore, chemical characterization of the lytic compound(s) may determine which genes are involved in their production. In contrast to the lytic strain, when the non-lytic strain of *A. fundyense* was exposed to grazing caged *P. kofoidii*, the non-lytic strain increased expression of genes for proteins involved in isoprenoid and polyketide biosynthesis (Wohlrab et al. 2016) suggesting that the non-lytic strain may possess an as of yet undescribed, inducible chemical defense. The differences in gene expression in response to the predator were not as strong as the initial differences between the two strains (Wohlrab et al. 2016). When these same strains were exposed to caged or uncaged copepod predators (*Centropages typicus*), both strains shifted toward smaller cell size and shorter chains (Wohlrab et al. 2017). Direct grazing resulted in increased production of PSTs in both strains but only the lytic strain increased production of PSTs in response to chemical cues from copepods alone (Wohlrab et al. 2017). Wohlrab and colleagues argued that in the absence of predation the non-lytic strain is already in a more defended phenotype based on the lower grazing rates on the non-lytic strain compared to the lytic strain at the start of the copepod grazing experiment; therefore, the non-lytic strain does not need to change as much to defend itself (2017). On the other hand, the lytic strain is more vulnerable to some predators; however, once there are grazer cues the lytic strain drastically changes its phenotype to a more defended state which results in lower grazing rates (Wohlrab et al. 2017). In general, this resulted in the lytic strain more closely resembling the non-lytic strain (Wohlrab et al. 2017). These two studies (Wohlrab et al. 2016, Wohlrab et al. 2017) highlight the complexity

and specificity of chemical interactions within phytoplankton species and between phytoplankton and their predators.

In a partner study to a 2015 study which investigated how variability in calcification and DMSP (**20**) production in the coccolithophore *Emiliana huxleyi* strains affect predation by several microzooplankton (Harvey et al.), Poulson-Ellestad and colleagues found that the metabolites exuded by four different strains of *E. huxleyi* were affected by grazing by the dinoflagellate *Oxyrrhis marina* (2016). *O. marina* grazing coefficient, a function of grazing rate adjusted for prey and predator concentrations, and growth rate were variable across the four strains, independent of calcification. Using metabolomics, the authors discovered substantial variability in the metabolites exuded by *E. huxleyi* strains with less than 25% similarity between any two strains that had been exposed to *O. marina* grazing. Additionally, no single metabolite changed the same way in all of the strains (Poulson-Ellestad et al. 2016). Nevertheless, the concentration of 4-methyl-5-thiazoleethanol (**60**), a metabolite produced by both *O. marina* and *E. huxleyi*, positively correlated with the grazing coefficient of *O. marina* on three of the four strains of *E. huxleyi* (Poulson-Ellestad et al. 2016). However, its concentration was variable across the strains with regard to ingestion and growth rate of *O. marina* suggesting the change in concentration of **60** in response to grazing pressure was not uniform across the three strains (Poulson-Ellestad et al. 2016). Overall, this study illuminates how chemically different strains of the same species can be and how even their response to predation may not unify their metabolism. Differences in metabolism and response to predation is strain-specific and important to keep in mind as we work to better understand

the chemical interactions involved in predator-prey interactions, especially when it comes to studying chemical defenses and predation cues.



4-methyl-5-thiazoleethanol (60)

Figure 1.14 Chemical structure of 4-methyl-5-thiazoleethanol (60), a metabolite produced by both *Oxyrrhis marina* and *Emiliania huxleyi*.

1.8 Community and ecosystem effects

1.8.1 Community and ecosystem effects

The allelopathic effects of diatom-produced secondary metabolites on multiple pelagic trophic levels are not well understood. It has been suggested that diatom polyunsaturated aldehyde (PUA) production functions mainly to deter microzooplankton herbivory (Flynn and Irigoien 2009) and suppress the growth of competitors (Casotti et al. 2005). However, a more recent study did not observe growth suppression of competing phytoplankton in the presence of diatom-produced PUAs. In a tritrophic system where copepods eat both microzooplankton and phytoplankton, Franzè and colleagues found evidence that PUAs reduce ciliate microzooplankton grazing while increasing predation by the copepod *Acartia tonsa* (2017). This suggests a cost-benefit tradeoff for diatoms; however the study did not determine whether the effect on copepods was general or species-specific. While PUA treatments contained natural ratios and

concentrations, only (2*E*,4*E*)-2,4-octadienal (**61**) and (2*E*,4*E*)-2,4-heptadienal (**62**) were used to create these conditions, excluding many other PUAs that have previously been associated with diatoms (Franzè et al. 2017). Further experiments that utilize a more comprehensive mixture of PUAs may reveal whether different classes of bloom-associated metabolites will produce similar trophic cascade effects.

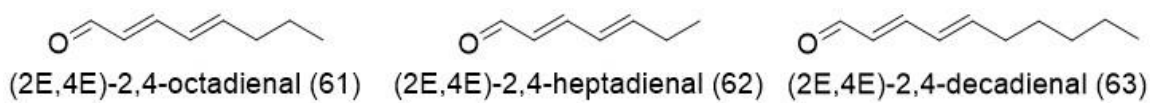


Figure 1.15 Polyunsaturated aldehydes produced by diatoms: (2*E*,4*E*)-2,4-octadienal (61**), (2*E*,4*E*)-2,4-heptadienal (**62**), and (2*E*,4*E*)-2,4-decadienal (**63**).**

In communities living on particulate matter in the open ocean, PUAs were found to affect bacteria that metabolize particulate organic carbon derived from phytoplankton (Edwards et al. 2015). Bacterial metabolic activity increased at PUA concentrations of 1 and 10 μM as was measured by respiration, cellular growth, hydrolysis of lipids, and acid phosphatase activity associated with the release of inorganic phosphorus into the water column. In contrast, high concentrations of PUAs, near 100 μM , were inhibitory and caused a shift in the composition of the microbial community (Edwards et al. 2015). Naturally occurring PUAs (**61**, **62**, and (2*E*,4*E*)-2,4-decadienal (**63**)) that diffused from naturally acquired particulate organic carbon were measured at micromolar concentrations (Edwards et al. 2015). These concentrations are much higher than the previously reported picomolar concentrations in the open ocean (Vidoudez et al. 2011, Bartual et al. 2014), but the observed changes in bacterial response may indicate that

sinking organic particles act as PUA hotspots. These results also suggest that PUAs modulate the remineralization of particulate organic carbon at shallow ocean depths which could reduce the ocean's efficiency as a carbon sink.

Mechanisms for how domoic acid (**44**) is transferred from the plankton to the benthos are understudied, and Schnetzer and colleagues suggest that exposure to **44** produced by the diatom *Pseudo-nitzschia australis* could be high for particle-associated microbes associated with marine snow (2017). Under colder, darker conditions, decomposition of marine snow contributed to an increase in dissolved **44**, but the acute toxicity and consequences of chronic exposure for organisms associated with these degrading aggregates was not tested (Schnetzer et al. 2017). Diatom toxins such as **44** have also been found to bioaccumulate in eukaryotic organisms with the potential to affect growth, reproduction, and behavior, thus having a large effect on food web dynamics. High concentrations of **44** associated with *Pseudo-nitzschia* spp. blooms were reported during the 2015 *Eubalaena australis* whale calving season in Golfo Nuevo, Argentina (D'Agostino et al. 2017). Copepods were the most abundant mesozooplankton in the study area and the authors suggested that they were the primary vector for transferring **44** to *E. australis*. However, other mesozooplankton could not be excluded as the primary vector since rates of **44** bioaccumulation and detoxification in different species were not determined (D'Agostino et al. 2017). In another study it was suggested that Scottish harbor seal (*Phoca vitulina*) populations may be negatively affected by **44** associated with *Pseudo-nitzschia* spp. Blooms (Jensen et al. 2015). A correlation was observed between **44** in *P. vitulina* urine and their decline in population on the east coast of Scotland. Additionally, *P. vitulina* from the eastern and northern Scottish coasts were

more likely to show **44** urine contamination than those found along the west coast (Jensen et al. 2015). Detection of **44** and PSTs (*e.g.* **22-30**) in fecal samples suggested that seals are exposed to these toxins through several fish including plaice, dab, and cod (Jensen et al. 2015). Fish collected in the same area contained detectable levels of both types of toxins making them plausible vectors for transferring toxins to seals (Jensen et al. 2015).

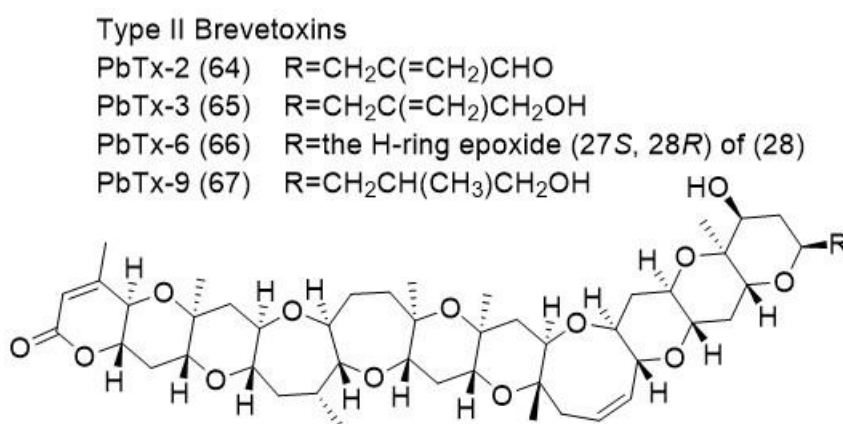


Figure 1.16 Brevetoxins (PbTx) -2 (64), -3 (65), -6 (66), and -9 (67) produced by the dinoflagellate *Karenia brevis*.

Bioaccumulation of dinoflagellate toxins in turtles and shellfish continues to be a problem along the Florida gulf coast where toxic *Karenia brevis* blooms occur. One study showed a correlation between total tumor score and accumulation of brevetoxins (**64-67**) in green sea turtles (*Chelonia mydas*), a species known to suffer from fibropapillomatosis (Perrault et al. 2017). However, plasma concentrations of brevetoxins measured in green and Kemp's ridley sea turtles in this study were the lowest recorded, which may indicate that detoxification pathways are upregulated or that brevetoxins do not bioaccumulate in

the plasma of all turtle species. Perrault and colleagues suggested that abundance of brevetoxins in plasma was low because sampled turtles were exposed to the end of a bloom. In another study, the invasive green mussel *Perna viridis* retained brevetoxins at high concentrations after a *K. brevis* bloom (McFarland et al. 2015). The detoxification of this mussel was slower than that of native oysters *Crassostrea virginica* and clams *Mercenaria mercenaria* posing a risk for the transfer of *K. brevis* toxins to higher trophic levels (McFarland et al. 2015). Previous studies investigated how the New Zealand green-lipped mussel, *Perna canaliculus*, accumulated brevetoxins from a *Karenia selliformis* bloom (Morohashi et al. 1995, Ishida et al. 2004a, Ishida et al. 2004b), but McFarland and colleagues are the first to study brevetoxins accumulation in *P. viridis*.

Another investigation reported that feeding on PSTs (e.g. 22-30) and bioactive extracellular compound (BEC) producing *Alexandrium minutum* strains had strain-specific effects on the escape response of juvenile *Pecten maximus* scallops to a predatory starfish (Borcier et al. 2017). After feeding on the BEC-producing strain scallops reacted more slowly, whereas, after feeding on the strain which produces PSTs scallops had normal reaction times but still failed to escape (Borcier et al. 2017). This is in agreement with previous findings that clams exposed to PST-producing *A. tamarense* experienced muscle paralysis from bioaccumulated PSTs which made them more vulnerable to predators (Bricelj et al. 2005). On the other hand, the scallops exposed to the BEC-producing strain experienced the greatest reduction in filtration rate (Borcier et al. 2017). This illuminates the need to characterize the bioactive extracellular compounds of *A. minutum*. Additionally, these results suggest that both classes of compounds produced by *A. minutum* reduce behavioral responses of *P. maximus*, although the effects of PSTs and

BEC strains do not appear to be chronic (Borcier et al. 2017). Most importantly, this study highlights the necessity of not assuming that the known toxins, in this case the PSTs, of prey are responsible for all deleterious effects on predators (Borcier et al. 2017).

In addition, a recent study by Toth and colleagues presented evidence that teredinid shipworm larvae find wood (*Picea abies*) using waterborne chemical cues (2015). Field experiments showed shipworm larvae to prefer nets with wood over nets without wood. Future experiments could test larval attraction to extracts of multiple types and sizes of wood. Maximum and average larval swimming speeds were also determined (Toth et al. 2015); however, this part of the study used veliger blue mussel (*Mytilus edulis*) larvae instead of shipworms. Therefore, it will be important to determine whether teredinid and veliger larvae swim faster when exposed to wood-based chemical attractants.

1.8.2 Bacterial dynamics

Several studies reported how bacterial quorum sensing molecules affect bacteria-phytoplankton community dynamics. Harvey and colleagues found that *Pseudoalteromonas piscicida* produces the autoinducer precursor 2-heptyl-4-quinolone (**68**) which, at nanomolar concentrations, stops growth in the coccolithophore *Emiliana huxleyi* (Harvey et al. 2016). Since **68** alone did not recapitulate the rapid mortality caused by the whole exudate of *P. piscicida* it is likely that a mixture of compounds kills coccolithophores as seen under natural conditions. While *P. piscicida* concentrations in these experiments were above those found in nature, the authors suggest that their experimental design mimics the natural environment of bacteria co-occurring with algae

(Harvey et al. 2016). In addition, **68** had no effect on microalgae *Dunaliella tertiolecta* or *Phaeodactylum tricornutus* which suggests that differences in growth suppression among various phytoplankton species have the potential to alter community dynamics (Harvey et al. 2016). A next logical step would be to investigate the effect of **68** in microcosm experiments involving *P. piscicida* and multiple species of phytoplankton.

Acyl homoserine lactones, a class of quorum sensing autoinducers, were found to affect hydrolytic enzyme activity of particle-associated bacteria (Krupke et al. 2016). Acyl homoserine lactones variably inhibited or stimulated phosphatase, aminopeptidase, and lipase activities in samples from different study sites which shows that additional unknown factors are involved in enzymatic regulation of collected bacteria (Krupke et al. 2016). Quorum sensing autoinducers may be important for regulation of particulate organic carbon degradation, and ultimately carbon flux and biological pump efficiency, but the relationship remains unclear.

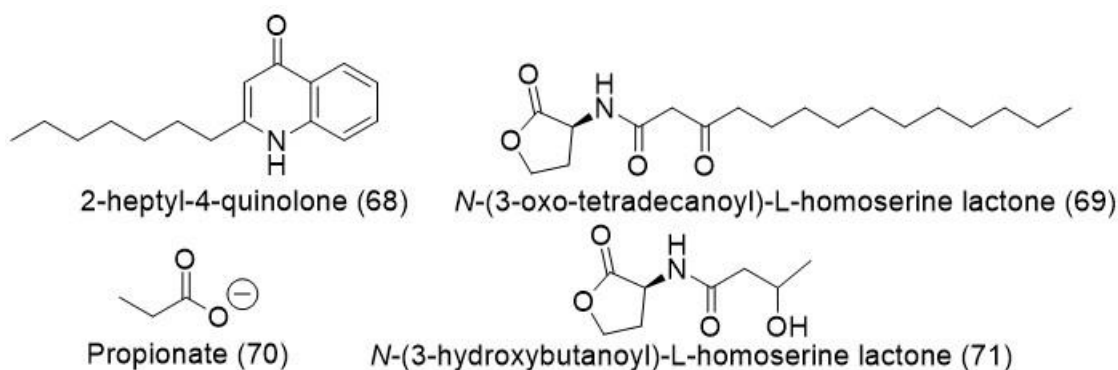


Figure 1.17 Bacterial quorum sensing molecules *N*-(3-oxo-tetradecanoyl)-L-homoserine lactone (**69**) and *N*-(3-hydroxybutanoyl)-L-homoserine lactone (**71**). Chemical structures of the autoinducer precursor 2-heptyl-4-quinolone (**68**), produced by *Pseudoalteromonas piscicida*, and propionate (**70**), a precursor of DMSP (**20**).

In a study by Johnson and colleagues, the bacterium *Ruegeria pomeroyi* was found to increase production of the quorum sensing autoinducer *N*-(3-oxotetradecanoyl)-L-homoserine lactone (**69**) when grown on algal-derived DMSP (**20**) (2016). However, when grown on propionate (**70**) which represents a portion of the structure of **20**, production of autoinducers did not increase indicating that **20** functions as signal in addition to being a food source. Therefore, production of **20** by other organisms has the potential to alter inter- and intra-species bacterial communication by upregulating production of signaling molecules (Johnson et al. 2016).

Bacteria associated with microalgae may play an important role in protecting aquaculture against pathogenic organisms. *Bacillus* sp. isolated from the microalga *Chaetoceros muelleri* degrades *N*-hexanoyl-L-homoserine lactone (**12**) and *N*-(3-hydroxybutanoyl)-L-homoserine lactone (**71**) (Pande et al. 2015). The latter is produced by pathogenic *Vibrio campbellii* and its removal by *Bacillus* sp. increases the survival of prawn (*Macrobrachium rosenbergii*) larvae raised in aquaculture (Pande et al. 2015). The strategy of using *Bacillus* sp. to remove *Vibrio* quorum sensing autoinducers could be extended to benefit other animals raised in the aquaculture industry as an alternative to using antibiotics.

There has been some evidence that intraspecific and interspecific competition among bacteria may be facilitated by algal blooms. A bacteria resource utilization model based on spatiotemporal response to lysed diatoms predicted that competition favors chemotaxis under bloom conditions (Smriga et al. 2016). While the model simplified dissolved organic matter to be a single substance, different diffusivity values predicted that motile bacteria's exposure to slowly diffusing molecules does not increase during

lysis of a diatom cell even though they are the main consumers of dissolved organic matter (Smriga et al. 2016). In an additional study, unique microbiomes were identified for harmful algal bloom-associated dinoflagellates *Alexandrium fundyense* and *Dinophysis acuminata* (Hattenrath-Lehmann and Gobler 2017). Exposure to exuded compounds of both algae resulted in specific bacterial profiles where growth was either suppressed or promoted (Hattenrath-Lehmann and Gobler 2017). However, the chemical components of the exudates have not been reported. While both types of algae were associated with microbiomes dominated by Flavobacteria, the assumption that allelochemicals suppress growth of competing bacteria is only one possible hypothesis and further work should be done to determine the chemicals that allow Flavobacteria to dominate microbial communities during harmful algal blooms (Hattenrath-Lehmann and Gobler 2017).

Bacterial communities associated with marine diatoms may play an important role in degrading aromatic hydrocarbons in crude oil and facilitating the production of marine oil snow. Mishamandani and colleagues found that there are transitions in dominance of bacterial community members associated with *Skeletonema costatum* when exposed to crude oil (2016). Specifically, an increase in *Methylophaga* population size was observed followed by increases in several species of hydrocarbonoclastic bacteria. These microbial communities were found to be capable of degrading polycyclic hydrocarbons naphthalene (**72**), phenanthrene (**73**), and some additional alkylated naphthalene derivatives (Mishamandani et al. 2016).

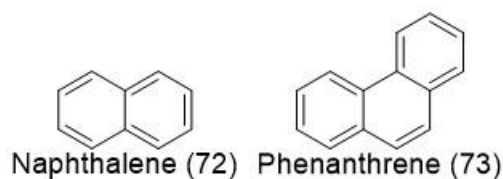


Figure 1.18 Polycyclic hydrocarbons, naphthalene (72) and phenanthrene (73), which are degraded by microbial communities associated with the diatom *Skeletonema costatum*.

Additionally, PUAs were shown to be more toxic to marine bacteria at higher concentrations and toxicity of these molecules increased with chain length for *2E,4E/Z*-dienals (e.g., **61-63**) (Pepi et al. 2017). The degree of saturation of membrane phospholipid fatty acids in the bacteria increased with increasing concentration of PUA exposure and decreasing cell growth (Pepi et al. 2017). However, the PUA concentrations used for these experiments (Pepi et al. 2017) were much higher than previously measured during a *Skeletonema marinoi* bloom in the Adriatic Sea (Vidoudez et al. 2011) and even higher than localized concentrations associated with marine particles in another report discussed earlier (Edwards et al. 2015). If PUAs are truly toxic for specific species of marine bacteria at natural concentrations, then these compounds have the potential to disrupt and alter natural microbial communities.

1.8.3 Effects of global change

Zooplankton preferences with respect to salinity, pH, and predator waterborne chemical cues were studied using larvae of the polychaete *Platynereis dumerilii* and the copepod *Euterpina acutifrons* as models (Ramanathan et al. 2015). A microfluidics chip designed for these experiments served as a useful instrument for observing zooplankton

larval behaviors under various conditions and has potential as a tool for studying ocean acidification (Ramanathan et al. 2015). *P. dumerilii* preferred pH ranges close to neutral and a salinity range comparable to and slightly above that of the open ocean (Ramanathan et al. 2015). Ramanathan and colleagues suggested that zooplankton larvae use high salinity as a proxy for nutrient richness. *E. acutifrons* had a slightly higher pH preference, just above neutral, which could have negative implications as ocean pH continues to decrease due to climate change (2015). Both zooplankton preferred natural sea water over waterborne chemical cues from sea bass, a predator (Ramanathan et al. 2015). In addition, *P. dumerilii* larvae preferred extracts of *Dunaliella* microalgae over *Isochrysis*, and when ciliated cells found in the larval foregut were ablated, the larval reaction time to the extract slowed (Ramanathan et al. 2015). One possibility is that these cells act as chemoreceptors and allow the larvae to detect potential food sources. Interactions between receptors in the larval foregut and metabolites released by algal prey is an area that should be further explored.

A study by Hattenrath-Lehmann and colleagues explored how increased levels of carbon dioxide impact the growth and toxicity of *Alexandrium fundyense* (2015). A strain from Northport Bay, New York, (USA) upon being treated with increasing CO₂ levels, displayed higher growth rates and toxicity attributed to increased concentrations of particularly toxic diastereomers GTX-1 (**24**) and -4 (**27**) (Oshima 1995, Hattenrath-Lehmann et al. 2015). However, toxicity of another strain, from the Bay of Fundy, Canada located about 700 km away, did not change with increasing carbon dioxide (Hattenrath-Lehmann et al. 2015). The results from this study suggest that increasing acidification of our oceans could facilitate *A. fundyense* harmful algal bloom formation

and make blooms more toxic, but not in a way predictable across genetically diverse populations.

1.9 Conclusions

The chemical ecology of the marine plankton continues to be an active field of research. Greater attention has been aimed at understanding the influence of bacteria on phytoplankton natural product biosynthesis, induction, and metabolism. Recent work has focused on the effects of quorum sensing of marine planktonic bacteria especially with respect to bacterial-algal relationships and community level interactions. Additionally, much attention has been devoted to phytoplankton chemical defenses, particularly PSTs (*e.g.* 22-30); however, there continues to be problems with assumptions being made that known phytoplankton “toxins” function as chemical defenses without explicitly demonstrating that they serve defensive functions. In comparison to the previous review (Schwartz et al. 2016) there have been more recent studies on intraspecific signaling and fewer studies on allelopathic interactions. However, there continues to be a relative scarcity of studies on chemical cues involved in parasitic interactions.

Full characterization and isolation of the compounds responsible for chemically mediated pelagic interactions remains problematic, evidenced by the small number of novel natural products published from these study systems during the reporting period. Small quantities, diffusion, and instability of many of these compounds has made it difficult to isolate individual compounds but continued advancements in techniques and instrumentation support improvements in the field. The use of -omics (metabolomics, proteomics, and transcriptomics) are revealing candidate signaling molecules and the

mechanisms of biological response to many chemical signals and cues. In fact, a recent review by Kuhlisch and Pohnert highlighted how metabolomics has successfully been applied in many chemical ecology studies (2015). Along with discerning the environmental impacts of algal toxins in their ecological communities, more studies could be undertaken to predict how they might influence interactions in other communities as many of the harmful algal bloom species expand and shift their niches due to climate change (Gobler et al. 2017). As the field advances scientists also need to persist in the hard work of using ecologically relevant approaches while studying allelopathy and chemical defenses, with consideration of natural concentrations verified from field samples, and testing defenses using appropriate ecological targets and compound dispersal methods. Albeit less studied than terrestrial or marine benthic systems, chemically mediated interactions are clearly important planktonic ecosystems and therefore represent a rich source of novel natural products yet to be discovered.

CHAPTER 2. HARMFUL ALGA TRADES OFF GROWTH AND TOXICITY IN RESPONSE TO CUES FROM DEAD PHYTOPLANKTON

This section is reproduced from Brown, E. R., and J. Kubanek. 2020. Harmful alga trades off growth and toxicity in response to cues from dead phytoplankton. *Limnology and Oceanography* 65:1723-1733; <https://doi.org/10.1002/lno.11414>.

2.1 Abstract

Organisms are under selection pressure to recognize predators and assess predation risk to avoid becoming prey. In some cases, the presence of injured competitors alerts individuals to the likelihood that predators are nearby. Previous studies have shown that the marine dinoflagellate *Alexandrium minutum* responds to chemical cues from copepods by dramatically upregulating sodium channel-blocking toxins that appear to function as defenses against copepod grazing. However, it is unknown whether *A. minutum* uses other cues, such as damaged phytoplankton, some of which are its competitors, to assess predation risk and subsequently increase its resistance to predators. To investigate the role of dead phytoplankton cues in chemical defense plasticity, *A. minutum* was exposed for three days to chemical cues from six different phytoplankton. Chemical cues from dead, unrelated, historically co-occurring phytoplankton species induced toxin production in *A. minutum* coincident with a decrease in growth. In contrast, exposure to chemical cues from more closely related dead phytoplankton, either conspecific or congeneric, suppressed toxin production in

A. minutum relative to their absence. This was coupled with a modest, yet significant, increase in growth. The consistent inverse relationship between toxin production and growth suggests that *A. minutum* experiences a trade-off. Together, these results reveal that relatedness of dead phytoplankton is important in how *A. minutum* utilizes resources for growth and defense.

2.2 Introduction

Predation is an important factor controlling phytoplankton populations (Sherr and Sherr 1988, Weisse 1991, Strom 2008). Filter-feeding animals and zooplankton have been implicated in the termination of phytoplankton blooms (Alpine and Cloern 1992, Smayda 2008). It is estimated that 60-75% of phytoplankton mortality in the oceans is due to microzooplankton grazing (Calbet and Landry 2004). Thus, like organisms in other ecosystems, phytoplankton are under selection pressure to recognize predators and assess predation risk to avoid becoming prey (Lima and Dill 1990).

Organisms can detect predators using visual, auditory, mechanical, or olfactory stimuli (Bollens et al. 1994, Lass and Spaak 2003, Malavasi et al. 2008). After perceiving predators some organisms undergo dramatic changes in behavior, morphology, and defense in order to avoid attack (Pohnert et al. 2007, Hay 2009, Scherer and Smee 2016). Both the copepod *Acartia hudsonica* and the cladoceran *Daphnia magna* recognize diurnal predatory fishes and avoid them through diel vertical migration. *A. hudsonica* employs visual and mechanical cues (Bollens et al. 1994), whereas *D. magna* utilizes chemical cues (Loose and Dawidowicz 1994, Hahn et al. 2019). Other *Daphnia* spp. react to compounds excreted by midge fly larva, water fleas, and freshwater copepods,

increasing their helmet size which allows them to avoid gape-limited predators (Laforsch and Tollrian 2004, Weiss et al. 2018). Compounds emitted by predators also trigger morphological and chemical defenses in single-celled organisms such as dinoflagellates and diatoms, which decrease chain length and increase toxin production after detecting copepods (Selander et al. 2006, Selander et al. 2011, Amato et al. 2018, Selander et al. 2019). Recently, toxin induction in *Alexandrium minutum* was attributed to a family of molecules called copepodamides excreted by copepods (Selander et al. 2015).

In addition to detection of predators, many organisms assess predation risk indirectly through feeding cues associated with predation events (Scherer and Smee 2016). For example, cues from grazing copepods stimulate greater toxin production in *A. minutum* than cues from starved copepods (Selander et al. 2006). This is likely due to increased copepodamide production when copepods are feeding (Selander et al. 2015) but may also be partly caused by cues released by grazed phytoplankton from sloppy feeding. For instance, *Alexandrium catenella* (previously *A. fundyense*) increases toxin production when exposed to lysed conspecifics (Senft-Batoh et al. 2015b). Similarly, compounds released from macerated conspecifics, and even some heterospecifics, elicit growth in defensive helmets in several species of *Daphnia* (Laforsch et al. 2006). In fact, many organisms from diverse taxa use cues from dead competitors when assessing predation risk (Chivers et al. 1997, Hazlett and McLay 2005, Schoeppner and Relyea 2005, Dalesman et al. 2007).

When organisms react to cues from dead competitors, their response may be correlated with either the phylogenetic relatedness or the historical, geographic co-occurrence of the competitor. Since competitors often share predators, cues from more

closely related competitors may trigger stronger anti-predatory behaviors due to greater risk of being attacked (Schoeppner and Relyea 2005, Dalesman et al. 2007). Therefore, cues from dead, closely related competitors are expected to be a reliable indication of high predation risk. Alternatively, an organism might respond strongly to cues from dead competitors that they frequently encounter as an indication that there is a hungry predator nearby (Chivers et al. 1997, Scherer and Smee 2016). The effects of cues from dead competitors and the influence of relatedness and co-occurrence of the competitors has been relatively well studied in animals (Chivers et al. 1997, Hazlett and McLay 2005, Schoeppner and Relyea 2005, Dalesman et al. 2007, Scherer and Smee 2016); however, there have been almost no studies in single-celled organisms such as phytoplankton.

The goal of the current study was to investigate whether *A. minutum* uses cues from dead phytoplankton, some of which act as competitors, to assess predation risk and subsequently upregulate toxin production. Furthermore, we endeavored to explore the relative importance of phylogenetic relatedness and historical, geographic co-occurrence of the dead phytoplankton as cues for predation risk. We hypothesized that *A. minutum* uses cues from dead phytoplankton as an indication of imminent predation risk and consequently upregulates toxin production if the cues were derived from closely related and historical co-occurring phytoplankton. Alternatively, *A. minutum* might invest less in chemical defense and more in growth in response to cues from closely related phytoplankton if its toxins are ineffective at preventing predation.

2.3 Materials and methods

2.3.1 Phytoplankton cultivation

Cultures of the dinoflagellates *Alexandrium minutum* strain CCMP 113, *Prorocentrum lima* strain CCMP 686, *Prorocentrum micans* strain CCMP 688, and *Coolia monotis* strain CCMP 304 were grown in monoculture at 15 °C with irradiance of 89-100 $\mu\text{mol m}^{-2}\text{s}^{-1}$ and *Alexandrium pacificum* strain CCMP 1493 and *Alexandrium tamarense* strain CCMP 2023 were maintained as monocultures at 21 °C with irradiance of 100-145 $\mu\text{mol m}^{-2}\text{s}^{-1}$. All cultures were acquired from NCMA Bigelow Laboratory and grew in filtered seawater from the Gulf of Maine (NCMA Bigelow Laboratory, 35 ppt) amended with full strength K media minus Si (Keller et al. 1987) in incubators set on a 12:12 h light:dark cycle. Cells were enumerated visually using at least two sets of 10 whipple disc grid fields of view and a minimum of 150 cells counted in a 125 μL Palmer-Maloney counting cell on an Olympus IX-50 inverted microscope after preservation with a 1% acidified Lugol's solution and by in vivo fluorescence using a Turner Design Trilogy fluorometer. Biomass for each phytoplankton species was calculated by first measuring their biovolumes, using 30 living cells visualized with an eyepiece reticle on an Olympus IX-50 microscope, noting the corresponding shapes for each phytoplankton species, as described by Hillebrand and colleagues (1999). Biomass for each phytoplankton was then calculated using the carbon to volume equation for all dinoflagellates from Menden-Deuer and Lessard (2000) (Table 2.1).

Table 2.1 Comparison of the cell size, biomass, and concentration of lysed phytoplankton added to *Alexandrium minutum* replicates for Experiments 1.

Lysed phytoplankton species	Biovolume ($\mu\text{m}^3 \text{ cell}^{-1}$)	Biomass (pgC cell^{-1})	Lysed phytoplankton -to- <i>A. minutum</i> ratio by biomass
<i>Alexandrium minutum</i>	6,963	1,064	1:3
<i>Alexandrium pacificum</i>	21,812	2,719	2.6:3
<i>Alexandrium tamarense</i>	11,112	1,565	1.5:3
<i>Prorocentrum lima</i>	14,158	1,908	1.8:3
<i>Prorocentrum micans</i>	16,764	2,192	2.1:3
<i>Coolia monotis</i>	15001	2,001	1.9:3

2.3.2 Experimental design

2.3.2.1 Preparation of chemical cues from dead phytoplankton

To investigate whether phylogenetic relatedness to *A. minutum* strain CCMP 113 and/or historical co-occurrence of a phytoplankton with *A. minutum* are important in determining the ability of *A. minutum* to use the damaged phytoplankton as an indication of predator presence, experiments were carried out similar to those conducted by Senft-Batoh and colleagues (2015b). By this design, phytoplankton lysates were added to cultures of *A. minutum* CCMP 113 in order to simulate nearby phytoplankton being grazed upon, without introducing cues from the grazers themselves. The following phytoplankton were used: a conspecific (individuals of the same strain of *A. minutum*, CCMP 113), a co-occurring congener (*A. tamarense*, CCMP 2023), a non-co-occurring congener (*A. pacificum*, CCMP 1493), and three co-occurring less closely related dinoflagellates (*P. lima*, CCMP 686; *P. micans*, CCMP 688; *C. monotis*, CCMP 304). These phytoplankton were chosen because they come from coastal waters of northern Spain (except *A. pacificum*) and are expected to share similar predators. Additionally,

despite some of the species tending to be mostly benthic (*P. lima* and *C. monotis*), they should each directly compete at least occasionally with *A. minutum* for nutrients, particularly due to the regular oscillation of upwelling and downwelling in the region which results in large-scale mixing of nutrients (Álvarez-Salgado et al. 2000, Tilstone et al. 2000). For both Experiments 1 and 2, aliquots which contained appropriate concentration of cells, or biomass, were harvested from each phytoplankton monoculture when they were in exponential growth phase. The cells were then concentrated by centrifugation and the media decanted to bring the final volume of each aliquot to approximately 2 mL. The aliquots were stored at -80 °C. Daily for three days, concentrated aliquots of phytoplankton cells were lysed via four freeze-thaw cycles with sonication via a bath (lysis was confirmed by microscopy) and added to *A. minutum* as described below.

2.3.2.2 Experiment 1

The first experiment was performed in six batches, each including a subset of the dead phytoplankton treatments as well as control cultures where *A. minutum* was grown with an equivalent volume of full strength K media added (“media control”) instead of the addition of lysed cells (Table 2.2). The total replicate number for each treatment across the six batches was as follows: $n=43$ for the media control, $n=12$ for the conspecific treatment, $n=12$ for the co-occurring congener treatment, $n=12$ for the non-co-occurring congener treatment, and for the less related co-occurring phytoplankton treatment $n=16$ for *P. lima*, $n=12$ for *P. micans*, and $n=12$ for *C. monotis*. Batches were initiated when *A. minutum* was in exponential growth phase at a population density of $\sim 15\text{-}20,000$ cells mL^{-1} . To initiate the experiment for each batch, a 1.0 mL aliquot of

A. minutum was preserved from each replicate with 1% acidified Lugol’s solution and visually enumerated. Phytoplankton lysates were prepared as described earlier and added daily for three days to cultures of *A. minutum* in a ratio of 1:3 lysed phytoplankton cells to *A. minutum* cells, as per Senft-Batoh et al. (2015b), corresponding to ratios of lysed phytoplankton to *A. minutum*, by biomass, as reported in Table 2.1. On the fourth day, a 1.0 mL aliquot of *A. minutum* from each replicate was preserved with 1% acidified Lugol’s solution and visually enumerated. The remaining *A. minutum* cells were harvested and extracted for intracellular toxin analysis, as described below. Percent growth was calculated using the cell counts from the start and end points of each *A. minutum* replicate.

Table 2.2 Distribution of treatments of chemical cues from dead phytoplankton and replicates across batches (Experiment 1).

Batch	Chemical cues from dead phytoplankton	Number of replicates
1	Media control	4
	<i>A. minutum</i>	4
	<i>A. pacificum</i>	4
	<i>A. tamarensis</i>	4
2	Media control	4
	<i>A. minutum</i>	4
	<i>A. pacificum</i>	4
	<i>A. tamarensis</i>	4
	<i>P. lima</i>	4
3	Media control	4
	<i>A. minutum</i>	4
	<i>A. pacificum</i>	4
	<i>A. tamarensis</i>	4
	<i>P. lima</i>	4
4	Media control	8
	<i>P. lima</i>	8
5	Media control	11
	<i>P. micans</i>	12
6	Media control	12
	<i>C. monotis</i>	12

2.3.2.3 Experiment 2

Experiment 2 was conceived separately to test the effects of nutrients and concentration of dead phytoplankton cues on toxin production and growth of *A. minutum* using similar methods to Experiment 1 but with lysates from only one dead phytoplankton, the non-co-occurring congener *A. pacificum* (CCMP 1493). In this experiment, *A. minutum* was grown with either daily additions of 2 mL of full strength K media (“media control”, $n=8$), modified K media diluted so that ammonia and nitrate concentrations were equivalent to the 2.6:3 treatment *A. pacificum* lysate (“dilute media control”, $n=8$), *A. pacificum* lysate at the same concentration ratio as Experiment 1 (1:3 lysed *A. pacificum* cells to *A. minutum* cells equivalent to 2.6:3 by biomass) (“2.6:3 treatment”, $n=8$), or *A. pacificum* lysate at a concentration ratio of 0.38:3 lysed *A. pacificum* cells to *A. minutum* cells (equivalent to 1:3 by biomass) (“1:3 treatment”, $n=8$) for three days. The *A. pacificum* lysates were prepared as described earlier. The experiment was initiated when *A. minutum* was at a population density of $\sim 19,000$ cells mL^{-1} and a 1.0 mL aliquot of *A. minutum* was preserved from each replicate for visual enumeration. On the first day, three additional aliquots of *A. pacificum* lysate were prepared for the 2.6:3 treatment for the purpose of having lysate available to measure ammonia and nitrate, which became the basis for the ammonia and nitrate concentrations in the dilute media controls. The cell debris from the lysates were pelleted by centrifugation and from the supernatant, 200 μL and 40 μL were collected for ammonia and nitrate analyses, respectively. Ammonia concentrations of the three *A. pacificum* lysate supernatants, three aliquots of seawater, and three aliquots of full strength K media were measured in duplicate (Table 2.3) using a Sigma-Aldrich Ammonia Assay Kit with

samples transferred into a 96 well plate and read at 340 nm on a Thermo Scientific Multiskan GO microplate spectrophotometer following the manufacturer's protocol (Sigma-Aldrich, St. Louis, MO, USA). For nitrate analysis, the three lysate supernatants were diluted 10-fold and three aliquots of full strength K media were diluted 50-fold with Cayman Chemicals Nitrate/Nitrite Assay Buffer. The nitrate concentrations of the *A. pacificum* lysates, K media, and three aliquots of seawater were measured in duplicate (Table 2.3) using a Cayman Chemical Nitrate/Nitrite Colorimetric Assay Kit read at 540 nm on a Thermo Scientific Multiskan GO microplate spectrophotometer following the manufacturer's protocol (Cayman Chemical, Ann Arbor, MI, USA). A bottle of modified K media was then prepared with all nutrients and vitamins, except ammonia, at 58% of standard concentrations and ammonia at 20% of standard concentration resulting in final concentrations of approximately 672 μM and 22 μM for nitrate and ammonia, respectively. This modified dilute K media was used in the "dilute media control" treatment, and the experiment proceeded as for experiment 1. On the fourth day, a 1.0 mL aliquot of *A. minutum* from each replicate was preserved with 1% acidified Lugol's solution and visually enumerated. The remaining cells were harvested and extracted for intracellular toxin analysis, as described below. The cell pellet from one dilute media control replicate was lost during the freeze-drying process resulting in $n=7$ for the dilute media controls for toxin analysis. Percent growth was calculated using the cell counts from the start and end points of each *A. minutum* replicate.

Table 2.3 Measured nutrient concentrations used to calculate concentrations of ammonia and nitrate used for dilute media control in Experiment 2.

Sample	Nitrate concentration (μM)	Ammonia concentration (μM)
Seawater	1.1 ± 0.4	61 ± 6
K media in seawater	1120 ± 25	107 ± 6
<i>A. pacificum</i> cell lysate	672 ± 6	22 ± 6

2.3.3 Intracellular toxin analysis

From the portion of each *A. minutum* replicate set aside for toxin analysis, cells were harvested by centrifuging at $3260 \times g$ for 10 min and the supernatant was inspected via microscopy to ensure no cells remained. In Experiment 1, a 2.0 mL aliquot of the supernatant was stored at $-20\text{ }^{\circ}\text{C}$ for later analysis of extracellular toxins. The cell pellets were then freeze-dried and suspended in 500 μL 1% aqueous acetic acid, and then subjected to four freeze-thaw cycles with sonication, via a bath, to lyse the cells and extract toxins (Anderson et al. 1990a). After the final thaw step the samples were centrifuged at $10,000 \times g$ for 10 min to pellet debris and the toxin-containing supernatant was filtered through a 0.2 μm nylon filter to remove precipitate, in preparation for liquid chromatography/mass spectrometric (LC/MS) analysis (Harju et al. 2015). Samples were chromatographically separated using a 20 minute isocratic elution of 60% aqueous acetonitrile with 0.001% formic acid on a TOSOH Bioscience 3 μm HILIC TSK-gel Amide-80 column (150 mm x 4.6 mm) with three rinses of the injection loop between samples on a Waters 2695 Separation Module attached to a Waters QDA mass spectrometer. Since the gonyautoxins (GTX) in standard solutions readily desulfated in the QDA, toxin concentrations were calculated using the area of the desulfated fragment

ion (m/z 332 for GTX 1 and 4 and m/z 316 for GTX 2 and 3, respectively) and the molecular ion (m/z 412 for GTX 1 and 4 and m/z 396 for GTX 2 and 3, respectively) peaks, compared with standards solutions obtained by dilution of certified reference calibration solutions purchased from The National Research Council of Canada. A calibration curve of external standards at six concentrations for each of the toxins showed a linear relationship between toxin concentration and area of mass spectral peaks. Gonyautoxins 1-4 were chosen for the toxin analysis because they are the primary paralytic shellfish toxins produced by *A. minutum* (Hwang and Lu 2000, Grzebyk et al. 2003, Selander et al. 2015, Senft-Batoh et al. 2015b).

2.3.4 Extracellular toxin analysis

The 2.0 mL aliquots of supernatant from experimental replicates in Experiment 1 were thawed and 100 μ L from each sample was diluted with Abraxis Seawater Matrix Sample Diluent. Similarly, GTX 1-4 standards were prepared in Abraxis Seawater Matrix Sample Diluent from certified reference calibration solutions obtained from The National Research Council of Canada. Each sample and standard was analyzed using the Abraxis saxitoxin (PSP) ELISA microtiter plate assay read at 450 nm on a Hidex Sense plate reader following the saxitoxin in seawater sample analysis protocol (Abraxis LLC, Warminster, PA, USA). Unfortunately, following communication with the manufacturer these measurements were deemed unreliable due to the inconsistent response of the ELISA antibody to the GTX standards and its potential to cross-react with other components in the exudates. Therefore, 450 μ L of the eight most toxic samples, as determined by ELISA results, were spiked with 5 μ L glacial acetic acid, to create a 1% aqueous acetic acid sample solution, and subjected to LC/MS analysis for comparison of

toxin concentrations as described above (Harju et al. 2015). When measured by LC/MS, the extracellular toxin concentrations were at or below the limits of detection. This limit of detection corresponded to concentrations which were 90% lower than those predicted by ELISA (data not shown), further reducing confidence in the use of ELISA for extracellular toxin analysis in these experiments. Therefore, the focus of the study was thereafter restricted to dynamics of intracellular toxins produced by *A. minutum*.

2.3.5 *Statistical analysis*

Cellular toxin concentration, growth, and bulk molar toxin concentration for Experiment 1 were analyzed using linear mixed effect models (nlme, package nlme) in R (v 3.4.2) (Pinheiro et al. 2017, R Development Core Team 2020). Models were selected by testing linear and linear mixed effect models via likelihood ratio tests to obtain the optimal model. The optimal model in all cases was a random intercept mixed effect models with batch set as a random effect and phytoplankton treatments set as fixed effects. Significance differences between treatments were tested using a generalized linear hypothesis test (glht) and Tukey test for multiple comparisons of mixed effects models (package multcomp) (Hothorn et al. 2008). Effects of phylogenetic relatedness and historical, geographic co-occurrence of the phytoplankton on toxin production and growth relative to the media controls in Experiment 1 were analyzed using nested ANOVAs (aov, base stats package) in R (Pinheiro et al. 2017, R Development Core Team 2020) . Additionally, the relationship between the mean cellular toxicity and mean growth for the media control and all phytoplankton treatment in Experiment 1 were analyzed using linear regression analysis (lm, base stats package) in R (R Development Core Team 2020). Cellular toxin concentration and percent growth for Experiment 2 were

analyzed using a Welch's ANOVA with a Games-Howell post-hoc test (oneway, userfriendlyscience package), due to unequal sample sizes resulting in unequal variance, in R (Peters et al. 2018). Graphs depicting data associated with the nested ANOVAs, Welch's ANOVA, and linear regression were constructed using the ggplot2 package in R (Wickham 2016).

2.4 Results

When *A. minutum* was exposed to chemical compounds from lysed phytoplankton, significant species-specific effects were observed on cellular concentrations of GTX 1-4 and on growth (Figure 2.1). Contrary to the primary original prediction, exposure to chemical cues from more closely related phytoplankton (one conspecific and two congeneric) suppressed *A. minutum* toxin production by 41-61% compared to media controls, whereas chemicals from any of three other phytoplankton stimulated *A. minutum* toxin production by 32-86% (Figure 2.1a). However, there were also finer-scale species-specific effects. Exposure to chemical cues from *A. pacificum* caused the greatest suppression of toxicity in *A. minutum* (61%) ($p < 0.001$). In contrast, cues from dead *P. lima* caused the greatest increase in cellular toxin production compared to media controls (86%) ($p < 0.001$), a significantly greater increase than was caused by *P. micans* and *C. monotis* at 32% ($p = 0.002$) and 39% ($p < 0.001$), respectively (Figure 2.1a). In general, cues from the six different dead phytoplankton each resulted in a distinct pattern of altered cellular toxicity.

A consistent, inverse relationship was observed between cellular toxicity and growth when *A. minutum* was exposed to chemicals from six different phytoplankton

(Figure 2.1). Exposure to chemical cues from congeners which suppressed toxin production increased *A. minutum* growth by 54-90% (Figure 2.1b) compared to media controls ($p < 0.001$ for all phytoplankton). In contrast, cues from the three less related phytoplankton that significantly induced cellular toxin production, suppressed *A. minutum* growth by 56-90% (Figure 2.1b) relative to media controls ($p < 0.001$ for all phytoplankton). In all six cases the cues from dead phytoplankton resulted in alteration of growth that was inverse to their effect on cellular toxicity, although the magnitude of differences were not generally equivalent. Additionally, when the mean growth and cellular toxicity for all treatments together are considered there was a significant inversely relationship ($p < 0.001$) (Figure A1). These findings suggest that the dead phytoplankton cues trigger a population level trade-off between toxin production, or defense, and growth in *A. minutum*.

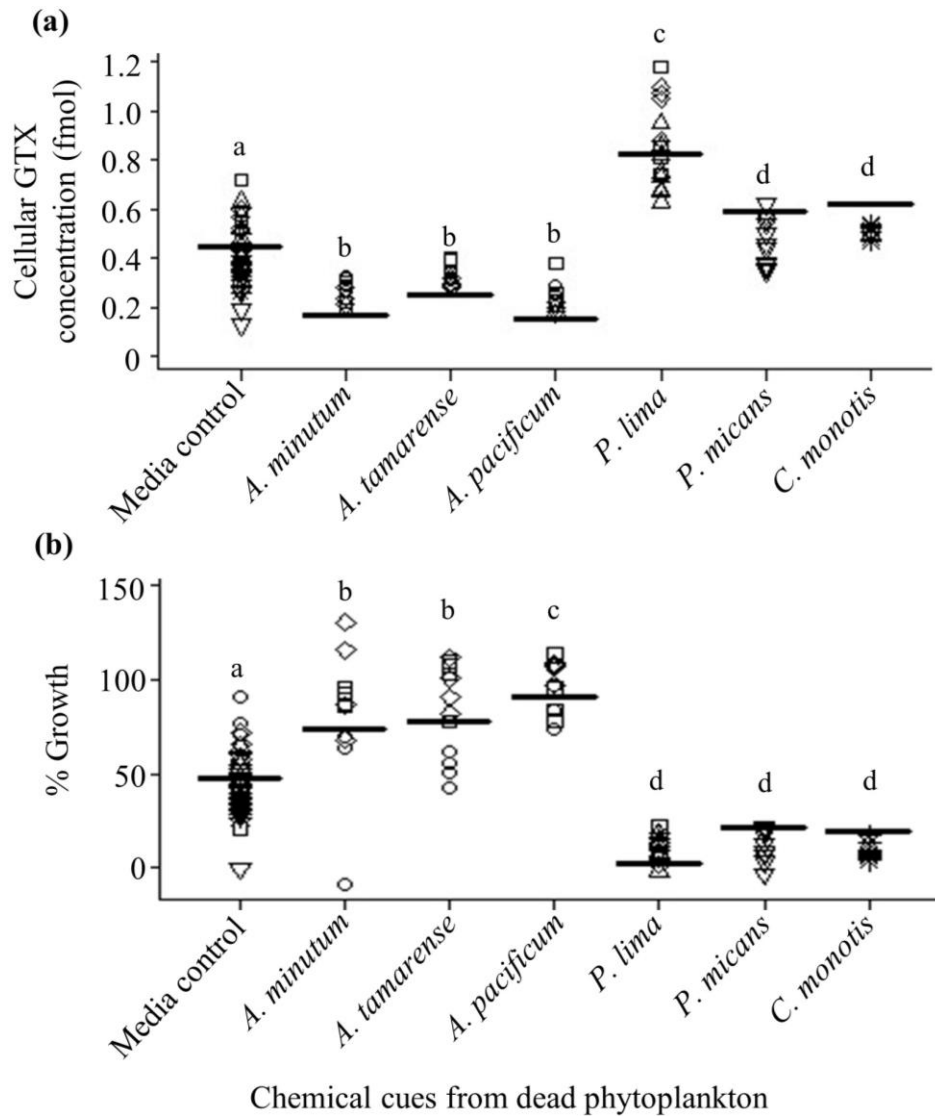


Figure 2.1 Effects of chemical cues from dead phytoplankton (as an indication of predation risk) on (a) cellular toxin concentration of GTX 1-4 and (b) percent growth of *Alexandrium minutum* (Experiment 1). Data were analyzed using a random intercept model whereby the dark bars represent the line of best fit and the symbols show the contribution of each batch to the mean. The lower case letters show statistical differences between treatments via Tukey tests ($p \leq 0.05$).

When toxicity was measured as bulk molar concentration instead of per cell, *A. minutum* exposed to chemical cues from lysed phytoplankton showed similar, but less extreme patterns, of toxin regulation (Figure 2.2). Exposure to cues from more closely related phytoplankton significantly suppressed toxin production of *A. minutum* by 33-58% compared to media controls ($p < 0.001$ for all phytoplankton), whereas cues from the three less related phytoplankton slightly stimulated *A. minutum* toxin production by 12-28% (Figure 2.2). Unlike cellular toxicity, bulk toxicity was only significantly increased relative to media controls when *A. minutum* was exposed to chemical cues from dead *P. lima* (28%) ($p = 0.003$); whereas, exposure to dead *P. micans* and *C. monotis* caused insignificant changes of 12% ($p = 1.0$) and 13% ($p = 0.30$), respectively (Figure 2.2). Overall, this suggests that changes in cellular toxicity of *A. minutum* in response to cues from dead phytoplankton are mostly, although with subtle differences, a reflection of actual toxin production and not an artifact of possible dilution among an increased number of cells.

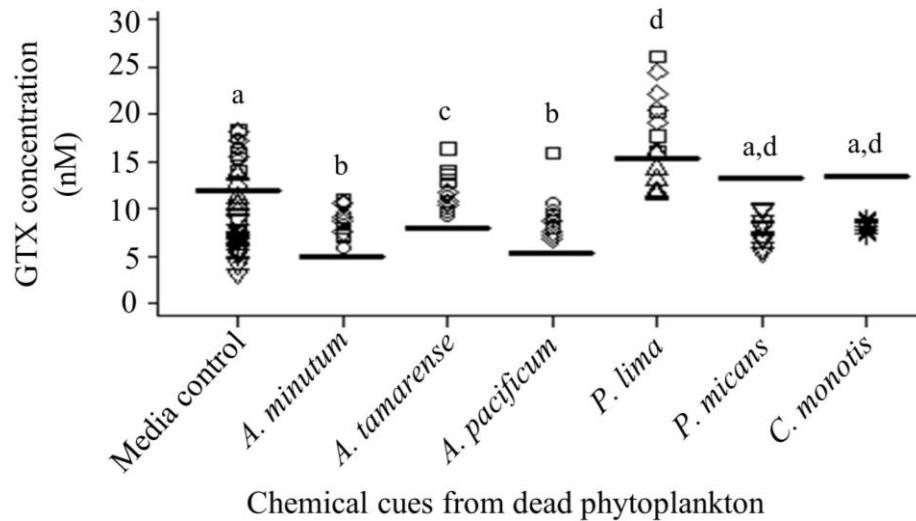


Figure 2.2 Effects of chemical cues from dead phytoplankton (as an indication of predation risk) on bulk (molar) toxin concentration of GTX 1-4 of *Alexandrium minutum* (Experiment 1). Data were analyzed using a random intercept model whereby the dark bars represent the line of best fit and the symbols show the contribution of each batch to the mean. The lower case letters show statistical differences between treatments via Tukey post-hoc test ($p \leq 0.05$).

When the toxicity-altering effects of chemical cues from conspecifics and congeners were considered as a group relative to less related phytoplankton, effects on *A. minutum* toxicity and growth were strongly reinforced (Figure 2.3). Upon exposure to chemical cues from dead, closely related phytoplankton considered as a group, *A. minutum* responded by decreasing its toxicity by 45% (Figure 2.3a) while increasing growth by 94% (Figure 2.3b) relative to media controls. Conversely, in response to cues from dead less related phytoplankton considered as a group, *A. minutum* increased toxin production by 64% (Figure 2.3a) and reduced growth by 74% (Figure 2.3b) compared to media controls. Overall, this suggests that phylogenetic relatedness of phytoplankton to *A. minutum* is a significant determining factor in how *A. minutum* responds to predation

risk via cues from dead phytoplankton both in terms of toxin regulation ($p < 0.001$, $F_{1,4} = 143.8$) and growth ($p < 0.001$, $F_{1,4} = 74.4$).

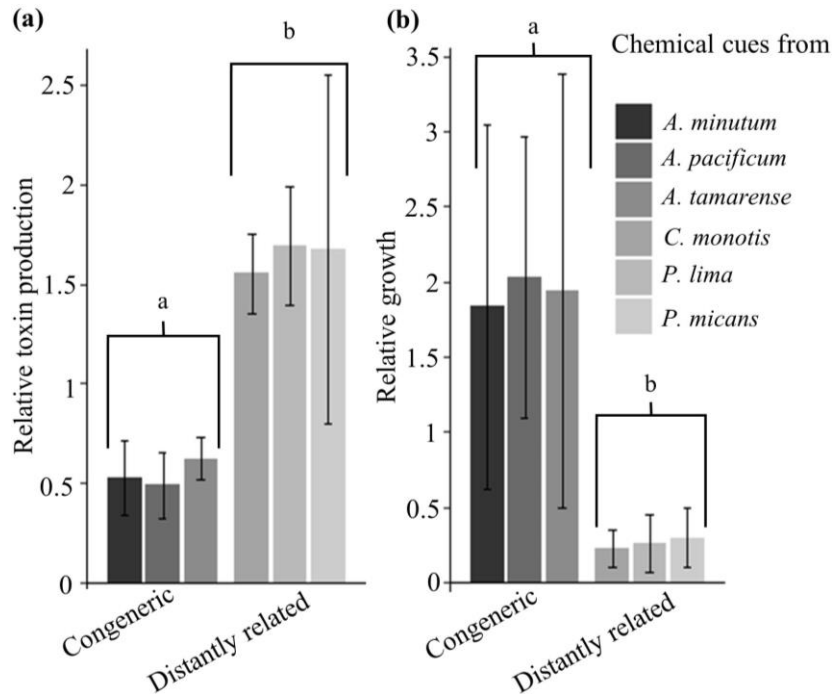


Figure 2.3 Effects of phylogenetic relatedness on (a) cellular toxin production of GTX 1-4 and (b) growth of *Alexandrium minutum* relative to controls in response to chemical cues from dead phytoplankton, as an indication of predation risk (Experiment 1). Data from exposure to chemical cues from *A. minutum*, *A. tamarense*, and *A. pacificum* are nested under “congeneric” and *P. lima*, *P. micans*, and *C. monotis* are nested under “distantly related”. Data are shown as mean \pm standard deviation and were analyzed using a nested ANOVA. Lower case letters show statistical differences between treatments ($p \leq 0.05$).

There were no strong effects on *A. minutum* toxicity and growth associated with historical co-occurrence when, to eliminate the confounding factor of relatedness, only the conspecific and congeners were considered (Figure 2.4). Surprisingly, *A. minutum* did not show a heightened sensitivity to cues from co-occurring phytoplankton relative

to phytoplankton with no known historical overlap with the geographic distribution of *A. minutum* (Figure 2.1a and Figure 2.4). In fact, between the two sets of phytoplankton (historically co-occurring or not) there was no significant difference in toxin production ($p=0.14$, $F_{1,1}=2.2$) or growth ($p=0.74$, $F_{1,1}=0.10$) in *A. minutum* (Figure 2.4). Instead, chemical cues from either co-occurring or non-co-occurring dead, related phytoplankton caused about a 50% reduction in toxin production (Figure 2.4a) and a nearly 100% increase in growth (Figure 2.4b) compared to media controls. Therefore, historical co-occurrence appears to not be an important factor when *A. minutum* is assessing potential predation risk in response to cues from dead phytoplankton.

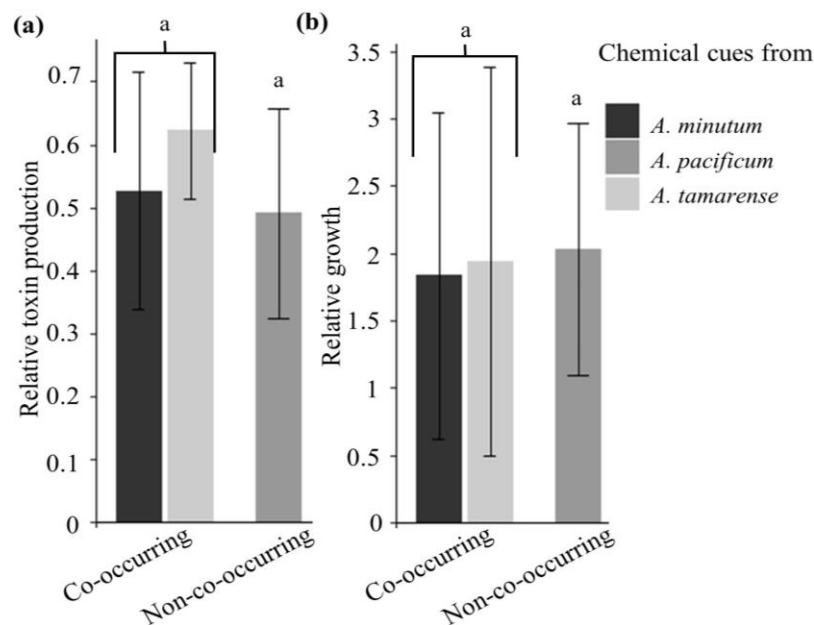


Figure 2.4 Effects of historical, geographic co-occurrence on (a) cellular toxin production of GTX 1-4 and (b) growth of *Alexandrium minutum* relative to controls, in response to chemical cues from dead phytoplankton, as an indication of predation risk (Experiment 1). Data from exposure to chemical cues from *A. minutum* and *A. tamarensis* are nested under “co-occurring” and *A. pacificum* is under “non-co-occurring”. Data are shown as mean \pm standard deviation and were analyzed using a nested ANOVA. Lower case letters show statistical differences between treatments ($p \leq 0.05$).

When the experiment with *A. pacificum* was repeated to include a more realistic control (“dilute media control”) in which ammonia and nitrate concentrations were manipulated to mimic concentrations in the lysed *A. pacificum* treatment, toxin suppression ($p < 0.001$, $F_{3,11.8} = 229.9$) and growth induction ($p < 0.001$, $F_{3,14.28} = 354.7$) patterns were again observed (Figure 2.5). On the other hand, impacts on toxicity ($p = 0.30$, $F_{3,11.8} = 229.9$) and growth ($p = 0.063$, $F_{3,14.28} = 354.7$) of *A. minutum* did not vary significantly between the full strength media control and the dilute media control, which imitated the ammonia and nitrate levels of the *A. pacificum* lysate (Figure 2.5). This suggests that chemical cues in the dead phytoplankton lysates, and not macronutrients from the lysates, are responsible for the changes in toxin production and growth observed in *A. minutum*.

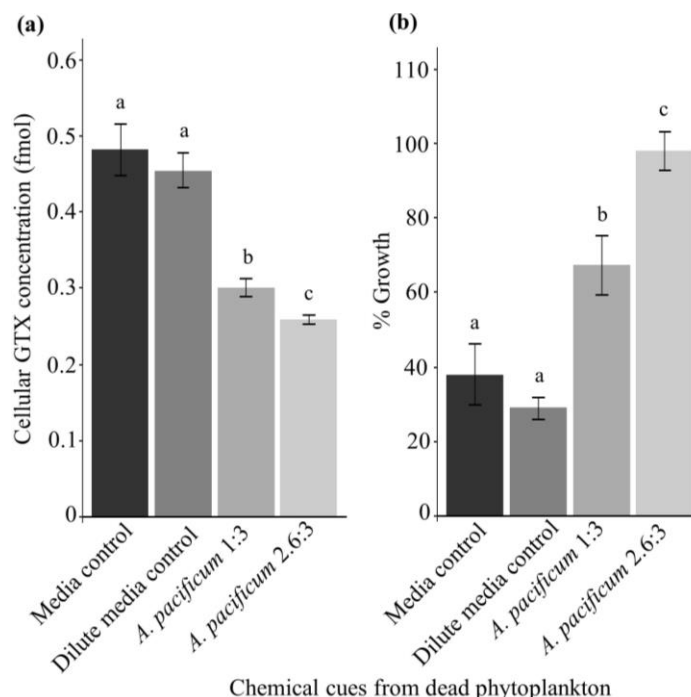


Figure 2.5 Effects of nutrients and chemical cues from dead *Alexandrium pacificum* (as an indication of predation risk) on (a) cellular toxin concentration of GTX 1-4 and (b) growth of *Alexandrium minutum* (Experiment 2). *A. minutum* was exposed to *A. pacificum* lysate at a 1:3 and 2.6:3 ratio of *A. pacificum* lysate biomass to *A. minutum* biomass, equivalent to 0.38:3 and 1:3 ratio of *A. pacificum* lysate to *A. minutum* by cell number. Additionally, either full strength K media (“media control”) or K media diluted to reflect the nitrate and ammonia concentration present in the 2.6:3 ratio of *A. pacificum* lysate biomass to *A. minutum* biomass (“dilute media control”) were added to *A. minutum* as controls. Data are shown as mean \pm standard deviation and were analyzed using a Welch’s ANOVA. Lower case letters show statistical differences between treatments via Games-Howell post-hoc test ($p \leq 0.05$).

The lower concentration of chemical cues in the “1:3 treatment” of Experiment 2 is likely still much higher than natural bulk concentrations of cell lysates from a sloppily feeding predator; however, it may still be ecologically relevant within short-lived hotspots of extremely high lysate concentrations created by actively feeding predators. The different concentrations of dead *A. pacificum* cue resulted in a graded response by *A. minutum* with the cues having a greater impact when applied at a higher concentration;

yet, still causing significant toxin suppression ($p < 0.001$, $F_{3,11.8} = 229.9$) and growth induction ($p < 0.001$, $F_{3,14.28} = 354.7$) at a lower, more realistic, concentration (Figure 2.5). Overall, this means that while the differences in the effective concentrations of the dead phytoplankton cues may have impacted the magnitude of the observed effects on toxin production and growth in *A. minutum* it likely did not impact the direction of the effects.

2.5 Discussion

The toxic marine dinoflagellate *A. minutum* responds to dead phytoplankton cues in a species-specific manner (Figure 2.1a and Figure 2.2). *A. minutum* responds to the presence of distantly related, but co-occurring, dead phytoplankton with enhanced chemical defenses, in the form of increased cellular toxin concentration (Figure 2.1a and Figure 2.3a). This is in agreement with recent findings that *A. catenella* increases toxin production in response to a lysed diatom and green alga (Griffin et al. 2019). However, cues from closely related phytoplankton suppressed toxin production in *A. minutum* (Figure 2.1a, Figure 2.2, Figure 2.3a, and Figure 2.5a); therefore, the original hypothesis that close relatedness among phytoplankton results in upregulation of toxin production was rejected. Additionally, the observed reduction of toxin production due to exposure to cues from related dead phytoplankton contrasts with recent findings in other studies (Senft-Batoh et al. 2015b, Griffin et al. 2019). In the study by Senft-Batoh and colleagues, *A. catenella* (previously *A. fundyense*) increased toxin production modestly, but significantly, in response to two strains of lysed conspecifics (Senft-Batoh et al. 2015b); whereas, Griffin et al. found that the same *A. catenella* strain did not significantly change its toxin production in response to the same two strains of lysed conspecifics (Griffin et al. 2019). Consequently, responses to dead phytoplankton cues by

Alexandrium species appear to be species-specific and not a conserved trait, given that some *Alexandrium* species respond to cues from conspecifics and congeners with decreased toxicity and others with either no change or enhanced toxicity. A distinction between the previous studies and the current one is that those experiments investigated the effects of cues from two conspecifics, whereas, the current study considered effects of a conspecific as well as two other congeneric species (plus three less related dinoflagellates).

Many studies have found that organisms respond to cues of other dead organisms consumed by common predators (Scherer and Smee 2016). However, Scherer and Smee reported that in more than 50% of studies analyzed, cues from conspecifics induced stronger defenses than cues from heterospecifics (Scherer and Smee 2016). For example, gray tree frog tadpoles decreased their activity level the most (Schoeppner and Relyea 2005) and pond snails spent the most time out of the water (Dalesman et al. 2007) in response to crushed conspecifics compared to other organisms that share a common predator. In contrast, in the current study toxicity in *A. minutum* was reduced by nearly 50% in response to cues from dead conspecifics; toxicity increased only in response to cues from less related phytoplankton (Figure 2.3a). One explanation for this pattern is that for *A. minutum*, cues from dead conspecifics may be an indication of bloom senescence (a regular occurrence for bloom-forming dinoflagellates) rather than sloppy predation. In this scenario, increased toxin production would not be adaptive, such that it may be more advantageous for *A. minutum* to use nutrients released by lysed cells to grow to offset mortality instead of investing in increased toxin production.

We originally hypothesized phytoplankton prey to be under selection pressure to respond to cues from other phytoplankton that they more frequently encounter, since those cues should reliably indicate predation risk. However, *A. minutum*'s response differed from studies in several other systems in that historical, geographic co-occurrence did not affect how it responded to cues from dead phytoplankton; instead, cues from both co-occurring and non-co-occurring closely related phytoplankton suppressed toxicity and increased growth (Figure 2.4). For example, both snails (Dalesman et al. 2007) and salamanders (Chivers et al. 1997) have been shown to engage in more antipredatory behavior in response to cues from dead closely related competitors and heterospecifics with which they cohabitate. In contrast, the marine crab *Heterozius rotundifrons* increased antipredatory posturing in response to crushed related crabs but not distantly related, co-occurring crabs (Hazlett and McLay 2005). Therefore, *A. minutum* and *H. rotundifrons* are similar in that genetic relatedness, rather than cohabitation, of the other organism is most important in determining how to respond to cues that an organism has died.

In the current study, there was an observed trade-off between growth and toxin production in response to dead phytoplankton cues (Figure 2.1, Figure 2.5, and Figure A1). Due to the similar magnitudes but opposite effects of cues on growth vs. toxin production in *A. minutum*, the most parsimonious explanation is that lysed phytoplankton caused a change in growth which in turn affected toxin concentration: if growth is suppressed, more resources are available for toxin induction; if growth is enhanced, existing toxins are diluted among daughter cells creating the appearance of toxin suppression. However, bulk toxin concentrations showed similar patterns to cellular

toxin concentrations (Figure 2.2). In the case of exposure to conspecific and congener cues, *A. minutum* produced less toxin, even taking into account that enhanced growth led to a greater number of cells containing these toxin molecules (Figure 2.2). This means that toxins were not just diluted because *A. minutum* cells divided more. However, when *A. minutum* was exposed to cues from less related dead phytoplankton, with the exception of *P. lima*, the observed increase in toxin production could be accounted for by reduced growth, via more synthesized toxin molecules and build-up of more toxins within fewer cells.

Another alternative hypothesis is that the decrease in toxin production by *A. minutum* in response to cues from dead conspecifics and congeners results from the cues being used as a quorum sensing-like mechanism. If dense blooms of *A. minutum* are not grazed upon at a greater rate than *A. minutum* growing at low population density, the chance of any one individual being eaten would decrease with increasing population concentration, in which case it would be adaptive to down-regulate (otherwise costly) toxin production during a dense bloom. One would then expect *A. minutum* to decrease toxin production the most in response to conspecific cues, which may be an indication of high population density, while decreasing toxicity less, if at all, in response to cues from congeners. This is contrary to what was discovered during the current study: *A. minutum* decreased toxin production the most, not in response to conspecific cues, but in response to cues from dead *A. pacificum*, with which it does not co-occur (Figure 2.1 a). Therefore, the alternative hypothesis that *A. minutum* uses cues from dead congeners for quorum sensing, suppressing toxin production, can likely be rejected.

Nutrients from phytoplankton lysates provided *A. minutum* with resources enabling toxin production and/or growth, but chemical cues likely enhanced the response. Phosphate limitation and high concentrations of nitrate and ammonia have previously been linked to toxin induction in *Alexandrium* species (John and Flynn 2000, Guisande et al. 2002, Leong et al. 2004, Selander et al. 2008). Conversely, nitrogen limitation has been linked to decreased toxin production (John and Flynn 2000). In the current experiment, when exposed to similar nitrate and ammonia conditions as *A. pacificum* lysate, but without phytoplankton chemical cues, *A. minutum* did not alter toxin production or growth relative to exposure to full strength media (Figure 2.5, “dilute media control” vs. “media control”). Instead, only exposure to cue containing *A. pacificum* lysates reduced toxin production in *A. minutum* (Figure 2.5). Although we did not measure phosphate in our controls or lysates, our diluted media control contained a 1.7-fold dilution of phosphate relative to the full strength media control; nevertheless toxins were neither induced nor suppressed when comparing *A. minutum* exposed to these two controls ($p = 0.30$). Therefore, it is likely that chemical cues in the lysate from dead congeners contributed to the observed suppression of toxin production.

A trade-off between defense and growth, as observed in this study, is in line with the optimal defense theory, which posits that defenses are expected to evolve in proportion to the risk of predation and inversely proportional to their cost (Rhoades 1979). Additionally, Rhoades proposed that defenses should be maintained at low or nonexistent levels in the absence of predators and increase in the presence of predators (i.e., be inducible). During the summer when *A. minutum* blooms under nutrient-depleted conditions with high grazing pressure, a reduction in growth, associated with toxin

induction, is worth the allocation cost if higher toxicity results in reduced grazing by copepods and a concomitant increase in the *A. minutum* population (Teegarden 1999, Selander et al. 2006). However, if copepods are even partially resistant to the toxins, the benefits of toxin production could be lost, as copepods would be capable of eating larger quantities of cells (Senft-Batoh et al. 2015b) with little ill effect and *A. minutum* may not grow fast enough to offset the mortality from predation.

Overall this study shows that *A. minutum* experiences a global trade-off between growth and toxin production upon exposure to cues from dead phytoplankton. Cues from more distantly related phytoplankton led to toxin induction, the magnitude of which was effectively accounted for by the reduced growth in *A. minutum* (i.e. *A. minutum* cells were dividing more slowly and made proportionally more toxin molecules). On the other hand, exposure to cues from both dead conspecifics and congeners enhanced *A. minutum* growth and dramatically suppressed toxin production beyond the extent expected by rapid cell division. Taken as a whole, these results reveal that *A. minutum* distinguished relatedness of dead phytoplankton, adjusting its growth and defense.

CHAPTER 3. PREDATOR CUES TARGET SIGNALING PATHWAYS IN TOXIC ALGAL METABOLOME

Brown, E. R., S. G. Moore, D. A. Gaul, and J. Kubanek. 2021. Predator Cues Target Signaling Pathways in Toxic Algal Metabolome. *In review*.

3.1 Abstract

Early detection of predators is critical to the survival of all living organisms. For phytoplankton, recognition and response to chemical cues from predators, as evidence of predation risk, is particularly crucial. The phytoplankton *Alexandrium minutum* upregulates its toxicity when exposed to copepodamides, a suite of compounds released by copepod predators. However, how *A. minutum* perceives these predatory cues and what metabolic pathways are involved in initiating toxin induction remains unknown. In this study LC/MS and NMR-based metabolomics uncovered subtle physiological responses of *A. minutum* to copepodamides, including dysregulation of valine biosynthesis and enhancement of butanoate metabolism and arginine biosynthesis. While we have yet to identify a chemoreceptor directly activated by copepod cues, based on the results of inhibition experiments detection of copepodamides appears to disrupt the activity of serine/threonine phosphatases leading to increased jasmonic acid biosynthesis and signaling, which leads to amplified gonyautoxin biosynthesis in *A. minutum*. This study is an important step toward a better understanding of chemosensory ecology of predator-prey interactions in phytoplankton.

3.2 Introduction

Perception and response to external stimuli are critical to all living organisms. Organisms respond to chemical, mechanical, visual, and auditory signals to find food and habitat, compete, avoid predation, and reproduce. Among stimulus modalities, chemical cues are arguably the most important for small organisms in planktonic environments when it comes to recognition of predators (Hay and Kubanek 2002, Lass and Spaak 2003, Brown et al. 2019).

Predator cues elicit physiological responses in a diverse array of phytoplankton prey (Van Donk et al. 2011, Selander et al. 2015, Selander et al. 2019). Zooplankton grazers are known to trigger formation of spines, increase silicification, and change chain length and colony size in phytoplankton (Van Donk et al. 2011). In addition to morphological changes, predator cues also induce chemical defenses in the form of toxins in some phytoplankton (Selander et al. 2015, Selander et al. 2019). However, only some zooplankton predators trigger particular defensive phenotypes (Senft-Batoh et al. 2015a, Lundholm et al. 2018) suggesting species-specific recognition of predator cues. In the case of predatory copepods, a suite of taurine lipid-derived metabolites called copepodamides (Selander et al. 2015) appear to be the primary cue leading to induced resistance in various phytoplankton prey (Selander et al. 2019, Arias et al. 2021). The particular cocktail of copepodamide molecules produced by copepods varies based on their species and diet (Grebner et al. 2019). Variation in copepodamide blend and overall concentration is likely used by phytoplankton in assessing predation risk.

Discovery of copepodamides and some other zooplankton cues have enabled manipulation of prey phenotypes in lab experiments (Yasumoto et al. 2005, Selander et al. 2015) yet little is known about how these chemical cues are recognized by prey or the molecular mechanisms by which they induce defensive phenotypes. Using transcriptomics and proteomics, two recent studies (Rocuzzo et al. 2020, Zhu et al. 2021) extensively mapped the signaling pathways and identified the physiological changes that result in increased colony formation in freshwater green algae in response to *Daphnia* zooplankton. Based on upregulation of G protein-coupled receptors (GPCRs), Zhu and colleagues suggested that these chemoreceptors are involved in green algal recognition of *Daphnia* grazing cues (Zhu et al. 2021). GPCRs have also been identified among diatom and dinoflagellate phytoplankton taxa (Mojib and Kubanek 2020); however, their potential role in predator cue recognition has not been deeply studied. To date only a handful of studies have pursued the signaling cascade in diatoms and dinoflagellates triggered by predatory zooplankton (Wohlrab et al. 2010, Amato et al. 2018, Li and Ismar 2018, Harðardóttir et al. 2019). These studies predominantly relied on transcriptomics; yet functional annotation of diatom (Falciatore et al. 2020) and especially, dinoflagellate (Akbar et al. 2018) genes remains relatively limited. In short, our understanding of sensory ecology of predator-prey interactions in plankton is still underdeveloped.

In the current study, we utilized metabolomics to explore shifts in the metabolism of *Alexandrium minutum*, one of several *Alexandrium* species whose toxicity is upregulated in response to copepodamides (Selander et al. 2015), as a first step towards identifying the signaling pathway that leads to toxin induction. We also endeavored to

uncover how copepodamides are detected by *A. minutum* by testing the hypothesis that copepodamides behave as agonists of GPCRs and an alternative hypothesis that copepodamides disrupt *A. minutum* cell membranes triggering toxin production via physical stress.

3.3 Methods

3.3.1 Phytoplankton culturing

Cultures of the dinoflagellate *Alexandrium minutum* strain CCMP 113, acquired from NCMA Bigelow Laboratory, were grown in filtered seawater from the Gulf of Maine (NCMA Bigelow Laboratory, 35 ppt) amended with full strength K media (Keller et al. 1987). Cultures were arbitrarily arranged in a Percival incubator at 15 °C set to a 12:12 h light/dark cycle with irradiance of 89-100 $\mu\text{mol m}^{-2} \text{s}^{-1}$. Cell density was quantified by visual enumeration of cells in a Palmer-Maloney chamber on an Olympus IX-50 inverted microscope after preservation with 1% acidified Lugol's solution.

3.3.2 Metabolomics experimental design and execution

To investigate the effect of copepod chemical cues on the metabolome of *A. minutum*, cultures in exponential growth phase at 15,000 cells mL⁻¹ were exposed to copepodamides (Appendix B.1.1 Copepodamide extraction and isolation). Twice, first at the start of the experiment and again 24 h later, 1.5 mL of either 0.2 μM copepodamides in DMSO (treatment, n=20) or DMSO alone (control, n=20) were added aseptically to 300 mL cultures of *A. minutum* resulting in a final concentration of 1 nM copepodamides. A blank media sample consisting of seawater amended with K media at

a 1.7-fold dilution, mimicking concentrations of macronutrients in spent media based on preliminary experiments (data not shown), was also incubated for the same length of time. At both the start, prior to the first addition of copepodamides, and end of the experiment, prior to harvesting, a 1.0 mL aliquot from each culture was preserved with Lugol's solution to measure cell concentrations, which was used to calculate *A. minutum* growth over the course of the experiment. An unpaired t-test, performed in GraphPad Prism 9.0, was used to compare growth between *A. minutum* and *A. minutum* exposed to copepodamides.

After about 40 h, all cultures were harvested with processing of treatments and controls intermixed over about 2.5 h within 4 h of the start of the light cycle. An aliquot of each culture was harvested by centrifugation for targeted toxin analysis, using methods similar to those described in Brown and Kubanek (2020), and an unpaired Welch's t-test was performed in GraphPad Prism 9.0 to compare toxin concentrations between treatments and controls. The remaining portion of each culture was harvested by vacuum filtration and extracted in a manner similar to Poulson-Ellestad et al. (2014). Both the polar and non-polar metabolomes were compared, separately, by ultrahigh performance liquid chromatography-mass spectrometry (UPLC/MS) and ¹H NMR spectroscopy (Appendix B.1.2 Harvesting and extraction of *Alexandrium minutum* for metabolomics experiment and B.1.3 Metabolomic sample preparation and spectral data acquisition).

3.3.3 *Metabolite analysis and annotation*

After acquisition, UPLC/MS and ¹H NMR data were pre-processed and analyzed by multivariate statistics (Appendix B.1.4 Data processing and analysis). In brief, principal component analysis (PCA) and orthogonalized partial least-squares discriminant analysis (oPLS-DA) were used to compare both the non-polar and polar metabolome, separately, of *A. minutum* treatments and controls. These analyses were completed using Metabolab and PLS-Toolbox (Eigenvector Research) in Matlab for ¹H NMR data and Compound Discoverer (ThermoFisher Scientific) and XCMS Online for UPLC-MS data (Ludwig and Günther 2011, Gowda et al. 2014). Metabolites that were found to be significantly different between controls and treatments and which contributed to discrimination of the metabolomes were tentatively annotated using a local spectral database as well as several publicly available databases (Appendix B.1.5 Metabolite annotation).

3.3.4 Signaling pathway inhibition experiments and cell membrane permeability assay

Based on the metabolomics results a series of inhibition experiments were performed to explore the involvement of jasmonic acid biosynthesis and signaling pathway and G protein-coupled receptors (GPCRs) (Appendix B.1.6 Signaling pathway inhibition experiments). In brief, cantharidin was used to inhibit serine/threonine protein phosphatases (Honkanen 1993), which regulate jasmonic acid biosynthesis (Bajsa et al. 2011), neomycin was used to inhibit jasmonic acid signaling (Vadassery et al. 2019), and SCH-202676 was used to inhibit GPCRs (Fawzi et al. 2001). Growth and cellular toxin concentrations were analyzed for these experiments. Additionally, an alternative hypothesis that copepodamides induce toxicity via disruption of cell membranes was assessed using a cell membrane permeability assay (Poulin et al.

2018) (Appendix B.1.7 Cell membrane permeability assay). All statistical analyses were executed using GraphPad Prism 9.0.

3.4 Results

3.4.1 *Copepodamides trigger subtle but measurable changes in the metabolome of *Alexandrium minutum**

Previous studies have shown that copepodamides, released by diverse copepod species (Grebner et al. 2019), induce toxin production in *A. minutum* (Selander et al. 2015) but have not explored other metabolic changes they trigger nor the signaling pathways involved in toxin induction. Therefore, in the current study UPLC/MS and ¹H NMR metabolomics were employed to investigate changes in the metabolome of *A. minutum* in response to these predatory copepod cues. Before metabolomic analysis, toxin induction from copepodamide exposure was verified by LC/MS quantification of gonyautoxins, the neurotoxins produced by *A. minutum* (Figure 3.1). Copepodamides caused a significant increase in *A. minutum* toxicity ($t = 13.5$, $df = 25.7$, $p \ll 0.001$; Figure 3.1a) and a somewhat unexpected significant reduction in growth ($t = 5.6$, $df = 38$, $p \ll 0.001$; Figure 3.1b) with no observed changes in cell size (data not shown). However, the 19% reduction in *A. minutum* growth was modest compared to the 103% increase in toxicity (Figure 3.1), suggesting that toxin induction did not substantially disrupt cellular function.

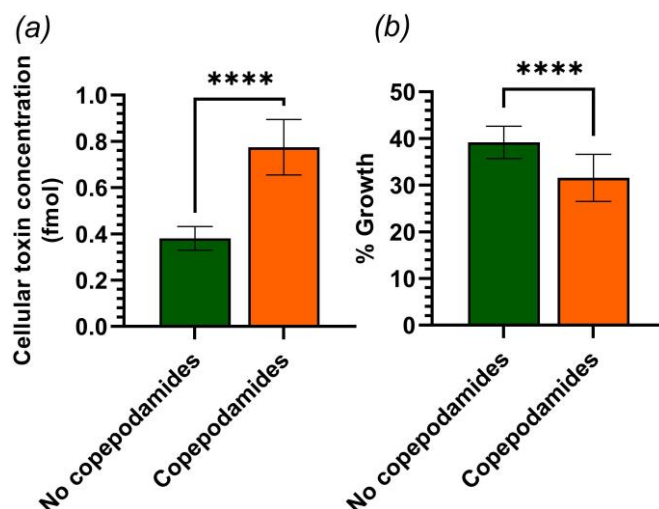


Figure 3.1 Exposure to copepodamides induced toxicity and reduced growth in *Alexandrium minutum*. Bars represent the mean \pm standard deviation of (a) cellular toxin concentration of gonyautoxins 1-4 and (b) percent growth of *A. minutum* when exposed to a solvent control (No copepodamides) or 1 nM copepodamides (Copepodamides). Data were analyzed using an unpaired Welch's t-test for the toxin analysis and an unpaired t-test for the growth analysis. Asterisks indicate level of statistical significance; **** $p << 0.001$.

Principal component analysis (PCA) of UPLC/MS and orthogonal partial least squares discriminant analysis (oPLS-DA) of ^1H NMR datasets each partially distinguished metabolomes of *A. minutum* based on exposure to copepodamides (Figure 3.2 and Figure B1). The UPLC/MS analysis revealed 24,914 polar features and 53,776 non-polar features in the metabolomes of *A. minutum* regardless of copepodamide exposure. Effects of copepodamide exposure on *A. minutum* were partially explained by 464 and 1,271 mass spectral features associated with the polar (Figure 3.2a and Figure 3.2c) and non-polar (Figure 3.2b and Figure 3.2d) metabolomes, respectively. Incomplete separation within each PCA model occurred over the first principal component which accounted for 19-30% of the variance among replicates.

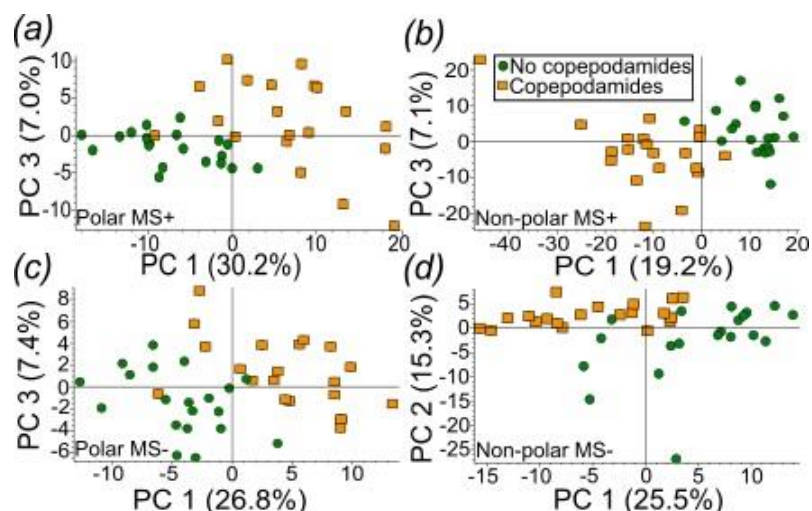


Figure 3.2 PCA models of UPLC/MS data revealed that both polar and non-polar metabolites moderately distinguished metabolomes of *Alexandrium minutum* based on copepodamide exposure. Orange squares represent metabolomes of *A. minutum* exposed to copepodamides and green circles represent metabolomes of *A. minutum* not exposed to copepodamides (controls). PCA scores plots from UPLC/MS analysis using positive (*a* and *b*) and negative (*c* and *d*) mode MS for both polar (*a* and *c*) and non-polar (*b* and *d*) metabolites.

Features from the MS-based metabolomics analysis led to identification of about a dozen metabolites (Table B1) implicated in *A. minutum* response to copepodamide exposure (Table 3.1). Several metabolites associated with butanoate metabolism were in significantly higher abundance in *A. minutum* exposed to copepodamides, suggesting overall upregulation of this pathway (Table 3.1). Additionally, both polar and non-polar NMR metabolomics analysis indicated enrichment, in copepodamide-exposed *A. minutum*, of compounds containing aliphatic acyl (2.0-2.5 ppm) and aldehyde (9.0-10.0 ppm) functional groups (Figure B1*b* and Figure B1*d*), which are highly prevalent in butanoate metabolism. Arginine biosynthesis may also have been upregulated in *A. minutum* upon exposure to copepodamides, evidenced by a significant increase in concentrations of glutamic acid and guanidinobutanamide, two of three metabolites

identified from the pathway (Table 3.1). However, arginine itself was not found to differ significantly in concentration (Table B1). Nicotinate and nicotinamide metabolism may be dysregulated in *A. minutum* after exposure to copepodamides: the loadings plot of the polar metabolome (Figure B1b) indicated that NMR signals at 7.81, 7.90, 8.45, and 8.66 ppm corresponding to a doublet, two singlets, and a doublet in the ¹H NMR spectra, respectively, were distinguishing features of *A. minutum* exposed to copepodamides. Signals in this region are typically associated with substituted pyridine rings which, when coupled with the 40% increase in concentration of an unknown metabolite similar to nicotiny alcohol ($p = 0.008$; Table B1), provided support for upregulation of nicotinate and nicotinamide metabolism. Unsurprisingly, several toxin intermediates and the byproduct succinic acid previously identified as part of the saxitoxin, or paralytic shellfish toxin, biosynthetic pathway (Cho et al. 2019) were observed in concentrations that were 100 to 160% higher in *A. minutum* when exposed to copepodamides (Table 3.1). Additionally, an analog of saxitoxin, decarbamoyloxysaxitoxin, that has not been previously described in *A. minutum* (Akbar et al. 2020), was tentatively identified and found to be in significantly higher concentration when copepodamides were present (Table B1).

Table 3.1 *Alexandrium minutum* metabolites and pathways tentatively identified by UPLC/MS to be affected by copepodamide exposure. Change in concentration and fold-change are based on *A. minutum* exposed to copepodamides relative to *A. minutum* exposed to a solvent control. *P* values were calculated using an unpaired t-test.

Pathway	Metabolites	Fold-change	<i>P</i> value
<i>Valine biosynthesis</i>			
Down	α -Ketoisovaleric acid	0.78	0.04
Up	2-aceto-2-hydroxy-butanoate	1.2	0.006
<i>Butanoate metabolism</i>			
Up	Maleic acid	1.5	0.03
Up	Hydroxyglutaric acid	1.3	0.04
<i>Arginine biosynthesis</i>			
Up	Glutamic acid	1.1	0.04
Down	4-Acetamidobutanoate	0.71	0.02
Up	4-Guanidinobutanamide	1.3	0.0004
<i>Paralytic shellfish toxin biosynthesis</i>			
Up	Intermediate-A'	2.6	0.0008
Up	Cyclic-C'	2.1	7.7E-12
Up	Intermediate-E	2.2	1.3E-15
Up	Succinic acid	1.1	0.004
Up	Decarbamoyloxysaxitoxin	3.0	7.6E-15
<i>Jasmonic acid biosynthesis</i>			
Up	Jasmonic acid	1.2	0.004
Up	Linolenic acid	1.2	0.03

3.4.2 *Jasmonic acid biosynthesis and signaling are involved in toxin production initiated by copepodamides*

Surprisingly, as a part of the UPLC/MS metabolomics analysis, jasmonic acid and its precursor linolenic acid (Wasternack and Strnad 2018) were identified as being distinguishing features of the metabolome of *A. minutum* exposed to copepodamides (Table 3.1). The identity of jasmonic acid was confirmed by matching MS spectral data from the quality control samples, including retention time, $[M-H]^-$ and $[M+H]^+$ *m/z*

values, and MS/MS fragmentation pattern in positive mode, to a commercial standard (Table B1). Key identifying features of linolenic acid included: $[M-H]^-$ and $[M+H]^+$ m/z values and MS/MS fragmentation pattern in positive mode consistent with spectra from a publicly available database (2020), and positive NMR loadings signals (Figure B1a), also present in representative NMR spectra from experimental replicates characteristic of the omega-3 terminal methyl (triplet at 1.00 ppm) and internal allylic methylene groups (multiplets at 5.29 and 5.30 ppm). Both jasmonic acid and linolenic acid increased in concentration by 20% in *A. minutum* responding to copepodamides (Table 3.1), indicating that biosynthesis of jasmonic acid is involved in enhanced toxin production.

A set of inhibition experiments were performed to directly test the involvement of jasmonic acid biosynthesis in toxin induction in *A. minutum*. Serine/threonine phosphatases are known to stimulate jasmonic acid biosynthesis (Bajsa et al. 2011); when such phosphatases were inhibited using cantharidin (Honkanen 1993), toxicity in *A. minutum* increased significantly, by 11% ($F_{1,31} = 80.5$, $p \ll 0.001$; Figure 3.3a). Toxin production was further enhanced upon exposure to copepodamides, regardless of inhibition of serine/threonine phosphatases ($F_{1,31} = 299$, $p \ll 0.001$; Figure 3.3a). In fact, induction due to copepodamides was slightly higher greater (23%) when serine/threonine phosphatases were inhibited than when these phosphatases functioned without interference (21%) (Figure 3.3a). Not surprisingly, inhibition of these cell-critical phosphatases came at a substantial cost to growth (phosphatase inhibition: $F_{1,32} = 312$, $p \ll 0.001$; copepodamide exposure: $F_{1,32} = 20.4$, $p \ll 0.001$; Figure B2a). Overall, the findings indicate that jasmonic acid biosynthesis is a part of toxin regulation in *A. minutum* both constitutively and as a part of the induced response to copepodamides.

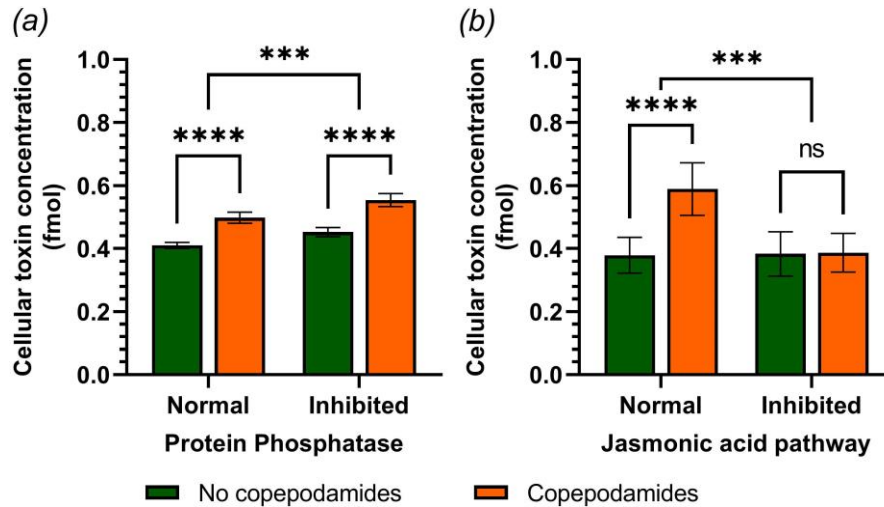


Figure 3.3 Jasmonic acid biosynthesis and signaling are involved in toxin production in *Alexandrium minutum* induced by copepodamide exposure. Bars represent the mean \pm standard deviation of cellular toxin concentration of gonyautoxins 1-4 in *A. minutum* in response to inhibition of (a) serine/threonine phosphatases by cantharidin and (b) jasmonic acid signaling by neomycin when exposed to a solvent control (No copepodamides, green) or 1 nM copepodamides (Copepodamides, orange). Data were analyzed using two-way ANOVAs with a Tukey HSD post hoc tests for multiple comparisons. Asterisks indicate the level of statistical significance; **** $p < 0.001$, *** $p < 0.001$, ns = not significantly different.

The induced biosynthesis of jasmonic acid observed upon copepodamide exposure led to the hypothesis that jasmonic acid signaling is part of the signal transduction leading to toxicity in *A. minutum*. Inhibition of the jasmonic acid signaling pathway via neomycin (Vadassery et al. 2019) resulted in a loss of copepodamide-induced toxicity in *A. minutum* (jasmonic acid signaling inhibition: $F_{1,31} = 17.8$, $p < 0.001$; copepodamide exposure: $F_{1,31} = 20.8$, $p < 0.001$; interaction effect: $F_{1,31} = 19.5$, $p < 0.001$; Tukey's HSD, $p = 0.99$; Figure 3.3b). However, interruption of the pathway had no effect on toxin concentrations in the absence of copepodamides (Tukey's HSD, $p = 1$; Figure 3.3b), implying that jasmonic acid signaling is not necessary for constitutive toxin production by *A. minutum*. Unlike with inhibition of serine/threonine

phosphatases, inhibition of jasmonic acid signaling had no direct impact on growth of *A. minutum*, although as in earlier experiments toxin induction associated with copepodamide exposure resulted in mild growth inhibition (jasmonic signaling inhibition: $F_{1,32} = 1.82$, $p = 0.22$; copepodamide exposure: $F_{1,32} = 6.13$, $p = 0.02$; interaction effect: $F_{1,32} = 1.53$, $p = 0.2$; Figure B2b). Curiously, and perhaps not surprisingly, it appears to be toxin induction – rather than copepodamide exposure per se – that slows growth, since *A. minutum* with blocked jasmonic acid signaling was observed to be both insensitive to copepodamide-induced toxin induction and insensitive to its growth-limiting effects (Tukey’s HSD, inhibited no copepodamide and copepodamide growth comparison: $p = 0.8$; Figure B2b). Taken all together, the results of both inhibition assays strongly suggest that jasmonic acid, via both its biosynthesis and signaling pathway, is involved in the signal transduction triggered by copepodamides that results in toxin induction in *A. minutum*.

3.4.3 *Copepodamides appear not to behave as GPCR agonists and do not disrupt cell membranes in Alexandrium minutum*

Based on prior studies (Wohlrab et al. 2010, Amato et al. 2018, Li and Ismar 2018, Harðardóttir et al. 2019, Mojib and Kubanek 2020), copepodamides were hypothesized to act as agonists of G protein-coupled receptors (GPCRs), triggering a signaling cascade that results in amplified toxin production in *A. minutum*. However, when the GPCR inhibitor SCH-202676 was applied to *A. minutum* to prevent binding of ligands to GPCRs (Fawzi et al. 2001), toxin concentrations rose significantly (GPCR inhibition: $F_{1,32} = 9.3$, $p = 0.004$; Figure B3a). Copepodamide-mediated toxin induction in *A. minutum* was further heightened by blocking GPCR chemoreception with toxin

concentrations increasing by 43% upon treatment with the GPCR inhibitor compared to only 27% in uninhibited *A. minutum* (copepodamide exposure: $F_{1,32} = 62.8$, $p \ll 0.001$; interaction effect: $F_{1,32} = 3.16$, $p = 0.08$; Figure B3a). Both inhibition of GPCRs and exposure to copepodamides induced toxin production without hindering growth in *A. minutum* in this experiment (GPCR inhibition: $F_{1,32} = 3.06$, $p = 0.09$; copepodamide exposure: $F_{1,32} = 2.3$, $p = 0.14$; interaction effect: $F_{1,32} = 0.122$, $p = 0.73$; Figure B3b). If GPCRs are critical to toxin induction, one would have expected abolition of their function to suppress copepodamide sensitivity in *A. minutum*; this was not observed, therefore our original hypothesis was rejected. To account for the likelihood that GPCR response is dose-dependent, a range of inhibitor concentrations (0.025 μM to 0.5 μM) was applied to *A. minutum*, and at all doses copepodamide-exposed cells were found to be more toxic than those not exposed to copepodamides (non-linear regression, $F_{4,16} = 15.54$, $p \ll 0.001$; Figure 3.4a). In fact, counter to the original hypothesis, greater inhibition of GPCRs was associated with augmented sensitivity as copepodamide-mediated toxin induction rose from 21 to 30%, with up to and including 0.1 μM SCH-202676 (Figure 3.4a). The slightly reduced sensitivity observed at the highest concentration of inhibitor (0.5 μM ; Figure 3.4a) was likely due to the extreme reduction in growth (Figure B4). Thus, GPCRs may play a role in toxin induction, but copepodamides appear not to act as agonists of GPCRs; instead copepodamides and a GPCR signaling cascade might interact via a more complex mechanism that leads to toxin induction.

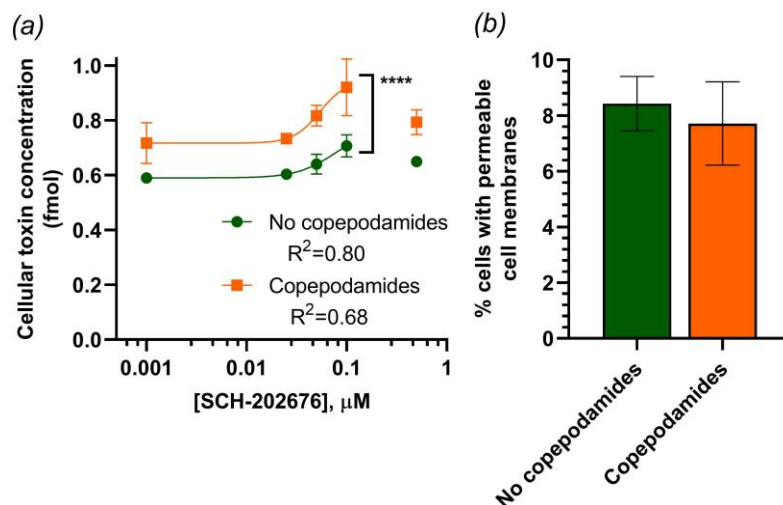


Figure 3.4 Copepodamides appear not to be agonists of GPCRs nor do they disrupt cell membranes in *Alexandrium minutum*. (a) Points represent the mean \pm standard percent growth of *A. minutum* in response to inhibition of GPCRs by SCH-202676 at varying doses when exposed to a solvent control (No copepodamides, green circles) or 1 nM copepodamides (Copepodamides, orange squares). The data were analyzed using a sigmoidal fitted non-linear regression, excluding the highest dose. (b) Bars represent the mean \pm standard deviation percent *A. minutum* cells alive with permeable cell membranes when exposed to a solvent control (No copepodamides) or 1 nM copepodamides (Copepodamides). Data were analyzed using an unpaired t-test. Asterisks indicate the level of statistical significance; ** $p << 0.001$.**

An alternative hypothesis to receptor recognition of copepodamides is that they trigger toxin production through physical stress, resulting from disruption of *A. minutum* cell membranes. However, *A. minutum* cells whose toxicity was significantly induced by copepodamide exposure did not suffer significant cell membrane permeability ($t = 1.1$, $df = 12$, $p = 0.3$, $n = 7$; Figure 3.4b). Therefore, this alternative hypothesis was rejected. Nonetheless, these results do not exclude the possibility that copepodamides enter the cells through other mechanisms.

3.5 Discussion

Perception of the predatory copepod cue, copepodamides, triggers targeted changes in the metabolome of the toxic dinoflagellate *A. minutum* (Figure 3.5). Copepodamide exposure did not result in a complete rearrangement of the algal metabolome but instead caused subtle changes that were partially resolved using multivariate statistics (Figure 3.2 and Figure B1). Metabolism of the amino acids valine and arginine were both impacted (Table 3.1), consistent with disruptions to amino acid metabolism observed, via transcriptomics, in *Pseudo-nitzschia seriata*, *Phaeodactylum tricornutum*, and *Alexandrium tamarense* in the presence of copepods (Wohlrab et al. 2010, Amato et al. 2018, Li and Ismar 2018, Harðardóttir et al. 2019). Butanoate metabolism is closely associated with the TCA cycle, arginine metabolism, and fatty acid degradation (Ogata et al. 1999); therefore the upregulation of this pathway may be tied to the observed increases in arginine biosynthesis and jasmonic acid biosynthesis (Table 3.1), which begins with fatty acid degradation (Wasternack and Strnad 2018). Enhancement of arginine biosynthesis (Table 3.1) is unsurprising in the context of *A. minimum* toxin induction as two arginines are required for the synthesis of each gonyautoxin molecule (Cho et al. 2019). The observed increase in concentration of the gonyautoxins (Figure 3.1a) was expected. However, our detection of paralytic shellfish toxin precursors (Table 3.1) is relatively novel as previously these have only been identified in *Alexandrium catenella* as a part of a stable isotope labelled feeding experiment (Cho et al. 2019).

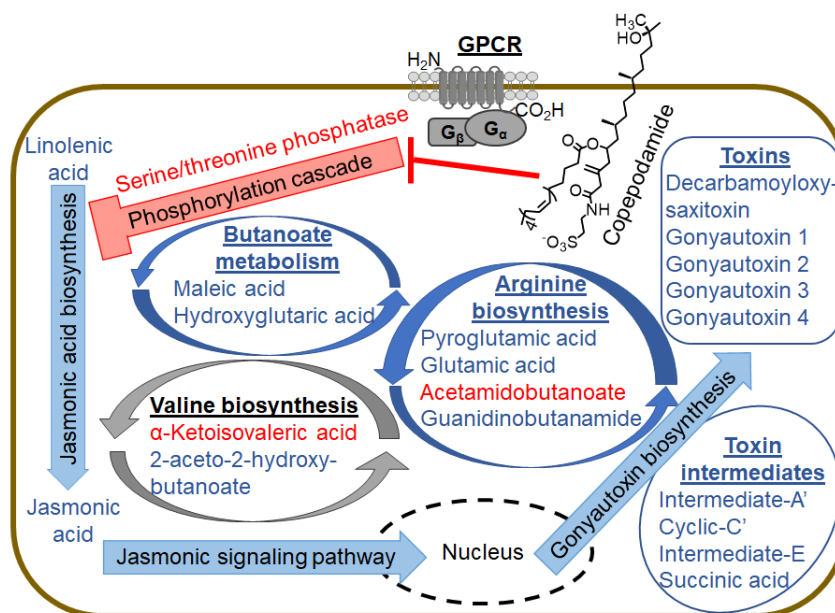


Figure 3.5 Cellular pathways and metabolites impacted in *Alexandrium minutum* by copepodamide exposure based on data from MS and NMR metabolomics, pathway inhibition experiments, and toxin analysis. Metabolites, enzymes, and pathways upregulated in response to copepodamides are indicated in blue. Red designates pathway and metabolites downregulated in response to copepodamides. Grey indicates equivocal regulation in response to copepodamides.

Copepodamide-induced toxicity appears to incur an inconsistent cost to *A. minutum* growth. In the original metabolomics experiment, exposure to copepodamides, and consequential 103% increase in toxicity, resulted in a 19% reduction in growth (Figure 3.1b). Additionally, *A. minutum* experienced 12 and 20% reductions in growth upon copepodamide exposure in the protein phosphatase and GPCR dose-dependent inhibition experiments, respectively (Figure B2a and Figure B4). Conversely, equivocal effects on growth occurred with copepodamide exposure in our jasmonic acid signaling and original GPCR inhibition experiments (Fig. S2b and S3b). The presence of the (albeit variably) observed trade-off between growth and toxin production in response to copepod cues stands in contrast to a recent study which reported no cost to toxicity

under varying levels of nitrogen limitation for the same strain of *A. minutum* (Ryderheim et al. 2021). While these authors observed no reduction in growth rate, *A. minutum* cells shrank when exposed to copepodamides, an effect not seen in the current study. This discrepancy may be due to the higher cell densities and lower phosphate concentrations utilized in the current study, compared to the study by Ryderheim and colleagues (2021), which would be expected to intensify competition for a limiting resource (phosphate). The elevated competition in the current study explains the realized cost of toxin production in the form of reduced growth. In juxtaposition to the Ryderheim study, Park and Dam found a 17-39% decrease in net growth rate in *A. tamarense* associated with toxin production in the presence of copepods (2021). Therefore, the true cost of toxin induction in *Alexandrium* spp remains unclear.

The mechanism by which *A. minutum* recognizes copepodamides remains ambiguous. Prior studies reported dysregulation of enzymes related to cyclic AMP (cAMP) and other GPCR signaling components in various phytoplankton taxa responding defensively to copepods and copepod cues (Wohlrab et al. 2010, Amato et al. 2018, Li and Ismar 2018, Harðardóttir et al. 2019), leading to a reasonable hypothesis that copepodamides act as GPCR agonists, triggering a signaling cascade via intracellular second messengers that culminates in upregulated toxin biosynthesis. However, in the current study inhibition of GPCRs by the general inhibitor SCH-202676 resulted in slightly increased, not decreased, toxin induction in *A. minutum* exposed to copepodamides (Figure 3.4a and Figure B3a); therefore, the original hypothesis was rejected. Nonetheless, this does not preclude the involvement of GPCR signaling altogether, as the chosen inhibitor is known to only act on the receptor, and not on other

G protein signaling components (Fawzi et al. 2001), leaving open the possibility that copepodamides interact downstream in this signaling pathway. Additionally, a previous study found that SCH-202676 actually increases antagonist binding to GPCRs (Göblyös et al. 2005) due to interactions with cysteine bonds in the GPCR (Göblyös et al. 2005, Lewandowicz et al. 2006). Therefore, it is possible that the observed augmentation of toxicity when GPCRs were inhibited immediately prior to copepodamide exposure was due to SCH-202676 assisting copepodamides in binding to GPCRs in an antagonistic manner, stopping a signaling pathway that normally limits toxin production. Another possibility is that copepodamides trigger defensive phenotypes differently in diatoms and dinoflagellates. In the diatom *Skeletonema marinoi*, copepod cues boosted cAMP activity (Amato et al. 2018) whereas in *A. tamarense* cAMP was reduced (Wohlrab et al. 2010). This is likely due to dramatic differences in the structures and functions of the predominant GPCRs and G protein signaling in diatoms and dinoflagellates (Mojib and Kubanek 2020). Perhaps copepodamides interact further upstream in the pathway in diatoms. Alternatively, due to the shorter length of the N-terminus and differences in the transmembrane domains in the more primitive dinoflagellate GPCRs (Mojib and Kubanek 2020), copepodamides may act as antagonists to dinoflagellate GPCRs and as agonists in diatoms. Consequently, further studies are warranted to tease out the mechanism by which copepodamides might interact with GPCRs and G protein signaling.

Despite their amphipathic, lipid-based structures, copepodamides do not disrupt cell membranes in *A. minutum*, dismissing an alternative hypothesis that they induce toxicity as a physical stress response. This hypothesis arose at least partly because

copepodamides with long chain fatty acyl groups that would be expected to insert into phospholipid-based cell membranes are an order of magnitude more potent than copepodamides lacking this functionality (Selander et al. 2015). However, since copepodamides did not significantly increase *A. minutum* cell membrane permeability (Figure 3.4b), this alternative hypothesis was rejected. Nevertheless, copepodamides might passively diffuse through phytoplankton cell membranes without causing substantial cell leakage, activating signaling pathways from within rather than via a membrane-bound GPCR. The femtomolar-to-nanomolar sensitivity of phytoplankton to copepodamides (Selander et al. 2015, Selander et al. 2019, Arias et al. 2021) supports the involvement of signal amplification via secondary messengers.

Signal transduction triggered by copepodamides in *A. minutum* is hypothesized to take place via inhibition of serine/threonine phosphatases, stimulation of jasmonic acid biosynthesis, and activation of the jasmonic acid signaling pathway (Figure 3.5). Inhibition of serine/threonine phosphatases, which negatively regulates jasmonic acid biosynthesis in vascular plants (Bajsa et al. 2011), augmented toxicity in *A. minutum* (Figure 3.3a). These results align with prior studies whereby copepod cues caused down-regulation of serine/threonine phosphatases in *P. seriata*, *P. tricornutum*, and *A. tamarense* (Wohlrab et al. 2010, Li and Ismar 2018, Harðardóttir et al. 2019). In the current study, overall upregulation of jasmonic acid biosynthesis was demonstrated by a 20% increase in jasmonic acid concentration in *A. minutum* exposed to copepodamides (Table 1). Jasmonic acid biosynthesis begins with the degradation of fatty acids and ends with formation of the carboxylic acid side chain of jasmonic acid via β -oxidation (Wasternack and Strnad 2018). While not all the biosynthetic steps were captured by the

current study, several transcriptomic studies of phytoplankton exposed to copepod cues have found consistent upregulation of lipid metabolism and β -oxidation (Wohlrab et al. 2010, Amato et al. 2018, Harðardóttir et al. 2019). Additionally, these studies found strong regulation of mitogen-activated protein kinase (MAPK) cascades, particularly those related to calcium-dependent protein kinases (Wohlrab et al. 2010, Amato et al. 2018, Li and Ismar 2018, Harðardóttir et al. 2019) which are required for jasmonic acid biosynthesis in many plants (Wasternack and Hause 2013). In vascular plants, increased intracellular pools of jasmonic acid promote transcription of defense-related genes (Wasternack and Strnad 2018); therefore, we hypothesized jasmonic acid in *A. minutum* to be involved in jasmonic acid signaling. This hypothesis was supported when inhibition of jasmonic acid signaling by neomycin eliminated copepodamide-induced enhanced toxicity (Figure 3.3*b*). Interestingly, phospholipase C (an enzyme which cleaves phospholipids) was recently identified as a regulator of jasmonic acid signaling (Kiba et al. 2020) and has also been labeled as an effector of GPCR signaling in both diatoms and dinoflagellates (Mojib and Kubanek 2020).

This study is the first in which jasmonic acid has been discovered in dinoflagellates. While jasmonic acid is known to act as a hormone involved in inducible defenses in vascular plants, it has not been found as readily among phytoplankton (Han 2016). It has been identified in only a handful of unicellular green algae and a single cyanobacterium. Confirmation of the jasmonic acid signaling pathway in phytoplankton has been even rarer because in most studies with phytoplankton, jasmonic acid has been added exogenously rather than being measured intracellularly (Newberger et al. 2006, Han 2016, Johnson et al. 2020). When addition of jasmonic acid resulted in phenotypic

changes, the involvement of the jasmonic acid signaling pathway was inferred but not probed further (Newberger et al. 2006, Han 2016, Johnson et al. 2020). However, in this study we not only measured an increase in endogenous jasmonic acid but also manipulated its signaling pathway to demonstrate its involvement in copepodamide-mediated toxin induction. This suggests that jasmonic acid signaling is a much older defense mechanism than anticipated (Han 2016) and provides further evidence that it pre-dates colonization of land by plants.

In conclusion, using metabolomics and inhibition experiments this study explored the subtle rearrangement of *A. minutum*'s metabolome in response to copepod predator cues and illuminated molecular mechanisms which result in increased toxicity. While a receptor of copepodamides was not identified, this study provided critical information about the potential involvement of G protein signaling and revealed the importance of jasmonic acid signaling in copepodamide-mediated toxin induction. Further research is needed to elucidate the receptor used by *A. minutum* and other phytoplankton in the chemosensation of copepodamides.

CHAPTER 4. DIFFERENTIATING TOXIC AND NONTOXIC CONGENERIC HARMFUL ALGAE USING THE NON-POLAR METABOLOME

Brown, E. R., S. G. Moore, D. A. Gaul, and J. Kubanek. 2021. Differentiating toxic and nontoxic congeneric harmful algae using the non-polar metabolome. *In review*.

4.1 Abstract

Recognition and rejection of chemically defended prey is critical to maximizing fitness for predators. Paralytic shellfish toxins (PSTs) which strongly inhibit voltage-gated sodium channels in diverse animal taxa are produced by several species of the bloom-forming algal genus *Alexandrium* where they appear to function as chemical defenses against grazing copepods. Despite PSTs being produced and localized within phytoplankton cells, some copepods distinguish toxic from non-toxic prey, selectively ingesting less toxic cells, in ways that suggest cell surface recognition perhaps associated with non-polar metabolites. In this study LC/MS and NMR-based metabolomics revealed that the non-polar metabolomes of two toxic species (*Alexandrium catenella* and *Alexandrium pacificum*) vary considerably from their non-toxic congener *Alexandrium tamarense* despite all three being very closely related. Toxic and non-toxic *Alexandrium* spp. were distinguished from each other by metabolites belonging to seven lipid classes. Of these, 17 specific metabolites were significantly more abundant in both toxic *A. catenella* and *A. pacificum* compared to non-toxic *A. tamarense* suggesting that just a small portion of the observed metabolic variability is associated with toxicity. Future

experiments aimed at deciphering chemoreception mechanisms of copepod perception of *Alexandrium* toxicity should consider these metabolites, and the broader lipid classes phosphatidylcholines and sterols, as potential candidate cues.

4.2 Introduction

The dinoflagellate genus *Alexandrium* is one of the most taxonomically and chemically diverse harmful algal bloom-forming genera (Anderson et al. 2012). Among the approximately 35 known species, at least half produce toxins of which there are three distinct classes: paralytic shellfish toxins (PSTs), spirolides, and goniodomins (Anderson et al. 2012, Murray et al. 2020). PSTs, which include saxitoxin, gonyautoxins, and *N*-sulfocarbamoyl and decarbamoyl analogs of saxitoxins (Anderson et al. 2012, Murray et al. 2020), are so named for their extreme inhibition of voltage-gated sodium channels leading to muscle paralysis, respiratory arrest, and occasionally death in humans (Faber 2012). At the time of their discovery, it was unclear what fitness advantages PSTs bestow on the phytoplankton cells that produce them. Many studies now support the hypothesis that PSTs function as induced chemical defenses against grazing zooplankton such as copepods (Selander et al. 2006, Bergkvist et al. 2008, Wohlrab et al. 2010, Turner 2014, Senft-Batoh et al. 2015a, Xu et al. 2017, Xu and Kiørboe 2018).

Consumption of toxic *Alexandrium* cells negatively impacts copepods. In a meta-analysis of experiments involving marine copepods and harmful algae, 19 studies were determined to have demonstrated adverse effects on copepods consuming *Alexandrium* cells (Turner 2014). The most commonly reported deleterious consequences are decreased fecundity and survivorship of juvenile copepods (nauplii)

(Frangopulos et al. 2000, Barreiro et al. 2007, Roncalli et al. 2016b, Abdulhussain et al. 2021), followed by disruption of swimming behavior (Turner 2014, Lasley-Rasher et al. 2016, Xu et al. 2018). However, some copepods that co-occur with toxic *Alexandrium* populations have evolved partial resistance to PSTs, appearing to not be deterred by or suffering adverse effects from PSTs (Colin and Dam 2007, Wohlrab et al. 2010). Unlike clams (Bricelj et al. 2005), heritable resistance to PSTs among copepods does not appear to involve mutations to sodium channels (Finiguerra et al. 2014, Finiguerra et al. 2015). Instead, recent transcriptome studies suggest that resistance to PSTs may be conferred by tight regulation of digestive enzymes to limit toxin assimilation and by detoxification pathways (Roncalli et al. 2016a, Roncalli et al. 2017, Han et al. 2021). However, for copepods that are sensitive to PSTs, selective consumption of non-toxic cells is expected to be advantageous.

Several studies have suggested that copepods actively favor non-toxic over toxic *Alexandrium* cells (Teegarden 1999, Selander et al. 2008, Senft-Batoh et al. 2015b). A foundational study by Teegarden showed that when simultaneously offered toxic *Alexandrium fundyense* and non-toxic *Alexandrium tamarense*, copepods belonging to three species preferentially grazed on non-toxic *A. tamarense* (1999). These *Alexandrium* spp. belong to a species complex whose cells are of similar size, shape, and nitrogen and carbon content (Balech 1990, Scholin et al. 1995), limiting variability among traits other than toxicity. Therefore, the Teegarden study provided initial support for the hypothesis that copepods are deterred by *Alexandrium* toxins. This selective feeding hypothesis has been explored further over the years using natural assemblages of phytoplankton (Teegarden et al. 2008), copepods with different feeding modalities (Xu et al. 2018) and

degrees of naïveté to toxic *Alexandrium* populations (Senft-Batoh et al. 2015b), and additional *Alexandrium* species (Xu et al. 2017, Xu and Kiørboe 2018, Abdulhussain et al. 2020). Data from these lab experiments have largely supported the selective feeding hypothesis with the exception of a study using the copepod *Temora longicornis* (Xu et al. 2017). However, in that case the non-toxic prey offered in choice experiments was not a congener, raising the possibility that the lack of observed preference could have been explained by other phytoplankton traits such as nutritional value. In contrast, the copepod *Acartia tonsa* consumed relatively fewer *A. minutum* cells when simultaneously offered non-toxic *Prorocentrum micans*, especially when *A. minutum* cells doubled their PST production upon exposure to copepod feeding cues (Selander et al. 2006). This study proposed that the copepods recognized that the induced cells were more toxic and discriminated against *A. minutum* in proportion to its toxicity. Taken together these studies strongly suggest that copepod feeding behavior is driven by toxicity in *Alexandrium* spp..

The simplest mechanism by which copepods might be expected to discern toxicity in prey would be to sense the toxins themselves. However, PSTs are synthesized and retained within *Alexandrium* cells and only released into the marine environment when cells lyse, making it improbable that copepods sense PSTs before consuming intact phytoplankton (Anderson et al. 1990b). Recent studies have suggested that copepods detect and select prey using near-field chemoreception, akin to taste, as opposed to far-field chemoreception, akin to smell (Gonçalves and Kiørboe 2015, Kiørboe et al. 2016, Xu et al. 2017). Therefore, we hypothesized that copepods use chemical cue(s) associated

with cell surfaces as indirect proxies for toxicity states among *Alexandrium* cells, as they come into contact with potential prey.

Glycoconjugates (Reuter and Gabius 1999) and cell membrane constituents (de Carvalho and Caramujo 2018) are frequently involved in cellular recognition. Lectins, which bind specific sugar moieties on glycoproteins and glycolipids, have previously been implicated in recognition of algal cells by oysters and zooplankton (Wootton et al. 2007, Espinosa et al. 2010). However, some algae may not be fully distinguishable by sugar moieties alone (Strom et al. 2003), so predators may need to assess other biochemical components of the cell membrane. Sterols, fatty acids, and other lipids have been found to act as biomarkers of various phytoplankton taxa (Véron et al. 1998, Martin-Creuzburg and Elert 2009, Řezanka et al. 2014, Řezanka et al. 2017) and impact the fluidity and three dimensional structure of cell membranes (de Carvalho and Caramujo 2018). Thus, their composition may also be integral to the chemosensory ability of zooplankton, including copepods, to distinguish prey. Therefore, in the current study exploring chemical cue(s) copepods may use to differentiate phytoplankton prey of varying toxicity levels, we chose to investigate the non-polar metabolome of three *Alexandrium* species. Quantitative analysis of their non-polar metabolomes was performed in two pairwise experiments: 1) toxic *Alexandrium catenella* was compared to non-toxic *Alexandrium tamarense* using the same strains as the foundational Teegarden study (1999); and 2) a more closely related toxic species, *Alexandrium pacificum*, was compared to the same non-toxic *A. tamarense* strain. Using this approach, we identified classes of lipids and other non-polar metabolites enriched in

both toxic species, presenting candidates for future experiments to decipher the chemoreception mechanism of copepod perception of *Alexandrium* toxicity.

4.3 Materials and methods

4.3.1 *Phytoplankton culturing*

Cultures of the non-toxic dinoflagellate *Alexandrium tamarense* strain CCMP 2023 (synonymous with CCMP 115 and CCAP 1119/1), and the toxic dinoflagellates *Alexandrium catenella* strain CCMP 1719 (synonymous with GTCA 28, previously named *Alexandrium fundyense* (John et al. 2014, Prud'homme van Reine 2017)) and *Alexandrium pacificum* strain CCMP 1493 (synonymous with ATCI01, previously named *A. tamarense* (John et al. 2014)), were acquired from NCMA Bigelow Laboratory. Cultures were arbitrarily arranged in a Percival incubator at 20 °C set to a 12:12 h light/dark cycle with irradiance of 100-123 $\mu\text{mol m}^{-2} \text{s}^{-1}$ and grown in filtered seawater from the Gulf of Maine (NCMA Bigelow Laboratory, a salinity of 35) amended with full strength K media (Keller et al. 1987). Cell density was quantified after preservation of cells with 1% acidified Lugol's solution by visual enumeration in a Palmer-Maloney chamber on an Olympus IX-50 inverted microscope.

4.3.2 *Experimental design*

To explore non-polar molecules associated with toxicity in *Alexandrium*, the non-polar metabolome of a single non-toxic species (*A. tamarense*) was compared with each of two toxic congeners (*A. catenella* and *A. pacificum*). *A. catenella* and *A. pacificum* were chosen due to their toxicity and phylogenetic relatedness to the well-studied non-

toxic *A. tamarensis*. *A. catenella* CCMP 1719 is known to produce saxitoxin, neosaxitoxin, gonyautoxins 1-5, and *N*-sulfocarbamoylgonyautoxin 3 (commonly known as C2) at concentrations of 12-31 pgSTXeq cell⁻¹ (Teegarden 1999, Orr et al. 2011). Prior feeding preference assays showed that copepods selectively feed on non-toxic *A. tamarensis* when offered alongside toxic *A. catenella* (Teegarden 1999). Therefore, we chose to compare these two strains for our first experiment. The *A. pacificum* strain chosen for this study, CCMP 1493, is also toxic, producing neosaxitoxin, gonyautoxins 1 and 3-5, and *N*-sulfocarbamoylgonyautoxins 2 and 3 (more commonly known as C1 and C2) at concentrations of 24-27 pgSTXeq cell⁻¹ (Orr et al. 2011, Blossom et al. 2019); however, copepod feeding preferences associated with this strain have not been established. Historically, all three species used in this study have been considered members of the *A. tamarensis* 'species complex', with *A. catenella* CCMP 1719 in Clade I, Group I and *A. tamarensis* CCMP 2023 and *A. pacificum* CCMP 1493 both in Clade II in the subclade Groups III and IV, respectively (Scholin et al. 1995, John et al. 2014). More recently, a series of phylogenetic studies were undertaken to better understand the genetic relationships between these groups and more clearly define species within the genus *Alexandrium* which resulted in reclassification of many strains, including CCMP 1719 from *A. fundyense* to *A. catenella* and CCMP 1493 from *A. tamarensis* to *A. pacificum* (Orr et al. 2011, John et al. 2014, Wang et al. 2014, Prud'homme van Reine 2017). Furthermore, Wang and colleagues who used ribosomal internal transcribed spacer rDNA found the estimated genetic distance between *A. tamarensis* and *A. catenella* to be 0.181, the distance between *A. tamarensis* and *A. pacificum* to be 0.161, and the distance between *A. catenella* and *A. pacificum* to be 0.196 (for reference, the maximum

intra-clade species difference was 0.066 and the inter-clade differences ranged from 0.134 to 0.216) (Wang et al. 2014). This means that toxic *A. pacificum* and non-toxic *A. tamarense* are more closely related to each other than toxic *A. catenella* is to *A. tamarense* and that both the toxic species, *A. catenella* and *A. pacificum*, are more distantly related to each other than either is to *A. tamarense*. Therefore, despite a lack of documented copepod feeding preferences, *A. pacificum* was chosen for second comparison to *A. tamarense* because its closer phylogenetic relationship means it likely has fewer confounding physiological differences other than toxicity.

Accordingly, metabolomes of toxic versus non-toxic species were compared using the following experimental pairings: *A. tamarense* (n=15) with *A. catenella* (n=15) (Experiment 1) and *A. tamarense* (n=15) with *A. pacificum* (n=15) (Experiment 2). The same non-toxic strain of *A. tamarense* was used in both experiments but the two experiments were conducted separately, in different months, to make the experiment manageable based on availability of batches grown from stock cultures. Due to the experiments being performed independently, quantitative comparisons were made only within and not between experiments. For both experiments, *Alexandrium* spp. cultures at a cell density of 12,000 to 13,000 cells mL⁻¹ were split into fifteen 300 mL subcultures of each species which grew for two days. At the end of each experiment, during harvesting, a 1.0 mL aliquot from each culture was preserved with Lugol's solution to measure cell concentrations.

4.3.3 *Harvesting and extraction*

Cultures were harvested with handling of replicates and treatments intermixed over approximately 2 h within 6 h of the start of the light cycle. Harvesting and extraction of cells was carried out as reported by Brown et al. (submitted), involving a slight modification of methods used by Poulson-Ellestad et al. (2014) in order to broadly extract non-polar metabolites, including sterols, fatty acids, glycosylated lipids, and various other classes of lipids. An aliquot of 50 mL of each culture was harvest by centrifugation at 3,260 x g for 10 min. The resulting cell pellets were freeze-dried and stored in a -80 °C freezer for later toxin analysis (see section 4.3.4). The remaining cells were harvested under vacuum onto muffled GF/F filters (Whatman #1825-110). Cell metabolism was then quenched with liquid nitrogen and cells were stored at -80 °C in muffled foil pouches until extraction. Cells were extracted with 30 mL of ice-cold 3:2:1 methanol/acetone/acetonitrile (OmniSolv, >99.5%, MilliporeSigma) by grinding the frozen filters with a liquid nitrogen-chilled mortar and pestle. To remove filter particulates, the extracts were centrifuged four times at 800 x g for 15 min. Solid materials were rinsed each time with fresh solvent and rinses combined with the supernatant to create one 53 mL extract. To remove remaining small particulates, extracts were filtered with a 0.2 µm nylon syringe filter (Acrodisc, Pall Laboratory) before being dried *in vacuo* using a Thermo Savant Speedvac concentrator. Non-polar and polar metabolites were separated by partitioning extracts in a biphasic mixture of 9:10:15 water/methanol/chloroform (OmniSolv, >99.5%, MilliporeSigma). Extracts were then dried again *in vacuo* with non-polar extracts used for further analysis and polar extracts set aside.

4.3.4 Toxin analysis

The cell pellet from each 50 mL aliquot was suspended in 500 μ L 1% aqueous acetic acid and subjected to four freeze-thaw cycles with sonication in a water bath to lyse cells and extract toxins (Devlin et al. 2011). Each sample was then centrifuged at 10,000 \times g for 5 min to pellet debris and the toxin-containing supernatant was filtered through a 0.2 μ m nylon syringe filter to remove precipitate. Toxin extracts were analyzed using positive electrospray ionization on a Waters QDA mass spectrometer (Waters Corporation) coupled to a Waters 2695 Separation Module (Waters Corporation). Chromatographic separation of the extracts was achieved by injecting of 20.0 μ L onto HILIC TSKgel Amide-80 column (4.6 \times 150 mm, 3 μ m particle size; TOSOH Bioscience), operated at 30 $^{\circ}$ C, fitted to the LC system with 5 rinses of the injection loop between samples. A flow rate of 1.0 mL min^{-1} was used with the following mobile phase gradient acidified with 0.1% formic acid: equilibration at 60% aqueous acetonitrile; 0-1 min hold at 60% aqueous acetonitrile; 1-9 min ramp to 20% aqueous acetonitrile; 9-11 min hold at 20% aqueous acetonitrile; 11 min return to 60% aqueous acetonitrile and reequilibration until 19 min. Toxin concentrations were calculated using the integrated area of the following ion signals via single ion recording: m/z 300.1 for saxitoxin, m/z 316.1 for neosaxitoxin, m/z 332.1 for gonyautoxin 1, m/z 396.1 for gonyautoxin 2 and 3, C1, and C2, and m/z 412.1 for gonyautoxin 4 (Yang et al. 2017, Huang et al. 2020). The integrated areas of ion peaks were compared with standard solutions, interspersed after every four samples, obtained by dilution of certified reference calibration solutions purchased from The National Research Council of Canada. A calibration curve of external standards at seven concentrations for each of the toxins plus a solvent blank

showed a linear relationship between toxin concentrations and area of mass spectral peaks. The limit of detection for each toxin was as follows: 0.085 μM for saxitoxin, 0.15 μM for neosaxitoxin, 0.010 μM for gonyautoxin 1, 0.35 μM for gonyautoxin 3, C1, and C2 combined, and 0.17 μM for gonyautoxin 4 or 0.76 μM for total toxin concentration. Toxin measurements are reported as the total concentration of all detected toxins.

4.3.5 NMR sample preparation and spectral data acquisition

Non-polar extracts were dissolved with volumes calculated to account for different cell densities at the time of harvesting, to a concentration equivalent to 1.62×10^7 *Alexandrium* cells mL^{-1} in dimethyl sulfoxide- d_6 (99.9% atom d_6 -DMSO; Cambridge Isotope Labs) containing 0.1% trimethylsilane (TMS) as internal standard for ^1H nuclear magnetic resonance (NMR) spectroscopy analysis. The extracts were transferred to 3 mm NMR tubes. Extracts from Experiment 1 (*A. tamarense*-*A. catenella*) were analyzed using a Bruker Avance IIIHD 800 MHz NMR spectrometer equipped with a 3 mm triple resonance broadband cryoprobe. Extracts from Experiment 2 (*A. tamarense*-*A. pacificum*) were analyzed using a Bruker Avance IIIHD 700 MHz NMR spectrometer equipped with a 5 mm indirect broadband cryoprobe, because the 800 MHz instrument was unavailable at the time of data acquisition. Spectra of non-polar extracts from both experiments were acquired using a Bruker zg30 pulse sequence ^1H NMR experiment compiled from 320 scans.

4.3.6 NMR spectral processing and analysis

Spectra were pre-processed using Metabolab version 2019.12.08.1237 (Ludwig and Günther 2011) in Matlab R2013a version 8.1.0.604. The spectra from both experiments were processed separately but using the same parameters. Both sets of spectra were aligned using the TMS internal standard (0.00 ppm), manually phased, spline baseline corrected to improve peak integration, and segmentally aligned. The following spectral regions were removed: -0.50 to 0.30 ppm (excess upfield region), 2.49-2.53 ppm (residual DMSO), 3.30-3.45 ppm (water), and 10.70-11.50 ppm (excess downfield region). The spectra were filtered to reduce the impact of noise, binned (0.005 ppm), and probabilistic quotient normalized to minimize minute differences in dilution (Dieterle et al. 2006). The data were generalized logarithmic transformed to minimize technical variance and highlight biological variance (Parsons et al. 2007) using $\lambda = 7.4690 \times 10^{-9}$ for Experiment 1 (*A. tamarense*-*A. catenella*) and $\lambda = 8.2594 \times 10^{-9}$ for Experiment 2 (*A. tamarense*-*A. pacificum*). Finally, the data for both experiments were mean centered.

PLS-Toolbox version 8.0.2 (Eigenvector Research) in Matlab was used to generate orthogonalized partial least-squares discriminant analysis (oPLS-DA) models which were cross-validated using Venetian blinds methods with five data splits for each comparison. Due to poor NMR spectral quality one *A. tamarense* replicate spectrum was removed from analysis of Experiment 1 (*A. tamarense*-*A. catenella*) and two *A. pacificum* and four *A. tamarense* replicate spectra were removed for Experiment 2. The loadings of the first principal component and first latent variable of the PCA and

oPLS-DA models, respectively, were used to identify spectroscopic features that were significantly different between the non-polar metabolomes in each experiment.

4.3.7 UPLC/MS sample preparation and data acquisition

Unlike with ^1H NMR spectroscopy, extracts for both experiments were prepared and analyzed by ultra-high performance liquid chromatography tandem mass spectrometer (UPLC/MS) together. Using LCMS grade 2:1 isopropyl alcohol/acetonitrile (OmniSolv, >99.5%, MilliporeSigma) extracts were reconstituted at a concentration equivalent to 4.54×10^6 *Alexandrium* cells mL^{-1} in and centrifuged at $21,100 \times g$ for 5 min to pellet minute particulates. Unfortunately, two *A. pacificum* samples from Experiment 2 were lost due to vials breaking during reconstitution. A small portion of all remaining samples were combined to create nine pooled quality control samples. The pooled quality samples were analyzed after every 10 injections of the randomly interspersed *Alexandrium* extracts to monitor instrumental drift. Additionally, a solvent blank was analyzed at the beginning and end of the analysis.

Extracts were analyzed using a Orbitrap ID-X Tribrid Mass Spectrometer (ThermoFisher Scientific) coupled to a Vanquish UPLC system (ThermoFisher Scientific). Chromatographic separation of the extracts was achieved by injecting of $2.0 \mu\text{L}$ onto an Accucore C30 silica column ($2.1 \times 150 \text{ mm}$, $2.6\text{-}\mu\text{m}$ particle size; ThermoFisher Scientific), operated at $50 \text{ }^\circ\text{C}$, fitted to the UPLC system. Mobile phase A was 40:60 water/acetonitrile and mobile phase B was 10% acetonitrile in isopropyl alcohol with both containing 10 mM ammonium formate and 0.1% formic acid buffer (Optima, LCMS, Fischer Scientific). A flow rate of 0.4 mL min^{-1} was used with the

following mobile phase gradient: equilibration at 80% A; 0-1 min ramp to 40% A; 1-5 min ramp to 30% A; 5-5.5 min ramp to 15% A; 5.5-8 min ramp to 10% A; 8-8.2 min ramp to 0% A; 8.2-10.5 min hold at 0% A; 10.5-10.7 min return to 80% A and re-equilibration at 80% A until 12 min.

Mass spectrometric analysis was accomplished using the ID-X Tribrid spectrometer which possesses a resolution power of 500,000 FWHM at 200 m/z and mass accuracy of <1 ppm. Extracts were analyzed twice, first in negative ionization mode with a spray voltage of 2.5 kV and then in positive ionization mode with a spray voltage of 3.5 kV. Other than spray voltage, all other instrument settings were the same. The heated electrospray ionization source was run at a vaporizer temperature of 275 °C with nitrogen gas flows at 40, 8, and 1 L h⁻¹ for sheath, auxiliary, and sweep, respectively. Data was acquired using a scan range of 70-1050 m/z and an automatic gain control set at 1×10^5 ions. Tandem mass spectrometry (MS/MS) data were acquired in a data-dependent manner with a resolution of 30,000 and an isolation window of 0.8 m/z with a cycle time of 1.5 s. Dynamic exclusion was set to 10 s and data-dependent MS/MS was activated by higher energy collisional dissociation with stepped normalized collision energies of 15, 30, and 45 % or collision-induced dissociation energy of 30%. AcquireX Deep Scan was performed with four iterations to maximize number of collected MS/MS scans. Data acquisition was carried out using Compound Discoverer V3.0 (ThermoFisher Scientific).

4.3.8 UPLC/MS data processing and analysis

After UPLC/MS acquisition, spectral features (retention time, m/z) were extracted from chromatograms using Compound Discoverer version 3.1 (ThermoFisher Scientific) and XCMS online (Gowda et al. 2014). This was accomplished by aligning chromatograms, picking and integrating peak pickings, followed by extraction and normalization of peak areas. Spectral features were filtered for noise using the following parameters: peak areas had to be five times greater than baseline, as determined by the blank samples, and features had to be present in greater than 50% of the pooled quality control samples and have a relative standard deviation of less than 30%.

Principal component analysis (PCA) was used to examine differences in non-polar metabolomes of *A. tamarense* vs. *A. catenella* (Experiment 1) and *A. tamarense* vs. *A. pacificum* (Experiment 2), using Compound Discoverer. Each dataset was log 10-transformed and PCA models generated based on spectral features with a fold change greater than or equal to 1.1 or less than or equal to 0.9 and $p \leq 0.05$ via t-test when comparing the metabolomes within each experiment. Additionally, spectral features extracted by XCMS online were entered into LIPID Metabolites and Pathways Strategy (LIPID MAPS) Online Tools (Fahy et al. 2007) to generate volcano plots using a fold-change threshold of 1.1 and $p \leq 0.05$ in order to identify significantly different features in each experiment.

4.3.9 Metabolite annotation

Lipids whose concentrations were positively associated with both toxic *Alexandrium* species, *A. pacificum* and *A. catenella*, were sought by comparing the

non-polar metabolomes of each toxic species with non-toxic *A. tamarensis* from their respective experiment. Specifically, metabolites were prioritized for identification if they were more abundant, by similar proportions, in both toxic species relative to *A. tamarensis* from their respective experiment, and had minimal differences in abundance between *A. tamarensis* in both experiments. Metabolite characterization was predominately dependent on UPLC/MS and MS/MS data. (¹H NMR spectroscopy data were mainly used for identification of functional groups and metabolite classes.) Using Compound Discoverer, elemental formulae were generated based on exact mass and isotopic patterns from UPLC/MS data. The elemental formulae along with [M-H]⁻ and [M+H]⁺ *m/z* ions, MS/MS fragmentation patterns, retention time, and isotopic patterns were compared to a local spectral database, built from curated experimental data, as well as these publicly available databases: ChemSpider, LIPID MAPS classification and database (Sud et al. 2006, Fahy et al. 2009), MassBank of North America (MoNA)(2020), the human metabolome database (HMDB) (Wishart et al. 2007), mzVault (in house database), and mzCloud. Additionally, the LOBSTAHS database (Collins et al. 2016) and LIPID MAPS Online Tools (Fahy et al. 2007) were used to putatively identify some MS features, by matching exact mass and adduct patterns. Retention time and characteristic MS/MS fragmentation patterns were also used to place metabolites into broader lipid classes even when full identification was not achieved (Brügger et al. 1997, Piretti et al. 1997, Hsu et al. 2007, Taguchi 2009, Murphy and Axelsen 2011, Zianni et al. 2013, Hsu 2016). KEGG (Ogata et al. 1999) and LIPID MAPS were utilized to map the significant metabolites onto known metabolic pathways.

4.4 Results

4.4.1 *The non-polar metabolomes of Alexandrium spp. vary considerably between closely related toxic and non-toxic species*

A. pacificum and *A. catenella* produce suites of structurally similar paralytic shellfish toxins (PSTs) including saxitoxin, neosaxitoxin, gonyautoxins 1-5, and *N*-sulfocarbamoylgonyautoxins 2 and 3 (more commonly known as C1 and 2) whereas the *A. tamarense* strain used in this study is traditionally classified as non-toxic (Orr et al. 2011, John et al. 2014). Using LC/MS analysis, *A. catenella* and *A. pacificum* were found to produce 16.6 ± 1.9 and 0.733 ± 0.005 fmol of total PSTs per cell, respectively (n = 3 for each species), based on detection of gonyautoxins 2/3 and 1/4, C1/2, neosaxitoxin, and saxitoxin in *A. catenella*; and gonyautoxins 1 and 2/3, C1/2, and neosaxitoxin in *A. pacificum*. While these concentrations are lower than previously reported, there is precedence for decreased toxin concentrations at lower growth rates (Juhl et al. 2001, Devlin et al. 2011). No toxins were detected in *A. tamarense* despite a limit of detection of 0.76 μ M, corresponding to approximately 0.4 fmol per cell (n = 6).

The non-polar metabolomes of *A. pacificum* and *A. catenella* differed substantially from their non-toxic congener *A. tamarense* based on analysis by principal component analysis (PCA) and orthogonal partial least squares discriminant analysis (oPLS-DA) on UPLC/MS and ¹H NMR datasets, respectively (Figure 4.1 and Figure 4.2). In Experiment 1, *A. catenella* metabolomes were fully distinguishable from *A. tamarense* metabolomes across the first principal component, which captured an average of 63.4% of the variance, using both ionization modes of MS data analysis

(Figure 4.1A and B) and over the first latent variable, which captured 2.8% of the variance, based on NMR spectral data analysis (Figure 4.2A). Distinctions between metabolomes were driven by 15,581 unique mass spectral features which varied significantly between *A. catenella* and *A. tamarensis*. Of these unique features, 2,998 did not vary substantially in *A. tamarensis* between Experiments 1 and 2. In contrast, the metabolomes of *A. pacificum* and *A. tamarensis* in Experiment 2 were mostly but not completely separated over the first principal component via MS analysis (Figure 4.1C and D) and over the first latent variable from NMR data analysis (Figure 4.2C), which captured an average of 49.7%, across both MS ionization modes and 63.9% of the NMR variance. Only 6,878 unique mass spectral features varied significantly between *A. pacificum* and *A. tamarensis* and 1,121 of these features did not vary substantially in *A. tamarensis* between Experiments 1 and 2.

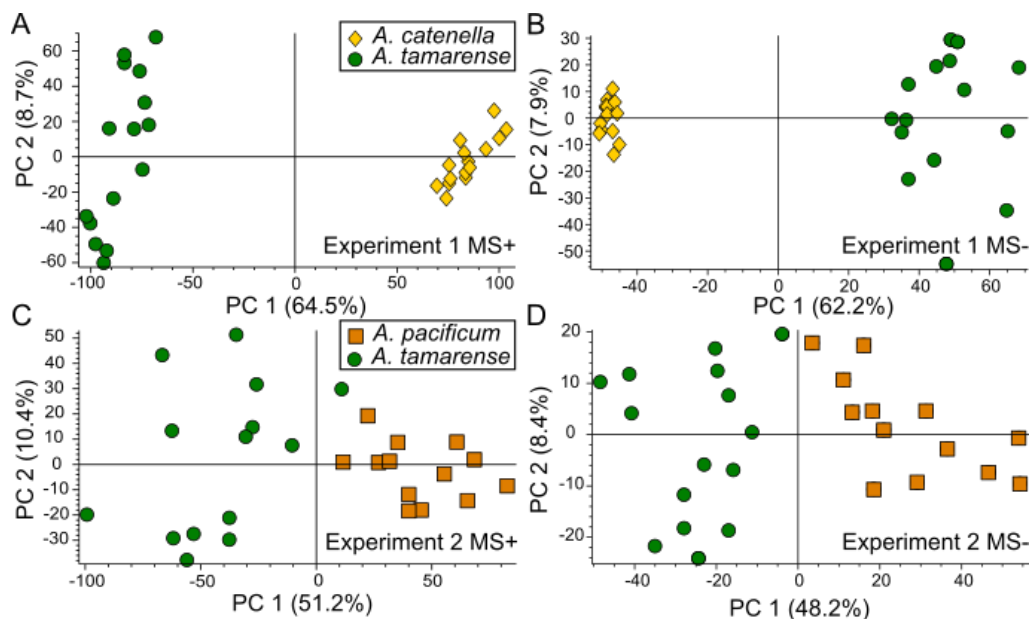


Figure 4.1 The non-polar metabolomes of toxic *Alexandrium* species, *A. catenella* and *A. pacificum*, differ considerably from non-toxic *A. tamarensis* based on PCA models from UPLC/MS data. Yellow diamonds represent metabolomes of *A. catenella*, orange squares represent metabolomes of *A. pacificum*, and green circles represent metabolomes of *A. tamarensis*. Scores plots from PCA models based on UPLC/MS analysis of Experiment 1 (A and B) and 2 (C and D) metabolites using both positive (A and C, “MS+”) and negative mode (B and D, “MS-”).

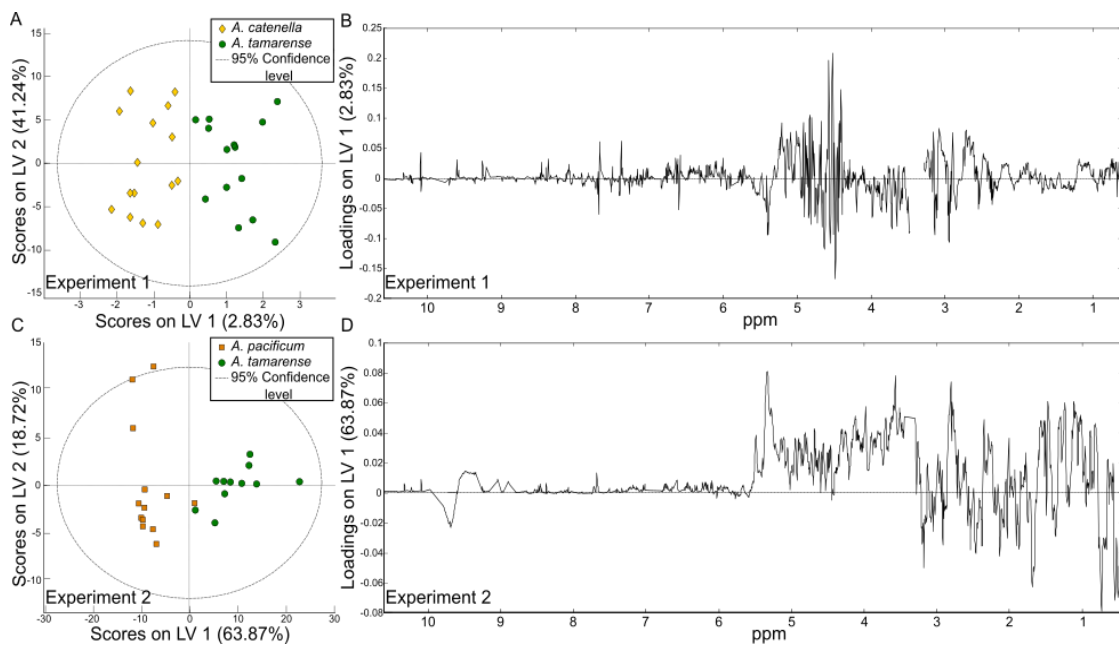


Figure 4.2 oPLS-DA models of NMR spectral data revealed that non-polar metabolomes of toxic *Alexandrium* (*A. catenella* and *A. pacificum*) species differ from non-toxic *A. tamarensis*. Yellow diamonds represent metabolomes of *A. catenella*, orange squares represent metabolomes of *A. pacificum*, and green circles represent metabolomes of *A. tamarensis*. oPLS-DA models based on ^1H NMR spectral analysis of Experiment 1 (A and B) and 2 (C and D) with scores plots (A and C) and their corresponding loadings plots on the first latent variable (B and D). Positive loading values signify metabolites in greater concentration in *A. catenella* (B) and *A. pacificum* (D) than *A. tamarensis*, whereas negative loads show metabolites enhanced in *A. tamarensis*.

MS-based metabolomics analysis led to putative identification of 34 metabolites belonging to seven lipid classes that were in significantly different concentrations either between *A. catenella* and *A. tamarensis* (Experiment 1, Table C1) or between *A. pacificum* and *A. tamarensis* (Experiment 2, Table C2). All but two of these metabolites were more abundant in at least one of the toxic species than in non-toxic *A. tamarensis* (Table 4.1). For both *A. catenella* and *A. pacificum*, the metabolites whose concentrations were most enhanced relative to *A. tamarensis* belonged to the

triacylglycerol class (Table 4.1). Additionally, the majority of tentatively identified metabolites which were in higher concentration in *A. catenella* were triacylglycerols, whereas glycerophospholipids were the most represented class in *A. pacificum* (Table 4.1).

Table 4.1 Lipid classes identified by MS-based models with significantly different concentrations in toxic *Alexandrium catenella* or *Alexandrium pacificum* compared to non-toxic *A. tamarense*. The number of compounds in each class and the average fold-change is included for each class. Average fold-change is the mean change in concentration for each lipid in *A. catenella* relative to *A. tamarense* (Experiment 1) and in *A. pacificum* relative to *A. tamarense* (Experiment 2).

Lipid class	<i>A. catenella</i>		<i>A. pacificum</i>	
	# of metabolites	Average fold-change	# of metabolites	Average fold-change
Free fatty acids	1	4.9	2	1.6
Monoacylglycerols	1	1.5	1	2.0
Diacylglycerols	3	8.4	-	-
Triacylglycerols	12	11.1*	1	2.4
Sphingolipids	3	2.2	-	-
Glycerophospholipids	7	4.7 [§]	5	1.4 [§]
Sterols	2	1.7 [§]	1	2.3

*Average calculated using at least one metabolite whose fold-change value was uncertain.

[§] Average includes a metabolite which was less abundant in the toxic species.

4.4.2 Only a small portion of the non-polar metabolome of *Alexandrium* spp. is likely associated with toxicity

The majority of the identified metabolites differed significantly in concentration in either *A. catenella* or *A. pacificum*, but not both, relative to *A. tamarense* (Table C1 and Table C2). In fact, only 747 features from the MS metabolomics analysis varied significantly between both toxic species and *A. tamarense*. This was consistent with the

NMR spectral analysis (Figure 4.2B and D) which pointed to different components of the non-polar metabolomes as critical to distinguishing metabolomes of the toxic species from *A. tamarensis* in each experiment. Notably, NMR spectral features with chemical shifts of 3.5-4.0 ppm, indicative of metabolites containing alcohols, ethers, or halides, were more strongly associated with toxic *A. pacificum* than non-toxic *A. tamarensis* in Experiment 2 (Figure 4.2B and Figure C1A), whereas in Experiment 1 they were slightly more enhanced in non-toxic *A. tamarensis* than toxic *A. catenella* (Figure 4.2D and Figure C1A). However, there were some chemical features which seemed to be consistently more highly represented in both toxic species. For example, some aromatic metabolites appear to be associated with *A. catenella* and *A. pacificum* rather than *A. tamarensis* based on enrichment in protons in the regions from 6.0-6.2 ppm, 6.6-6.8 ppm, 7.0-7.2 ppm, 7.7-7.8 ppm, and 8.0-8.2 ppm in toxic metabolomes (Figure 4.2B and D and Figure C1B). Additionally, 17 metabolites were found by MS metabolomics to be significantly more abundant in both *A. catenella* and *A. pacificum* relative to *A. tamarensis* of which three were partially identified (Table 4.2). One metabolite, a 20 carbon dihydroxy sterol glycosylated with glucuronic acid, was detected at concentrations that were 190% and 130% greater in toxic *A. catenella* and *A. pacificum*, respectively, compared to *A. tamarensis* (Table 4.2). A phosphatidylinositol containing two fatty acyl chains with a total of 35 carbons and 5 double bonds and a triacylglycerol containing three fatty acyl chains with a total of 49 carbons and 3 double bonds were also in higher abundance in *A. catenella* and *A. pacificum* (Table 4.2). In contrast, a phosphatidylcholine containing two fatty acyl chains with a total of 48 carbons and 12 double bonds, was 46% and 38%,

respectively, less concentrated in both toxic species compared to *A. tamarensis* (Table 4.2).

Table 4.2 Candidate metabolites tentatively identified that were in significantly different concentrations in both toxic *Alexandrium catenella* and *Alexandrium pacificum* compared to non-toxic *A. tamarensis*. The change in concentration is the compound's concentration in *A. catenella* relative to *A. tamarensis* (Experiment 1) and its concentration in *A. pacificum* relative to *A. tamarensis* (Experiment 2). P values were calculated using an unpaired t-test. Lipid classifications: phosphatidylcholines (PCs), phosphatidylinositols (PIs), and triacylglycerols (TGs).

Metabolite	<i>A. catenella</i>		<i>A. pacificum</i>	
	Fold-change	P value	Fold-change	P value
PI 35:5	1.6	1.5 E -3	1.5	0.003
Sterol 20:1; O2; glucuronide	2.9	1.4 E -5	2.3	0.02
TG 49:3; O3	4.9	1.2 E -8	2.4	0.004
PC 48:12	0.54	6.9 E -12	0.62	6.7 E -9

4.5 Discussion

The non-polar metabolomes of toxic and non-toxic *Alexandrium* vary considerably despite being closely related congeners. The species in this study all belong to what has historically been referred to as the *A. tamarensis* species complex (Scholin et al. 1995) with the two toxic species each being more phylogenetically similar to actual *A. tamarensis* than to each other (Wang et al. 2014). Moreover, until 2014 the strains used in Experiment 2 (non-toxic *A. tamarensis* CCMP 2023 and toxic *A. pacificum* 1493) were considered members of the same species (John et al. 2014, Wang et al. 2014). Therefore, the observed clear statistical separation of the non-polar metabolomes of non-toxic *A. tamarensis* from each toxic species in both experiments (Figure 4.1 and Figure 4.2A

and C) may at first seem surprising. However, a hallmark of *Alexandrium* populations, particularly those in the *A. tamarensis* species complex, is their great genetic and phenotypic diversity, even within some of its species (Alpermann et al. 2009, Tillmann et al. 2009, Anderson et al. 2012, Brandenburg et al. 2018). For example, among 15 geographically overlapping strains of *Alexandrium ostenfeldii*, maximum growth rate varied by 3.3-fold, toxicity varied by 74-fold, and cellular carbon-to-nitrogen ratios varied by 3.0-fold (Brandenburg et al. 2018). Thus, our discovery of 15,581 spectral features varying significantly in abundance between *A. catenella* and *A. tamarensis*, and 6,878 spectral features differing between *A. pacificum* and *A. tamarensis* consistent with our expectations based on prior knowledge of this harmful alga.

As generalist consumers of single-celled algae, many copepod species favor non-toxic *Alexandrium* cells over cells rich in PSTs when offered a choice (Teegarden 1999, Selander et al. 2008, Senft-Batoh et al. 2015b). Since PSTs are intracellular (Anderson et al. 1990b) and copepods select prey after handling but before consuming them (Gonçalves and Kiørboe 2015, Xu et al. 2017), copepods may be recognizing cell surface chemical cues that are associated with toxicity rather than the toxins themselves. Various classes of lipids and other cell membrane components can act as phylogenetic biomarkers (Véron et al. 1998, Martin-Creuzburg and Elert 2009, Řezanka et al. 2014, Řezanka et al. 2017) and have even been linked to detection of algal prey by grazers (Wootton et al. 2007, Espinosa et al. 2010). Therefore, it is possible that some of the compounds in the non-polar metabolome that vary in abundance between toxic *Alexandrium* species (*A. catenella* and *A. pacificum*) and non-toxic *A. tamarensis* may facilitate copepod selection of less chemically defended prey.

Metabolites belonging to seven different lipid classes were implicated in the separation of the non-polar metabolomes of *Alexandrium* species based on toxicity; however, some classes are less likely than others to function as cues for copepods. Among these, fatty acids, mono- and triacylglycerols, glycerophospholipids, and sterols were in greater abundance in both toxic *A. catenella* and *A. pacificum* relative to non-toxic *A. tamarense* (Table 4.1). Free fatty acids have previously been used to distinguish classes of algae (Mansour et al. 1999, Mansour et al. 2003, Cañavate et al. 2017, de Carvalho and Caramujo 2018). However, their quantities and composition are often variable throughout the growth phases of phytoplankton (Mansour et al. 2003, Hammann et al. 2013), making them unreliable indicators of a cell's toxicity. Similarly, triacylglycerol concentrations fluctuate throughout the life of phytoplankton cells (Mansour et al. 2003, Cañavate et al. 2017) due to their primary function in energy storage (Manoharan et al. 1999). Monoacylglycerols are also storage metabolites (de Carvalho and Caramujo 2018) as well as breakdown products of triacylglycerols (Goutx et al. 2003), thus exhibiting high variability, making them poor candidates as cues for grazing copepods.

Among the glycerophospholipid class of lipids, phosphatidic acids, phosphatidylinositols, and phosphatidylcholines were the sub-classes most enhanced in both toxic species relative to their non-toxic congener (Table C1 and Table C2). Phosphatidic acids and phosphatidylinositols predominantly serve as building blocks for other lipid classes and intracellular signaling molecules (Řezanka et al. 2017, de Carvalho and Caramujo 2018). In fact, phosphatidylinositols have been linked to biomineralization in *Emiliania huxleyi* (Nam et al. 2020) and symbiosis in *Symbiodinium* (Rosic et al.

2015). As principally intracellular compounds it is improbable that phosphatidic acids or phosphatidylinositols would be associated with cell surfaces and therefore available for sensing by copepods to differentiate potential prey.

Phosphatidylcholines and sterols are the most likely candidates for non-polar metabolites that could be used by planktonic organisms such as copepods to differentiate toxic and non-toxic *Alexandrium* cells. In contrast to the other subclasses of glycerophospholipids, phosphatidylcholines – while only a minor component of the lipidome of phytoplankton – are typically located on the extracellular face of plasma membranes (Van Mooy et al. 2009, Cañavate et al. 2017). Additionally, a recent study found phosphatidylcholine concentrations to be relatively stable throughout various phases of phytoplankton growth (Cañavate et al. 2017) making a them a potentially important lipid class for cellular recognition by other organisms. Sterols, like phosphatidylcholines, remain at a reasonably consistent concentration throughout the cell cycle and are mainly localized to the exterior cell membrane (Hallegraeff et al. 1991, Mansour et al. 1999, Cañavate et al. 2017). Furthermore, sterol composition has been shown to be fairly species- (Piretti et al. 1997, Véron et al. 1998, Mansour et al. 1999) and even strain-specific (Volkman et al. 1999, Mansour et al. 2003). These qualities, coupled with their presence at double the concentration in toxic *A. catenella* and *A. pacificum* compared to *A. tamarense*, make sterols a potentially important class of metabolites to investigate as potential chemical cues associated with cell surfaces that copepods could use to distinguish toxic and non-toxic *Alexandrium* cells.

Only a few individual metabolites from the non-polar metabolomes of *Alexandrium* spp. are likely related to toxicity. Among the five classes of lipids discussed

above, only 745 individual metabolites were categorized as exhibiting significantly different concentrations in both toxic species, *A. catenella* (Experiment 1) and *A. pacificum* (Experiment 2), relative to *A. tamarensis*. This implies that just 4.8% of the metabolites in Experiment 1 and 11% of the metabolites in Experiment 2 are possibly associated with toxicity. Similarly, proteomics studies found only a 12% difference in the proteomes of toxic *A. minutum* and non-toxic *A. tamutum* (Subong et al. 2021) and a 5.3% difference between toxic and non-toxic strains of *A. catenella* (Zhang et al. 2015a). Interestingly, proteins involved in lipid biosynthesis/metabolism and membrane formation were classified as varying significantly in abundance based on cellular toxicity in both studies (Zhang et al. 2015a, Subong et al. 2021). Non-polar metabolites of *Alexandrium* that could be detected by copepods as a proxy for toxicity would presumably be enhanced in both *A. catenella* and *A. pacificum* and would not be expected vary substantially in *A. tamarensis* between experiments of similar design, as *A. tamarensis* was found to produce no detectable levels of toxins in both experiments. Based on the MS metabolomics analysis, only 17 metabolites fit these criteria. Three of these metabolites were broadly annotated by comparison of exact mass and characteristic MS/MS fragmentation patterns to database features as a glycosylated and hydroxylated 20 carbon sterol; a phosphatidylinositol containing two fatty acyl chains with a total of 35 carbons and 5 double bonds; and a triacylglycerol containing three fatty acyl chains with a total of 49 carbons and 3 double bonds (Table 4.2). Consequently, further studies are warranted to characterize the full molecular structures of these metabolites and to test their candidacy as potential chemical cues that could be used by copepods to select for non-toxic over toxic *Alexandrium* cells.

In conclusion, this metabolomics-based study identified components of the non-polar metabolome which differentiate toxic and non-toxic *Alexandrium* species. We pinpointed sterols and phosphatidylcholines as broad classes of metabolites, plus several individual metabolites, that were enriched in both toxic species. These lipid classes and metabolites may be candidates for future experiments aimed at deciphering chemoreception mechanisms of copepod perception of toxicity among *Alexandrium* cells. Investigation of these potential cell surface chemical cues will greatly benefit from new techniques such as live single cell mass spectrometry (Baumeister et al. 2019, Baumeister et al. 2020) and recent improvements in single cell surface-enhanced Raman scattering, which allow for greater sensitivity (Yan et al. 2020) and analysis of living cells (Kuku et al. 2017, Nam et al. 2019). Insight into the chemosensory mechanisms utilized by grazers to carefully select palatable, non-toxic prey, which is imperative for their survival and production of viable progeny, will allow us to better understand how these predator-prey interactions shape community structure and dynamics.

CHAPTER 5. CONCLUSIONS AND FUTURE DIRECTIONS

Interspecific interactions that shape planktonic communities are often mediated by chemical cues (Brown et al., 2019; Hay and Kubanek, 2002; Pohnert et al., 2007). A decade ago Roberts and colleagues urged us to improve our awareness of the chemical mechanisms behind predator-prey interactions in planktonic environments (Roberts et al., 2011); however, other than studies involving the model zooplankton *Daphnia* (Weiss, 2019), this area of plankton ecology is still relatively underdeveloped. The current body of work investigates chemosensory mechanisms involved in predator-prey interactions by assessing the metabolic response of a chemically defended phytoplankton to predator cues and quantitatively examining differences in the non-polar metabolome between toxic and non-toxic phytoplankton congeners that may be utilized by predators in prey selection. Additionally, the studies herein explore potential cues used by a phytoplankton to assess predation risk.

An important question to evaluate is whether the same types of chemical cues that govern interactions among macroscopic organisms scale down to microscopic planktonic communities. Responses of prey to predator cues has been demonstrated in both large and microscopic organisms (Lass and Spaak, 2003; Scherer and Smee, 2016; Wolfe, 2000). However, studies exploring response to cues from injured or dying conspecifics and competitors have mostly been restricted to larger, multicellular organisms (Scherer and Smee, 2016). When a preliminary study showed that lysate from dead conspecifics induced production of paralytic shellfish toxins (PSTs), a suite of defensive compounds, in the marine phytoplankton *Alexandrium catenella* (Senft-Batoh et al., 2015), it inspired

the investigation into factors that impact the potential use of dissolved metabolites from dead competitors as cues for assessment of predation risk as reported in Chapter 2 (Brown and Kubanek, 2020). In larger organisms evolutionary and ecological relatedness of competitors tends to influence whether compounds released by the injured or dead organism are utilized for predation risk assessment and how the perceiving organism responds (Dalesman et al., 2007; Scherer and Smee, 2016). The relative importance of phylogenetic relatedness and historical co-occurrence, in how the cue is interpreted varies based on the primary predator of the prey organism and the cost of defense (Scherer and Smee, 2016). In our study we found that the phytoplankton *Alexandrium minutum*, like larger prey, responds to dead competitors and that phylogenetic relatedness of the competitor (rather than geographic co-occurrence) is the most important determinant in its response (Brown and Kubanek, 2020) (Chapter 2). In line with the optimal defense theory (Rhoades, 1979), *A. minutum* exhibited a trade-off between growth and defense in its response to the dead competitor cues. The trade-off may be due in part to the metabolites leaked from dead competitors simultaneously acting as a cue and providing nutrients that *A. minutum* can use to grow. However, we demonstrated that enhancement of growth and suppression of defense from exposure to congeneric competitors was not exclusively due to increased resource availability. The observed decrease in defense in *A. minutum* was a bit perplexing but as both congeners employ the same toxins for chemical defense, excess dissolved metabolites from dead congeners may signal that the predator is resistant to this particular defense. Under this scenario, the nutrients liberated by the dead cells are more effectively dedicated to growth than defense. An important next step is to test the universality of the observed trade-off between growth and defense

in response to dead competitor cues among phytoplankton. While larger organisms often also experience trade-offs when investing in defenses (Stamp, 2003), the impacts on growth may be more apparent in phytoplankton because of their ability to immediately utilize the nutrients released by a dead competitor.

A better understanding of the biochemical mechanisms behind predator-prey interactions may also assist in determining the energy and resources phytoplankton expend to produce chemical defenses. Whether or not production of PSTs comes at a cost to growth in *Alexandrium* species is currently being debated within the literature (Park and Dam, 2021; Ryderheim et al., 2021). In Chapter 2 we observed a strong trade-off between PST production and growth with decreased PST production allowing for enhanced growth (Brown and Kubanek, 2020). In other interactions we observed induction of PSTs resulting in reduced growth in *A. minutum* (Chapters 2 and 3). However, the observed growth-related cost of induced toxicity was inconsistent across the many experiments that went into this thesis. In response to cues from dead unrelated competitors, PST concentrations in *A. minutum* increased nearly proportionally to the measured decreases in growth; whereas exposure to copepodamides caused growth reductions that varied between non-significant and up to two-thirds of the proportional increase in toxicity. Why growth-related costs of PST production appears to vary so much is not immediately apparent but could make for interesting future studies. Additionally, elucidation of the processes that go into induction and biosynthesis will assist in more accurate measurement of the physiological costs of PST production.

In Chapter 3 we uncovered some of the biochemical processes involved in copepodamide-induced toxicity in *A. minutum*. Transcriptomic studies aimed at

identifying the signaling pathway activated by copepod cues have had little success (Li and Ismar, 2018; Wohlrab et al., 2010) due to limited functional annotation of dinoflagellate genes and high frequency of posttranscriptional gene regulation (Akbar et al., 2018). Therefore, we reasoned that applying metabolomics, as the most downstream “-omics” technique, might be productive. Our analysis revealed that very little of *A. minutum*'s metabolome was reorganized in response to copepodamides making it straightforward to identify a few key pathways that were impacted by exposure to predator cues, based on changes in metabolite concentrations. Interestingly, jasmonic acid was among the metabolites that were in higher abundance in *A. minutum* exposed to copepodamides. As jasmonic acid is involved in defense induction in higher order plants (Han, 2016) we hypothesized that it was key to the signal cascade leading to toxin upregulation. Using inhibition experiments we provided further support for our hypothesis, piecing together parts of the cellular pathway in *A. minutum* activated by copepodamides. Discovery of components of the jasmonic acid signaling pathway in *A. minutum* was exciting as this is the first time it was identified in phytoplankton outside of cyanobacteria or the phylum Chlorophyta. Pending exploration of other dinoflagellates and Chromalveolata this may indicate that jasmonic acid signaling is an older evolutionary trait than previously suggested (Han, 2016).

Despite great effort, the receptor(s) used by phytoplankton to sense predator cues remain unidentified, due to their recent discovery, the limited availability of copepodamides for experimentation, and the complexity of phytoplankton genomes and gene regulation. Owing to their potency as predator cues, copepodamides elicit a response in phytoplankton at very low concentrations allowing us to study the

physiological changes they trigger with only micrograms of partially purified compounds. However, non-computational receptor-ligand studies typically require higher quantities of pure compounds. Fortunately, another research group is nearing completion of a total synthesis scheme for copepodamides which should provide material for many more avenues of study. For example, fluorescent tags could be amended to copepodamides enabling localization of the receptor and attachment of biotin would create a pull-down probe which could be used for isolation and characterization of the receptor. Once the receptor is characterized this may illuminate how such a diverse array of plankton seem to detect and react to copepodamides via induced toxicity, bioluminescence, decreased chain length, and changes in diel feeding and swimming behavior (Arias et al., 2021; Grebner et al., 2019; Lindström et al., 2017; Lundholm et al., 2018; Prevett et al., 2019; Selander et al., 2019).

Finally, it is important that we also examine the predator side of predator-prey interactions as we may be able to exploit the biomarkers used by zooplankton predators in prey selection to predict and even manipulate the toxicity of algal blooms. As copepods are notoriously unaccepting of artificial food, the application of bioassay-guided fractionation to isolate cues used by copepods to differentiate toxic and non-toxic prey is risky. Thankfully, metabolomics has greatly advanced in the last decade allowing us to narrow down the list of potential compounds that should be tested (Poulin and Pohnert, 2019). In Chapter 4 we utilized this technique to propose candidate compounds that copepods use to differentiate toxic and non-toxic *Alexandrium* cells. However, further studies are needed to fully characterize and test the compounds. Also, worth investigating is whether the identified compounds change in concentrations when *Alexandrium* cells

increase toxin production in response to either predators or their abiotic environment. Compounds that fluctuate with cellular toxicity would make better cues but may be harder for copepods to “learn”.

While this thesis exclusively used phytoplankton from the genus *Alexandrium* to explore chemosensory components of predator-prey interactions, similar studies can and should be applied to a wide spectrum of phytoplankton. In doing so we can ask questions such as: Is there still a trade-off between growth and defense when a phytoplankton defense is exuded rather than intracellular? Or if a defense is unstable and short lived, such as bioluminescence? What if the defense is structural rather than chemical? How many other phytoplankton use jasmonic acid signaling in defense induction? How old is jasmonic acid as a defense mechanism? And do copepods use similar classes of compounds to distinguish chemically defended cells in other genera?

Chemical ecologists are becoming more adept at identifying planktonic predator chemical cues (Grebner et al., 2019; Hahn et al., 2019; Selander et al., 2015; Weiss et al., 2018), but we still have much to learn about how these cues are perceived and interpreted by prey (Mitchell et al., 2017). Knowledge of the biochemical mechanisms behind these predator-prey interactions will allow us to ask more targeted questions about the evolutionary arms races between many zooplankton predators and phytoplankton. Additionally, a greater familiarity with the mechanisms will aid in predictions of how interactions may be impacted by global change including ocean acidification, allowing us to anticipate changes in community dynamics as population ranges shift with global warming.

APPENDIX A. SUPPLEMENTARY FIGURES FOR CHAPTER 2

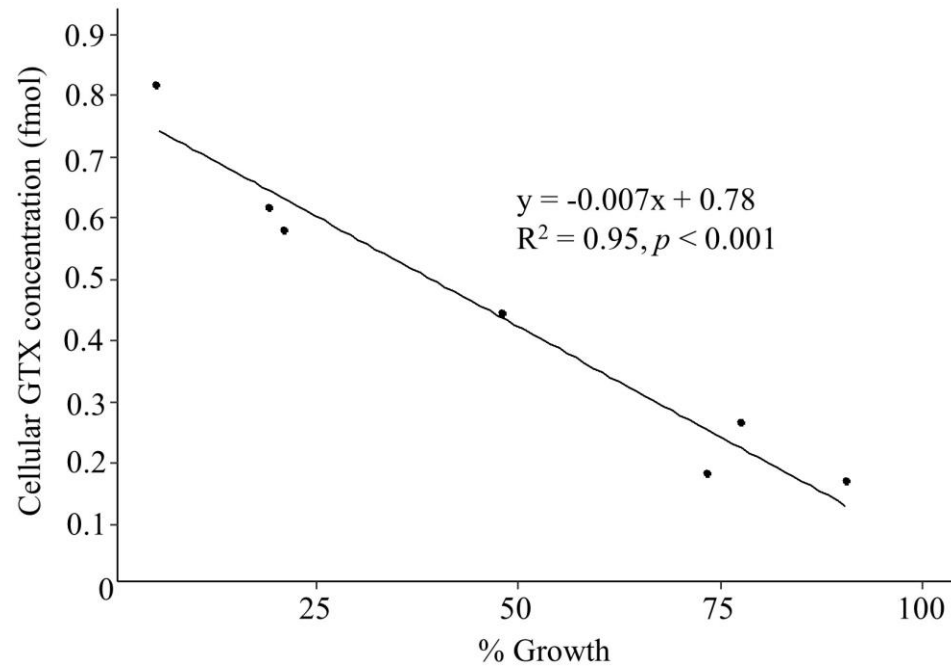


Figure A1 Relationship between cellular toxicity and growth in *Alexandrium minutum* in response to chemical cues from dead phytoplankton (Experiment 1). Data were analyzed by linear regression analysis using the mean growth and toxicity for the media control and each dead phytoplankton treatment.

APPENDIX B. SUPPLEMENTARY MATERIALS FOR CHAPTER 3

B.1 Methods

B.1.1 Copepodamide extraction and isolation

Extraction and isolation of copepodamides was carried out in a manner similar to Selander et al. (2015). Frozen *Calanus finmarchicus* (Calanus AS Product #19900) was freeze-dried, and 500 g of dry mass was extracted three times with a total of 17.5 L methanol. Crude extracts were combined and dried. Extracts were resuspended in 98:2 methanol/water with 1% ammonia (600 mL) and fractionation by liquid-liquid partitioning against 98:2 hexane/methanol (900 mL). The methanol/water fraction was retained and washed two more times with 600 mL each of the hexane mixture. The methanol/water fraction was then further separated by reversed phase solid phase extraction (ENVI-18, 10 g; Supelco) with a stepwise gradient of aqueous methanol. Lyso-copepodamide and lyso-dihydrocopepodamide eluted with 50% aqueous methanol and this fraction was set aside. Copepodamides and dihydrocopepodamides other than lyso-copepodamide and lyso-dihydrocopepodamide eluted with 90% aqueous methanol, a portion of which was subjected to further purification by silica gel column chromatography, eluting with a stepwise gradient from hexanes to ethyl acetate to isopropanol. Copepodamides and dihydrocopepodamides eluted in the fractions between 1:1 and 2:3 ethyl acetate/isopropanol which were combined and further purified by reversed phase HPLC using a Zorbax SB-C18 column (4.6 x 250 mm, 5 μ m particle size; Agilent Technologies, Inc) attached to a Waters 1525 Binary HPLC pump (Waters Corporation). The column was operated at room temperature with a flow rate of 1

mL min⁻¹ for 40 min and a mobile phase of 88% 40:45:15 acetonitrile/methanol/water with 0.2% formic acid, 0.1% ammonia, and 5 µM phosphoric acid and 12% isopropanol with 0.2% formic acid, 0.1% ammonia, and 5 µM phosphoric acid. Fractions between 14 and 26 min were collected and found to contain a natural blend of copepodamides containing 22:6, 20:5, and 18:4 copepodamides and 22:6, 20:5, and 18:4 dihydrocopepodamides based on single ion reaction monitoring of *m/z* 758.5, 732.5, 706.5, 760.5, 734.5, and 708.5 using a Waters QDA mass spectrometer (Waters Corporation) operated in negative ionization mode, coupled to a Waters 2695 Separation Module (Waters Corporation). It is likely that other copepodamides and dihydrocopepodamides were also present in this blend but they were not fully characterized. Quantitative ¹H NMR spectroscopy was performed on a Bruker Avance IIIHD 800 MHz NMR spectrometer equipped with a 3 mm triple resonance broadband cryoprobe using characteristic proton signals, shared by both copepodamides and dihydrocopepodamides, to determine the combined total concentration of all copepodamides and dihydrocopepodamides for use in the metabolomics experiment. Throughout the paper this blend is referred to simply as copepodamides.

B.1.2 Harvesting and extraction of Alexandrium minutum for metabolomics experiment

A 50 mL aliquot from each culture and the blank media sample was collected in a 50 mL centrifuge tube for toxin analysis. as described below in Toxin analysis (Appendix B.1.2.1.1). The remaining *A. minutum* cells were harvested by vacuum onto GF/F filters (Whatman #1825-110, previously muffled for 3 h at 450 °C) and quenched with liquid nitrogen. Frozen cells with filters were stored in foil (previously muffled for 3 h at 450 °C) at -80 °C until extraction. Frozen filters containing cells were ground with

a liquid nitrogen-chilled mortar and pestle and extracted with 30 mL of ice-cold 3:2:1 methanol/acetone/acetonitrile (OmniSolve, >99.5%, Millapore Sigma). Filter particulates were removed by centrifugation (800 x g for 15 min) and the supernatant was transferred to a new vial. The filter pellets were rinsed with fresh solvent and centrifuged three times with a total of 23 mL of extraction solvent. All supernatants for each replicate culture were combined and filtered with a 0.2 µm nylon syringe filter (Acrodisc, Pall Laboratory) to remove remaining small particulates, and then dried *in vacuo* using a Thermo Savant speedvac. Dried extracts were dissolved in a biphasic mixture of 9:10:15 water/methanol/chloroform (OmniSolve, >99.5%, Millapore Sigma) to separate polar (water/methanol) and non-polar (methanol/chloroform) metabolites, and then dried again *in vacuo*.

Polar extracts were re-dissolved completely in 1.0 mL 50% aqueous methanol, with 25% of the mixture aliquoted for UPLC/MS and the other 75% reserved for ¹H NMR spectroscopy. Both the UPLC/MS samples as well as the ¹H NMR spectroscopy samples were then dried *in vacuo*. Excess, insoluble inorganic salts were removed from polar ¹H NMR spectroscopy samples by twice triturating with ice-cold methanol and filtering through combusted glass pipettes with glass wool plugs. Methanol was removed from the triturated polar ¹H NMR spectroscopy *in vacuo*. Non-polar extracts were not aliquoted as 100% of the extracts were analyzed first by ¹H NMR spectroscopy followed by UPLC/MS analysis.

B.1.2.1.1 Toxin analysis

Aliquots collected for toxin analysis were centrifuged at 3,260 x *g* for 10 min. Supernatants were then removed and the remaining cell pellets lyophilized. After lyophilization cell pellets were re-suspended in 500 μ L 1% aqueous acetic acid, and subjected to four freeze-thaw cycles with sonication to lyse the cells (Anderson et al. 1990a). Lysates were centrifuged at 10,000 x *g* for 10 min to pellet cell debris and the supernatant (toxin extract) was filtered with a 0.2 μ m nylon syringe filter (Acrodisc, Pall Laboratory) to remove small particulates, in preparation for high performance liquid chromatography/mass spectrometric (HPLC/MS) analysis (Harju et al. 2015). Chromatographic separation of supernatants was achieved using 20 μ L injections onto a HILIC TSK-gel Amide-80 column (150 mm x 4.6 mm, 3- μ m particle size; TOSOH Bioscience Corporation) on an Agilent 1260 Infinity Binary LC System (Agilent Technologies). The column was operated at a room temperature with a flow rate of 0.5 mL min⁻¹. Mobile phase A was water and mobile phase B was acetonitrile and both mobile phases were modified with 0.1% formic acid (Optima, LCMS, Fischer Scientific). The toxins were eluted using a 40 min isocratic method of 40% A. The LC system was coupled to a Bruker amaZon SL ion trap mass spectrometer (Bruker Daltonics Inc.) used for mass spectrometric detection of gonyautoxins (GTX) 1-4. Analysis of the HPLC/MS data was carried out using MZMine 2 (Pluskal et al. 2010) after conversion of the file formats to mzXML using ProteoWizard (Chambers et al. 2012). GTX concentrations were calculated by comparison of mass spectral peak areas with interspersed standard solutions of certified reference calibration solutions purchased from The National Research Council of Canada. Since the gonyautoxins (GTX) in standard solutions readily

underwent sulfate hydrolysis in the mass spectrometer, toxin concentrations were calculated using the area of the sulfate-hydrolyzed fragment ion (m/z 332 for GTX 1 and 4 and m/z 316 for GTX 2 and 3, respectively) and the molecular ion (m/z 412 for GTX 1 and 4 and m/z 396 for GTX 2 and 3, respectively) peaks. A calibration curve composed of five toxin concentrations plus a blank sample showed a linear relationship between toxin concentration and area of mass spectral peaks. GTX concentrations and cell concentrations were then used to calculate cellular toxin concentrations. An unpaired t-test was used to compare toxin concentrations between *A. minutum* exposed and not exposed to copepodamides. Statistical analyses were performed using GraphPad Prism 9.0.

B.1.3 Metabolomic sample preparation and spectral data acquisition

B.1.3.1 ^1H NMR spectroscopy

In order to compare metabolomes without the confounding factor of different number of cells having been extracted across replicates, each sample was dissolved in a volume of solvent for ^1H NMR spectroscopy analysis that accounted for its cell concentration at the time of harvest.

B.1.3.1.1 Non-polar extracts

Non-polar extracts were dissolved at a concentration equivalent to 2.27×10^7 *A. minutum* cells mL^{-1} in dimethyl sulfoxide- d_6 (99.9% atom d_6 -DMSO; Cambridge Isotope Labs) containing 0.1% trimethylsilane (TMS), as internal standard. The media blank extract was prepared in the smallest volume of solvent possible (175 μL). The

non-polar extracts were transferred to 3 mm NMR tubes, and analyzed using a Bruker Avance IIIHD 800 MHz NMR spectrometer equipped with a 3 mm triple resonance broadband cryoprobe. Spectra of non-polar extracts were acquired using a simple ^1H NMR experiment (Bruker zg30 pulse sequence) with a spectral width of 9.6 kHz centered at 4400.00 Hz over 320 scans. One treatment replicate was lost and therefore its spectrum was not acquired.

B.1.3.1.2 Polar extracts

Polar extracts were dissolved at a concentration equivalent to 1.70×10^7 *A. minutum* cells mL^{-1} in 90:10 $\text{H}_2\text{O}/\text{D}_2\text{O}$ (99.96% atom D_2O ; Cambridge Isotope Labs) with 0.2 mM phosphate buffer (pH 7.4) and 0.25 mM 3-(trimethylsilyl)propionic-2,2,3,3- d_4 acid (TMSP), as internal standard, for ^1H NMR spectroscopy analysis. The media blank extract was prepared in the smallest volume of solvent possible (175 μL). Particulates were excluded by briefly centrifuging the samples and then carefully transferring the extracts into 3 mm NMR tubes. The extracts were analyzed using a Bruker Avance IIIHD 800 MHz NMR spectrometer equipped with a 3 mm triple resonance broadband cryoprobe. Spectra for the polar extracts were acquired using a 1D water presaturation (Bruker zgpr pulse sequence) with a spectral width of 12 kHz centered at 3758.36 Hz, with a relaxation delay 3 s, over 480 scans.

B.1.3.2 UPLC/MS

Similar to ^1H NMR sample preparation and spectroscopic analysis, non-polar and polar extracts were prepared for and analyzed by UPLC/MS separately. Each extract was dissolved in a volume of solvent appropriate for its final cell concentration, and all

samples were centrifuged at 21,100 x g for 5 min to pellet minute particulates. During analysis of both non-polar and polar extracts, treatment and control extracts and the media blank extract were randomly interspersed with pooled quality control samples acquired after every 10 sample injections. The pooled sample was used for quality control monitoring, drift correction, and MS/MS collection. Additionally, a sample blank was created using the same volume of solvent as the pooled quality control sample.

B.1.3.2.1 Non-polar extracts

Non-polar extracts were dissolved at a concentration equivalent to 4.54×10^6 *A. minutum* cells mL⁻¹ in LCMS grade 2:1 isopropyl alcohol/acetonitrile (OmniSolv, >99.5%, MilliporeSigma). The media blank extract was prepared in the smallest volume of solvent possible (1000 μ L). Eight pooled quality control samples were then generated by combining a small portion of all samples. Extracts were analyzed using a Q Exactive HF Hybrid Quadrupole-Orbitrap Mass Spectrometer (ThermoFisher Scientific) coupled to a Vanquish UPLC system (ThermoFisher Scientific). Chromatographic separation of the extracts was accomplished by injecting of 2.0 μ L onto an Accucore C30 column (2.1 x 150 mm, 2.6- μ m particle size; ThermoFisher Scientific) fitted to the UPLC system. The column was operated at a temperature of 50 °C with a flow rate of 0.4 mL min⁻¹. Mobile phase A was 40:60 water/acetonitrile and mobile phase B was 10:90 acetonitrile/isopropyl alcohol. Both mobile phases contained 10 mM ammonium formate and 0.1% formic acid buffer. All solvents and modifiers were LCMS grade (Optima, LCMS, Fischer Scientific). The following mobile phase gradient was used: equilibration at 80% A; 0-1 min ramp to 40% A; 1-5 min ramp to 30% A; 5-5.5 min ramp

to 15% A; 5.5-8 min ramp to 10% A; 8-8.2 min ramp to 0% A; 8.2-10.5 min hold at 0% A; 10.5-10.7 min return to 80% A and re-equilibration at 80% A until 12 min.

Mass spectrometric analysis of the non-polar extracts was performed using the Q Exactive HF Hybrid Quadrupole-Orbitrap which possesses a resolution power of 240,000 FWHM at 200 m/z and mass accuracy of <3 ppm. Each extract was analyzed twice, once in negative ionization mode and then in positive ionization mode using similar instrument settings except that a spray voltage of 3.5 kV was used for positive mode whereas 2.8 kV was used for negative mode. The heated electrospray ionization (HESI) source was operated at a vaporizer temperature of 425 °C. The sheath, auxiliary, and sweep nitrogen gas flows were 60, 18, and 4 L h⁻¹, respectively. The mass spectrometric scan range was 150-2000 m/z . Tandem MS data were acquired in a data-dependent manner with a resolution of 120,000 and the dd-MS² collected at a resolution of 30,000 with an isolation window of 0.4 m/z with a loop count of top 5. Stepped normalized collision energies were set at 10, 30, and 50 eV for fragmentation in the higher-energy collisional dissociation (HCD) cell prior to ion analysis in the orbitrap. Dynamic exclusion was set at 10 s and ions with charges greater than 2 omitted. Data acquisition was undertaken using Compound Discoverer version 3.0 (ThermoFisher Scientific).

B.1.3.2.2 Polar extracts

Polar extracts were dissolved at a concentration equivalent to 4.54 x 10⁶ *A. minutum* cells mL⁻¹ in 30% aqueous acetonitrile (OmniSolv, LCMS MilliporeSigma). The media blank extract was prepared in the smallest volume of solvent possible

(250 μ L). As with non-polar extracts, prior to analysis seven pooled quality control samples consisting of a small portion of all samples were generated. Analysis was completed using an Orbitrap ID-X Tribrid Mass Spectrometer (ThermoFisher Scientific) coupled to a Vanquish UPLC system. Chromatographic separation of the extracts was achieved using 2.0 μ L injections on a Waters Acquity UPLC BEH HILIC column (2.1 x 150 mm, 1.7- μ m particle size; Waters Corporation) fitted to the UPLC system. The column was operated at a temperature of 40 °C with a flow rate of 0.4 mL min⁻¹. Mobile phase A was 80:20 water/acetonitrile with 10 mM ammonium formate and 0.1% formic acid and mobile phase B was acetonitrile with 0.1% formic acid. All solvents and modifiers for both mobile phases were LCMS grade (Optima, LCMS, Fischer Scientific). The following mobile phase gradient was used: equilibration at 5% A; 0-0.5 min hold at 5% A; 0.5-9 min ramp to 70% A (curve 7); 9-9.4 min hold at 70% A; 9.4-9.5 min return to 5% A and re-equilibration at 5% A until 12 min.

The Orbitrap ID-X Tribrid used to analyze the polar extracts possesses a resolution power of 500,000 FWHM at 200 m/z and mass accuracy of <1 ppm. Extracts were analyzed first in negative ionization mode and then in positive ionization mode using similar instrument settings except that a spray voltage of 3.5 kV for positive mode and 2.5 kV for negative mode. The HESI source was operated at a vaporizer temperature of 320 °C. The sheath, auxiliary, and sweep nitrogen gas flows were 40, 8, and 1 L h⁻¹, respectively. The mass spectrometric scan range was 70-1050 m/z with an automatic gain control target set at 1×10^5 ions. Tandem MS data was acquired in a data-dependent manner with a full scan resolution of 120,000 and dd-MS² at a resolution of 30,000 with an isolation window of 0.8 m/z with a cycle time of 1.5 s. Stepped normalized collision

energies were set at 15, 30, and 45 eV for fragmentation in the HCD cell prior to ion analysis in the orbitrap. Dynamic exclusion was set at 8 s and ions with charges greater than 2 omitted. As with the non-polar extracts, data acquisition was carried out using Compound Discoverer.

B.1.4 Data processing and analysis

B.1.4.1 ¹H NMR spectroscopy

¹H NMR spectra were pre-processed using Metabolab version 2019.12.08.1237 (Ludwig and Günther 2011) in Matlab R2013a version 8.1.0.604. Only extracts derived from *A. minutum* cultures, not the blank media extracts, were analyzed using Metabolab.

B.1.4.1.1 Non-polar extracts

Spectra from non-polar extracts were aligned to TMS at 0.00 ppm, manually phased, spline baseline corrected, and segmentally aligned. The spectral regions associated with TMS (-0.50 to 0.60 ppm), the residual DMSO signal (2.45-2.65 ppm), water (3.30-3.46 ppm), and the excess downfield region that contained no signals (10.40-11.50 ppm) were removed and noise filtration applied. Spectra were then binned (0.005 ppm), probabilistic quotient normalized to account for minute concentration differences (Dieterle et al. 2006), generalized logarithmic transformed to reduce bias toward metabolites with high concentrations ($\lambda = 6.5012 \times 10^{-9}$) (Parsons et al. 2007), and mean centered.

B.1.4.1.2 Polar extracts

Similar to the non-polar extract analyses, NMR spectra from polar extracts were aligned to TMS at 0.00 ppm, manually phased, spline baseline corrected, and segmentally aligned. For polar extracts the spectral regions around TMS (-2.60 to 0.50 ppm), processing contaminant (2.63-2.84 ppm), water (4.71-5.23 ppm), and the excess downfield region (9.50-12.50 ppm) were removed and noise filtration applied. Spectra were then binned (0.005 ppm), probabilistic quotient normalized, generalized logarithmic transformed ($\lambda = 5.210 \times 10^{-9}$), and mean centered.

B.1.4.1.3 Analysis

PLS-Toolbox version 8.0.2 (Eigenvector Research) in Matlab was used to generate an oPLS-DA model which was cross-validated using Venetian blinds methods with seven data splits to capture the maximum variance between control and treatment samples in the first latent variable (LV). During model generation for the polar extracts, spectra for two control replicates and one treatment replicate were removed due to poor NMR spectral quality. Differences between metabolomes of *A. minutum* exposed and not exposed to copepodamides were examined using the oPLS-DA model with the loadings of the first latent variable used to identify spectroscopic features that were significantly different between treatments.

B.1.4.2 UPLC/MS

After UPLC/MS acquisition, spectral features (retention time, m/z) were extracted from chromatograms via alignment, peak picking and integration, and peak area

extraction using Compound Discoverer version 3.1 (ThermoFisher Scientific) and XCMS Online (Gowda et al. 2014). The data were then normalized and scaled by the median peak area across all samples. Spectral features that were not five times greater than background peaks, based on the media blank sample, were removed from the dataset. Additionally, features that were present in fewer than 50% of the pooled quality control samples and had a relative standard deviation of greater than 30% were excluded from the dataset.

PCA was used to examine differences in polar and non-polar metabolomes, separately, of *A. minutum* (control) and *A. minutum* exposed to copepodamides (treatment) using both Compound Discoverer and XCMS Online. Using XCMS platform spectral features were identified as being significantly different between treatment and controls using Welch's t-test (Gowda et al. 2014). In Compound Discoverer, the data was log 10 transformed. The PCA model was then generated using spectral features with an absolute value fold change greater than or equal to 1.1 in metabolomes of *A. minutum* exposed to copepodamides when compared with standard *A. minutum* metabolomes and p values less than 0.05 based on a t-test.

B.1.5 Metabolite annotation

Structure identification was attempted for all features that were identified as significantly different between *A. minutum* exposed versus not exposed to copepodamides. Identification was predominately dependent on MS/MS data with ¹H NMR spectroscopy being largely used for confirmation of functional groups. From the UPLC/MS data, elemental formulae were generated based on exact mass and isotopic

patterns. The elemental formulae along with $[M-H]^-$ and $[M+H]^+$ ions, MS/MS fragmentation patterns, retention time, isotopic patterns, and significant 1H NMR chemical shifts were compared to a local spectral database, built from curated experimental data, as well as these publicly available databases: Metlin database (Smith et al. 2005), MassBank of North America (MoNA)(2020), the human metabolome database (HMDB) (Wishart et al. 2007), ChemSpider (Pence and Williams 2010), Kyoto Encyclopedia of Genes and Genomes (KEGG) database (Ogata et al. 1999), LIPID Metabolites and Pathways Strategy (LIPID MAPS) database (Sud et al. 2006), SpectraBase (John Wiley & Sons 2020), mzVault (in house database), and mzCloud. Additionally, *in silico* fragmentation of potential structural matches was calculated and scored against experimental data using FISH coverage scoring in Compound Discoverer. Select metabolite identities were further confirmed via comparisons of retention times, $[M-H]^-$ and $[M+H]^+$ ions, and MS/MS fragmentation patterns to purchased standards. KEGG (Ogata et al. 1999) and MetaCyc (Caspi et al. 2017) were used to determine pathways in which significant metabolites were involved. Additionally, a review by Bromke (2013) was consulted when examining the amino acid biosynthetic pathways and a review by Wasternack and Strnad (2018) was consulted for biosynthesis of jasmonic acid.

B.1.6 Signaling pathway inhibition experiments

B.1.6.1 Serine/threonine protein phosphatases

Cantharidin inhibits serine/threonine protein phosphatases types 1 and 2A (Honkanen 1993), which have been found to negatively regulate jasmonic acid

biosynthesis and signaling in plants (Bajsa et al. 2011). In order to examine jasmonic acid production and signaling in *A. minutum*, cultures in exponential growth phase at a cell density of about 15,000 cells mL⁻¹ were exposed to 5 µM cantharidin and 1 nM copepodamides. At the start of the experiment and again after 24 h, 250 µL of either 2 mM cantharidin in DMSO (inhibition treatment) or DMSO (inhibition control) were added aseptically to 100 mL cultures of *A. minutum* resulting in a final concentration of 5 µM cantharidin. Additionally, the inhibition treatments and controls were either subjected to 1 nM copepodamide or solvent through aseptic addition of 250 µL of 0.4 µM copepodamides in DMSO or DMSO, respectively, 1 h after the addition of cantharidin or DMSO. Overall, this resulted in the following 4 treatments of 9 replicates each: control (DMSO additions), copepodamide-exposed (DMSO and copepodamide additions), phosphatase-inhibited control (cantharidin and DMSO additions), and phosphatase-inhibited copepodamide-exposed (cantharidin and copepodamide additions). A 1.0 mL aliquot from each culture was preserved with Lugol's solution at the start, prior to the first addition of cantharidin or copepodamides, and at the end of the experiment, immediately before harvesting, to measure cell concentrations. After about 40 h, all cultures were harvested with processing of all treatments intermixed over about 3 h. The cultures were harvested by equally distributing each culture into two aliquots in 50 mL centrifuge tubes and centrifuging them at 3,260 x g for 10 min. Supernatants were removed resulting in two cell pellets for each replicate culture which were then lyophilized. Both sets of cell pellets were then extracted in 1% aqueous acetic acid as described in Appendix B.1.2 Harvesting and extraction of *Alexandrium minutum* for metabolomics experiment.1.1. After removing particulates, one set of extracts was

reserved for HPLC/MS toxin analysis (Appendix B.1.2 Harvesting and extraction of *Alexandrium minutum* for metabolomics experiment.1.1) and the other was prepared for jasmonic acid extraction (Appendix B.1.6.1.1). One phosphatase-inhibited copepodamide-exposed sample was lost due to a broken vial during toxin analysis. Growth and cellular toxin concentrations were compared between treatments using a two-way ANOVA with a Tukey HSD post hoc test for multiple comparisons in GraphPad Prism 9.0.

B.1.6.1.1 Jasmonic acid extraction and analysis

The jasmonic acid extraction and analysis was adapted from a method developed for extraction of phytohormones by Durgbanshi and colleagues (2005). Briefly, 500 μL of 1% aqueous acetic acid extracts, at a pH of about 2.75, were partitioned twice against 500 μL diethyl ether. The diethyl ether extracts were combined and the solvent evaporated in a chemical fume hood. The extract was then dissolved in 300 μL 10% aqueous methanol with 0.01% acetic acid in preparation for HPLC/MS analysis (Gamir et al. 2012). The extracts were chromatographically separated with 20 μL injections onto a Kinetex EVO C18 silica column (50 mm x 2.1 mm, 5- μm particle size; Phenomenex Inc) on Waters 2695 Separation Module (Waters Corporation) coupled to a Waters QDA mass spectrometer (Waters Corporation). The column was maintained at a 40 °C with a flow rate of 0.3 mL min⁻¹. The following mobile phase gradient was used (acidified with 0.01% acetic acid): 0-6 min ramp from water to 90% aqueous methanol; 6-8 min hold 90% aqueous methanol; 8-8.5 min ramp to 100% methanol. Jasmonic acid elution was tracked via the QDA operating in negative mode with ion extraction of m/z 209.21 representing $[\text{M}-\text{H}]^-$. A calibration curve composed of jasmonic acid standards (Cayman

Chemicals) at six concentrations plus a blank sample showed a linear relationship between jasmonic acid and area of integrated mass spectral peaks. Therefore, jasmonic acid quantification was attempted by comparison of mass spectral peak areas in the samples with interspersed jasmonic acid standards. Unfortunately, the jasmonic acid concentration in the extracts was at or below the 2.6 nM limit of detection of the QDA.

B.1.6.2 Jasmonic acid signaling pathway

To further investigate the involvement of jasmonic acid signaling in the response of *A. minutum* to copepod chemical cues, *A. minutum* cultures in exponential growth phase at a cell density of about 18,000 cells mL⁻¹ were exposed to 3 μM neomycin, a jasmonic acid signaling inhibitor (Vadassery et al. 2019), and 1 nM copepodamides. At the start of the experiment and again 24 h later, 250 μL of either 0.6 mM aqueous neomycin sulfate (inhibition treatment) or water (inhibition control) were added aseptically to 50 mL cultures of *A. minutum* resulting in a final concentration of 3 μM neomycin. Additionally, the inhibition treatments and controls were either subjected to 1 nM copepodamide or solvent. This was accomplished by aseptic addition of 250 μL of either 0.2 μM copepodamides in DMSO (copepodamide treatment) or DMSO alone (control) 1 h after the addition of neomycin or water. Overall, this resulted in 4 treatments of 9 replicates each: control (water and DMSO additions), copepodamide-exposed (water and copepodamide additions), jasmonic acid-inhibited control (neomycin and DMSO additions), and jasmonic acid-inhibited copepodamide-exposed (neomycin and copepodamide additions). Prior to the first addition of neomycin or copepodamides and at the end of the experiment, just before harvesting, a 1.0 mL aliquot from each culture was preserved with Lugol's solution to measure cell concentrations, which were later

used to calculate *A. minutum* growth and change in cellular toxin concentrations. After about 40 h, all cultures were harvested for toxin analysis with processing of all treatments intermixed over about 1.5 h. Toxin concentrations were analyzed using the methods outlined in Appendix B.1.2 Harvesting and extraction of *Alexandrium minutum* for metabolomics experiment.1.1. One control sample was lost due to a broken vial during toxin analysis. Growth and cellular toxin concentrations were compared between treatments using a two-way ANOVA with a Tukey HSD post hoc test for multiple comparisons in GraphPad Prism 9.0.

B.1.6.3 G protein-coupled receptors (GPCRs)

Based on previous transcriptomic studies involving exposure of phytoplankton to copepod grazing (Wohlrab et al. 2010, Amato et al. 2018, Li and Ismar 2018) and a meta-analysis of the presence of GPCRs in *A. minutum* and other eukaryotic phytoplankton (Mojib and Kubanek 2020), the role of GPCRs in recognition of copepodamides was explored. *A. minutum* cultures in exponential growth phase at a cell density of about 13,000 cells mL⁻¹ were exposed to 0.1 μM SCH-202676, a known inhibitor of ligand binding to GPCRs (Fawzi et al. 2001), and 1 nM copepodamides. At the start of the experiment and 24 h later 250 μL of either 0.02 mM SCH-202676 in DMSO (inhibition treatment) or DMSO alone (inhibition control) was added aseptically to 50 mL cultures of *A. minutum* resulting in a final concentration of 0.1 μM SCH-202676. Aseptic addition of 250 μL of either 0.2 μM copepodamides in DMSO, resulting in a final concentration of 1 nM, or DMSO alone took place 1 h later. Overall, this resulted in 4 treatments of 9 replicates each: control (DMSO additions), copepodamide-exposed (DMSO and copepodamide additions), GPCR-inhibited control (SCH-202676 and DMSO additions),

and GPCR-inhibited copepodamide-exposed (SCH-202676 and copepodamide additions). A 1.0 mL aliquot from each culture was preserved with Lugol's solution prior to the first addition of SCH-202676 or copepodamides. Additionally, at the end of the experiment and just before harvesting, another 1.0 mL aliquot was taken from each culture with 500 μ L preserved with Lugol's solution to measure cell concentrations and 500 μ L set aside for a cell membrane permeability analysis. After about 40 h, all cultures were harvested by centrifugation with processing of all treatments intermixed over about 1.5 h. Toxin concentrations were analyzed using the methods outlined in Appendix B.1.2

Harvesting and extraction of *Alexandrium minutum* for metabolomics experiment.1.1. Growth and cellular toxin concentrations were compared between treatments using a two-way ANOVA with a Tukey HSD post hoc test for multiple comparisons in GraphPad Prism 9.0.

B.1.6.4 Dose-dependence of GPCR inhibition

Based on the results of the GPCR inhibition assay, a dose-dependent analysis of the impact of GPCR inhibition on the response of *A. minutum* to copepodamides was executed. The assay was performed by exposing *A. minutum* cultures in exponential growth phase at a cell density of about 14,500 cells mL⁻¹ to four concentrations of SCH-202676 and 1 nM copepodamides. At the start of the experiment and 24 h later four concentrations of SCH-202676, accomplished through either 125 μ L DMSO or SCH-202676 in DMSO at concentrations of 0.01 mM, 0.02 mM, 0.04 mM, and 0.2 mM, were added aseptically to 50 mL cultures of *A. minutum*. These GPCR inhibition treatments were further split into either controls or 1 nM copepodamide-exposed treatments via the aseptic addition of either 125 μ L DMSO alone or 0.4 μ M

copepodamides in DMSO 1 h after the addition of DMSO or SCH-202676. Overall, this resulted in 10 treatments of 3 replicates each: control (DMSO additions), 0.025 μM SCH-202676 GPCR-inhibited control (0.01 mM SCH-202676 and DMSO additions), 0.05 μM SCH-202676 GPCR-inhibited control (0.02 mM SCH-202676 and DMSO additions), 0.1 μM SCH-202676 GPCR-inhibited control (0.04 mM SCH-202676 and DMSO additions), 0.5 μM SCH-202676 GPCR-inhibited control (0.2 mM SCH-202676 and DMSO additions), uninhibited copepodamide-exposed (DMSO and copepodamide additions), 0.025 μM SCH-202676 GPCR-inhibited copepodamide-exposed (0.01 mM SCH-202676 and copepodamide additions), 0.05 μM SCH-202676 GPCR-inhibited copepodamide-exposed (0.02 mM SCH-202676 and copepodamide additions), 0.1 μM SCH-202676 GPCR-inhibited copepodamide-exposed (0.04 mM SCH-202676 and copepodamide additions), and 0.5 μM SCH-202676 GPCR-inhibited copepodamide-exposed (0.2 mM SCH-202676 and copepodamide additions). At both the start, prior to the first addition of SCH-202676 and copepodamides, and end of the experiment, immediately before harvesting, a 1.0 mL aliquot from each culture was preserved with Lugol's solution to measure cell concentrations. After about 40 h, all cultures were harvested in 50 mL centrifuge tube by centrifugation over the course of about 1.5 h with processing of all treatments intermixed. Toxin concentrations were analyzed using the methods outlined in Appendix B.1.2 Harvesting and extraction of *Alexandrium minutum* for metabolomics experiment.1.1. In order to statistically compare growth and cellular toxin concentrations, the data were log-transformed to create dose-response curves. The uninhibited solvent controls were assigned a dose of 0.001 μM for the purposes of log-transformation. The data were fit using a sigmoidal fitted non-linear

regression, excluding the highest dose due to an extreme reduction in growth (Figure B4). The dose response curves of *A. minutum* either exposed to copepodamides or DMSO were then compared using non-linear regression analysis in GraphPad Prism 9.0.

B.1.7 Cell membrane permeability assay

Aliquots (500 μL), set aside from the GPCR inhibition assay, were stained by addition of 20 μL of aqueous 0.05% w/v Neutral Red (Mallinckrodt Chemical) followed 30 min later by the addition of 10 μL of 50 μM SYTOX Green in DMSO (Invitrogen Molecular Probes), to test for live and permeable cells, respectively. The stained cells were incubated for 1 h in the dark at room temperature to allow *A. minutum* to absorb the dyes prior to counting. All cells were counted within 3 h of staining, using fluorescence with a FITC filter cube (to detect SYTOX Green) and bright-field microscopy (to detect Neutral Red) on an Olympus IX-50 inverted microscope with a Palmer-Maloney settling chamber, at 400X magnification (40X objective and 10X eyepiece). This enabled comparison of the percentage of living cells with disrupted cell membranes (red and fluorescent green) in uninhibited control and copepodamide-exposed *A. minutum* ($n = 7$) (Poulin et al. 2018). Statistical analyses were performed using an unpaired t-test in GraphPad Prism 9.0.

B.2 Results: Supplementary figures and tables

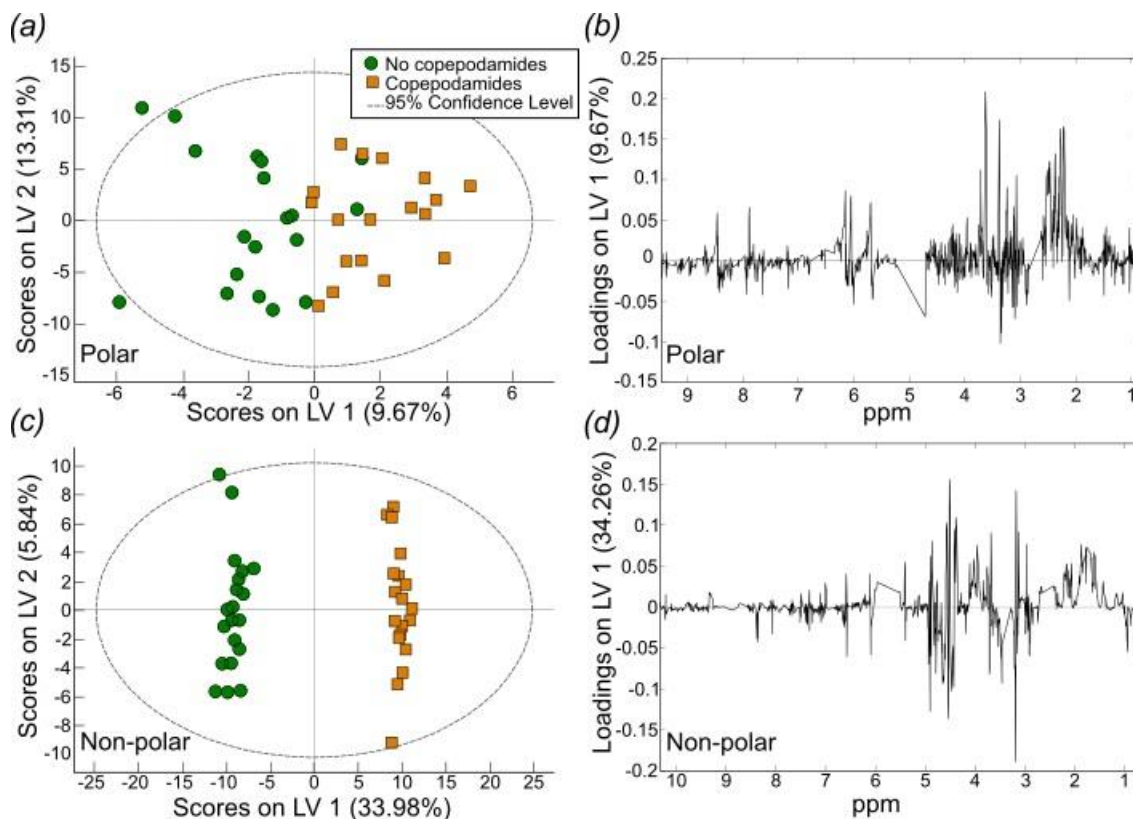


Figure B1 oPLS-DA models of NMR data revealed that both polar and non-polar metabolomes of *Alexandrium minutum* change in response to copepodamide exposure. Orange squares represent metabolomes of *A. minutum* exposed to copepodamides and green circles represent metabolomes of *A. minutum* not exposed to copepodamides (controls). oPLS-DA scores plots from ^1H NMR analysis (a and c) and their corresponding loadings plots on the first latent variable (b and d) for both polar (a and b) and non-polar (c and d) metabolomes, which are composed of 1,176 and 1,305 features, respectively.

Table B1 Identification of metabolites whose concentrations differed in *Alexandrium minutum* based upon exposure to copepodamides, based on UPLC/-MS data. The retention time (in minutes), *m/z*, detected ion, molecular formula, and mass error (ppm) are provided for each tentatively identified metabolite. Additionally, the fold-change based on *A. minutum* exposed to copepodamides relative to *A. minutum* exposed to a solvent control is provided where possible. Confidence levels were assigned based on available spectral details. Confidence level 1: exact match both in fragmentation and retention time to an authentic standard; 2: observed MS/MS data and shifts in the ¹H NMR loadings plots and raw spectra were consistent with predicted spectra from databases; 3: observed MS/MS data were consistent with predicted spectra from databases; 4: relatively high FISH coverage calculated by Compound Discoverer and retention time relative to other metabolites matches the literature; 5: close match mass match and retention time relative to other metabolites matches the literature.

Metabolite	Fold-change	Retention time (min)	<i>m/z</i>	Detected ion	Molecular formula	Mass error (ppm)	Confidence
Maleic acid	1.5	1.39	115.0038	[M-H] ⁻	C ₄ H ₄ O ₄	1.52	1
Arginine	1	7.13	175.1184	[M+H] ⁺	C ₆ H ₁₄ N ₄ O ₂	-0.03	1
Glutamic acid	1.1	6.02	148.0604	[M+H] ⁺	C ₅ H ₉ NO ₄	0.14	1
Pyroglutamic acid*	1.1	1.88	128.0354	[M-H] ⁻	C ₅ H ₇ NO ₃	0.03	3
Succinic acid	1.1	1.39	117.0195	[M-H] ⁻	C ₄ H ₆ O ₄	0.80	1
Succinic anhydride	1.2	1.52	99.0089	[M-H] ⁻	C ₄ H ₄ O ₃	2.47	4
Hydroxyglutarate	1.3	1.38	147.0298	[M-H] ⁻	C ₅ H ₈ O ₅	-0.92	2
4-Guanidinobutanamide	1.3	4.99	145.1084	[M+H] ⁺	C ₅ H ₁₂ N ₄ O	-0.06	3
4-Acetamidobutanate	0.71	1.42	146.0811	[M+H] ⁺	C ₆ H ₁₁ NO ₃	0.24	3
Jasmonic acid	1.2	1.75	211.1329	[M+H] ⁺	C ₁₂ H ₁₈ O ₃	0.06	1
Linolenic acid	1.2	4.62	277.2168	[M-H] ⁻	C ₁₈ H ₃₀ O ₂	-1.71	2
Oxo-phytodienoic acid (OPDA)#	-	7.47	293.2107	[M+H] ⁺	C ₁₈ H ₂₈ O ₃	-1.61	5
Valine	0.9	5.31	118.0629	[M+H] ⁺	C ₅ H ₁₁ NO ₂	0.26	3
α-Ketoisovaleric acid	0.78	1.22	115.0401	[M-H] ⁻	C ₅ H ₈ O ₃	0.14	2
2-aceto-2-hydroxybutanoate	1.2	1.51	145.0506	[M-H] ⁻	C ₆ H ₁₀ O ₄	-0.26	3
Intermediate-A'	2.6	6.12	187.1553	[M+H] ⁺	C ₈ H ₁₈ N ₄ O	0	3 [§]
Cyclic-C'	2.1	6.85	209.1510	[M+H] ⁺	C ₉ H ₁₆ N ₆	0.48	3 [§]
Intermediate-E	2.2	6.79	225.1458	[M+H] ⁺	C ₉ H ₁₆ N ₆ O	0.44	3 [§]
Decarbamoyloxy-saxitoxin	3.0	6.89	241.1408	[M+H] ⁺	C ₉ H ₁₇ N ₆ O ₂	-2.07	4 [%]

Table B1 (continued)

Unknown; similar to nicotinyl alcohol	1.4	5.03	110.0601	[M+H] ⁺	C ₆ H ₇ NO	0.38	3
---	-----	------	----------	--------------------	----------------------------------	------	---

*glutamine artifact derived from in source cyclization (Purwaha et al. 2014)

#fold-change uncertain due to poor peak integration

\$based on fragmentation from Cho et al. (2019) and high resolution mass spectrometry analysis in Tsuchiya et al. (2016)

%Mass error based on high resolution mass spectrometry in Iwamoto et al. (2007)

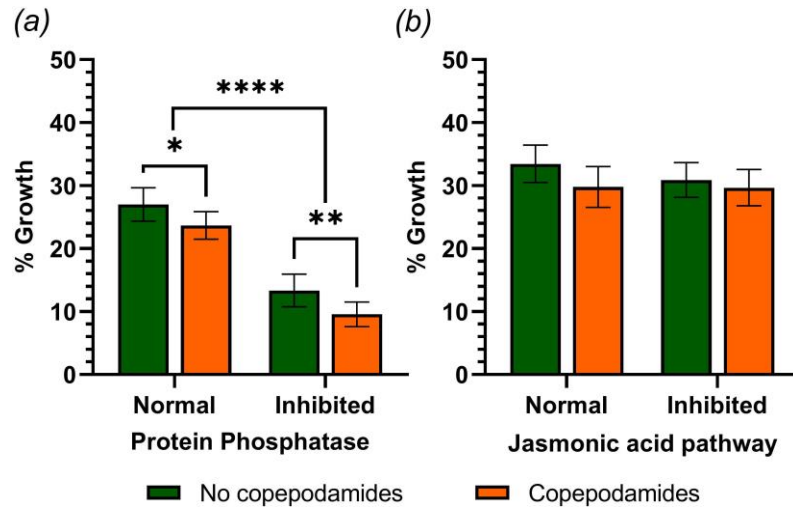


Figure B2 Inhibition of jasmonic acid biosynthesis reduced growth and exposure to copepodamides had variable impacts on growth in *Alexandrium minutum*. Bars represent the mean \pm standard deviation of percent growth of *A. minutum* in response to inhibition of (a) serine/threonine phosphatases by cantharidin and (b) jasmonic acid signaling by neomycin when exposed to a solvent control (No copepodamides, green) or 1 nM copepodamides (Copepodamides, orange). Data were analyzed using two-way ANOVAs with a Tukey HSD post hoc tests for multiple comparisons. Asterisks indicate the level of statistical significance; ** $p < 0.001$, *** $p < 0.001$.**

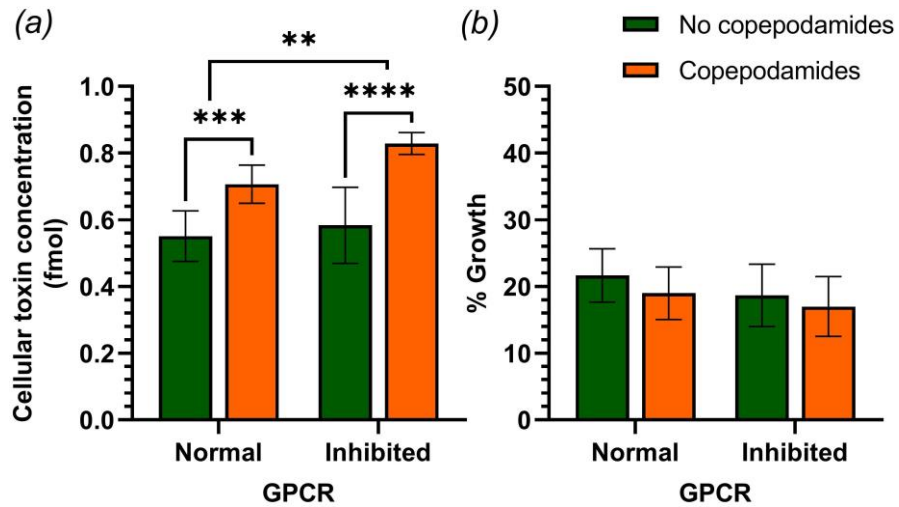


Figure B3 Inhibition of GPCRs did not block induction of toxin production or cause reduction in growth in *Alexandrium minutum*. Bars represent the mean \pm standard deviation of (a) cellular toxin concentration of gonyautoxins 1-4 and (b) percent growth of *A. minutum* in response to inhibition of GPCRs by SCH-202676 when exposed to a solvent control (No copepodamides, green) or 1 nM copepodamides (Copepodamides, orange). Data were analyzed using two-way ANOVAs with a Tukey HSD post hoc tests for multiple comparisons. Asterisks indicate the level of statistical significance; ** $p < 0.001$, *** $p < 0.001$, ** $p < 0.01$.**

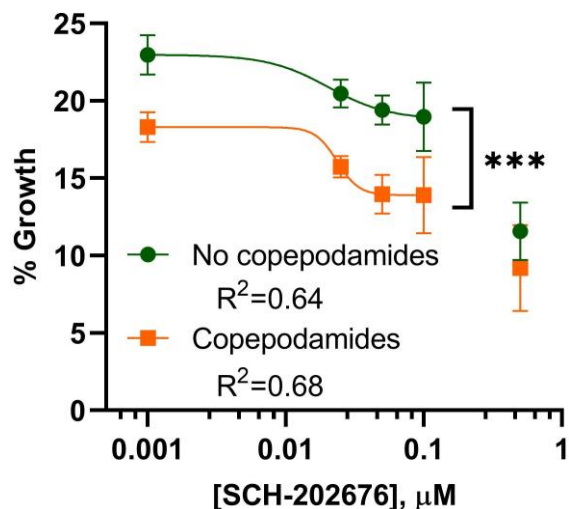


Figure B4 Exposure to copepodamides when GPCRs were inhibited caused a reduction in growth in *Alexandrium minutum*. Points represent the mean \pm standard percent growth of *A. minutum* in response to inhibition of GPCRs by SCH-202676 at varying doses when exposed to a solvent control (No copepodamides, green) or 1 nM copepodamides (Copepodamides, orange). The uninhibited solvent controls were assigned a dose of 0.001 μM for the purposes of log-transformation. The data were analyzed using a non-linear regression, excluding the highest dose. Asterisks indicate the level of statistical significance; *** $p < 0.001$.

**APPENDIX C. SUPPLEMENTARY FIGURE AND TABLES FOR
CHAPTER 4**

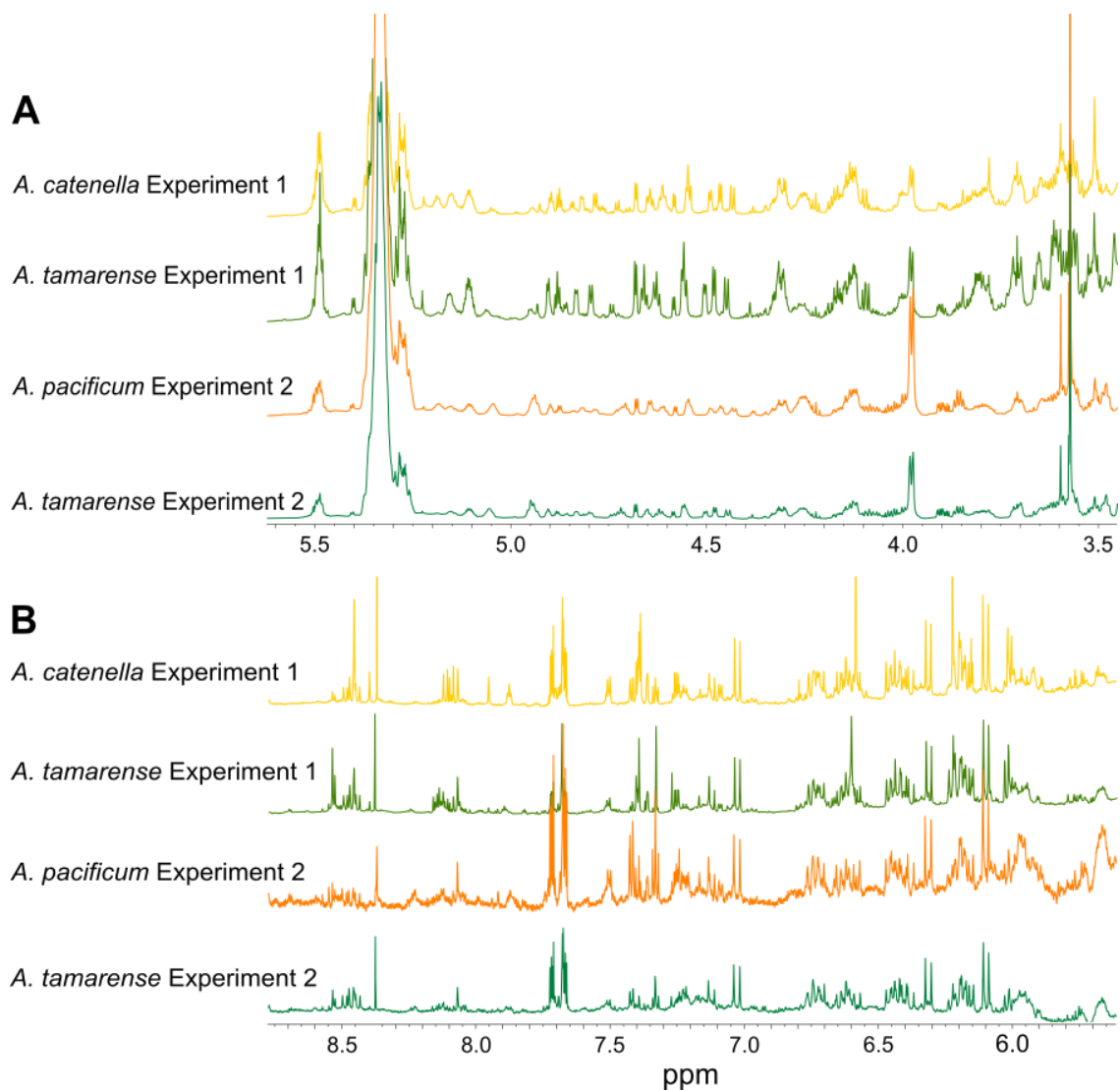


Figure C1 Representative ^1H NMR spectra from NMR metabolomics experiments 1-2. A single representative ^1H NMR spectrum of the non-polar metabolome from each *Alexandrium* species: *A. catenella* (yellow) and *A. tamarensis* (light green) (Experiment 1) and *A. catenella* (yellow) and *A. tamarensis* (dark green) (Experiment 2) from (A) 3.5-5.6 ppm and (B) 5.7-8.7 ppm.

Table C1 Putatively identification of metabolites whose concentrations are significantly different in *Alexandrium catenella* compared to *Alexandrium tamarense* based on UPLC/MS data from experiment 1. The *m/z*, detected ion, molecular formula, and mass error (mDa), and lipid class are provided for each tentatively identified metabolite which differs significantly in concentration between *A. catenella* and *A. tamarense* from Experiment 1 but do not differ significantly between *A. tamarense* from Experiment 1 and 2. Additionally, the *p*-value and fold-change based on *A. catenella* relative to *A. tamarense* is provided. Confidence levels were assigned based on available spectral details. Confidence level 1: exact match both in fragmentation and retention time to a purchased standard; 2: observed MS/MS data consistent with predicted spectrum from databases and exact mass match in LOBSTAHS or LIPDMAPS to corresponding lipid class; 3: exact mass match in LOBSTAHS or LIPDMAPS to corresponding lipid class or partial match of MS/MS data to databases.

m/z (mass error, Da)	Detected ion	Molecular formula	Metabolites	Lipid class	Fold- change	P value	Confidence
257.2122 (0.0001)	[M-H] ⁻	C ₁₅ H ₃₀ O ₃	hydroxy- pentadecan- oic acid	Free fatty acids	4.9	3.4 E -11	2
393.2777 (0.0001)	[M+Cl] ⁻	C ₂₁ H ₄₂ O ₄	MG (18:0)	Mono- acylglycerols	1.5	2.8 E -6	3
580.4941 (0.0005)	[M+CHOO] ⁻	C ₃₄ H ₆₅ NO ₃	Cer (d34:2)	Sphingolipids	1.3	0.0001	2
775.7552 (0.0003)	[M-H] ⁻	C ₅₁ H ₁₀₀ O ₄	DG (O-48:1)	Di- acylglycerols	2.8	0.02	3
859.6669 (0)	[M-H] ⁻	C ₅₂ H ₉₃ O ₉	TG 49:4; O3	Tri- acylglycerols	40*	1.6 E -13	2
921.7192 (0.0003)	[M-H] ⁻	C ₅₈ H ₉₉ O ₈	TG 55:7; O2	Tri- acylglycerols	10.6	1.7 E -09	2
1022.700 4 (0.0014)	[M-H] ⁻	C ₆₀ H ₉₉ NO ₁₀ P	PS 54:10	Glycero- phospholipids	14.4	1.1 E -17	2
479.2658 (0.0007)	[M-H] ⁻	C ₂₆ H ₄₀ O ₈	Sterol 20:1; O2; GlcA	Sterols	2.9	1.4 E -5	2
918.6107 (0.0088)	[M-CH ₃] ⁻	C ₅₆ H ₈₈ NO ₈ P	PC 48:12	Glycero- phospholipids	0.54	6.9 E -12	2
1037.780 2 (0.0010)	[M-H] ⁻	C ₆₀ H ₁₁₁ O ₁₁ P	SLBPA (C18:1/ C18:1/ C18:1)	Glycero- phospholipids	3.9	4.4 E -13	3
377.1959 (0)	[M+H] ⁺	C ₂₁ H ₂₈ O ₆	18- oxocortisol	Sterols	0.58	0.03	3
634.5407 (0.0002)	[M+NH ₄] ⁺	C ₃₉ H ₆₈ O ₅	DG (18:1/18:3)	Di- acylglycerols	2.1	1.9 E -6	2

Table C1 (continued)

638.5723 (0.0005)	[M+NH ₄] ⁺	C ₃₉ H ₇₂ O ₅	DG (18:1/18:1)	Di- acylglycerols	20.2	1.1 E -18	2
689.5116 (0)	[M+H] ⁺	C ₃₈ H ₇₃ O ₈ P	PA (35:1)	Glycero- phospholipids	3.2	4.3 E -8	3
736.7181 (0.0004)	[M+H] ⁺	C ₄₇ H ₉₂ NO ₄	Cer 47:1; O3	Sphingolipids	3.2	2.3 E -11	2
738.6613 8 (0.0006)	[M+NH ₄] ⁺	C ₄₅ H ₈₄ O ₆	TG (14:0\14:0\ 14:1)	Tri- acylglycerols	4.5	1.2 E -17	2
726.5880 (0.0001)	[M+H] ⁺	C ₄₂ H ₇₉ NO ₈	Glucosyl- ceramide (d18:1/18:1)	Sphingolipids	2.0	2.1 E -8	2
778.6920 (0.0001)	[M+NH ₄] ⁺	C ₄₈ H ₈₈ O ₆	TG 45:2	Tri- acylglycerols	4.4	1.7 E -14	3
878.8146 (0.0025)	[M+NH ₄] ⁺	C ₅₅ H ₁₀₄ O ₆	TG (16:0/18:0/1 8:1)	Tri- acylglycerols	15.5	4.9 E -17	2
881.7564 (0.0005)	[M+Na] ⁺	C ₅₅ H ₁₀₂ O ₆	TG (16:0/18:1/1 8:1)	Tri- acylglycerols	4.2	7.7 E -21	2
883.7725 (0.0007)	[M+Na] ⁺	C ₅₅ H ₁₀₄ O ₆	TG (16:0/18:0/1 8:1)	Tri- acylglycerols	5.4	2.6 E -17	2
922.7864 (0.0006)	[M+NH ₄] ⁺	C ₅₉ H ₁₀₀ O ₆	TG 56:7	Tri- acylglycerols	7.9	3.7 E -13	2
962.9114 (0)	[M+NH ₄] ⁺	C ₆₁ H ₁₁₆ O ₆	TG 58:1	Tri- acylglycerols	6.5	1.2 E -22	2
977.7058 (0.0006)	[M+H]	C ₅₃ H ₁₀₁ O ₁₃ P	PI 44:1	Glycero- phospholipids	6.5	2.3 E -15	3
1002.848 3 (0.0001)	[M+NH ₄] ⁺	C ₆₅ H ₁₀₈ O ₆	TG 62:9	Tri- acylglycerols	24.3*	2.8 E -16	2
1032.989 5 (0.0002)	[M+NH ₄] ⁺	C ₆₆ H ₁₂₆ O ₆	TG 63:1	Tri- acylglycerols	4.8	5.1 E -19	2
1068.801 3 (0.0046)	[M+Na] ⁺	C ₆₂ H ₁₁₂ NO ₉ P	PE 57:6; O	Glycero- phospholipids	2.6	1.7 E -11	3
843.5017 (0.0001)	[M+H] ⁺	C ₄₄ H ₇₅ O ₁₃ P	PI 35:5	Glycero- phospholipids	1.6	1.5 E -3	3
880.6666 (0.0003)	[M+NH ₄] ⁺	C ₅₂ H ₉₄ O ₉	TG 49:3; O3	Tri- acylglycerols	4.9	1.2 E -8	3

*Fold change value uncertain due to extremely low concentration of lipids in *A. tamarense* or

high level of variability.

Table C2 Putatively identification of metabolites whose concentrations different significantly in *Alexandrium pacificum* compared to *Alexandrium tamarense* based on UPLC/MS data from experiment 2. The *m/z*, detected ion, molecular formula, and mass error (mDa), and lipid class are provided for each tentatively identified metabolite which differs significantly in concentration between *A. pacificum* and *A. tamarense* from Experiment 2 but do not differ significantly between *A. tamarense* from Experiment 1 and 2. Additionally, the *p*-value and fold-change based on *A. pacificum* relative to *A. tamarense* is provided. Confidence levels were assigned based on available spectral details. Confidence level 1: exact match both in fragmentation and retention time to a purchased standard; 2: observed MS/MS data consistent with predicted spectrum from databases and exact mass match in LOBSTAHS or LIPDMAPS to corresponding lipid class; 3: exact mass match in LOBSTAHS or LIPDMAPS to corresponding lipid class or partial match of MS/MS data to databases.

m/z (Mass error, Da)	Detected ion	Molecular formula	Metabolites	Lipid class	Fold- change	P value	Confidence
479.2658 (0.0007)	[M-H] ⁻	C ₂₆ H ₄₀ O ₈	Sterol 20:1; O2; GlcA	Sterols	2.3	0.02	2
918.6107 (0.0088)	[M-CH ₃] ⁻	C ₅₆ H ₈₈ NO ₈ P	PC 48:12	Glycero- phospholipids	0.62	6.7 E -9	2
1037.780 2 (0.0010)	[M-H] ⁻	C ₆₀ H ₁₁₁ O ₁₁ P	SLBPA (C18:1/ C18:1/ C18:1)	Glycero- phospholipids	1.5	3.5 E -5	2
359.2224 (0.0004)	[M-H] ⁻	C ₂₂ H ₃₂ O ₄	Dihydroxy- docosa- hexaenoic acid	Free fatty acids	1.6	0.009	3
604.4612 (0.0005)	[M-H] ⁻	C ₃₂ H ₆₅ NO ₄ S	NAT 30:0	Free fatty acids/amides	1.6	0.002	3
719.4948 (0.0073)	[M-H] ⁻	C ₄₂ H ₇₃ O ₇ P	PA O-39:6	Glycero- phospholipids	1.2	0.003	2
777.6000 (0.0015)	[M+CHOO] ⁻	C ₄₂ H ₈₅ O ₇ P	PA O-39:0	Glycero- phospholipids	2.1	5.1 E -4	2
553.5195 (0.0005)	[M+H] ⁺	C ₃₅ H ₆₈ O ₄	MG O-32:2	Mono- acylglycerols	2.0	0.05	3
843.5017 (0.0001)	[M+H] ⁺	C ₄₄ H ₇₅ O ₁₃ P	PI 35:5	Glycero- phospholipids	1.5	0.003	2
880.6666 (0.0003)	[M+NH ₄] ⁺	C ₅₂ H ₉₄ O ₉	TG 49:3; O3	Tri- acylglycerols	2.4	0.004	3

REFERENCES

2020. MassBank of North America (MoNA) Fiehn lab.
- Abdulhussain, A. H., K. B. Cook, A. D. Turner, A. M. Lewis, T. S. Bibby, and D. J. Mayor. 2021. The influence of the toxin-producing dinoflagellate, *Alexandrium catenella* (1119/27), on the survival and reproduction of the marine copepod, *Acartia tonsa*, during prolonged exposure. *Frontiers in Marine Science* **8**.
- Abdulhussain, A. H., K. B. Cook, A. D. Turner, A. M. Lewis, M. A. Elsafi, and D. J. Mayor. 2020. The influence of the toxin producing dinoflagellate, *Alexandrium catenella* (1119/27), on the feeding and survival of the marine copepod, *Acartia tonsa*. *Harmful Algae* **98**:101890.
- Abi-Khalil, C., D. S. Finkelstein, G. Conejero, J. Du Bois, D. Destoumieux-Garzon, and J. L. Rolland. 2017. The paralytic shellfish toxin, saxitoxin, enters the cytoplasm and induces apoptosis of oyster immune cells through a caspase-dependent pathway. *Aquatic Toxicology* **190**:133-141.
- Abi-Khalil, C., C. Lopez-Joven, E. Abadie, V. Savar, Z. Amzil, M. Laabir, and J.-L. Rolland. 2016. Exposure to the paralytic shellfish toxin producer *Alexandrium catenella* increases the susceptibility of the oyster *Crassostrea gigas* to pathogenic *Vibrios*. *Toxins* **8**:24.
- Akbar, M., A. Ahmad, G. Usup, and H. Bunawan. 2018. Current Knowledge and Recent Advances in Marine Dinoflagellate Transcriptomic Research. *Journal of Marine Science and Engineering* **6**:13.
- Akbar, M. A., N. Y. Mohd Yusof, N. I. Tahir, A. Ahmad, G. Usup, F. K. Sahrani, and H. Bunawan. 2020. Biosynthesis of Saxitoxin in Marine Dinoflagellates: An Omics Perspective. *Marine Drugs* **18**:103.
- Alpermann, T. J., B. Beszteri, U. W. E. John, U. Tillmann, and A. D. Cembella. 2009. Implications of life-history transitions on the population genetic structure of the toxigenic marine dinoflagellate *Alexandrium tamarense*. *Molecular Ecology* **18**:2122-2133.

- Alpine, A. E., and J. E. Cloern. 1992. Trophic interactions and direct physical effects control phytoplankton biomass and production in an estuary. *Limnology and Oceanography* **37**:946-955.
- Álvarez-Salgado, X. A., J. Gago, B. M. Míguez, M. Gilcoto, and F. F. Pérez. 2000. Surface waters of the NW Iberian margin: Upwelling on the shelf versus outwelling of upwelled waters from the Rías Baixas. *Estuarine, Coastal and Shelf Science* **51**:821-837.
- Amato, A., V. Sabatino, G. M. Nylund, J. Bergkvist, S. Basu, M. X. Andersson, R. Sanges, A. Godhe, T. Kiørboe, E. Selander, and M. I. Ferrante. 2018. Grazer-induced transcriptomic and metabolomic response of the chain-forming diatom *Skeletonema marinoi*. *The ISME Journal* **12**:1594–1604.
- Amin, S. A., L. R. Hmelo, H. M. van Tol, B. P. Durham, L. T. Carlson, K. R. Heal, R. L. Morales, C. T. Berthiaume, M. S. Parker, B. Djunaedi, A. E. Ingalls, M. R. Parsek, M. A. Moran, and E. V. Armbrust. 2015. Interaction and signalling between a cosmopolitan phytoplankton and associated bacteria. *Nature* **522**:98-101.
- Anderson, D., D. Kulis, J. Sullivan, and S. Hall. 1990a. Toxin composition variations in one isolate of the dinoflagellate *Alexandrium fundyense*. *Toxicon* **28**:885-893.
- Anderson, D., D. Kulis, J. Sullivan, S. Hall, and C. Lee. 1990b. Dynamics and physiology of saxitoxin production by the dinoflagellates *Alexandrium* spp. *Marine biology* **104**:511-524.
- Anderson, D. M., T. J. Alpermann, A. D. Cembella, Y. Collos, E. Masseret, and M. Montresor. 2012. The globally distributed genus *Alexandrium*: Multifaceted roles in marine ecosystems and impacts on human health. *Harmful Algae* **14**:10-35.
- Arias, A., E. Selander, E. Saiz, and A. Calbet. 2021. Predator Chemical Cue Effects on the Diel Feeding Behaviour of Marine Protists. *Microbial Ecology*:Epub ahead of print.
- Astuya, A., C. Carrera, V. Ulloa, A. Aballay, G. Núñez-Acuña, H. Hégaret, and C. Gallardo-Escárate. 2015. Saxitoxin modulates immunological parameters and gene transcription in *Mytilus chilensis* hemocytes. *International Journal of Molecular Sciences* **16**:15235-15250.

- Bajsa, J., Z. Pan, and S. O. Duke. 2011. Serine/threonine protein phosphatases: Multi-purpose enzymes in control of defense mechanisms. *Plant signaling & behavior* **6**:1921-1925.
- Balech, E. 1990. A short diagnostic description of *Alexandrium*. Page 77 in S. B. Graneli E, Edler L, Anderson DM, editor. Toxic marine phytoplankton. Elsevier, New York.
- Barreiro, A., C. Guisande, I. Maneiro, A. R. Vergara, I. Riveiro, and P. Iglesias. 2007. Zooplankton interactions with toxic phytoplankton: Some implications for food web studies and algal defence strategies of feeding selectivity behaviour, toxin dilution and phytoplankton population diversity. *Acta Oecologica* **32**:279-290.
- Bartual, A., N. Arandia-Gorostidi, A. Cózar, S. Morillo-García, M. Ortega, M. Vidal, A. Cabello, J. González-Gordillo, and F. Echevarría. 2014. Polyunsaturated aldehydes from large phytoplankton of the Atlantic Ocean surface (42°N to 33°S). *Marine Drugs* **12**:682-699.
- Basu, S., S. Patil, D. Mapleson, M. T. Russo, L. Vitale, C. Fevola, F. Maumus, R. Casotti, T. Mock, M. Caccamo, M. Montresor, R. Sanges, and M. I. Ferrante. 2017. Finding a partner in the ocean: molecular and evolutionary bases of the response to sexual cues in a planktonic diatom. *New Phytologist* **215**:140-156.
- Baumeister, T. U. H., M. Vallet, F. Kaftan, L. Guillou, A. Svatoš, and G. Pohnert. 2020. Identification to species level of live single microalgal cells from plankton samples with matrix-free laser/desorption ionization mass spectrometry. *Metabolomics* **16**:28.
- Baumeister, T. U. H., M. Vallet, F. Kaftan, A. Svatoš, and G. Pohnert. 2019. Live single-cell metabolomics with matrix-free laser/desorption ionization mass spectrometry to address microalgal physiology. *Frontiers in Plant Science* **10**:172-172.
- Bergkvist, J., E. Selander, and H. Pavia. 2008. Induction of toxin production in dinoflagellates: The grazer makes a difference. *Oecologia* **156**:147-154.
- Blossom, H. E., B. Markussen, N. Daugbjerg, B. Krock, A. Norlin, and P. J. Hansen. 2019. The cost of toxicity in microalgae: Direct evidence from the dinoflagellate *Alexandrium*. *Frontiers in Microbiology* **10**:1065-1065.

- Bollens, S. M., B. W. Frost, and J. R. Cordell. 1994. Chemical, mechanical and visual cues in the vertical migration behavior of the marine planktonic copepod *Acartia hudsonica*. *Journal of Plankton Research* **16**:555-564.
- Borcier, E., R. Morvezen, P. Boudry, P. Miner, G. Charrier, J. Laroche, and H. Hegaret. 2017. Effects of bioactive extracellular compounds and paralytic shellfish toxins produced by *Alexandrium minutum* on growth and behaviour of juvenile great scallops *Pecten maximus*. *Aquatic Toxicology* **184**:142-154.
- Brahamsha, B. 1996. An abundant cell-surface polypeptide is required for swimming by the nonflagellated marine cyanobacterium *Synechococcus*. *Proceedings of the National Academy of Sciences* **93**:6504-6509.
- Brandenburg, K. M., S. Wohlrab, U. John, A. Kremp, J. Jerney, B. Krock, and D. B. Van de Waal. 2018. Intraspecific trait variation and trade-offs within and across populations of a toxic dinoflagellate. *Ecology Letters* **21**:1561-1571.
- Bricelj, V. M., L. Connell, K. Konoki, S. P. MacQuarrie, T. Scheuer, W. A. Catterall, and V. L. Trainer. 2005. Sodium channel mutation leading to saxitoxin resistance in clams increases risk of PSP. *Nature* **434**:763-767.
- Bromke, M. A. 2013. Amino acid biosynthesis pathways in diatoms. *Metabolites* **3**:294-311.
- Brown, E. R., M. R. Cepeda, S. J. Mascuch, K. L. Poulson-Ellestad, and J. Kubanek. 2019. Chemical ecology of the marine plankton. *Natural Product Reports* **36**:1093-1116.
- Brown, E. R., and J. Kubanek. 2020. Harmful alga trades off growth and toxicity in response to cues from dead phytoplankton. *Limnology and Oceanography* **65**:1723-1733.
- Brügger, B., G. Erben, R. Sandhoff, F. T. Wieland, and W. D. Lehmann. 1997. Quantitative analysis of biological membrane lipids at the low picomole level by nano-electrospray ionization tandem mass spectrometry. *Proceedings of the National Academy of Sciences* **94**:2339-2344.
- Calbet, A., and M. R. Landry. 2004. Phytoplankton growth, microzooplankton grazing, and carbon cycling in marine systems. *Limnology and Oceanography* **49**:51-57.

- Cañavate, J. P., I. Armada, and I. Hachero-Cruzado. 2017. Polar lipids analysis of cultured phytoplankton reveals significant inter-taxa changes, low influence of growth stage, and usefulness in chemotaxonomy. *Microbial Ecology* **73**:755-774.
- Casotti, R., S. Mazza, C. Brunet, V. Vantrepotte, A. Ianora, and A. Miralto. 2005. Growth inhibition and toxicity of the diatom aldehyde 2-trans, 4-trans-decadienal on *Thalassiosira weissflogii* (Bacillariophyceae). *Journal of Phycology* **41**:7-20.
- Caspi, R., R. Billington, C. A. Fulcher, I. M. Keseler, A. Kothari, M. Krummenacker, M. Latendresse, P. E. Midford, Q. Ong, W. K. Ong, S. Paley, P. Subhraveti, and P. D. Karp. 2017. The MetaCyc database of metabolic pathways and enzymes. *Nucleic Acids Research* **46**:D633-D639.
- Chambers, M. C., B. Maclean, R. Burke, D. Amodei, D. L. Ruderman, S. Neumann, L. Gatto, B. Fischer, B. Pratt, J. Egertson, K. Hoff, D. Kessner, N. Tasman, N. Shulman, B. Frewen, T. A. Baker, M.-Y. Brusniak, C. Paulse, D. Creasy, L. Flashner, K. Kani, C. Moulding, S. L. Seymour, L. M. Nuwaysir, B. Lefebvre, F. Kuhlmann, J. Roark, P. Rainer, S. Detlev, T. Hemenway, A. Huhmer, J. Langridge, B. Connolly, T. Chadick, K. Holly, J. Eckels, E. W. Deutsch, R. L. Moritz, J. E. Katz, D. B. Agus, M. MacCoss, D. L. Tabb, and P. Mallick. 2012. A cross-platform toolkit for mass spectrometry and proteomics. *Nature Biotechnology* **30**:918-920.
- Charpentier, C. L., and J. H. Cohen. 2015. Chemical cues from fish heighten visual sensitivity in larval crabs through changes in photoreceptor structure and function. *Journal of Experimental Biology* **218**:3381-3390.
- Charpentier, C. L., A. J. Wright, and J. H. Cohen. 2017. Fish kairomones induce spine elongation and reduce predation in marine crab larvae. *Ecology* **98**:1989-1995.
- Chen, J., Q. Ye, H.-F. Gu, H.-Y. Li, S.-H. Lv, J.-S. Liu, and W.-D. Yang. 2015. Variability in the allelopathic action of the *Alexandrium tamarense* species complex along the coast of China. *Harmful Algae* **47**:17-26.
- Chen, L. 2010. A molecular approach to the study of saxitoxin resistance in copepods. Doctoral. University of Connecticut, ProQuest Dissertations and Theses Publishing.

- Chi, W., L. Zheng, C. He, B. Han, M. Zheng, W. Gao, C. Sun, G. Zhou, and X. Gao. 2017. Quorum sensing of microalgae associated marine *Ponticoccus* sp. PD-2 and its algicidal function regulation. *AMB Express* **7**:59.
- Chivers, D. P., J. M. Kiesecker, E. L. Wildy, M. T. Anderson, and A. R. Blaustein. 1997. Chemical alarm signalling in terrestrial salamanders: Intra- and interspecific responses. *Ethology* **103**:599-613.
- Cho, Y., S. Tsuchiya, T. Omura, K. Koike, H. Oikawa, K. Konoki, Y. Oshima, and M. Yotsu-Yamashita. 2019. Metabolomic study of saxitoxin analogues and biosynthetic intermediates in dinoflagellates using ¹⁵N-labelled sodium nitrate as a nitrogen source. *Scientific Reports* **9**:3460.
- Christy, J. H. 2011. Timing of hatching and release of larvae by brachyuran crabs: Patterns, adaptive significance and control. *Integrative and Comparative Biology* **51**:62-72.
- Cohen, J. H., and R. B. Forward Jr. 2003. Ctenophore kairomones and modified aminosugar disaccharides alter the shadow response in a larval crab. *Journal of Plankton Research* **25**:203-213.
- Cohen, J. H., C. K. Hanson, A. I. Dittel, D. C. Miller, and C. E. Tilburg. 2015. The ontogeny of larval swimming behavior in the crab *Hemigrapsus sanguineus*: Implications for larval transport. *Journal of Experimental Marine Biology and Ecology* **462**:20-28.
- Colin, S. P., and H. G. Dam. 2007. Comparison of the functional and numerical responses of resistant versus non-resistant populations of the copepod *Acartia hudsonica* fed the toxic dinoflagellate *Alexandrium tamarense*. *Harmful Algae* **6**:875-882.
- Collins, J. R., B. R. Edwards, H. F. Fredricks, and B. A. S. Van Mooy. 2016. LOBSTAHS: An adduct-based lipidomics strategy for discovery and identification of oxidative stress biomarkers. *Analytical Chemistry* **88**:7154-7162.
- Cronin, T. W. 1982. Estuarine retention of larvae of the crab *Rhithropanopeus harrisi*. *Estuarine, Coastal and Shelf Science* **15**:207-220.

- D'Agostino, V. C., M. Degradi, V. Sastre, N. Santinelli, B. Krock, T. Krohn, S. L. Dans, and M. S. Hoffmeyer. 2017. Domoic acid in a marine pelagic food web: Exposure of southern right whales *Eubalaena australis* to domoic acid on the Península Valdés calving ground, Argentina. *Harmful Algae* **68**:248-257.
- D'Alelio, D., A. Amato, A. Luedeking, and M. Montresor. 2009. Sexual and vegetative phases in the planktonic diatom *Pseudo-nitzschia multistriata*. *Harmful Algae* **8**:225-232.
- D'Alvise, P. W., S. Lillebø, M. J. Prol-Garcia, H. I. Wergeland, K. F. Nielsen, Ø. Bergh, and L. Gram. 2012. *Phaeobacter gallaeciensis* reduces *Vibrio anguillarum* in cultures of microalgae and rotifers, and prevents vibriosis in cod larvae. *PLoS ONE* **7**:e43996.
- Dadon-Pilosof, A., K. R. Conley, Y. Jacobi, M. Haber, F. Lombard, K. R. Sutherland, L. Steindler, Y. Tikochinski, M. Richter, and F. O. Glöckner. 2017. Surface properties of SAR11 bacteria facilitate grazing avoidance. *Nature microbiology* **2**:1608–1615
- Dalesman, S., S. D. Rundle, D. T. Bilton, and P. A. Cotton. 2007. Phylogenetic relatedness and ecological interactions determine antipredator behavior. *Ecology* **88**:2462-2467.
- de Carvalho, C. C. C. R., and M. J. Caramujo. 2018. The various roles of fatty acids. *Molecules (Basel, Switzerland)* **23**:2583.
- Deeds, J. R., R. E. Hoesch, A. R. Place, and J. P. Y. Kao. 2015. The cytotoxic mechanism of karlotoxin 2 (KmTx 2) from *Karlodinium veneficum* (Dinophyceae). *Aquatic Toxicology* **159**:148-155.
- Detree, C., G. Núñez-Acuña, S. Roberts, and C. Gallardo-Escárate. 2016. Uncovering the complex transcriptome response of *Mytilus chilensis* against saxitoxin: Implications of harmful algal blooms on mussel populations. *PLoS ONE* **11**:e0165231.
- Devlin, R. A., K. Campbell, K. Kawatsu, and C. T. Elliott. 2011. Physical and immunoaffinity extraction of paralytic shellfish poisoning toxins from cultures of the dinoflagellate *Alexandrium tamarense*. *Harmful Algae* **10**:542-548.

- Dieterle, F., A. Ross, G. Schlotterbeck, and H. Senn. 2006. Probabilistic quotient normalization as robust method to account for dilution of complex biological mixtures. Application in ^1H NMR metabonomics. *Analytical Chemistry* **78**:4281-4290.
- Doberva, M., S. Sanchez-Ferandin, E. Toulza, P. Lebaron, and R. Lami. 2015. Diversity of quorum sensing autoinducer synthases in the Global Ocean Sampling metagenomic database. *Aquatic Microbial Ecology* **74**:107-119.
- Durgbanshi, A., V. Arbona, O. Pozo, O. Miersch, J. V. Sancho, and A. Gómez-Cadenas. 2005. Simultaneous determination of multiple phytohormones in plant extracts by liquid chromatography–electrospray tandem mass spectrometry. *Journal of Agricultural and Food Chemistry* **53**:8437-8442.
- Durham, B. P., S. P. Dearth, S. Sharma, S. A. Amin, C. B. Smith, S. R. Campagna, E. V. Armbrust, and M. A. Moran. 2017. Recognition cascade and metabolite transfer in a marine bacteria-phytoplankton model system. *Environmental Microbiology* **19**:3500-3513.
- Durham, B. P., S. Sharma, H. Luo, C. B. Smith, S. A. Amin, S. J. Bender, S. P. Dearth, B. A. S. Van Mooy, S. R. Campagna, E. B. Kujawinski, E. V. Armbrust, and M. A. Moran. 2015. Cryptic carbon and sulfur cycling between surface ocean plankton. *Proceedings of the National Academy of Sciences* **112**:453-457.
- Edwards, B. R., K. D. Bidle, and B. A. S. Van Mooy. 2015. Dose-dependent regulation of microbial activity on sinking particles by polyunsaturated aldehydes: Implications for the carbon cycle. *Proceedings of the National Academy of Sciences* **112**:5909-5914.
- Espinosa, E. P., M. Perrigault, J. E. Ward, S. E. Shumway, and B. Allam. 2010. Microalgal cell surface carbohydrates as recognition sites for particle sorting in suspension-feeding bivalves. *The Biological Bulletin* **218**:75-86.
- Faber, S. 2012. Saxitoxin and the induction of paralytic shellfish poisoning. *Journal of Young Investigators* **23**:1-7.
- Fahy, E., S. Subramaniam, R. C. Murphy, M. Nishijima, C. R. H. Raetz, T. Shimizu, F. Spener, G. van Meer, M. J. O. Wakelam, and E. A. Dennis. 2009. Update of the LIPID MAPS comprehensive classification system for lipids. *Journal of Lipid Research* **50**:S9-S14.

- Fahy, E., M. Sud, D. Cotter, and S. Subramaniam. 2007. LIPID MAPS online tools for lipid research. *Nucleic Acids Research* **35**:W606-W612.
- Falciatore, A., M. Jaubert, J.-P. Bouly, B. Bailleul, and T. Mock. 2020. Diatom Molecular Research Comes of Age: Model Species for Studying Phytoplankton Biology and Diversity. *The Plant Cell* **32**:547-572.
- Fawzi, A. B., D. Macdonald, L. L. Benbow, A. Smith-Torhan, H. Zhang, B. C. Weig, G. Ho, D. Tulshian, M. E. Linder, and M. P. Graziano. 2001. SCH-202676: An allosteric modulator of both agonist and antagonist binding to G protein-coupled receptors. *Molecular Pharmacology* **59**:30-37.
- Fernández-Herrera, L. J., C. J. Band-Schmidt, D. J. López-Cortés, C. J. Hernández-Guerrero, J. J. Bustillos-Guzmán, and E. Núñez-Vázquez. 2016. Allelopathic effect of *Chattonella marina* var. *marina* (Raphidophyceae) on *Gymnodinium catenatum* (Dinophyceae). *Harmful Algae* **51**:1-9.
- Finiguerra, M., D. E. Avery, and H. G. Dam. 2014. Sodium channel expression in the copepod *Acartia hudsonica* as a function of exposure to paralytic shellfish toxin (PST). *Harmful Algae* **39**:75-80.
- Finiguerra, M., D. E. Avery, and H. G. Dam. 2015. Determining the advantages, costs, and trade-offs of a novel sodium channel mutation in the copepod *Acartia hudsonica* to paralytic shellfish toxins (PST). *PLoS ONE* **10**:e0130097.
- Finiguerra, M. B. 2013. Determining the role of a novel sodium channel mutation on tolerance to paralytic shellfish toxins in the marine copepod *Acartia hudsonica*. Doctoral University of Connecticut, DigitalCommons@UConn.
- Flynn, K. J., and X. Irigoien. 2009. Aldehyde-induced insidious effects cannot be considered as a diatom defence mechanism against copepods. *Marine Ecology Progress Series* **377**:79-89.
- Frangopulos, M., C. Guisande, I. Maneiro, I. Riveiro, and J. Franco. 2000. Short-term and long-term effects of the toxic dinoflagellate *Alexandrium minutum* on the copepod *Acartia clausi*. *Marine Ecology Progress Series* **203**:161-169.
- Franzè, G., J. J. Pierson, D. K. Stoecker, and P. J. Lavrentyev. 2017. Diatom-produced allelochemicals trigger trophic cascades in the planktonic food web. *Limnology and Oceanography* **63**:1093-1108.

- Gallo, C., G. d'Ippolito, G. Nuzzo, A. Sardo, and A. Fontana. 2017. Autoinhibitory sterol sulfates mediate programmed cell death in a bloom-forming marine diatom. *Nature Communications* **8**:1292.
- Gamir, J., V. Pastor, M. Cerezo, and V. Flors. 2012. Identification of indole-3-carboxylic acid as mediator of priming against *Plectosphaerella cucumerina*. *Plant Physiology and Biochemistry* **61**:169-179.
- Gleason, F. H., T. G. Jephcott, F. C. Küpper, M. Gerphagnon, T. Sime-Ngando, S. A. Karpov, L. Guillou, and F. F. van Ogtrop. 2015. Potential roles for recently discovered chytrid parasites in the dynamics of harmful algal blooms. *Fungal Biology Reviews* **29**:20-33.
- Gobler, C. J., O. M. Doherty, T. K. Hattenrath-Lehmann, A. W. Griffith, Y. Kang, and R. W. Litaker. 2017. Ocean warming since 1982 has expanded the niche of toxic algal blooms in the North Atlantic and North Pacific oceans. *Proceedings of the National Academy of Sciences* **114**:4975-4980.
- Göblyös, A., H. de Vries, J. Brussee, and A. P. Ijzerman. 2005. Synthesis and Biological Evaluation of a New Series of 2,3,5-Substituted [1,2,4]-Thiadiazoles as Modulators of Adenosine A1 Receptors and Their Molecular Mechanism of Action. *Journal of Medicinal Chemistry* **48**:1145-1151.
- Gonçalves, R. J., and T. Kiørboe. 2015. Perceiving the algae: How feeding-current feeding copepods detect their nonmotile prey. *Limnology and Oceanography* **60**:1286-1297.
- González, J. M., R. P. Kiene, and M. A. Moran. 1999. Transformation of sulfur compounds by an abundant lineage of marine bacteria in the α -subclass of the class Proteobacteria. *Applied and Environmental Microbiology* **65**:3810-3819.
- Goutx, M., C. Guigue, and L. Striby. 2003. Triacylglycerol biodegradation experiment in marine environmental conditions: Definition of a new lipolysis index. *Organic Geochemistry* **34**:1465-1473.
- Gowda, H., J. Ivanisevic, C. H. Johnson, M. E. Kurczy, H. P. Benton, D. Rinehart, T. Nguyen, J. Ray, J. Kuehl, B. Arevalo, P. D. Westenskow, J. Wang, A. P. Arkin, A. M. Deutschbauer, G. J. Patti, and G. Siuzdak. 2014. Interactive XCMS online: Simplifying advanced metabolomic data processing and subsequent statistical analyses. *Analytical Chemistry* **86**:6931-6939.

- Grebner, W., E. C. Berglund, F. Berggren, J. Eklund, S. Harðadóttir, M. X. Andersson, and E. Selander. 2019. Induction of defensive traits in marine plankton—new copepodamide structures. *Limnology and Oceanography* **64**:820-831.
- Griffin, J. E., G. Park, and H. G. Dam. 2019. Relative importance of nitrogen sources, algal alarm cues and grazer exposure to toxin production of the marine dinoflagellate *Alexandrium catenella*. *Harmful Algae* **84**:181-187.
- Grzebyk, D., C. Béchemin, C. J. Ward, C. Vérité, G. A. Codd, and S. Y. Maestrini. 2003. Effects of salinity and two coastal waters on the growth and toxin content of the dinoflagellate *Alexandrium minutum*. *Journal of Plankton Research* **25**:1185-1199.
- Guisande, C., M. Frangópulos, I. Maneiro, A. R. Vergara, and I. Riveiro. 2002. Ecological advantages of toxin production by the dinoflagellate *Alexandrium minutum* under phosphorus limitation. *Marine Ecology Progress Series* **225**:169-176.
- Hahn, M. A., C. Effertz, L. Bigler, and E. von Elert. 2019. 5 α -cyprinol sulfate, a bile salt from fish, induces diel vertical migration in *Daphnia*. *eLife* **8**:e44791.
- Hallegraeff, G. M., P. D. Nichols, J. K. Volkman, S. I. Blackburn, and D. A. Everitt. 1991. Pigments, fatty acids, and sterols of the toxic dinoflagellate *Gymnodinium catenatum*. *Journal of Phycology* **27**:591-599.
- Hammann, S., U. Tillmann, M. Schröder, and W. Vetter. 2013. Profiling the fatty acids from a strain of the microalgae *Alexandrium tamarense* by means of high-speed counter-current chromatography and gas chromatography coupled with mass spectrometry. *J Chromatogr A* **1312**:93-103.
- Han, G.-Z. 2016. Evolution of jasmonate biosynthesis and signaling mechanisms. *Journal of Experimental Botany* **68**:1323-1331.
- Han, J., J. S. Park, J. Lee, Y. Park, H. H. Shin, Y.-U. Choi, and K.-W. Lee. 2021. Effects of toxic dinoflagellate *Alexandrium minutum* on the expression of detoxification-related genes in the marine copepod *Tigriopus japonicus*. *Journal of Experimental Marine Biology and Ecology* **540**:151563.
- Harðadóttir, S., M. Pančić, A. Tammilehto, B. Krock, E. F. Møller, T. G. Nielsen, and N. Lundholm. 2015. Dangerous relations in the Arctic marine food web:

Interactions between toxin producing *Pseudo-nitzschia* diatoms and Calanus Copepodites. *Marine Drugs* **13**:3809-3835.

Harðardóttir, S., S. Wohlrab, D. M. Hjort, B. Krock, T. G. Nielsen, U. John, and N. Lundholm. 2019. Transcriptomic responses to grazing reveal the metabolic pathway leading to the biosynthesis of domoic acid and highlight different defense strategies in diatoms. *BMC Molecular Biology* **20**:7.

Harju, K., M.-L. Rapinoja, M.-A. Avondet, W. Arnold, M. Schär, S. Burrell, W. Luginbühl, and P. Vanninen. 2015. Optimization of sample preparation for the identification and quantification of saxitoxin in proficiency test mussel sample using liquid chromatography-tandem mass spectrometry. *Toxins* **7**:4868-4880.

Harvey, E. L., K. D. Bidle, and M. D. Johnson. 2015. Consequences of strain variability and calcification in *Emiliana huxleyi* on microzooplankton grazing. *Journal of Plankton Research* **37**:1137-1148.

Harvey, E. L., R. W. Deering, D. C. Rowley, A. El Gamal, M. Schorn, B. S. Moore, M. D. Johnson, T. J. Mincer, and K. E. Whalen. 2016. A bacterial quorum-sensing precursor induces mortality in the marine coccolithophore, *Emiliana huxleyi*. *Frontiers in Microbiology* **7**:59.

Hattenrath-Lehmann, T. K., and C. J. Gobler. 2017. Identification of unique microbiomes associated with harmful algal blooms caused by *Alexandrium fundyense* and *Dinophysis acuminata*. *Harmful Algae* **68**:17-30.

Hattenrath-Lehmann, T. K., J. L. Smith, R. B. Wallace, L. R. Merlo, F. Koch, H. Mittelsdorf, J. A. Goleski, D. M. Anderson, and C. J. Gobler. 2015. The effects of elevated CO₂ on the growth and toxicity of field populations and cultures of the saxitoxin-producing dinoflagellate, *Alexandrium fundyense*. *Limnology and Oceanography* **60**:198-214.

Hay, M. E. 2009. Marine chemical ecology: Chemical signals and cues structure marine populations, communities, and ecosystems. *Annual review of Marine Science* **1**:193-212.

Hay, M. E., and J. Kubanek. 2002. Community and ecosystem level consequences of chemical cues in the plankton. *Journal of Chemical Ecology* **28**:2001-2016.

- Hazlett, B. A., and C. McLay. 2005. Responses of the crab *Heterozius rotundifrons* to heterospecific chemical alarm cues: Phylogeny vs. ecological overlap. *Journal of Chemical Ecology* **31**:671-677.
- Heuschele, J., L. Nemming, L. Tolstrup, T. Kiørboe, G. M. Nylund, and E. Selander. 2016. The sex specific metabolic footprint of *Oithona davisae*. *Journal of Sea Research* **117**:1-6.
- Heuschele, J., and E. Selander. 2014. The chemical ecology of copepods. *Journal of Plankton Research* **36**:895-913.
- Hillebrand, H., C.-D. Dürselen, D. Kirschtel, U. Pollinger, and T. Zohary. 1999. Biovolume calculation for pelagic and benthic microalgae. *Journal of Phycology* **35**:403-424.
- Hinow, P., J. R. Strickler, and J. Yen. 2017. Olfaction in a viscous environment: The “color” of sexual smells in *Temora longicornis*. *The Science of Nature* **104**:46.
- Honkanen, R. E. 1993. Cantharidin, another natural toxin that inhibits the activity of serine/threonine protein phosphatases types 1 and 2A. *FEBS Letters* **330**:283-286.
- Hothorn, T., F. Bretz, and P. Westfall. 2008. Simultaneous inference in general parametric models. *Biometrical Journal* **50**:346-363.
- Høyland-Kroghsbo, N. M., R. B. Mærkedahl, and S. L. Svenningsen. 2013. A quorum-sensing-induced bacteriophage defense mechanism. *mBio* **4**:00362-00312.
- Hsu, F.-F. 2016. Complete structural characterization of ceramides as [M-H]⁺ ions by multiple-stage linear ion trap mass spectrometry. *Biochimie* **130**:63-75.
- Hsu, F.-F., J. Turk, K. Zhang, and S. M. Beverley. 2007. Characterization of inositol phosphorylceramides from *Leishmania major* by tandem mass spectrometry with electrospray ionization. *Journal of the American Society for Mass Spectrometry* **18**:1591-1604.
- Huang, H.-N., J.-L. Lu, S.-E. Lin, R.-J. Zheng, and J. Lin. 2020. Simultaneous determination of twelve paralytic shellfish poisoning toxins in bivalve molluscs

- by UPLC-MS/MS and its applications to a food poisoning incident. *Toxicon* **174**:1-7.
- Hwang, D. F., and Y. H. Lu. 2000. Influence of environmental and nutritional factors on growth, toxicity, and toxin profile of dinoflagellate *Alexandrium minutum*. *Toxicon* **38**:1491-1503.
- Ianora, A., M. Bastianini, Y. Carotenuto, R. Casotti, V. Roncalli, A. Miralto, G. Romano, A. Gerech, A. Fontana, and J. T. Turner. 2015. Non-volatile oxylipins can render some diatom blooms more toxic for copepod reproduction. *Harmful Algae* **44**:1-7.
- Imai, I., Y. Ishida, and Y. Hata. 1992. Isolation and properties of a bacterium inhibiting the growth of *Gymnodinium nagasakiense*. *Nippon Suisan Gakkaishi* **58**:1073-1077.
- Imai, I., Y. Ishida, and Y. Hata. 1993. Killing of marine phytoplankton by a gliding bacterium *Cytophaga* sp., isolated from the coastal sea of Japan. *Marine Biology* **116**:527-532.
- Ishida, H., A. Nozawa, H. Nukaya, L. Rhodes, P. McNabb, P. T. Holland, and K. Tsuji. 2004a. Confirmation of brevetoxin metabolism in cockle, *Austrovenus stutchburyi*, and greenshell mussel, *Perna canaliculus*, associated with New Zealand neurotoxic shellfish poisoning, by controlled exposure to *Karenia brevis* culture. *Toxicon* **43**:701-712.
- Ishida, H., A. Nozawa, H. Nukaya, and K. Tsuji. 2004b. Comparative concentrations of brevetoxins PbTx-2, PbTx-3, BTX-B1 and BTX-B5 in cockle, *Austrovenus stutchburyi*, greenshell mussel, *Perna canaliculus*, and Pacific oyster, *Crassostrea gigas*, involved neurotoxic shellfish poisoning in New Zealand. *Toxicon* **43**:779-789.
- Iwamoto, O., H. Koshino, D. Hashizume, and K. Nagasawa. 2007. Total synthesis of (-)-decarbamoxyloxysaxitoxin. *Angewandte Chemie International Edition* **46**:8625-8628.
- Jatt, A. N., K. Tang, J. Liu, Z. Zhang, and X.-H. Zhang. 2015. Quorum sensing in marine snow and its possible influence on production of extracellular hydrolytic enzymes in marine snow bacterium *Pantoea ananatis* B9. *FEMS Microbiology Ecology* **91**:1-13.

- Jauffrais, T., A. Contreras, C. Herrenknecht, P. Truquet, V. Séchet, U. Tillmann, and P. Hess. 2012. Effect of *Azadinium spinosum* on the feeding behaviour and azaspiracid accumulation of *Mytilus edulis*. *Aquatic Toxicology* **124-125**:179-187.
- Jensen, S.-K., J.-P. Lacaze, G. Hermann, J. Kershaw, A. Brownlow, A. Turner, and A. Hall. 2015. Detection and effects of harmful algal toxins in Scottish harbour seals and potential links to population decline. *Toxicon* **97**:1-14.
- John, E. H., and K. J. Flynn. 2000. Growth dynamics and toxicity of *Alexandrium fundyense* (Dinophyceae): the effect of changing N:P supply ratios on internal toxin and nutrient levels. *European Journal of Phycology* **35**:11-23.
- John, U., R. W. Litaker, M. Montresor, S. Murray, M. L. Brosnahan, and D. M. Anderson. 2014. Formal revision of the *Alexandrium tamarensis* species complex (Dinophyceae) taxonomy: The introduction of five species with emphasis on molecular-based (rDNA) classification. *Protist* **165**:779-804.
- John Wiley & Sons, I. 2020. SpectraBase.
- Johnson, M. D., B. R. Edwards, D. J. Beaudoin, B. A. S. Van Mooy, and A. Vardi. 2020. Nitric oxide mediates oxylipin production and grazing defense in diatoms. *Environmental Microbiology* **22**:629-645.
- Johnson, W. M., M. C. Kido Soule, and E. B. Kujawinski. 2016. Evidence for quorum sensing and differential metabolite production by a marine bacterium in response to DMSP. *The ISME Journal* **10**:2304-2316.
- Jonasdottir, S., T. Kiørboe, K. W. Tang, M. St. John, A. Visser, E. Saiz, and H. Dam. 1998. Role of diatoms in copepod production: Good, harmless or toxic? *Marine Ecology-Progress Series* **172**:305-308.
- Juhl, A. R., V. L. Trainer, and M. I. Latz. 2001. Effect of fluid shear and irradiance on population growth and cellular toxin content of the dinoflagellate *Alexandrium fundyense*. *Limnology and Oceanography* **46**:758-764.
- Keller, M. D., R. C. Selvin, W. Claus, and R. R. L. Guillard. 1987. Media for the culture of oceanic ultraphytoplankton. *Journal of Phycology* **23**:633-638.

- Kiba, A., M. Nakano, M. Hosokawa, I. Galis, H. Nakatani, T. Shinya, K. Ohnishi, and Y. Hikichi. 2020. Phosphatidylinositol-phospholipase C2 regulates pattern-triggered immunity in *Nicotiana benthamiana*. *Journal of Experimental Botany* **71**:5027-5038.
- Kim, J. H., H. J. Jeong, A. S. Lim, J. R. Rho, and S. B. Lee. 2016. Killing potential protist predators as a survival strategy of the newly described dinoflagellate *Alexandrium pohangense*. *Harmful Algae* **55**:41-55.
- Kjørboe, T., A. Andersen, V. J. Langlois, and H. H. Jakobsen. 2010. Unsteady motion: Escape jumps in planktonic copepods, their kinematics and energetics. *Journal of The Royal Society Interface* **7**:1591-1602.
- Kjørboe, T., R. J. Goncalves, D. Couespel, H. van Someren Gréve, E. Saiz, and P. Tiselius. 2016. Reply to comment: Prey perception in feeding-current feeding copepods. *Limnology and Oceanography* **61**:1169-1171.
- Krock, B., U. Tillmann, É. Potvin, H. Jeong, W. Drebing, J. Kilcoyne, A. Al-Jorani, M. Twiner, Q. Göthel, and M. Köck. 2015. Structure elucidation and in vitro toxicity of new azaspiracids isolated from the marine dinoflagellate *Azadinium poporum*. *Marine Drugs* **13**:6687-6702.
- Krupke, A., L. R. Hmelo, J. E. Ossolinski, T. J. Mincer, and B. A. S. Van Mooy. 2016. Quorum sensing plays a complex role in regulating the enzyme hydrolysis activity of microbes associated with sinking particles in the ocean. *Frontiers in Marine Science* **3**:55.
- Kuhlisch, C., and G. Pohnert. 2015. Metabolomics in chemical ecology. *Natural Product Reports* **32**:937-955.
- Kuku, G., M. Altunbek, and M. Culha. 2017. Surface-enhanced raman scattering for label-free living single cell analysis. *Analytical Chemistry* **89**:11160-11166.
- Labeeuw, L., J. Khey, A. R. Bramucci, H. Atwal, A. P. de la Mata, J. Harynuk, and R. J. Case. 2016. Indole-3-acetic acid is produced by *Emiliania huxleyi* coccolith-bearing cells and triggers a physiological response in bald cells. *Frontiers in Microbiology* **7**:e00828.
- Laforsch, C., L. Beccara, and R. Tollrian. 2006. Inducible defenses: The relevance of chemical alarm cues in *Daphnia*. *Limnology and Oceanography* **51**:1466-1472.

- Laforsch, C., and R. Tollrian. 2004. Inducible defenses in multipredator environments: Cyclomorphosis in *Daphnia cucullata*. *Ecology* **85**:2302-2311.
- Landa, M., A. S. Burns, S. J. Roth, and M. A. Moran. 2017. Bacterial transcriptome remodeling during sequential co-culture with a marine dinoflagellate and diatom. *The ISME Journal* **11**:2677-2690.
- Lasley-Rasher, R. S., K. Nagel, A. Angra, and J. Yen. 2016. Intoxicated copepods: Ingesting toxic phytoplankton leads to risky behaviour. *Proceedings of the Royal Society B: Biological Sciences* **283**:20160176.
- Lass, S., and P. Spaak. 2003. Chemically induced anti-predator defences in plankton: A review. *Hydrobiologia* **491**:221-239.
- Lassudrie, M., P. Soudant, J.-L. Nicolas, C. Fabioux, C. Lambert, P. Miner, J. Le Grand, B. Petton, and H. Hégaret. 2015. Interaction between toxic dinoflagellate *Alexandrium catenella* exposure and disease associated with herpesvirus OsHV-1 μ Var in Pacific oyster spat *Crassostrea gigas*. *Harmful Algae* **45**:53-61.
- Lassudrie, M., P. Soudant, J.-L. Nicolas, P. Miner, J. Le Grand, C. Lambert, N. Le Goïc, H. Hégaret, and C. Fabioux. 2016. Exposure to the toxic dinoflagellate *Alexandrium catenella* modulates juvenile oyster *Crassostrea gigas* hemocyte variables subjected to different biotic conditions. *Fish & Shellfish Immunology* **51**:104-115.
- Lauritano, C., Y. Carotenuto, A. Miralto, G. Procaccini, and A. Ianora. 2012. Copepod population-specific response to a toxic diatom diet. *PLoS ONE* **7**:e47262.
- Lauritano, C., Y. Carotenuto, V. Vitiello, I. Buttino, G. Romano, J.-S. Hwang, and A. Ianora. 2015. Effects of the oxylipin-producing diatom *Skeletonema marinoi* on gene expression levels of the calanoid copepod *Calanus sinicus*. *Marine Genomics* **24**:89-94.
- Lee, B., and M. G. Park. 2017. Different life cycle strategies of the dinoflagellates *Fragilidium duplocampanaeforme* and its prey *Dinophysis acuminata* may explain their different susceptibilities to the infection by the parasite *Parvilucifera infectans*. *Harmful Algae* **65**:1-8.

- Leong, S. C. Y., A. Murata, Y. Nagashima, and S. Taguchi. 2004. Variability in toxicity of the dinoflagellate *Alexandrium tamarensis* in response to different nitrogen sources and concentrations. *Toxicon* **43**:407-415.
- Lewandowicz, A. M., J. Vepsäläinen, and J. T. Laitinen. 2006. The 'allosteric modulator' SCH-202676 disrupts G protein-coupled receptor function via sulphhydryl-sensitive mechanisms. *British Journal of Pharmacology* **147**:422-429.
- Li, S., and S. M. H. Ismar. 2018. Transcriptome, Biochemical and Growth Responses of the Marine Phytoplankton *Phaeodactylum Tricornutum* Bohlin (Bacillariophyta) to Copepod Grazer Presence. *Cellular Physiology and Biochemistry* **46**:1091-1111.
- Li, Z., S. Lin, X. Liu, J. Tan, J. Pan, and H. Yang. 2014. A freshwater bacterial strain, *Shewanella* sp. Lzh-2, isolated from Lake Taihu and its two algicidal active substances, hexahydropyrrolo [1, 2-a] pyrazine-1, 4-dione and 2, 3-indolinedione. *Applied Microbiology and Biotechnology* **98**:4737-4748.
- Lim, A. S., H. J. Jeong, J. H. Kim, and S. Y. Lee. 2015. Description of the new phototrophic dinoflagellate *Alexandrium pohangense* sp. nov. from Korean coastal waters. *Harmful Algae* **46**:49-61.
- Lima, S. L., and L. M. Dill. 1990. Behavioral decisions made under the risk of predation: A review and prospectus. *Canadian Journal of Zoology* **68**:619-640.
- Lindström, J., W. Grebner, K. Rigby, and E. Selander. 2017. Effects of predator lipids on dinoflagellate defence mechanisms - increased bioluminescence capacity. *Scientific Reports* **7**:13104.
- Loose, C. J., and P. Dawidowicz. 1994. Trade-offs in diel vertical migration by zooplankton: The costs of predator avoidance. *Ecology* **75**:2255-2263.
- López-Cortés, D. J., C. J. Band-Schmidt, I. Gárate-Lizárraga, J. J. Bustillos-Guzmán, F. E. Hernández-Sandoval, and E. J. Núñez-Vázquez. 2011. Co-ocurrencia de *Chattonella marina* y *Gymnodinium catenatum* en la Bahía de La Paz, Golfo de California (primavera 2009). *Hidrobiológica* **21**:185-196.
- Lu, Y., S. Wohlrab, M. Groth, G. Glöckner, L. Guillou, and U. John. 2016. Transcriptomic profiling of *Alexandrium fundyense* during physical interaction

with or exposure to chemical signals from the parasite *Amoebophrya*. *Molecular Ecology* **25**:1294-1307.

Ludwig, C., and U. L. Günther. 2011. MetaboLab - Advanced NMR data processing and analysis for metabolomics. *BMC Bioinformatics* **12**:366.

Lundholm, N., B. Krock, U. John, J. Skov, J. Cheng, M. Pančić, S. Wohlrab, K. Rigby, T. G. Nielsen, E. Selander, and S. Harðardóttir. 2018. Induction of domoic acid production in diatoms—Types of grazers and diatoms are important. *Harmful Algae* **79**:64-73.

Maibam, C., P. Fink, G. Romano, M. C. Buia, E. Butera, and V. Zupo. 2015. *Centropages typicus* (Crustacea, Copepoda) reacts to volatile compounds produced by planktonic algae. *Marine Ecology* **36**:819-834.

Malavasi, S., V. Georgalas, D. Mainardi, and P. Torricelli. 2008. Antipredator responses to overhead fright stimuli in hatchery-reared and wild European sea bass (*Dicentrarchus labrax* L.) juveniles. *Aquaculture Research* **39**:276-282.

Manoharan, K., T. K. Lee, J. M. Cha, J. H. Kim, W. S. Lee, M. Chang, C. W. Park, and J. H. Cho. 1999. Acclimation of *Prorocentrum minimum* (dinophyceae) to prolonged darkness by use of an alternative carbon source from triacylglycerides and galactolipids. *Journal of Phycology* **35**:287-292.

Mansour, M. P., J. K. Volkman, and S. I. Blackburn. 2003. The effect of growth phase on the lipid class, fatty acid and sterol composition in the marine dinoflagellate, *Gymnodinium* sp. in batch culture. *Phytochemistry* **63**:145-153.

Mansour, M. P., J. K. Volkman, A. E. Jackson, and S. I. Blackburn. 1999. The fatty acid and sterol composition of five marine dinoflagellates. *Journal of Phycology* **35**:710-720.

Martin-Creuzburg, D., and E. v. Elert. 2009. Ecological significance of sterols in aquatic food webs. Pages 43-64 in M. Kainz, M. T. Brett, and M. T. Arts, editors. *Lipids in Aquatic Ecosystems*. Springer New York, New York, NY.

McCarren, J., and B. Brahamsha. 2007. Swmb, a 1.12-megadalton protein that is required for nonflagellar swimming motility in *Synechococcus*. *Journal of Bacteriology* **189**:1158-1162.

- McCarren, J., J. Heuser, R. Roth, N. Yamada, M. Martone, and B. Brahamsha. 2005. Inactivation of *swmA* results in the loss of an outer cell layer in a swimming *Synechococcus* strain. *Journal of Bacteriology* **187**:224-230.
- McFarland, K., F. Jean, P. Soudant, and A. K. Volety. 2015. Uptake and elimination of brevetoxin in the invasive green mussel, *Perna viridis*, during natural *Karenia brevis* blooms in southwest Florida. *Toxicon* **97**:46-52.
- Menden-Deuer, S., and E. J. Lessard. 2000. Carbon to volume relationships for dinoflagellates, diatoms, and other protist plankton. *Limnology and Oceanography* **45**:569-579.
- Mishamandani, S., T. Gutierrez, D. Berry, and M. D. Aitken. 2016. Response of the bacterial community associated with a cosmopolitan marine diatom to crude oil shows a preference for the biodegradation of aromatic hydrocarbons. *Environmental Microbiology* **18**:1817-1833.
- Mojib, N., and J. Kubanek. 2020. Comparative transcriptomics supports the presence of G protein-coupled receptor-based signaling in unicellular marine eukaryotes. *Limnology and Oceanography* **65**:762-774.
- Morohashi, A., M. Satake, K. Murata, H. Naoki, H. F. Kaspar, and T. Yasumoto. 1995. Brevetoxin B3, a new brevetoxin analog isolated from the greenshell mussel *Perna canaliculus* involved in neurotoxic shellfish poisoning in New Zealand. *Tetrahedron Letters* **36**:8995-8998.
- Murphy, R. C., and P. H. Axelsen. 2011. Mass spectrometric analysis of long-chain lipids. *Mass spectrometry reviews* **30**:579-599.
- Murray, S., U. John, H. Savela, and A. Kremp. 2020. Chapter 4 *Alexandrium* spp.: Genetic and ecological factors influencing saxitoxin production and proliferation. Pages 133-166 *Climate Change and Marine and Freshwater Toxins*. De Gruyter.
- Nam, O., I. Suzuki, Y. Shiraiwa, and E. Jin. 2020. Association of phosphatidylinositol-specific phospholipase C with calcium-induced biomineralization in the coccolithophore *Emiliana huxleyi*. *Microorganisms* **8**:1389.
- Nam, W., X. Ren, S. A. S. Tali, P. Ghassemi, I. Kim, M. Agah, and W. Zhou. 2019. Refractive-index-insensitive nanolaminated SERS substrates for label-free

- raman profiling and classification of living cancer cells. *Nano Letters* **19**:7273-7281.
- Newberger, N. C., L. K. Ranzer, J. M. Boehnlein, and R. G. Kerr. 2006. Induction of terpene biosynthesis in dinoflagellate symbionts of Caribbean gorgonians. *Phytochemistry* **67**:2133-2139.
- Ogata, H., S. Goto, K. Sato, W. Fujibuchi, H. Bono, and M. Kanehisa. 1999. KEGG: Kyoto encyclopedia of genes and genomes. *Nucleic Acids Research* **27**:29-34.
- Orr, R. J. S., A. Stüken, T. Rundberget, W. Eikrem, and K. S. Jakobsen. 2011. Improved phylogenetic resolution of toxic and non-toxic *Alexandrium* strains using a concatenated rDNA approach. *Harmful Algae* **10**:676-688.
- Oshima, Y. 1995. Postcolumn derivatization liquid chromatographic method for paralytic shellfish toxins. *Journal of AOAC International* **78**:528-532.
- Paffenhöfer, G. A., and H. Jiang. 2016. Comment: On phytoplankton perception by calanoid copepods. *Limnology and Oceanography* **61**:1163-1168.
- Pande, G. S. J., F. M. I. Natrah, A. V. B. Flandez, U. Kumar, Y. Niu, P. Bossier, and T. Defoirdt. 2015. Isolation of AHL-degrading bacteria from micro-algal cultures and their impact on algal growth and on virulence of *Vibrio campbellii* to prawn larvae. *Applied Microbiology and Biotechnology* **99**:10805-10813.
- Park, G., and H. G. Dam. 2021. Cell-growth gene expression reveals a direct fitness cost of grazer-induced toxin production in red tide dinoflagellate prey. *Proceedings of the Royal Society B: Biological Sciences* **288**:20202480.
- Parsons, H. M., C. Ludwig, U. L. Günther, and M. R. Viant. 2007. Improved classification accuracy in 1- and 2-dimensional NMR metabolomics data using the variance stabilising generalised logarithm transformation. *BMC Bioinformatics* **8**:234.
- Pence, H. E., and A. Williams. 2010. ChemSpider: An online chemical information resource. *Journal of Chemical Education* **87**:1123-1124.

- Pepi, M., H. J. Heipieper, C. Balestra, M. Borra, E. Biffali, and R. Casotti. 2017. Toxicity of diatom polyunsaturated aldehydes to marine bacterial isolates reveals their mode of action. *Chemosphere* **177**:258-265.
- Perrault, J. R., N. I. Stacy, A. F. Lehner, C. R. Mott, S. Hirsch, J. C. Gorham, J. P. Buchweitz, M. J. Bresette, and C. J. Walsh. 2017. Potential effects of brevetoxins and toxic elements on various health variables in Kemp's ridley (*Lepidochelys kempii*) and green (*Chelonia mydas*) sea turtles after a red tide bloom event. *Science of The Total Environment* **605-606**:967-979.
- Peters, G.-J. Y., P. Verboon, and J. Green. 2018. {userfriendlyscience}: Quantitative analysis made accessible. <http://userfriendlyscience.com>, <http://userfriendlyscience.com>.
- Pinheiro, J., D. Bates, S. DebRoy, D. Sarkar, and R Core Team. 2017. nlme: Linear and nonlinear mixed effects models. <https://CRAN.R-project.org/package=nlme>.
- Piretti, M. V., G. Pagliuca, L. Boni, R. Pistocchi, M. Diamante, and T. Gazzotti. 1997. Investigation of 4-methyl sterols from cultured dinoflagellate algal strains. *Journal of Phycology* **33**:61-67.
- Pluskal, T., S. Castillo, A. Villar-Briones, and M. Orešič. 2010. MZmine 2: Modular framework for processing, visualizing, and analyzing mass spectrometry-based molecular profile data. *BMC Bioinformatics* **11**:395.
- Pohnert, G., M. Steinke, and R. Tollrian. 2007. Chemical cues, defence metabolites and the shaping of pelagic interspecific interactions. *Trends in Ecology & Evolution* **22**:198-204.
- Poulin, R. X., S. Hogan, K. L. Poulson-Ellestad, E. Brown, F. M. Fernández, and J. Kubanek. 2018. *Karenia brevis* allelopathy compromises the lipidome, membrane integrity, and photosynthesis of competitors. *Scientific Reports* **8**:9572.
- Poulson-Ellestad, K. L., E. L. Harvey, M. D. Johnson, and T. J. Mincer. 2016. Evidence for strain-specific exometabolomic responses of the coccolithophore *Emiliania huxleyi* to grazing by the dinoflagellate *Oxyrrhis marina*. *Frontiers in Marine Science* **3**:1.

- Poulson-Ellestad, K. L., C. M. Jones, J. Roy, M. R. Viant, F. M. Fernández, J. Kubanek, and B. L. Nunn. 2014. Metabolomics and proteomics reveal impacts of chemically mediated competition on marine plankton. *Proceedings of the National Academy of Sciences* **111**:9009-9014.
- Poulson, K. L., R. D. Sieg, and J. Kubanek. 2009. Chemical ecology of the marine plankton. *Natural Product Reports* **26**:729-745.
- Prud'homme van Reine, W. F. 2017. Report of the nomenclature committee for algae: 15. *Taxon* **66**:191-192.
- Purwaha, P., L. P. Silva, D. H. Hawke, J. N. Weinstein, and P. L. Lorenzi. 2014. An artifact in LC-MS/MS measurement of glutamine and glutamic acid: In-source cyclization to pyroglutamic acid. *Analytical Chemistry* **86**:5633-5637.
- R Development Core Team. 2020. R: A language and environment for statistical computing. R Foundation for Statistical Computing, <https://www.R-project.org/>, Vienna, Austria.
- Ramanathan, N., O. Simakov, C. A. Merten, and D. Arendt. 2015. Quantifying preferences and responsiveness of marine zooplankton to changing environmental conditions using microfluidics. *PLoS ONE* **10**:e0140553.
- Rasmussen, S. A., A. J. C. Andersen, N. G. Andersen, K. F. Nielsen, P. J. Hansen, and T. O. Larsen. 2016a. Chemical diversity, origin, and analysis of phycotoxins. *Journal of Natural Products* **79**:662-673.
- Rasmussen, S. A., S. B. Binzer, C. Hoeck, S. Meier, L. S. de Medeiros, N. G. Andersen, A. Place, K. F. Nielsen, P. J. Hansen, and T. O. Larsen. 2017. Karmitoxin: An amine-containing polyhydroxy-polyene toxin from the marine dinoflagellate *Karlodinium armiger*. *Journal of Natural Products* **80**:1287-1293.
- Rasmussen, S. A., S. Meier, N. G. Andersen, H. E. Blossom, J. Ø. Duus, K. F. Nielsen, P. J. Hansen, and T. O. Larsen. 2016b. Chemodiversity of ladder-frame prymnesin polyethers in *Prymnesium parvum*. *Journal of Natural Products* **79**:2250-2256.
- Reuter, G., and H. J. Gabius. 1999. Eukaryotic glycosylation: Whim of nature or multipurpose tool? *Cellular and Molecular Life Sciences CMLS* **55**:368-422.

- Řezanka, T., J. Lukavský, L. Nedbalová, and K. Sigler. 2017. Lipidomic profile in three species of dinoflagellates (*Amphidinium carterae*, *Cystodinium* sp., and *Peridinium aciculiferum*) containing very long chain polyunsaturated fatty acids. *Phytochemistry* **139**:88-97.
- Řezanka, T., L. Nedbalová, L. Procházková, and K. Sigler. 2014. Lipidomic profiling of snow algae by ESI-MS and silver-LC/APCI-MS. *Phytochemistry* **100**:34-42.
- Roccuzzo, S., N. Couto, E. Karunakaran, R. V. Kapoore, T. O. Butler, J. Mukherjee, E. M. Hansson, A. P. Beckerman, and J. Pandhal. 2020. Metabolic Insights Into Infochemicals Induced Colony Formation and Flocculation in *Scenedesmus subspicatus* Unraveled by Quantitative Proteomics. *Frontiers in Microbiology* **11**.
- Roelke, D., A. Barkoh, B. Brooks, J. Grover, K. D. Hambright, J. LaClaire, II, P. R. Moeller, and R. Patino. 2016. A chronicle of a killer alga in the west: Ecology, assessment, and management of *Prymnesium parvum* blooms. *Hydrobiologia* **764**:29-50.
- Rolland, J. I., D. Stien, S. Sanchez-Ferandin, and R. Lami. 2016. Quorum sensing and quorum quenching in the phycosphere of phytoplankton: A case of chemical interactions in ecology. *Journal of Chemical Ecology* **42**:1201-1211.
- Rolton, A., P. Soudant, J. Vignier, R. Pierce, M. Henry, S. E. Shumway, V. M. Bricelj, and A. K. Voley. 2015. Susceptibility of gametes and embryos of the eastern oyster, *Crassostrea virginica*, to *Karenia brevis* and its toxins. *Toxicon* **99**:6-15.
- Roncalli, V., M. J. Jungbluth, and P. H. Lenz. 2016a. Glutathione S-transferase regulation in *Calanus finmarchicus* feeding on the toxic dinoflagellate *Alexandrium fundyense*. *PLoS ONE* **11**:e0159563.
- Roncalli, V., P. H. Lenz, M. C. Cieslak, and D. K. Hartline. 2017. Complementary mechanisms for neurotoxin resistance in a copepod. *Scientific Reports* **7**:14201.
- Roncalli, V., J. T. Turner, D. Kulis, D. M. Anderson, and P. H. Lenz. 2016b. The effect of the toxic dinoflagellate *Alexandrium fundyense* on the fitness of the calanoid copepod *Calanus finmarchicus*. *Harmful Algae* **51**:56-66.

- Rosic, N., E. Y. S. Ling, C.-K. K. Chan, H. C. Lee, P. Kaniewska, D. Edwards, S. Dove, and O. Hoegh-Guldberg. 2015. Unfolding the secrets of coral–algal symbiosis. *The ISME Journal* **9**:844-856.
- Roth, P. B., M. J. Twiner, Z. Wang, M. Y. B. Dechraoui, and G. J. Doucette. 2007. Fate and distribution of brevetoxin (PbTx) following lysis of *Karenia brevis* by algicidal bacteria, including analysis of open A-ring derivatives. *Toxicon* **50**:1175-1191.
- Roy, J. S., K. L. Poulson-Ellestad, R. Drew Sieg, R. X. Poulin, and J. Kubanek. 2013. Chemical ecology of the marine plankton. *Natural Product Reports* **30**:1364-1379.
- Ryderheim, F., E. Selander, and T. Kiørboe. 2021. Predator-induced defence in a dinoflagellate generates benefits without direct costs. *The ISME Journal*.
- Sala-Pérez, M., T. J. Alpermann, B. Krock, and U. Tillmann. 2016. Growth and bioactive secondary metabolites of arctic *Protoceratium reticulatum* (Dinophyceae). *Harmful Algae* **55**:85-96.
- Sañudo-Wilhelmy, S. A., L. Gómez-Consarnau, C. Suffridge, and E. A. Webb. 2014. The role of B Vitamins in marine biogeochemistry. *Annual review of Marine Science* **6**:339-367.
- Scalco, E., K. Stec, D. Iudicone, M. I. Ferrante, and M. Montresor. 2014. The dynamics of sexual phase in the marine diatom *Pseudo-nitzschia multistriata* (Bacillariophyceae). *Journal of Phycology* **50**:817-828.
- Scherer, A. E., and D. L. Smee. 2016. A review of predator diet effects on prey defensive responses. *Chemoecology* **26**:83-100.
- Schnetzer, A., R. H. Lampe, C. R. Benitez-Nelson, A. Marchetti, C. L. Osburn, and A. O. Tatters. 2017. Marine snow formation by the toxin-producing diatom, *Pseudo-nitzschia australis*. *Harmful Algae* **61**:23-30.
- Schoeppner, N. M., and R. A. Relyea. 2005. Damage, digestion, and defence: the roles of alarm cues and kairomones for inducing prey defences. *Ecology Letters* **8**:505-512.

- Scholin, C. A., G. M. Hallegraeff, and D. M. Anderson. 1995. Molecular evolution of the *Alexandrium tamarense* 'species complex' (Dinophyceae): Dispersal in the North American and west Pacific regions. *Phycologia* **34**:472-485.
- Scholz, B., F. Küpper, W. Vyverman, H. Ólafsson, and U. Karsten. 2017. Chytridiomycosis of marine diatoms—The role of stress physiology and resistance in parasite-host recognition and accumulation of defense molecules. *Marine Drugs* **15**:26.
- Schwartz, E. R., R. X. Poulin, N. Mojib, and J. Kubanek. 2016. Chemical ecology of marine plankton. *Natural Product Reports* **33**:843-860.
- Segev, E., T. P. Wyche, K. H. Kim, J. Petersen, C. Ellebrandt, H. Vlamakis, N. Barteneva, J. N. Paulson, L. Chai, J. Clardy, and R. Kolter. 2016. Dynamic metabolic exchange governs a marine algal-bacterial interaction. *eLife* **5**:e17473.
- Selander, E., E. C. Berglund, P. Engström, F. Berggren, J. Eklund, S. Harðardóttir, N. Lundholm, W. Grebner, and M. X. Andersson. 2019. Copepods drive large-scale trait-mediated effects in marine plankton. *Science Advances* **5**:eaat5096.
- Selander, E., G. Cervin, and H. Pavia. 2008. Effects of nitrate and phosphate on grazer-induced toxin production in *Alexandrium minutum*. *Limnology and Oceanography* **53**:523-530.
- Selander, E., T. Fagerberg, S. Wohlrab, and H. Pavia. 2012. Fight and flight in dinoflagellates? Kinetics of simultaneous grazer-induced responses in *Alexandrium tamarense*. *Limnology and Oceanography* **57**:58-64.
- Selander, E., J. Heuschele, G. M. Nylund, G. Pohnert, H. Pavia, O. Bjærke, L. A. Pender-Healy, P. Tiselius, and T. Kiørboe. 2016. Solid phase extraction and metabolic profiling of exudates from living copepods. *PeerJ* **4**:e1529.
- Selander, E., H. H. Jakobsen, F. Lombard, and T. Kiørboe. 2011. Grazer cues induce stealth behavior in marine dinoflagellates. *Proceedings of the National Academy of Sciences* **108**:4030-4034.
- Selander, E., J. Kubanek, M. Hamberg, M. X. Andersson, G. Cervin, and H. Pavia. 2015. Predator lipids induce paralytic shellfish toxins in bloom-forming algae. *Proceedings of the National Academy of Sciences* **112**:6395-6400.

- Selander, E., P. Thor, G. Toth, and H. Pavia. 2006. Copepods induce paralytic shellfish toxin production in marine dinoflagellates. *Proceedings of the Royal Society of London B: Biological Sciences* **273**:1673-1680.
- Senft-Batoh, C. D., H. G. Dam, S. E. Shumway, and G. H. Wikfors. 2015a. A multi-phylum study of grazer-induced paralytic shellfish toxin production in the dinoflagellate *Alexandrium fundyense*: A new perspective on control of algal toxicity. *Harmful Algae* **44**:20-31.
- Senft-Batoh, C. D., H. G. Dam, S. E. Shumway, G. H. Wikfors, and C. D. Schlichting. 2015b. Influence of predator-prey evolutionary history, chemical alarm-cues, and feeding selection on induction of toxin production in a marine dinoflagellate. *Limnology and Oceanography* **60**:318-328.
- Seuront, L., and H. E. Stanley. 2014. Anomalous diffusion and multifractality enhance mating encounters in the ocean. *Proceedings of the National Academy of Sciences* **111**:2206-2211.
- Seyedsayamdost, M. R., R. J. Case, R. Kolter, and J. Clardy. 2011. The Jekyll-and-Hyde chemistry of *Phaeobacter gallaeciensis*. *Nature Chemistry* **3**:331-335.
- Sherr, E., and B. Sherr. 1988. Role of microbes in pelagic food webs: A revised concept. *Limnology and Oceanography* **33**:1225-1227.
- Sieg, R. D., K. L. Poulson-Ellestad, and J. Kubanek. 2011. Chemical ecology of the marine plankton. *Natural Product Reports* **28**:388-399.
- Śliwińska-Wilczewska, S., J. Maculewicz, A. Barreiro Felpeto, V. Vasconcelos, and A. Latała. 2017a. Allelopathic activity of picocyanobacterium *Synechococcus* sp. on filamentous cyanobacteria. *Journal of Experimental Marine Biology and Ecology* **496**:16-21.
- Śliwińska-Wilczewska, S., J. Maculewicz, J. Tuszer, K. Dobosz, D. Kulasa, and A. Latała. 2017b. First record of allelopathic activity of the picocyanobacterium *Synechococcus* sp. on a natural plankton community. *Ecohydrology & Hydrobiology* **17**:227-234.
- Śliwińska-Wilczewska, S., F. Pniewski, and A. Latała. 2016. Allelopathic activity of the picocyanobacterium *Synechococcus* sp. under varied light, temperature, and salinity conditions. *International Review of Hydrobiology* **101**:69-77.

- Smayda, T. J. 2008. Complexity in the eutrophication–harmful algal bloom relationship, with comment on the importance of grazing. *Harmful Algae* **8**:140-151.
- Smith, C. A., G. O. Maille, E. J. Want, C. Qin, S. A. Trauger, T. R. Brandon, D. E. Custodio, R. Abagyan, and G. Siuzdak. 2005. METLIN: A metabolite mass spectral database. *Therapeutic Drug Monitoring* **27**:747-751.
- Smriga, S., V. I. Fernandez, J. G. Mitchell, and R. Stocker. 2016. Chemotaxis toward phytoplankton drives organic matter partitioning among marine bacteria. *Proceedings of the National Academy of Sciences* **113**:1576-1581.
- Snell, T. W. 2017. Analysis of proteins in conditioned medium that trigger monogonont rotifer mictic reproduction. *Hydrobiologia* **796**:245-253.
- Stahl, A., and M. S. Ullrich. 2016. Proteomics analysis of the response of the marine bacterium *Marinobacter adhaerens* HP15 to the diatom *Thalassiosira weissflogii*. *Aquatic Microbial Ecology* **78**:65-79.
- Stauffer, B. A., A. G. Gellene, D. Rico, C. Sur, and D. A. Caron. 2017. Grazing of the heterotrophic dinoflagellate *Noctiluca scintillans* on dinoflagellate and raphidophyte prey. *Aquatic Microbial Ecology* **80**:193-207.
- Strom, S., K. Bright, K. Fredrickson, and B. Brahamsha. 2017. The *Synechococcus* cell surface protein SwmA increases vulnerability to predation by flagellates and ciliates. *Limnology and Oceanography* **62**:784-794.
- Strom, S., G. Wolfe, J. Holmes, h. Stecher, C. Shimeneck, S. Lambert, and E. Moreno. 2003. Chemical defense in the microplankton I: Feeding and growth rates of heterotrophic protists on the DMS-producing phytoplanker *Emiliana huxleyi*. *Limnology and Oceanography* **48**:217-229.
- Strom, S. L. 2008. Microbial ecology of ocean biogeochemistry: A community perspective. *Science* **320**:1043-1045.
- Subong, B. J. J., A. O. Lluisma, R. V. Azanza, and L. A. Salvador-Reyes. 2021. Differentiating two closely related *Alexandrium* species using comparative quantitative proteomics. *Toxins* **13**:7.

- Sud, M., E. Fahy, D. Cotter, A. Brown, E. A. Dennis, C. K. Glass, A. H. Merrill, Jr, R. C. Murphy, C. R. H. Raetz, D. W. Russell, and S. Subramaniam. 2006. LMSD: LIPID MAPS structure database. *Nucleic Acids Research* **35**:D527-D532.
- Sun, S., Q. X. M. Tay, S. Kjelleberg, S. A. Rice, and D. McDougald. 2015. Quorum sensing-regulated chitin metabolism provides grazing resistance to *Vibrio cholerae* biofilms. *The ISME Journal* **9**:1812-1820.
- Taguchi, R. 2009. Advances in lipid analysis/lipidomics – analyses of phospholipids by recent application of mass spectrometry. Pages 1-20 in A. Lajtha, G. Tettamanti, and G. Goracci, editors. *Handbook of neurochemistry and molecular neurobiology: Neural lipids*. Springer US.
- Tammilehto, A., T. G. Nielsen, B. Krock, E. F. Møller, and N. Lundholm. 2015. Induction of domoic acid production in the toxic diatom *Pseudo-nitzschia seriata* by calanoid copepods. *Aquatic Toxicology* **159**:52-61.
- Tan, D., A. Dahl, and M. Middelboe. 2015a. Vibriophages differentially influence biofilm formation by *Vibrio anguillarum* strains. *Applied and Environmental Microbiology* **81**:4489-4497.
- Tan, D., L. Gram, and M. Middelboe. 2014. Vibriophages and their interactions with the fish pathogen *Vibrio anguillarum*. *Applied and Environmental Microbiology* **80**:3128-3140.
- Tan, D., S. L. Svenningsen, and M. Middelboe. 2015b. Quorum sensing determines the choice of antiphage defense strategy in *Vibrio anguillarum*. *mBio* **6**:e00627-00615.
- Teegarden, G. J. 1999. Copepod grazing selection and particle discrimination on the basis of PSP toxin content. *Marine Ecology Progress Series* **181**:163-176.
- Teegarden, G. J., R. G. Campbell, D. T. Anson, A. Ouellet, B. A. Westman, and E. G. Durbin. 2008. Copepod feeding response to varying *Alexandrium* spp. cellular toxicity and cell concentration among natural plankton samples. *Harmful Algae* **7**:33-44.
- Thiel, V., T. Brinkhoff, J. S. Dickschat, S. Wickel, J. Grunenberg, I. Wagner-Döbler, M. Simon, and S. Schulz. 2010. Identification and biosynthesis of tropone

derivatives and sulfur volatiles produced by bacteria of the marine *Roseobacter* clade. *Organic & biomolecular chemistry* **8**:234-246.

Tillmann, U., T. L. Alpermann, R. C. da Purificação, B. Krock, and A. Cembella. 2009. Intra-population clonal variability in allelochemical potency of the toxigenic dinoflagellate *Alexandrium tamarense*. *Harmful Algae* **8**:759-769.

Tilstone, G. H., B. M. Míguez, F. G. Figueiras, and E. G. Fermín. 2000. Diatom dynamics in a coastal ecosystem affected by upwelling: Coupling between species succession, circulation and biogeochemical processes. *Marine Ecology Progress Series* **205**:23-41.

Toth, G. B., A. I. Larsson, P. R. Jonsson, and C. Appelqvist. 2015. Natural populations of shipworm larvae are attracted to wood by waterborne chemical cues. *PLoS ONE* **10**:e0124950.

Toth, G. B., F. Noren, E. Selander, and H. Pavia. 2004. Marine dinoflagellates show induced life-history shifts to escape parasite infection in response to waterborne signals. *Proceedings of the Royal Society of London B* **271**:733-738.

Tran, D., A. Ciutat, A. Mat, J.-C. Massabuau, H. Hégaret, C. Lambert, N. Le Goic, and P. Soudant. 2015. The toxic dinoflagellate *Alexandrium minutum* disrupts daily rhythmic activities at gene transcription, physiological and behavioral levels in the oyster *Crassostrea gigas*. *Aquatic Toxicology* **158**:41-49.

True, A. C., D. R. Webster, M. J. Weissburg, and J. Yen. 2017. Copepod avoidance of thin chemical layers of harmful algal compounds. *Limnology and Oceanography* **63**:1041-1055.

Tsuchiya, S., Y. Cho, K. Konoki, K. Nagasawa, Y. Oshima, and M. Yotsu-Yamashita. 2016. Biosynthetic route towards saxitoxin and shunt pathway. *Scientific Reports* **6**:20340.

Turner, J. T. 2014. Planktonic marine copepods and harmful algae. *Harmful Algae* **32**:81-93.

Vadassery, J., D. J. Ballhorn, S. R. Fleming, C. Mazars, S. P. Pandey, A. Schmidt, M. C. Schuman, K.-W. Yeh, A. Yilamujiang, and A. Mithöfer. 2019. Neomycin: An effective inhibitor of jasmonate-induced reactions in plants. *Journal of Plant Growth Regulation* **38**:713-722.

- Van Donk, E., A. Ianora, and M. Vos. 2011. Induced defences in marine and freshwater phytoplankton: a review. *Hydrobiologia* **668**:3-19.
- Van Mooy, B. A. S., H. F. Fredricks, B. E. Pedler, S. T. Dyhrman, D. M. Karl, M. Koblížek, M. W. Lomas, T. J. Mincer, L. R. Moore, T. Moutin, M. S. Rappé, and E. A. Webb. 2009. Phytoplankton in the ocean use non-phosphorus lipids in response to phosphorus scarcity. *Nature* **458**:69-72.
- van Tol, H. M., S. A. Amin, and E. V. Armbrust. 2016. Ubiquitous marine bacterium inhibits diatom cell division. *The ISME Journal* **11**:31-42.
- Venuleo, M., J. A. Raven, and M. Giordano. 2017. Intraspecific chemical communication in microalgae. *New Phytologist* **215**:516-530.
- Véron, B., J.-C. Dauguet, and C. Billard. 1998. Sterolic biomarkers in marine phytoplankton. II. Free and conjugated sterols of seven species used in mariculture. *Journal of Phycology* **34**:273-279.
- Vidoudez, C., R. Casotti, M. Bastianini, and G. Pohnert. 2011. Quantification of dissolved and particulate polyunsaturated aldehydes in the Adriatic Sea. *Marine Drugs* **9**:500-513.
- Volkman, J. K., W. I. C. Rijpstra, J. W. de Leeuw, M. P. Mansour, A. E. Jackson, and S. I. Blackburn. 1999. Sterols of four dinoflagellates from the genus *Prorocentrum*. *Phytochemistry* **52**:659-668.
- Wang, H., J. Tomasch, V. Michael, S. Bhujji, M. Jarek, J. Petersen, and I. Wagner-Döbler. 2015. Identification of genetic modules mediating the Jekyll-and-Hyde interaction of *Dinoroseobacter shibae* with the dinoflagellate *Prorocentrum minimum*. *Frontiers in Microbiology* **6**:e01262.
- Wang, J., Y. Zhang, H. Li, and J. Cao. 2013. Competitive interaction between diatom *Skeletonema costatum* and dinoflagellate *Prorocentrum donghaiense* in laboratory culture. *Journal of Plankton Research* **35**:367-378.
- Wang, L., Y. Zhuang, H. Zhang, X. Lin, and S. Lin. 2014. DNA barcoding species in *Alexandrium tamarense* complex using ITS and proposing designation of five species. *Harmful Algae* **31**:100-113.

- Wang, R., É. Gallant, and M. R. Seyedsayamdost. 2016a. Investigation of the genetics and biochemistry of roseobacticide production in the *Roseobacter* clade bacterium *Phaeobacter inhibens*. *mBio* **7**:e02118-02115.
- Wang, R., J. Wang, Q. Xue, X. Sha, L. Tan, and X. Guo. 2017a. Allelopathic interactions between *Skeletonema costatum* and *Alexandrium minutum*. *Chemistry and Ecology* **33**:485-498.
- Wang, R., J. Wang, Q. Xue, L. Tan, J. Cai, and H. Wang. 2016b. Preliminary analysis of allelochemicals produced by the diatom *Phaeodactylum tricorutum*. *Chemosphere* **165**:298-303.
- Wang, R., Q. Xue, J. Wang, L. Tan, Q. Zhang, Y. Zhao, and D. M. Anderson. 2017b. Effects of an allelochemical in *Phaeodactylum tricorutum* filtrate on *Heterosigma akashiwo*: Morphological, physiological and growth effects. *Chemosphere* **186**:527-534.
- Wasternack, C., and B. Hause. 2013. Jasmonates: biosynthesis, perception, signal transduction and action in plant stress response, growth and development. An update to the 2007 review in *Annals of Botany*. *Annals of Botany* **111**:1021-1058.
- Wasternack, C., and M. Strnad. 2018. Jasmonates: News on Occurrence, Biosynthesis, Metabolism and Action of an Ancient Group of Signaling Compounds. *International Journal of Molecular Sciences* **19**:2539.
- Waters, A. L., J. Oh, A. R. Place, and M. T. Hamann. 2015. Stereochemical studies of the karlotoxin class using NMR spectroscopy and DP4 chemical-shift analysis: Insights into their mechanism of action. *Angewandte Chemie* **127**:15931-15936.
- Weiss, L. C., B. Albada, S. M. Becker, S. W. Meckelmann, J. Klein, M. Meyer, O. J. Schmitz, U. Sommer, M. Leo, J. Zagermann, N. Metzler-Nolte, and R. Tollrian. 2018. Identification of *Chaoborus* kairomone chemicals that induce defences in *Daphnia*. *Nature Chemical Biology* **14**:1133-1139.
- Weisse, T. 1991. The annual cycle of heterotrophic freshwater nanoflagellates: Role of bottom-up versus top-down control. *Journal of Plankton Research* **13**:167-185.
- Wickham, H. 2016. *ggplot2: Elegant Graphics for Data Analysis*. Springer-Verlag New York.

- Wishart, D. S., D. Tzur, C. Knox, R. Eisner, A. C. Guo, N. Young, D. Cheng, K. Jewell, D. Arndt, S. Sawhney, C. Fung, L. Nikolai, M. Lewis, M.-A. Coutouly, I. Forsythe, P. Tang, S. Shrivastava, K. Jeroncic, P. Stothard, G. Amegbey, D. Block, D. D. Hau, J. Wagner, J. Miniaci, M. Clements, M. Gebremedhin, N. Guo, Y. Zhang, G. E. Duggan, G. D. MacInnis, A. M. Weljie, R. Dowlatabadi, F. Bamforth, D. Clive, R. Greiner, L. Li, T. Marrie, B. D. Sykes, H. J. Vogel, and L. Querengesser. 2007. HMDB: The human metabolome database. *Nucleic Acids Research* **35**:D521-D526.
- Wohlrab, S., M. H. Iversen, and U. John. 2010. A molecular and co-evolutionary context for grazer induced toxin production in *Alexandrium tamarense*. *PLoS ONE* **5**:e15039.
- Wohlrab, S., E. Selander, and U. John. 2017. Predator cues reduce intraspecific trait variability in a marine dinoflagellate. *BMC ecology* **17**:8.
- Wohlrab, S., U. Tillmann, A. Cembella, and U. John. 2016. Trait changes induced by species interactions in two phenotypically distinct strains of a marine dinoflagellate. *The ISME Journal* **10**:2658-2668.
- Woodson, C. B., D. R. Webster, M. J. Weissburg, and J. Yen. 2007. Cue hierarchy and foraging in calanoid copepods: Ecological implications of oceanographic structure. *Marine Ecology Progress Series* **330**:163-177.
- Wootton, E. C., M. V. Zubkov, D. H. Jones, R. H. Jones, C. M. Martel, C. A. Thornton, and E. C. Roberts. 2007. Biochemical prey recognition by planktonic protozoa. *Environmental Microbiology* **9**:216-222.
- Woznica, A., J. P. Gerdt, R. E. Hulett, J. Clardy, and N. King. 2017. Mating in the closest living relatives of animals is induced by a bacterial chondroitinase. *Cell* **170**:1175-1183.
- Xu, J., P. J. Hansen, L. T. Nielsen, B. Krock, U. Tillmann, and T. Kiørboe. 2017. Distinctly different behavioral responses of a copepod, *Temora longicornis*, to different strains of toxic dinoflagellates, *Alexandrium* spp. *Harmful Algae* **62**:1-9.
- Xu, J., and T. Kiørboe. 2018. Toxic dinoflagellates produce true grazer deterrents. *Ecology* **99**:2240-2249.

- Xu, J., L. T. Nielsen, and T. Kiørboe. 2018. Foraging response and acclimation of ambush feeding and feeding-current feeding copepods to toxic dinoflagellates. *Limnology and Oceanography* **63**:1449-1461.
- Xu, N., Y. Z. Tang, J. Qin, S. Duan, and C. J. Gobler. 2015. Ability of the marine diatoms *Pseudo-nitzschia multiseriata* and *P. pungens* to inhibit the growth of co-occurring phytoplankton via allelopathy. *Aquatic Microbial Ecology* **74**:29-41.
- Yan, Y., Y. Nie, L. An, Y.-Q. Tang, Z. Xu, and X.-L. Wu. 2020. Improvement of surface-enhanced raman scattering method for single bacterial cell analysis. *Frontiers in Bioengineering and Biotechnology* **8**.
- Yang, Q., L. Chen, X. Hu, L. Zhao, P. Yin, and Q. Li. 2015. Toxic effect of a marine bacterium on aquatic organisms and its algicidal substances against *Phaeocystis globosa*. *PLoS ONE* **10**:e0114933.
- Yang, X., L. Zhou, Y. Tan, X. Shi, Z. Zhao, D. Nie, C. Zhou, and H. Liu. 2017. Development and validation of a liquid chromatography-tandem mass spectrometry method coupled with dispersive solid-phase extraction for simultaneous quantification of eight paralytic shellfish poisoning toxins in shellfish. *Toxins* **9**:206.
- Yasumoto, K., A. Nishigami, M. Yasumoto, F. Kasai, Y. Okada, T. Kusumi, and T. Ooi. 2005. Aliphatic sulfates released from *Daphnia* induce morphological defense of phytoplankton: isolation and synthesis of kairomones. *Tetrahedron Letters* **46**:4765-4767.
- Zhang, S.-F., Y. Zhang, Z.-X. Xie, H. Zhang, L. Lin, and D.-Z. Wang. 2015a. iTRAQ-based quantitative proteomic analysis of a toxigenic dinoflagellate *Alexandrium catenella* and its non-toxic mutant. *Proteomics* **15**:4041-4050.
- Zhang, Y., J. Wang, L. Tan, J. Cao, and H. Li. 2015b. Effect of allelopathy on the competition and succession of *Skeletonema costatum* and *Prorocentrum donghaiense*. *Marine Biology Research* **11**:1093-1099.
- Zhou, J., Y. Lyu, M. L. Richlen, D. M. Anderson, and Z. Cai. 2016. Quorum sensing is a language of chemical signals and plays an ecological role in algal-bacterial interactions. *Critical Reviews in Plant Sciences* **35**:81-105.

Zhu, X., Y. Sun, L. Zhang, J. Wang, L. Gu, Y. Huang, and Z. Yang. 2021. Multi-omics reveal the pathways involved in induced defensive colony formation of *Tetrademus obliquus* in response to *Daphnia* grazing cues. *Limnology and Oceanography*:1-13.

Zianni, R., G. Bianco, F. Lelario, I. Losito, F. Palmisano, and T. R. I. Cataldi. 2013. Fatty acid neutral losses observed in tandem mass spectrometry with collision-induced dissociation allows regiochemical assignment of sulfoquinovosyl-diacylglycerols. *Journal of Mass Spectrometry* **48**:205-215.